

POLITECNICO DI MILANO
Dipartimento di Chimica, Materiali e Ingegneria Chimica
“Giulio Natta”
Dottorato in Ingegneria dei Materiali XXIV Ciclo
2012

**POLYMER NANOCOMPOSITES
BASED ON CARBON NANOTUBES**



Supervisor: Prof. Stefano TURRI
Tutor: Prof.ssa Marinella LEVI
Coordinator: Prof.ssa Chiara CASTIGLIONI

Author: Diego MOLINA **Number:** 738606

>>
ABSTRACT

Carbon nanotubes (CNTs) have emerged as the most promising nanofiller for polymer nanocomposites due to their outstanding mechanical and electrical properties. Theoretical enhancement of properties are not easily accessible due to their strong tendency to form agglomerate and due to difficulties in processing their nanostructure in polymer systems. Despite the vast amount of data available in literature, a lot of controversial results are still present.

The most effective way to stabilize dispersion is by CNTs' surface functionalization that could also efficiently transfer external stress to nanotubes increasing the mechanical properties of the nanocomposites.

The first part of the thesis was directed in order to study the effectiveness and effects of CNTs' surface functionalization. Efficient functionalization methods were investigated to prepare MWCNT with carboxylic (COOH-CNT) and amine (NH₂-CNT) functionalities. The procedures were carried out with high yield obtaining functionalized carbon nanotubes. A quantitative characterization of the functionalities present on the external wall were exploited. Moreover, the functionalization methods developed didn't reduce significantly the peculiar aspect ratio of carbon nanotubes.

As widely known, achieving an homogenous dispersion of carbon nanotubes inside polymer matrices is the main objective in order to enhance the different properties of nanocomposites. Besides all the published works, obtaining a good dispersion in nanocomposites is not trivial. Moreover, a great interest in imparting conductivity in highly insulated materials by fabricating conductive polymer nanocomposites is increasingly present.

The second part of the thesis was focused on the dispersion of the functionalized CNTs, together with pristine grade (CNT), in two different polymer matrices, one thermoset epoxy resin and two different perfluoropolyether (PFPE) aqueous dispersions.

A dispersion method of the CNTs in a DGEBA (diglycidil ether of bisphenol A) based resin was developed with mechanical stirring and ultrasonication. Calorimetry characterizations were investigated to observe the effects of the insertion of different functionalized carbon nanotubes inside the nanocomposites. Extensive rheological characterizations showed at first a good reproducibility of the dispersion process. Nanocomposites containing COOH-CNT showed a lower effect on viscosity (easier processability) than the other CNT grades (NH₂-CNT and pristine CNT). Moreover, rheological measurements (steady and dynamic) were exploited to monitor the efficiency of the CNTs dispersion in the epoxy matrix. The percolation threshold between viscous liquid and solid-like behavior was investigated and related to the different functionalities and to the different CNTs' structure morphologies formed. Electrical characterization was also performed. A percolation threshold was observed when pristine CNTs and NH₂-CNTs were inserted. These observations suggested that CNTs could interact with the resin in

different ways, depending on the type of functionalities present on their external wall.

Conductivity induced by carbon nanotubes in those nanocomposites make them ideal candidates as damage evolution sensor.

A promising defect's sensitivity was registered even at low crack length, and the electrical response was found to be related on the concentration and on the different functionalities of carbon nanotubes inserted into the nanocomposites.

Two different perfluoropolyether polymers were investigated, inserting carboxylic functionalized CNTs. Those matrices are widely used to impart hydrophobic and oleophobic repellence and as lubricant in critical conditions. The creation of nanocomposites with the insertion of carbon nanotubes is realized in order to enhance the peculiar high performances of those polymers. COOH-CNTs were efficiently mixed with different perfluoropolyether polymers with mechanical stirring and ultrasonication. A shear thinning behavior was observed for the nanocomposites' dispersions and a presence of interconnected microstructures of CNTs was suggested. A clear enhancement of dynamic mechanical properties was observed at increasing carbon nanotubes concentration, with a more wide temperature range in which those nanocomposites could be efficiently used. These improvements were obtained without modifying the peculiar hydro/oleo-phobicity of those nanocomposites. Moreover, the insertion of carbon nanotubes clearly induced an electrical conductivity in those nanocomposites.

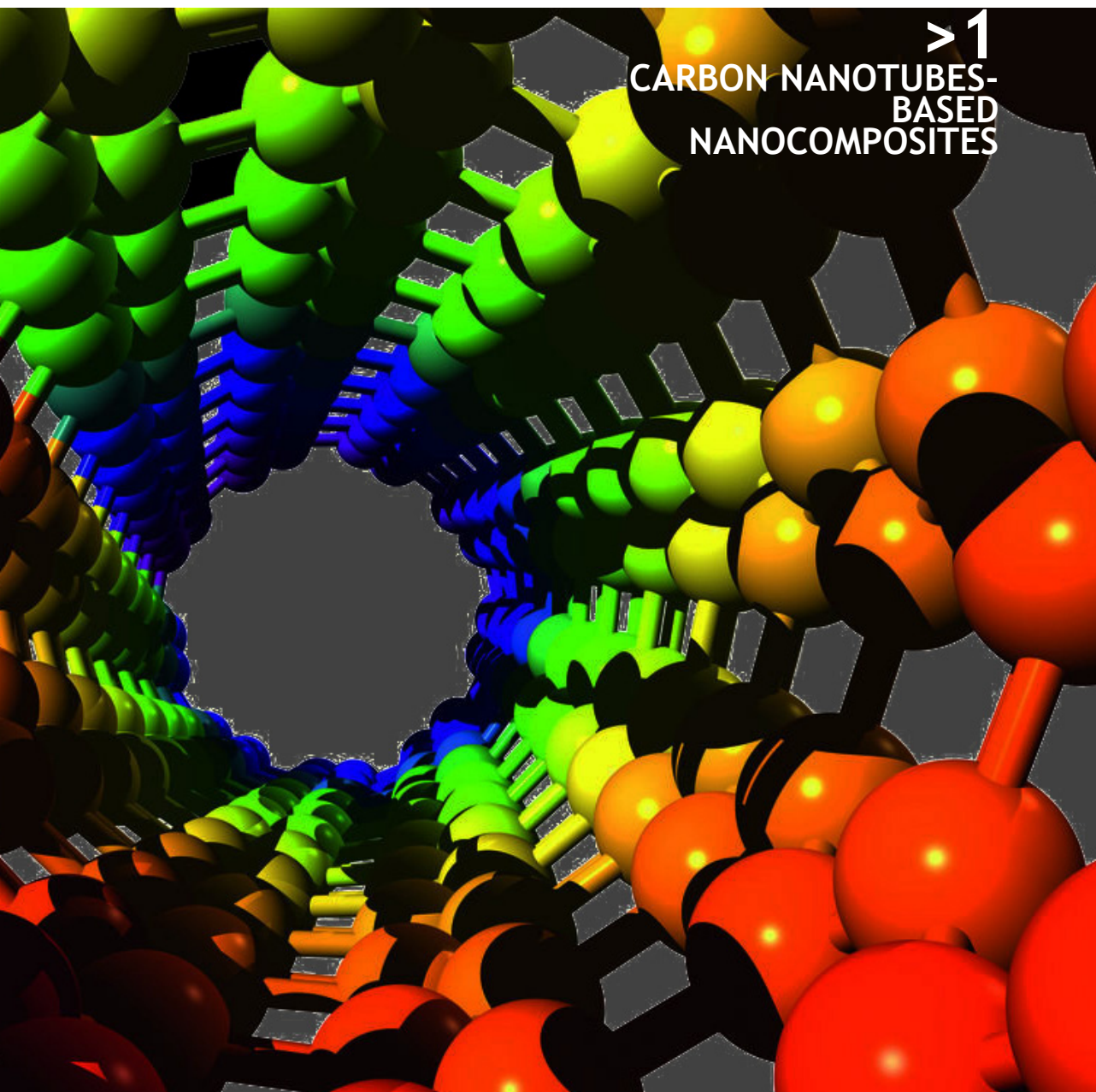
The induced conductivity observed for those nanocomposites could open their exploitation in different applications. One of the most promising is the exploitation of fluorinated CNT based nanocomposites as advanced hydrophobic surface treatments of Gas Diffusion Layer (GDL) for PEM fuel cells. GDL requires different and controversial properties, that could be fulfilled by using those nanocomposites as coating of carbon cloth, permitting to enhance the performances of pollutant free PEM fuel cell. Carbon cloths treated with perfluoropolyether polymer modified with COOH-CNT, showed a good hydrophobicity as required by GDL components. Moreover, an improvement in conductivity, respect to the standard PTFE coating method, was obtained at increasing concentration of carbon nanotubes. An high water vapor permeability was observed with limited film formation of perfluoropolyether coatings, marginally effected by CNTs insertion. GDLs hydrophobized with those fluorinated nanocomposites showed a clear improvement in electrochemical performances when used in PEM fuel cell systems, in comparison with standard GDL coated with PTFE.

**>>
TABLE OF CONTENTS**

| | | |
|----------|--|------------|
| 1 | Carbon nanotubes-based nanocomposites | 1 |
| 1.1 | Properties of carbon nanotubes | 5 |
| 1.2 | Functionalization of carbon nanotubes | 8 |
| 1.3 | Dispersion of carbon nanotubes | 10 |
| 1.4 | Mechanical and electrical properties of nanocomposites based on carbon nanotubes | 12 |
| 1.5 | Epoxy based nanocomposites | 14 |
| 1.6 | Nanocomposites based on nanotubes for polymer electrolyte membrane fuel cell application | 16 |
| 1.7 | References | 20 |
| 2 | Aim of the work | 27 |
| 2.1 | Functionalization of multiwalled carbon nanotubes | 30 |
| 2.2 | Epoxy-based nanocomposites | 31 |
| 2.3 | Fluorinated polymers-based nanocomposites | 32 |
| 3 | Functionalization of carbon nanotubes | 33 |
| 3.1 | Introduction | 34 |
| 3.2 | Experimental section | 36 |
| 3.3 | Results and discussion | 40 |
| 3.4 | Conclusions and future considerations | 49 |
| 3.5 | References | 50 |
| 4 | Epoxy nanocomposites containing carbon nanotubes | 53 |
| 4.1 | Introduction | 54 |
| 4.2 | Experimental section | 56 |
| 4.3 | Results and discussion | 64 |
| 4.4 | Conclusions and future considerations | 94 |
| 4.5 | References | 96 |
| 5 | Fluorinated nanocomposites containing carbon nanotubes | 101 |
| 5.1 | Introduction | 102 |
| 5.2 | Experimental section | 104 |
| 5.3 | Results and discussion | 109 |
| 5.4 | Conclusions and future considerations | 134 |
| 5.5 | References | 136 |

| | | |
|----------|---|------------|
| 6 | Fluorinated nanocomposites coatings on gas diffusion layer | 139 |
| 6.1 | Introduction | 140 |
| 6.2 | Experimental section | 143 |
| 6.3 | Results and discussion | 150 |
| 6.4 | Conclusions and future considerations | 172 |
| 6.5 | References | 174 |
| 7 | Conclusions | 177 |
| 7.1 | Functionalization of multiwalled carbon nanotubes | 179 |
| 7.2 | Epoxy-based nanocomposites | 180 |
| 7.3 | Fluorinated polymers nanocomposites | 181 |
| | Appendix 1 Glossary | 183 |
| | Appendix 2 List of publications | 185 |
| | Acknowledgements | 191 |

>1
CARBON NANOTUBES-
BASED
NANOCOMPOSITES



Polymer nanocomposites are the ideal solution for a new generation of composite material [1-5]. In the last 20 years, they are receiving significant attention, both in academia and industry, for the possibility of achieve high mechanical properties at lower filler loading. With nanofillers' dimensions of only a few nanometers, a large interfacial area per volume between the nano particle and polymer matrix are reached, resulting in enhancement toughness without sacrificing stiffness. Moreover, the possibilities opened by the insertion of nanofiller with peculiar electric, optical and mechanical properties, had widely increased the flexible field of application in which nanocomposites could be applied [2-5].

The demand for new high performance polymer nanocomposites for various applications in many different areas, has lead many interest in investigating the potential use of the carbon nanotubes (CNTs) as reinforcement of polymer matrix [1,5-11]. Compared to different range of other nanofillers, carbon nanotubes have emerged as the most promising nanofiller for polymer nanocomposites due to their remarkable mechanical and electrical properties [1,9,10]. No previous material has displayed the combination of thermal, electronic and mechanical properties showed by carbon nanotubes [12-14]. Since their discovery, the interest generated in such materials creates a huge activity in material science and engineering [6-10]. The peculiar conductivity, the high aspect ratio and their impressive mechanical properties, make them the ideal candidate to develop novel nanocomposites for unprecedented wide range of applications [6-11].

Despite the vast amount of data available in literature, a lot of controversial results are still present [6,9,10]. Taking into account only the promised mechanical improvement expected by the carbon nanotubes insertions in polymer nanocomposites, although the CNTs' high strength and stiffness, as well as the high aspect ratio observed, the actual measured enhancements of those properties in nanocomposites are below these expectation [6-8,11,15,16]. The potential of using CNTs as advanced nanofiller has not been realized mainly because of the difficulties in processing [6,15,16]. The nanometric size of carbon nanotubes intensifies their tendency to form agglomerates [6-8,13-15]. Moreover, van der Waals attraction of CNTs and their high aspect ratio make them held together as bundles and ropes, and they show a very low solubility in most solvents, and hence they show a low capability of be easily processed in most polymer matrix [8,15-18]. All the effective utilization of CNTs as novel nano fillers for fabricating nanocomposites strongly depends on the homogenous dispersion of CNTs throughout the matrix and their final morphology [6-8,15-18]. The same dispersion of the filler within the host matrix is important in any nanocomposites but, the peculiar aspect ratio, in which carbon nanotubes presents their self, makes this issues even more significant [2,6,16-18]. CNTs dispersion process still represents a critical topic to really exploit the potential usage of these nanostructure in advanced nanocomposites [6-8,15-18]. Various techniques are reported about different approach

to obtain a good dispersion of nanotubes in polymer matrix, even if those methods couldn't give a complete dispersion of the agglomerates^[6,8,16]. At the same time it is also important to stabilize the dispersion to prevent re-aggregation. CNTs, due to their large surface area and their carbon based outside face, are very well known to form agglomerate during compounding^[17]. The most effective way to resolve these problems, that needs to be coupled with finding a good dispersing method, is surface functionalization^[1,6,8,19]. This modification of the external wall prevents the re-aggregation of nanotubes and also leads to coupling CNTs with different polymer matrices. Coupling with polymer matrix within the composites is very important for an efficient transfer of external stress to the nanotubes^[6,8,20-22]. However surface modification leads to significant improvement in CNTs dispersion and stress transfer, the most used functionalization method developed in different works, caused deterioration of intrinsic properties of CNTs mainly due to tube fragmentation^[23,24]. It become obvious that dispersion and stabilization are not simple issues and compromises have to be made depending on the different applications for which the nanotubes based nanocomposites are required^[6-8,10,11]. The success of processing technique is directly related to the performances of nanocomposites^[6].

Even if the getting of the hypothesized properties for nanocomposites containing carbon nanotubes is not yet reached, their excellent range of properties, investigated in the first years after their discovery, has opened up a new age of advanced multifunctional materials^[1,6-11,25-27]. Incorporation of CNTs in polymer matrices provides materials that could be used for many high performance engineering applications such as nanoelectronics, quantum wire interconnects, field emission devices, chemical sensor, biosensor, detector, liquid crystal display, structural materials, fuel cells, and composites with unprecedented mechanical properties^[1,6-11,25-27]. Currently, the most widespread use of CNTs nanocomposites is in electronics^[1,25-29]. These nanocomposites could be used to shield electromagnetic interference and as discharge components. Moreover the microwave-adsorbing capability of carbon nanotubes could be exploited in structural material for heating^[1,25-27]. Thin layer of nanotubes in plastics could be used in transparent conducting composites^[1,25-27,30]. As expected the biggest near term market for CNTs based nanocomposites will be undoubtedly for high value applications that can sustain the added cost of the carbon nanotubes, and so also commercial sector such as electronics and energy^[1,6-11,25-27].

After almost two decades after the discovery of CNTs, and after the starting point of the so called "nanotubes rush", the nanotubes-based nanocomposites field is vital as ever before. The rate of publications and patent applications still continues to increase every year. There are no CNTs-based products currently on the market with mass market appeal, but some are in the making. This is not surprising because typically the time to market from a discovery takes more than a decade to

reach the applications. Nowadays the scientific community is beginning to move beyond the properties that interested in the past years, in which the main topic were focused on CNTs' characteristics, and now are beginning to be concentrated on nano-technological problematical, and in converting from a nano-science issues to a device issues ^[1,25-27].

One of the strength of CNTs' nanocomposites field, that differs from other similar appealing areas, is the wide field of promising applications ^[1,6-11,25-27]. Ranging from molecular electronics, fundamental science, and quantum computing to material science and medicine. All these different interests in the properties of carbon nanotubes, combined with an apparently unlimited potential for applications, have originated an unprecedented interdisciplinary collaborations that spread internationally and in far off disciplines, that finally interact with each other in a very beneficial cooperation ^[1,25-27]. For the moment, one of the most important near term outcomes from nanocomposites based on carbon nanotubes will be the knowledge that is gained about preparing them, for the development of the nanocomposites and future applications to come.

1.1 PROPERTIES OF CARBON NANOTUBES

Carbon nanotube is one of the different form of carbon allotropes, such as diamond, graphite, fullerene, graphene and amorphous carbon [12-14,19,31].

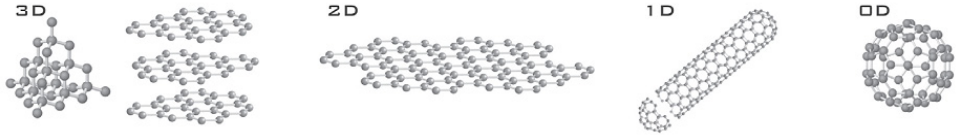


Figure 1 Crystal structure of different allotropes of carbon. Three-dimensional diamond and graphite (3D), two-dimensional graphene (2D), one dimensional nanotubes (1D) and zero dimensional buckyballs (0D) [31].

The one dimensional form is responsible for an aspect ratio values greater than 1000, that increase the scientific attention on this particular carbon allotropic form. The bonding in carbon nanotubes are in sp^2 form, i.e. each atom is joined with three neighbours, as in graphite. This structural bond, stronger than the sp^3 of diamonds, gives to the carbon nanotubes an unique strength. CNTs are long cylinders with covalently bonded carbon atoms, which possess extraordinary electronic and mechanical properties. All the peculiar properties of carbon nanotubes intimately depend on their atomic arrangements, on diameter and length of tubes, and on their morphology [12-14,19,31].

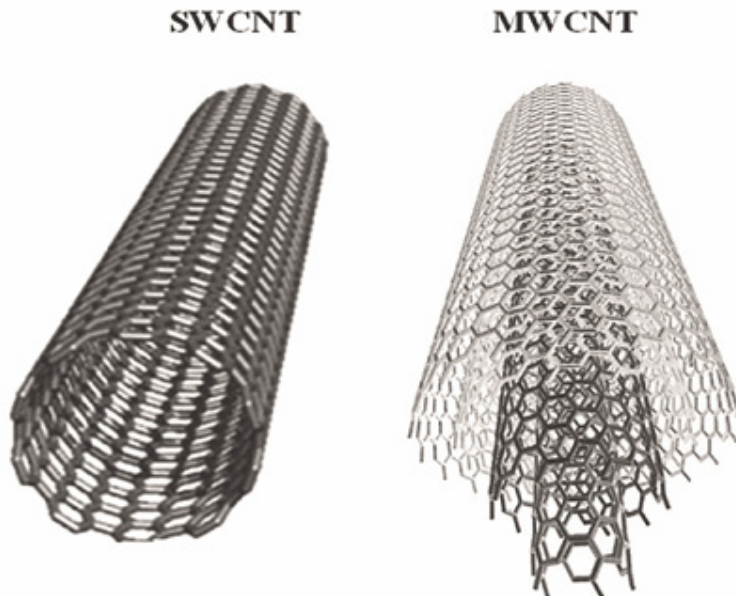


Figure 2 - Schematic diagrams of single wall carbon nanotubes (SWCNT) and multi walled carbon nanotubes (MWCNT).

There are mainly two type of carbon nanotubes [12]. Single wall nanotubes (SWCNTs) consist of a single sheet of graphene rolled seamlessly to form a cylinder with diameter of the order of 1 nm and a length of up to centimeters. Multi walled Carbon Nanotubes (MWCNTs) consist instead in an array of coaxial cylinder, separated by around 0,35 nm, similar to the basal plane separation in graphite. MWCNTs could have diameters from 2 to 100 nm and lengths of tens of microns, with most end capped with half of a fullerene molecules. They were first discovered by Endo in 1978, but the real interest in CNTs, that give the start to the “Nanotubes Rush”, was in 1991 when Iijima first reported it [6,8,10,12].

It is clear that CNTs have many advantages over other materials in terms of mechanical, electrical and thermal properties, although there is no consensus on the exact properties of CNTs [12-14,19,31-33]. The stiffness of CNTs was first determined by observing the amplitude of thermal vibration in transmission electron microscopy (TEM) and the theoretical average stiffness values were reported as 1,8 TPa for SWCNTs and 1,25 TPa for MWCNTs [13,14,32,33]. An *in situ* tensile test were carried out using a stressing stage operating inside a scanning electron microscopy. Experimental values showed that the strength of outer shell of MWCNT ranged from 11 to 63 GPa at fracture strains, and the modulus experimented were from 270 to 950 GPa [14,33]. It was observed that strength of nanotubes depends strongly on the number of defects presents, as well as interlayer interactions in MWCNTs, and so a great difference in properties is generated by the different method of preparations [1,7,21,27].

Electronics properties of CNTs strongly depend on helicity and wrapping morphology of the nanotubes, and these influence their metallic or semiconducting behavior [34-36]. Conductivity of SWCNTs is close to the in-plane conductivity of graphite, i.e. 10^6 S/m [34,35]. MWCNTs conductivities have been reported around 10^7 to 10^8 S/m depending on the helicities of the outermost shells or the presence of defects [34,35]. Axial thermal conductivity of SWCNTs is reported to be as high as 3300 W/mK [37]. All those experimented properties make the carbon nanotubes an unmatched material with the highest values in wide range of properties [1,25-27]. Those unprecedented properties were the starting blocks that pushed out the nanotube rush [1,6-8,25-27].

CNTs are usually prepared using three different methods: arc discharge, laser ablation and chemical vapor deposition (CVD) [1,25-27]. The most widely used synthesis technique is CVD, that permit a more control over the length and the structure of the produced nanotubes, compared to the other methods [38]. Even if during synthesis processes, impurities, in the form of catalyst particles, amorphous carbon and non-tubular fullerenes, are produced, CVD tends to a more pure nanotubes that could reduce the subsequent purification steps, often required to separate the tubes [38]. Moreover, CVD method could be scaled up to produce industrial quantity of CNTs, and so a reduction of the high production costs, that

nowadays limit the industrial access on those materials, could be achieved [1,25-27,38].

1.2 FUNCTIONALIZATION OF CARBON NANOTUBES

The full potentiality of CNTs when inserted in polymer matrix, has been severely limited due to poor interfacial interaction and difficulty in homogenous dispersion [6-8,10,11]. The nature of dispersion problem for CNTs is rather different from any other conventional fillers, such as spherical particles and carbon fibers [1,25-27]. This is due to the peculiarity of the small diameter, in nanometer scale, with high aspect ratio and so large surface area [6-8,10,11]. Moreover the CNTs are synthesized and supplied in the form of heavily entangled bundles, resulting in rather difficulties in dispersions. To resolve all these problems, some methods to modify surface properties of CNTs were developed [1,6,19,23,24,27]. A simple division of those approaches can be into chemical (covalent) and physical (noncovalent) functionalization. These functionalizations permit a better dispersion and interaction with different polymer matrices, that lead to an enhancement of the obtained properties of the nanocomposites [1,6-8,27].

The end caps of nanotubes tend to be composed by highly curved fullerene-like hemispheres, which show an elevated reactivity compared with the side walls [19]. Moreover, the side walls contain a lot of different defects such as, pentagon-heptagon pairs, sp^3 hybridized atoms and vacancies [19].

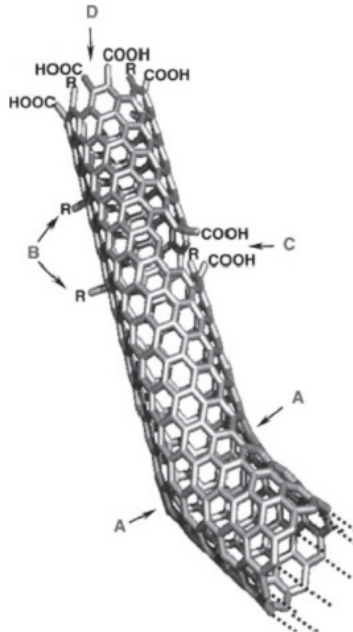


Figure 3 - Typical defect in SWCNT. A) five or seven membered rings in the carbon frameworks, leads to a bend in the tube, B) sp^3 hybridized defects, C) carbon framework damaged by oxidative conditions, which leaves a hole line with $-COOH$ groups, D) open end of SWCNT terminated with $COOH$ groups [19].

Covalent functionalization of CNTs can be achieved by the introduction of some functional groups on defects sites of carbon nanotubes by oxidative agents, like strong acid, which leave holes functionalized with different functional groups [23,24]. In particular, treatments of CNTs with strong acid such as H_2SO_4 and HNO_3 , tend to open the treated tubes, and create functional groups like carboxylic acid, alcohol and ester groups [23,24,39-43]. These functional groups could be used as precursor for further chemical reaction, such as silanation, thiolation and further amination [44-46]. Those functionalized carbon nanotubes show great stability in water and various organic solvents due to the presence of many functional groups such as polar or non-polar groups. Moreover, functionalized carbon nanotubes show significant improvement in interfacial bonding between CNTs and polymer matrices, driving to a stronger nanotube-polymer interaction that could lead to enhanced nanocomposites mechanical properties [6-8,15,23,24,40-46].

However this covalent functionalization method show some drawbacks. A large number of defects are inevitably created by the oxidative process on the CNTs sidewalls and, in some cases, could lead to a fragmentation of carbon nanotubes structure [39-43]. These damaging effects result in severe degradation in mechanical properties showed by CNTs, as well as the modification of the peculiar π electron systems in nanotubes, that extensively reduce the electrical and thermal properties [6-8,15,34-36,40-43,46]. As the break up into smaller pieces is increased, the high aspect ratio values showed by pristine carbon nanotubes falls down [40-43,46]. This further decrease the possible interactions between carbon nanotubes and polymer matrix, reducing the possible enhancement of nanocomposites properties [6-8,15,34-36,40-43,46].

The non-covalent functionalization is an alternative method to exploit the interfacial properties of carbon nanotubes with the preservation of the intrinsic properties of nanotubes [1,47-50]. Usually CNTs are functionalized by aromatic compounds and surfactants that could wrap around the nanotubes structure, and lead to individualization of nanotubes in aqueous or in organic solvent [49,50]. Even if this method is quite efficient in increasing the solubility of carbon nanotubes in common solvent, its exploitation is rather rare due to the difficulties in removing the wrapped structure in nanocomposites preparation [1,48].

Another different method of functionalization involve a plasma treatments in which the surface of carbon nanotubes firstly were covalently attached with fluorine and then exposed to polymerization initiator [51-54]. Plasma treatments represents a novel covalent approach, easy to scale up to industrial applications, with less drawbacks than standard covalent functionalization [5,51-54].

1.3 DISPERSION OF CARBON NANOTUBES

Carbon nanotubes based polymer nanocomposites are the biggest application area for CNTs and their extraordinary properties [1,25-27]. These nanocomposites are expected to be exploited in short term in a wide different fields including transportation, automotive, aerospace, sporting goods, energy and infrastructure sectors [1,25-27]. Such wide range applications are due to their high strength, light weight and processes flexibility. However, the effective utilization of CNTs for fabricating nanocomposites strongly depends on the homogenous dispersion of carbon nanotubes throughout the matrix without destroying their integrity [1,6-11,15,17,18,20-22,46,52].

It's very important to achieve high degree of CNTs dispersion during processing without affecting their properties [1,6-11]. As seen in discussing functionalization, carbon nanotubes have strong tendency to form aggregates due to their large surface area. These aggregates persist unless high shear forces are applied. When such strong mixing procedures are applied, damages on nanotubes' structure are observed, compromising their properties [1,6-11,25-27]. The biggest challenge in literature is to disperse individual nanotubes in the polymer matrices, and so to realize full potentiality of CNTs [6-8]. Surface modification of CNTs, as seen before, helps in dispersion, but long term stability is still a real challenge [1,6-8,25-27,55,56]. Several approaches have been successfully adopted to obtain a good mixing of nanotubes with polymer matrices, including dry powder mixing, solution blending, melt blending and surfactant assisted mixing [1,25-27].

The most common method for preparing carbon nanotubes based nanocomposites involves a mixing in suitable solvent [6-11]. The benefit of this systems comes mainly by the solvent that could facilitate the nanotubes to remain in a de-aggregated form, and so could help the effectiveness of dispersion [6-11]. Both organic and aqueous solutions were usually used to produce nanocomposites [1,6-11,15,17,25-27]. The dispersion is achieved by the use of a magnetic stirring, a mild shear mixing or commonly by ultrasonication. Ultrasonication can be provided by two forms, a gentle one with a sonicator bath or high-power sonication that involves sonicator tips. The use of high-power ultrasonication for a long period can shorten the nanotubes length and so a decrease of the nanocomposite properties could be observed [1,6-11,25-27]. In solvent blending, a good evaporation is mandatory to prevent the CNT aggregation. Usually a slow solvent evaporation could lead to elevated numbers of CNTs' bundles [1,25-27]. Different techniques are usually exploited in order to overcome all these problems, involving for example spin casting and drop casting [1,25-27]. Solution processing is the most used dispersion technique at lab scale for the suitable optimization and the good dispersion quality that could be obtained with "easy" operations [6-11].

While solution processing is a valuable technique for both nanotubes dispersion

and nanocomposites formation, it isn't suitable for industrial scale processes. Melt processing is a preferred choice for its low cost and simplicity to facilitate large scale production. All the melt blending knowledge applied on other composites are then transfer in carbon nanotubes based nanocomposites' preparation ^[1-5,25-27]. Some critical issues are opened considering the high shear force and the high temperature involved in this process, as high shear force could lead to carbon nanotubes fragmentations ^[1]. Optimization of shear rate and temperature is required to obtain a high dispersed nanocomposites without a deterioration of the nanotubes properties ^[1,6-8].

In recent year an *in situ* polymerization has been explored for the preparation of nanocomposites in which the nanotubes are grafted with polymer matrices ^[1,57]. This is a very convenient processing technique, which allows the preparation of nanocomposites with high nanotubes loading. More details studies on this technique are expected to come in near future ^[1, 25-27].

Besides all the published works related to different dispersion methods, most of these processes are limited in capacity and not powerful enough to separate the nanotubes agglomerates and to exploit properly all the wished enhancement in properties with the insertion of carbon nanotubes ^[6-8]. Moreover all different studies depends strongly on all the different variables associated with specific carbon nanotubes used, that makes difficult to compare all the results obtained ^[1,6-8]. Dispersion methods in fact need to consider the difference in length, diameter, average aspect ratio values of carbon nanotubes. Moreover every approach to create an homogenous dispersion needs to take into account the different functionalities present on the external surface and the concentration of those functionalities. It is generally observed that a particular processing method which is good for one property may not be good for another ^[6-8]. One such example is the surface modification of CNT. Functionalization as observed before, could give a better dispersion of carbon nanotubes in common solvent and, when supported, with for example, solution processing, could give a good dispersion in different polymer matrices. Those combination of good dispersion and surface modification generally enhance the mechanical properties of nanocomposites but, at the same time, the modification of the external wall deteriorates the electronic properties of the carbon nanotubes, and this could give a lower than expected conductivity of the nanocomposites itself. Unfortunately measuring the quality of dispersion in nanocomposites is not trivial. Most of the studies exploit microscopic methods to visualize the dispersion, even if these methods only provide a very local observation ^[1,25-27]. It was easily observed that a dispersion method needs to be optimized specifically on the different requirements that the nanocomposites have to fulfill in a specific application ^[6-8].

1.4 MECHANICAL AND ELECTRICAL PROPERTIES OF NANOCOMPOSITES BASED ON CARBON NANOTUBES

The excellent mechanical properties of CNTs suggest that incorporation of very small amount of CNTs into a polymer matrix can lead to structural materials with significantly high modulus and high strength [1,6-8,14,25-28]. Significant advancement has been made in improving the mechanical properties on different polymer matrices, mixing small fraction of CNTs [6-8]. The variation of many different CNTs' parameters and processing strategies has given some very good results, discussed in some excellent reviews, in fabricating relatively strong CNT-polymer composites [6-10]. Some outstanding reinforcement were obtained with insertion of superthorough composites fiber, and an average of more than 50% increase for the composite Young's modulus were observed in different polymer matrices with the insertion of small CNTs content [6,9]. As expected functionalized carbon nanotubes induced a greater enhancements in mechanical properties of the nanocomposites [6-10]. *In situ* polymerization shows some advantage over other nanocomposites processing methods with an average increase of Young's modulus of more than 80% [6]. Low reinforcement were instead observed when melt process were applied on bulk polymer matrix [6]. Moreover alignment of carbon nanotubes could produce some better reinforcement than random spread distribution [6].

In spite of the aggressive work that has been dedicated to this topic, experimental results are still not convergent and continuous research is needed [1,6-10,25-27]. However, the rapid growth of this field suggests that the solution to these problems are not very far.

Beside the mechanical improvements that could be obtained with carbon nanotubes insertion, a great interest in imparting conductivity in highly insulating material by fabricating conductive polymer nanocomposites is present [1,6-11,25,27-29,34,36,58-60]. The enhancement in electrical conductivity of insulating polymer by several order of magnitude has been achieved with very small loading of nanotubes in different polymer matrices [6,10,11,28,29,36,58-60]. This low CNTs' concentration helped in preserving all other performances showed by the polymers such as optical clarity, mechanical properties and low flow viscosities.

The electrical conductivity in nanocomposites increased with increasing CNTs concentrations till a critical loading, where a dramatic increase in conductivity values is observed [6,28,36,59]. This critical filler concentration is called electrical percolation threshold concentration. It was observed that, at percolation concentration, nanotubes fillers form a three-dimensional conductive network within the matrix, hence electron can tunnel from one filler to another, overcoming the high resistance of the insulating polymer matrix [1,6,28,36,59].

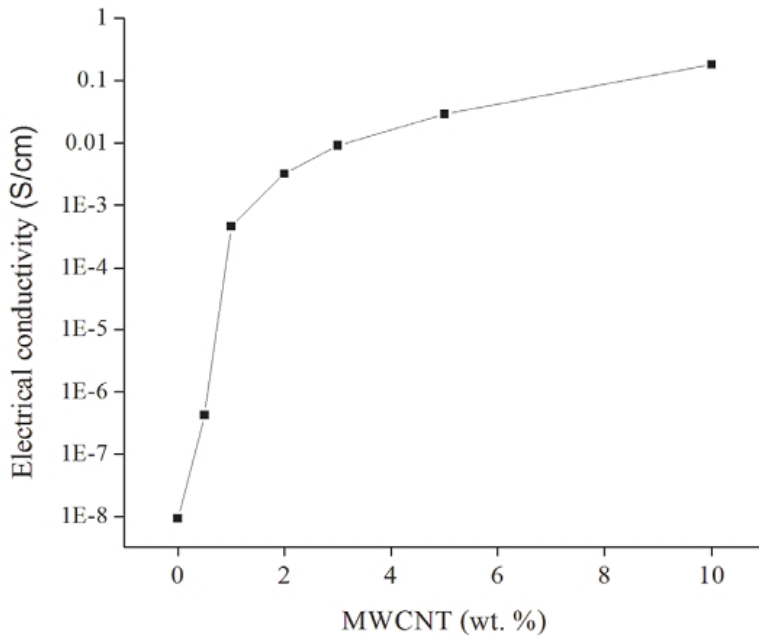


Figure 4 - Plot of dc electrical conductivity (σ) vs weight fraction of MWCNT in PTT/MWCNT composites^[1].

As observed in any other carbon nanotubes' induced properties, electrical conductivity of CNT-based nanocomposites and percolation concentration depend on aspect ratio of CNTs, intrinsic conductivity of carbon nanotubes, agglomeration structure in polymer matrix, degree of alignment and chemical functionalization of used CNTs ^[6,28,36,58-60]. As already observed, covalent functionalization with the benefits of inducing an easily dispersion and good load transfer, could disrupt the extended π conjugation of nanotubes and thereby reduce the electrical conductivity of the isolated nanotubes. Nevertheless, significant improvement in electrical conductivity of carbon nanotubes based nanocomposites lead to the development of novel materials for electronics, automotive and aerospace applications with use as electrostatic dissipation and conductive coatings. As observed the potential applications of those conductive nanocomposites makes electronics as the most near-terms application for those materials ^[1,6,25-27].

1.5 EPOXY BASED NANOCOMPOSITES

All the expected performances of carbon nanotubes based nanocomposites has not yet realized mainly because of difficulties in an homogenous dispersion, in a limitation of load transfer and in problems with an effective functionalization without modification of electronic behavior ^[6-8,10,11,15,16,28,46,49,59]. All those issues are open, often in conflict with each other and related to the processing of carbon nanotubes to create the wished nanocomposites. This is nowadays the main topic of interest to advance in CNTs based nanocomposites research ^[6,10,16,59].

Great attention were focused on CNTs based epoxy nanocomposites for their high technological interest ^[28,46,52,53,55,56,62-70]. Epoxy surface coatings are among the most widely used industrial finishes, providing superior adhesion, flexibility and corrosion resistance when applied to metallic substrates, and they could, when cured with various curing agents, create products with an almost unlimited range and variety of performance properties ^[61]. Some limitations of epoxy resin, such as the well know insulating behavior and their limited fracture toughness, could be overcome with the insertion of carbon nanotubes that could intensely widespread the possible performances of those nanocomposites ^[28,46,52,53,55,56,61-70]. Moreover those nanocomposites could be easily processed in lab scale ^[61]. This gives the possibility to focus the attention on all the different steps that carbon nanotubes took before nanocomposites reach the specific application, starting from synthesis to functionalization, and then to processing ^[62-69].

In spite of large amount of different works dedicated to these CNTs based epoxy nanocomposites, it is widely recognized that the experimental results are still not convergent and often some contradictory results are observed, leading to the need of continuous research for the development of the nanocomposites of the future ^[1, 6-11, 25-27,62].

Solution processing clearly produce good dispersion results, and in particular when ultrasonication is assisted ^[62]. All the results are aggressively dependent on the different morphological characteristics of the carbon nanotubes inserted, and a better dispersion, that produce an good enhancement of mechanical properties, coupled with a low percolation concentration for electrical conductivity, is observed when functionalized carbon nanotubes are blended, especially CNTs with higher functionalities concentrations ^[6]. All the parameters of the different dispersion methods need to be balanced to further clear the observed contradictory results. In most of the studies, microscopic techniques, in particular scanning electron microscopy, are used to describe the quality of the dispersion, even if those characterizations could give only local view of the microstructure, hence possible heterogeneities may go undetected ^[62-69].

On those particular epoxy nanocomposites it could be possible to perform extensive rheological studies providing a foundation for further studies of the dispersion

of carbon nanotubes and for effectiveness and effects of different functionalized carbon nanotubes on epoxy-nanocomposites behavior ^[71-74]. Rheology is confirmed to be a very powerful method to assess the quality of the dispersion, and hence it could suggest hints for a better processing of those materials ^[72-75]. Moreover rheology is very sensitive to changes in microstructure, integrated over all length scales ^[72-75]. Other characterizations that are inherently related to dispersion, such as electric conductivity, could further give suggestions for the comprehension of the microstructure morphology obtained and different functionalizations effectiveness. ^[69,70,74]

The employment of characterizations like rheology or electric conductivity, could give some useful information on the efficiency of the insertion of carbon nanotubes and, it could suggest the beneficial enhancement induced by carbon nanotubes for a specific application into which the epoxy-nanocomposites are supposed to be exploited. Combined rheological and conductivity measurements proved new experimental information for better understanding the microstructure that dispersed CNTs could create inside epoxy matrices ^[69-75]. Moreover those characterizations permit to comprehend how the differences in carbon nanotubes characteristics work to modify the CNTs' microstructure inside the polymer matrix, and also how this microstructure influences the enhancement of mechanical and electrical properties ^[69-75]. This methodological approach could be further extended to other polymer matrix as well ^[74,75]. More works are however needed to further comprehend all the mechanism that influence the creation of the microstructure and so the nanocomposites behavior.

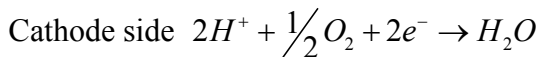
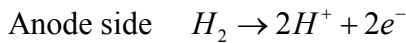
With the well known induced structural reinforcement and electrical conductivity, epoxy-nanocomposites based on carbon nanotubes can serve as a platform for sensing ^[1]. A particular and very promising application of the CNTs' induced conductivity on epoxy nanocomposites is the possibility to exploit the nanocomposites itself as a sensor for detecting nature and evolution of damage ^[76-79]. Carbon nanotubes efficiently dispersed in epoxy matrix, forming a conductive percolation network throughout the polymer matrix, could act as non invasive way to monitor damage ^[78]. Only few recent preliminary works are related to this very promising exploitation and, some better focusing on this non invasive technique are needed to better correlated the networked nanostructure formed by carbon nanotubes, to comprehend the effectiveness of damage sensor behavior.

1.6 NANOCOMPOSITES BASED ON CARBON NANOTUBES FOR POLYMER ELECTROLYTE MEMBRANE FUEL CELL APPLICATION

Carbon nanotubes with their unique combination of outstanding properties, such as high electrical and thermal conductivity, high mechanical strength and high surface area, are exploited, as observed before, in very wide applications. One of the most auspicious field in which are integrated is to enhance the performance of fuel cells ^[1, 25-27].

Fuel Cell (FC) is an electrochemical device which converts chemical energy of fuel directly into electrical energy ^[80]. FC could generate electricity in a single step without any moving parts and could operate without pollutant emission. Moreover, they are also run quietly and could be built in variety of size, making them attractive also for portable power devices.

There are many types of FCs, depending on the different electrolyte used. Among all the different types, Polymer Electrolyte Membranes (PEM) FCs are considered as the most promising candidate for automotive applications, for small scale stationary power generation and for portable power applications ^[80]. As an electrochemical energy converter, PEMFC converts energy of fuel (hydrogen) into electrical energy with a simple reaction: at the anode side the oxidation of hydrogen, and the reduction of oxygen at the cathode side.



Equation 1 - Fuel Cell electrochemical reactions.

The heart of PEM fuel cell is the proton conductive membrane that works as the electrolyte. Membrane realizes the proton transportation from anode to cathode side and, at the same time, it prevent gases to crossover. Moreover membrane needs to be electrical insulating. These peculiar requirements, necessary for a good electrochemical reaction, are usually fulfilled with a fluorinated copolymer with ionic tail. Nafion is the most common membrane used ^[80].

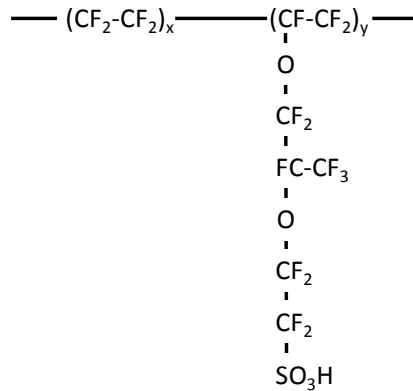


Figure 5 - Structure of perfluorocarbon-sulfonic acid ionomer (PFSA) polymer (Nafion).

Nafion efficiently transfers proton only when sufficiently hydrated, and this is the reason for the presence of sulfonic acid at the end of the side chain. Problems occurs at temperature higher than 80 °C, in which usually the membrane tends to de-hydrate, reducing its proton conductance and no further electrical insulating behavior is observed ^[80]. This dramatically reduces the performance of the fuel cell.

Around the electrolyte, the electrodes are placed. Electrodes are the place where the electrochemical reaction is conducted. There are three species that participate in the electrochemical reactions: gases, electrons and protons. Usually a Catalyst Layer (CL), that consist of a catalyst supported by conductive material, is used ^[80]. The most used CL is made of a carbon support and platinum as catalyst. Hydrogen oxidation takes place on the catalytic particles that are connected with the membrane ionomer, and so could be put in contact with protons. At the other side, the electrical conductive carbon supports the catalyst and it conducts electrons from outside the cell to the catalyst. Moreover CL needs to be porous in order to facilitate the gas distribution till the catalytic site.

One of the main problematic issues in fuel cell is the water management ^[81,82]. Excess water produced at the cathode side could results in flooding of the electrode and so in hindering the transport of gases, reducing the performance. At the same time, some hydration of the membrane is necessary. These conflicting issues are better handle with the insertion of a Gas Diffusion Layer (GDL) and a Microporous Layer (MPL) between the membrane electrode assembly (MEA) and the graphite plate that connect the cell with the load ^[80-82]. Different requirements are requested by GDL and MPL to increase the performances of the fuel cell. They need to be porous and electrically conductive. In order to prevent water flooding, particularly when fuel cell operates at high current density, a strong hydrophobic behavior is required. GDL is usually made of conductive carbon cloth or carbon paper ^[80-82]. An

hydrophobic treatment, usually made with polytetrafluoroethylene, is required to modify the surface of the conductive GDL. Gas diffusion layer usually shows macro-porous morphology, and helps to uniformly transport the gases. Moreover, the microporosity presented in GDL's structure helps to remove the produced water. MPL shows reduced pore and helps to nebulizer the water formed at cathode side ^[80]. Beneficial effects on produced water removal are well recognized when microporous layer is used ^[81-83]. MPL is usually made of carbon black and a hydrophobic binder. MPL provides a proper pore sized and hydrophobic behavior to allow a better water removal from the catalyst layer and gas transport to reaction sites. Moreover, Microporous Layer minimizes the electric contact resistance with the adjacent catalyst layer, and it enhance the mechanical compatibility between the GDL and CL.

All the components here described are summarized in Figure 6 that sketches the design of standard PEM fuel cell.

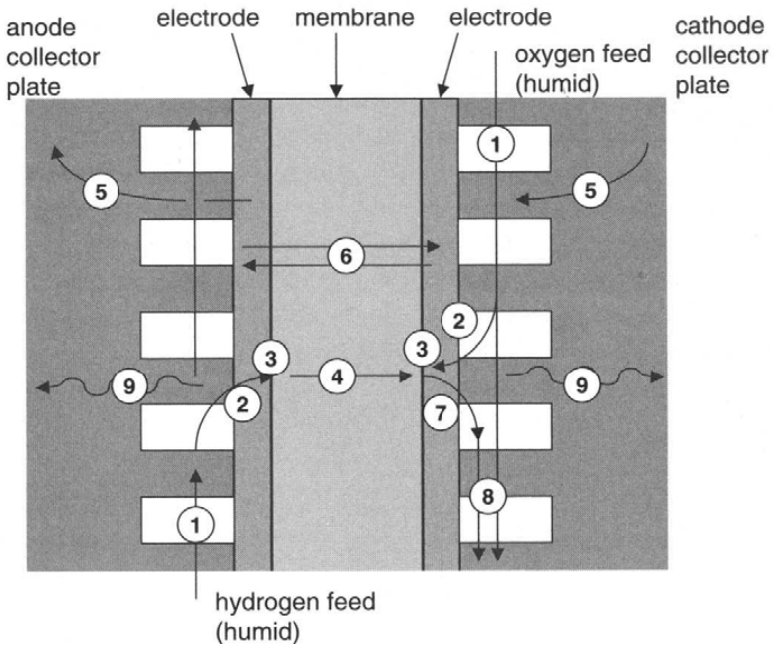


Figure 6 - PEM fuel cell components and processes. 1) gas flow through the channels of collector plate, 2) gas diffusion through porous media (GDL and MPL), 3) electrochemical reaction, 4) proton conduction through membrane, 5) electron conduction through conductive cell components, 6) water transport through polymer membrane, 7) water transport through porous catalyst layer and gas diffusion layer, 8) unused gas flow, 9) heat transfer.

PEM fuel cell, as observed, is a complex system, in which different components need to be optimized to increase the performance of the whole cell. Moreover any component requires different optimized conditions that are often conflicting with

each other, in order to enhance the fuel cell electric production. The improvement of the actual PEM fuel cell performances is a very challenging issue to open for industrial production these pollutant free devices ^[80-83].

Carbon nanotubes with the well known high electric conductivity, great chemical stability and peculiar high surface area, are nowadays exploited in different components of the PEMFCs to develop a novel high performances fuel cell ^[84-86].

With the unprecedented properties already discussed, CNTs are efficiently used in different components of PEMFCs. Carbon nanotubes are exploited as filler to a Nafion based nanocomposites, as a novel polymer electrolyte membrane with an improved mechanical stability ^[86]. The high aspect ratio showed by carbon nanotubes make them useful as catalytic layer with an increased performance than platinum. Moreover the excellent electronic conductivity and the good chemical stability make them ideal for supporting different catalytic system ^[84,87].

Among the many parameters that affect fuel cells' behavior, GDL plays an important role in the ultimate performance of the fuel cell ^[80,83]. The hydrophobization treatment of carbon cloth, required to deny the water flooding and the hindering of the reactant gases, is known to decrease the electric conductivity of GDL ^[80,83].

Carbon nanotubes based fluorinated nanocomposites could be the ideal candidate to replace the common polytetrafluoroethylene's coating of the gas diffusion layer. Carbon nanotubes insertion in a fluorinated polymer matrix is expected to increase the conductivity of treated gas diffusion layer, to minimize the electric contact resistance with the adjacent layers and to enhance the mechanical compatibility between the GDL and the catalyst layer. To the best of author's knowledge, carbon nanotubes based fluorinated nanocomposites have not been used for application as hydrophobic agent on GDL, even if their promising behavior for an enhancement of PEM fuel cells could be well hypothesized. An extensive optimization of the fluorinated nanocomposites' characteristics is needed to improve the properties required in the GDL coating, and so, to compete in increasing the performances of the polymer electrolyte membrane fuel cells.

1.7 REFERENCES

1. S. Yellampalli, *Carbon Nanotubes - Polymer Nanocomposites*, InTech (2011).
2. F. Hussain, M. Hojjati, M. Okamoto, R. Gorga, Polymer-matrix Nanocomposites, Processing, Manufacturing, and Application: An Overview, *Journal of Composite Materials*, 40 (17), 1511-1575 (2006).
3. P. Ajayan, L. Schadler, P. Braun, *Nanocomposite science and technology*, Wiley (2003).
4. Y. Mai, Z. Yu, *Polymer Nanocomposites*, CRC press (2006).
5. D. Paul, L. Robeson, Polymer nanotechnology: Nanocomposites, *Polymer*, 48, 3187-3204 (2008).
6. Z. Spitalsky, D. Tasis, K. Papagelis, C. Galiotis, Carbon nanotube-polymer composites: Chemistry, processing, mechanical and electrical properties, *Progress in Polymer Science*, 35, 357-401 (2010).
7. J. Coleman, U. Khan, W. Blau, Y. Gunko, Small but strong: A review of the mechanical properties of carbon nanotube-polymer composites, *Carbon*, 44, 1624-1652 (2006).
8. J. Coleman, U. Khan, Y. Gun'ko, Mechanical reinforcement of polymers using carbon nanotubes, *Advanced Material*, 18, 689-706 (2006).
9. J. Potts, D. Dreyer, C. Bielawski, R. Ruoff, Graphene-based polymer nanocomposites, *Polymer*, 52, 5-25 (2011).
10. H. Qian, E. Greenhalgh, M. Shaffer, A. Bismarck, Carbon nanotube-based hierarchical composites: a review, *Journal of Materials Chemistry*, 20, 4751-4762 (2010).
11. S. Bal, S. Samal, Carbon nanotube reinforced polymer composites-A state of the art, *Bulletin of Materials Science*, 30 (4), 379-386 (2007).
12. S. Iijima, Helical microtubules of graphitic carbon, *Nature*, 354, 56-58 (1991).
13. D. Qian, G. Wagner, W. Liu, M. Yu, Mechanics of carbon nanotubes, *Applied Mechanics Reviews*, 55, 495-533 (2002).
14. S. Xie, W. Li, Z. Pan, B. Chang, L. Sun, Mechanical and physical properties on carbon nanotube, *Journal of Physics and Chemistry of Solids*, 61 (7), 1153-1158 (2000).
15. X. Xie, Y. Mai X. Zhou, Dispersion and alignment of carbon nanotubes in polymer matrix: A review, *Materials Science and Engineering, Report*, 49, 89-112 (2005).

16. W. Wang, N. Murthy, Characterization of Nanotube-Reinforced Polymer Composites, in S. Yellampalli, *Carbon Nanotubes - Polymer Nanocomposites*, InTech (2011).
17. N. Grossiord, J. Loos, C. Koning, Strategies for dispersing carbon nanotubes in highly viscous polymers, *Journal of Materials Chemistry*, 15, 2349-2352 (2005).
18. L. Jin C. Bower, O. Zhoua, Alignment of carbon nanotubes in a polymer matrix by mechanical stretching, *Applied Physics Letters*, 73, 1197-1202 (1998).
19. A. Hirsch, Functionalization of single-walled carbon nanotubes, *Angewandte Chemie International Edition*, 41, 1853-1859 (2002).
20. M. Bryning, D. Milkie, M. Islam, K. Kikkawa, A. Yodh, Thermal conductivity and interfacial resistance in single-wall carbon nanotube epoxy composites. *Applied Physics Letters*, 87 (16), 161909 (2005).
21. L. Schadler, S. Giannaris, P. Ajayan, Load transfer in carbon nano tube epoxy composites, *Applied Physics Letters*, 73, 3842-2844 (1998).
22. G. Hwang, Y. Shieh, K. Hwang, Efficient load transfer to polymer-grafted multiwalled carbon nanotubes in polymer composites, *Advanced Functional Materials*, 14, 487-491 (2004).
23. J. Chen, M. Hamon, H. Hu, T. Chen, A. Rao, P. Eklund, R. Haddon, Solution properties of single-walled carbon nanotubes, *Science*, 282, 95-98 (1998).
24. C. Bower, A. Kleinhammes, Y. Wu, O. Zhou, Intercalation and partial exfoliation of single-walled carbon nanotubes by nitric acid, *Chemical Physics Letters*, 288, 481-486 (1998).
25. S. Bianco, *Carbon nanotubes from research to applications*, InTech (2011).
26. M. Meyyappan, *Carbon nanotubes science and applications*, Crc press (2005).
27. A. Jorio, G. Dresselhaus, M. Dresselhaus, *Carbon nanotubes Advanced topics in the synthesis, structure, properties and applications*, Springer (2008).
28. A. Sulong, N. Muhamad, R. Ramli, B Deros, J. Park, Electrical conductivity behavior of chemical functionalized MWCNTs epoxy composites, *European Journal of Scientific Research*, 29, 13-21 (2009).
29. S. Kim, S. Jang, S. Byum, J. Lee, J Yoo, S. Jeong, Electrical properties and EMI shielding characteristics of polypyrrole-nylon 6 composite fabrics, *Journal of Applied Polymer Science*, 87, 1969-1974 (2003).
30. M. Zhang, S. Fang, A. Zakhidov, S. Lee, A. Aliev, C. Qilliams, Strong,

- transparent, multifunctional, carbon nanotubes sheets, *Science*, 309, 1215-1219 (2005).
31. M. Katsnelson, Graphene: carbon in two dimensions, *Materials Today*, 10, 20-27 (2007).
 32. M. Yu, B. Files, S. Arepalli, R. Ruoff, Tensile loading of ropes of single wall carbon nanotubes and their mechanical properties, *Physical Review Letters*, 84, 5552-5555 (2000).
 33. M Yu, O. Lourie, M. Dyer, K Moloni, T. Kelly, R. Ruoff, Strength and breaking mechanism of multiwalled carbon nanotubes under tensile load, *Science*, 287, 637-640 (2000).
 34. T. Ebbesen, H. Lezec, H. Hiura, J. Bennet, H Ghaemi, T. Thio, Electrical conductivity of individual carbon nanotubes, *Nature*, 382, 54-56 (1996).
 35. J. Charlier, J. Issi, Electrical conductivity of novel forms of carbon , *Journal of Physics and Chemistry of Solids*, 57, 957-965 (1996).
 36. F. Du, J. Fisher, K. Winey, Effect of nanotube alignment on percolation conductivity in carbon nanotube/polymer composites, *Physical Review B, Condensed Matter and Materials Physics*, 72, 121401-121404 (2005).
 37. P. Kim, L. Shi, A. Majumdar, P. McEuen, Thermal transport measurements of individual multiwalled nanotubes, *Physical Review Letters*, 87, 215501-215504 (2004).
 38. C. See, A. Harris, A review of carbon nanotube synthesis via fluidized-bed chemical vapor deposition, *Industrial & Engineering Chemical Research*, 46, 997-1012 (2007).
 39. K. Esumi, M. Ishigami, A. Nakajima, K. Sawada, H. Honda, Chemical treatment of carbon nanotubes, *Carbon*, 34, 279-281 (1996).
 40. M. Marshall, S. Popanita, J. Shapter, Measurement of functionalized carbon nanotube carboxylic acid groups using a simple chemical process, *Carbon*, 44, 1137-1141 (2006).
 41. V. Datsyuk, M. Kalyva, K. Papagelis, J. Parthenios, D. Tasis, A. Siokou, I. Kallitsis, C. Galiotis, Chemical oxidation of multiwalled carbon nanotubes, *Carbon*, 46, 833-840 (2008).
 42. Y. Shieh, G. Liu, H. Wu, C. Lee, Effects of polarity and pH on the solubility of acid-treated carbon nanotubes in different media, *Carbon*, 45, 1880-1890 (2007).
 43. A. Osorio, I. Silveira, V. Bueno, C. Bergmann, $H_2SO_4/HNO_3/HCl$ - Functionalization and its effect on dispersion of carbon nanotubes in aqueous

- media, *Applied Surface Science*, 255, 2458-2489 (2008).
44. J. Liu, A. Rinzler, H. Dai, J. Hafner, R. Bradley, P. Boul, A. Lu, T. Iverson, K. Shelimov, C. Huffman, F. Rodriguez-Macias, Y. Shon, T. Randall Lee, D. Colber, R. Smalley, Fullerene Pipes, *Science*, 280, 1253-1256 (1998).
 45. P. Ma, J. Kim, B. Tang, Functionalization of carbon nanotubes using a silane coupling agent, *Carbon*, 44, 3232-3238 (2006).
 46. J. Wang, Z. Fang, A. Gu, L. Xu, F. Liu, Effect of amino-functionalization of multi-walled carbon nanotubes on the dispersion with epoxy resin matrix, *Journal of Applied Polymer Science*, 100, 97-104 (2006).
 47. Y. Zhao, J. Stoddard, Noncovalent functionalization of single-walled carbon nanotubes, *Accounts of Chemical Research*, 42 (8), 1161-1171 (2009).
 48. X. Gong, J. Liu, S. Baskaran, R. Voise, J. Young, Surfactant-assisted processing of carbon nanotube/polymer composites, *Chemistry of Materials*, 12 (4), 1049-1052 (2000).
 49. J. Yu, N. Grossiord, C. Koning, J. Loos, Controlling the dispersion of multi-wall carbon nanotubes in aqueous surfactant solution, *Carbon*, 45 (3), 618-623 (2007).
 50. S. Bergin, Z. Sun, P. Streich, J. Hamilton, J. Coleman, New solvents for nanotubes: approaching the dispersibility of surfactants, *Journal of Physical Chemistry C*, 114, 231-237 (2010).
 51. L. Valentini, D. Puglia, I. Armentano, J. Kenny, Sidewall functionalization of single-walled carbon nanotubes through CF_4 plasma treatment and subsequent reaction with aliphatic amines, *Chemical Physics Letters*, 403, 385-389 (2005).
 52. L. Valentini, D. Puglia, F. Carniato, E. Boccaleri, L. Marchese, J. Kenny, Use of plasma fluorinated single-walled carbon nanotubes for the preparation of nanocomposites with epoxy matrix, *Composites Science and Technology*, 68, 1008-1014 (2008).
 53. C. Tseng, C. Wang, C. Chen, Functionalizing carbon nanotubes by plasma modification for the preparation of covalent-integrated epoxy composites, *Chemistry of Materials*, 19, 308-315 (2007).
 54. G. Kalita, S. Adhikari, H. Aryal, R. Afre, T. Soga, M. Sharon, M. Umeno, Functionalization of multi-walled carbon nanotubes (MWCNTs) with nitrogen plasma for photovoltaic device application, *Current Applied Physics*, 9, 346-351 (2009).
 55. J. Zhu, J. Kim, H. Peng, J. Margrave, V. Khabashesku, E. Barrera, Improving

- the dispersion and integration of single-walled carbon nanotubes in epoxy composites through functionalization, *Nano Letters*, 3, 1107-1113 (2003).
56. J. Zhu, H. Peng, F. Rodriguez-Macias, J Margrave, V. Khabashesku, A. Imam, Reinforcing epoxy polymer composites through covalent integration of functionalized nanotubes, *Advanced Functional Materials*, 14, 643-648 (2004).
 57. C. Wu, Synthesis and characterization of poly(trimethylene terephthalate) composites incorporating multi-walled carbon nanotubes, *Journal of Applied Polymer Science*, 114, 1633-1642 (2009).
 58. J. Bai, A. Alloui, Effect of the length and the aggregate size of MWNTs on the improvement efficiency of the mechanical and electrical properties of composite – experimental investigation, *Composites, Part A*, 34A, 689-694 (2003).
 59. W. Bauhofer, J. Kovacs, A review and analysis of electrical percolation in carbon nanotube polymer composites, *Composites Science and Technology*, 69, 1486-1498 (2009).
 60. U. Sundararaj, M. Al-Saleh, Electromagnetic interference shielding mechanisms of CNT/polymer composites, *Carbon*, 47, 1738-1746 (2009).
 61. C. May, *Epoxy Resin: Chemistry and Technology*, 2nd Edition, CRC Press (1987).
 62. S. Pillai, S. Rai, Epoxy-based Carbon Nanotubes Reinforced Composites, in Boreddy Reddy, *Advances in Nanocomposites - Synthesis, Characterization and Industrial Applications*, InTech (2011).
 63. J. Shen, W. Huang, L. Wu, Y. Hu, M. Ye, The reinforcement role of different amino-functionalized multiwalled carbon nanotubes in epoxy nanocomposites, *Composites science and technology*, 67, 3041-3050 (2007).
 64. M. Abdalla, D. Dean, P. Robinson, E. Nyairo, Cure behavior of epoxy/MWCNT nanocomposites: The effect of nanotube surface modification, *Polymer*, 49, 3310-3317 (2008).
 65. J. Shen, W. Huang, L. Wu, Y. Hu, M. Ye, Study on amino-functionalized multiwalled carbon nanotubes, *Materials Science and Engineering: A*, 464, 151-156 (2007).
 66. P. Guo, H. Song, X. Chen, Interfacial properties and microstructure of multiwalled carbon nanotubes/epoxy composites, *Materials Science and Engineering A*, Vol 517 (1-2), 17-23 (2009).
 67. M. Abdalla, D. Dean, D. Adibempe, E. Nyairo, P. Robinson, G. Thompson, The effect of interfacial chemistry on molecular mobility and morphology

- of multiwalled carbon nanotubes epoxy nanocomposite, *Polymer*, 48, 5662-5670 (2007).
68. Z. Spitalsky, C. Krontiras, S. Georga, C. Galiotis, Effect of oxidation treatment of multiwalled carbon nanotubes on the mechanical and electrical properties of their epoxy composites, *Composites: Part A*, 40, 778-783 (2009).
 69. A. Battisti, A. Skordos, I. Partridge, Percolation threshold of nanotubes filled insature polyesters, *Composites Science and Technology*, 70, 633-637 (2010).
 70. I. Alig, T. Skipa, D. Lellinger, P. Potschke, Destruction and formation of a carbon nanotube network in polymer melts: Rheology and conductivity spectroscopy, *Polymer*, 49, 3524-2532 (2008).
 71. E. Hobbie, Shear rheology of carbon nanotube suspensions, *Rheologica Acta*, 49 (4), 323-334 (2010).
 72. Z. Fan, S. G. Advani, Rheology of multiwall carbon nanotube suspensions, *Journal of Rheology*, 51 (4), 585-604 (2007).
 73. M. J. Kayatin, V. A. Davis, Viscoelasticity and Shear Stability of Single-Walled Carbon Nanotube/Unsaturated Polyester Resin Dispersions, *Macromolecules*, Vol 42 (17), 6624-6632 (2009).
 74. M. Chapartegui, N. Markaide, S. Florez, C. Elizetxea, M. Fernandez, A. Santamaría, Specific rheological and electrical features of carbon nanotube dispersion in an epoxy resin, *Composites science and technology*, 70, 879-884 (2010).
 75. F. Galindo-Rosales, P. Moldenaers, J. Vermant, Assessment of the dispersion quality in polymer nanocomposites by rheological methods, *Macromolecular Materials and Engineering*, 296, 331-340 (2011).
 76. A. Lim, Q. An, T. Chou, E. Thostenson, Mechanical and electrical response of carbon nanotube-based fabric composites to Hopkinson bar loading, *Composites Science and Technology*, Vol 71 (5), 616-621 (2011).
 77. L. Gao, T. Chou, E. Thostenson, Z. Zhang, A comparative study of damage sensing in fiber composites using uniformly and non-uniformly dispersed carbon nanotubes, *Carbon*, Vol 48 (13), 3788-3794 (2010).
 78. E. Thostenson, T. Chou, Carbon Nanotube Networks: Sensing of Distributed Strain and Damage for Life Prediction and Self Healing, *Advanced Materials*, Vol 18 (21), 2837-2841 (2006).
 79. M. Rein, O. Breuer, H. Wagner, Sensors and sensitivity: Carbon nanotube buckypaper films as strain sensing devices, *Composites Science and Technology*, Vol 71 (3), 373-381 (2011).

80. F. Barbir, *"PEM Fuel Cells, Theory and Practice"*, Elsevier, 2005.
81. H. Li, Y. Tang, Z. Wang, Z. Shi, S. Wu, D. Song, J. Zhang, K. Fatih, J. Zhang, H. Wang, Z. Liu, R. Abouatallah, A. Mazza, A review of water flooding issues in the proton exchange membrane fuel cell, *Journal of Power Sources*, 178, 103-117 (2008).
82. L. Cindrella, A. Kannan, J. Lin, K. Saminathan, Y. Ho, C. Lin, J. Wertz, Gas Diffusion layer for proton exchange membrane fuel cells – A review, *Journal of Power Sources*, 194, 146-160 (2009).
83. C. Tseng, S. Lo, Effects of microstructure characteristics of gas diffusion layer and microporous layer on the performance of PEMFC, *Energy Conversion and Management*, 51, 677-684 (2010).
84. H. Gharibi, M. Javaheri, R. Mirzaie, The synergy between multi-wall carbon nanotubes and Vulcan XC72R in microporous layers, *International Journal of Hydrogen Energy*, 35, 9241-9251 (2010).
85. J. Tang, M. Itkis, C. Wang, X. Wang, Y. Yan, R. Haddon, Carbon nanotube free-standing membrane as gas diffusion layer in hydrogen fuel cells, *Micro and Nano Letters*, Volume 1 (1), 62–65 (2006).
86. V. Ijeri, L. Cappelletto, S. Bianco, S. Tortello, P. Spinelli, E. Tresso, Nafion and carbon nanotube nanocomposites for mixed proton and electron conduction, *Journal of Membrane Science*, 363, 265-270 (2010).
87. K. Lee, J. Zhang, H. Wang, D. Wilkinson, Progress in the synthesis of carbon nanotube- and nanofiber-supported Pt electrocatalysts for PEM fuel cell catalysis, *Journal of Applied Electrochemistry*, 36, 507-522 (2006).

>2
AIM OF THE WORK



The unprecedented combination of properties showed by carbon nanotubes have driven them to become the ideal candidate as nanofiller for advanced nanocomposites. CNTs' incorporation into different polymer matrices is expected to exploit their impressive mechanical strength and their high electrical /thermal conductivity, to obtain a nanocomposites with enhanced properties at very low nanofiller concentrations. Since carbon nanotubes discovery, the interest in such materials creates a vast activity in material science and engineering. These advanced nanocomposites have huge application potential in many diverse fields, ranging from structural material, nanoelectronics, chemical sensor, fuel cell, detector, liquid crystal display, ecc. These promised applications in widely different fields has lead the scientific community to create a vast activity on nanocomposites based on carbon nanotubes. Despite the amount of research that are increasing in number every year, a lot of controversial results are still present. The potential of using CNTs as advanced nanofiller has not been realized yet. The main problematical requirements, to effectively reach the promised mechanical and electrical enhancement expected by the carbon nanotubes insertion, are related to the homogenous dispersion of CNTs into the polymer matrices, without destroying their integrity and, to stabilize the dispersion preventing the re-aggregations. Moreover a control on the effective aspect ratio of the inserted carbon nanotubes is mandatory to permit the effective interfacial stress transfer between the matrix and nanofiller.

Different ways were practiced to effectively resolve those problems. The usage of surface functionalization and different dispersion approaches have reached a good compromise solution that create nanocomposites with a great mechanical enhancement and induced conductivity. Besides the results obtained, all the different studies depends strongly on the different characteristics associated with the specific carbon nanotubes used, and this makes difficult to compare all the outcome.

Therefore, to promote the nanocomposites based on carbon nanotubes applications, a better knowledge, on the different microstructures that the carbon nanotubes create inside different polymer matrices, is needed. Moreover, a comprehension of how these microstructures are formed, and how the functionalities, present on the external wall, modify the network of carbon nanotubes, is mandatory to better control the CNTs dispersion in different polymer matrices. The effects of the different dispersed microstructures on properties of nanocomposites must be further investigated to optimize the dispersion formation, in order to obtain a nanocomposites for specific advanced application.

The present research can be divided in three parts. The first is related to the functionalization of multiwalled carbon nanotubes with different functionalities, to clarify the behavior and the effect of those treated carbon nanotubes when inserted in different polymer matrices. The second part is focused on epoxy

based nanocomposites containing different functionalized carbon nanotubes, and in particular on the study of the relationship between the properties and the nanostructure formed by CNTs. The third part concerns perfluoropolyether based nanocomposites containing carboxylic carbon nanotubes and the induced properties modification when nanofillers are inserted, especially in a particular application like the hydrophobization coating of gas diffusion layer in polymer electrolyte membrane fuel cells.

2.1 FUNCTIONALIZATION OF MULTIWALLED CARBON NANOTUBES

Functionalization methods are usually produced by strong acid treatments followed by other different chemical reactions, to modify the functionalities present on the external wall. The functionalized carbon nanotubes show great stability in different solvent, and permit a better interfacial stress transfer with different polymer matrices.

The main objective of this study is focused on different chemical functionalization procedures, to induce carboxylic and amine functionalities on the external wall of multiwalled carbon nanotubes, in order to optimize the process, and to obtain an effective functionalized CNTs with light modification of the peculiar aspect ratio value. Moreover, the study is focused on a quantitative investigation of the functionalities induced on the external wall, and how these different concentrations modify the behavior of carbon nanotubes in common solvent and in various polymer matrices, to comprehend the optimized functionalization methodology to effectively enhance nanocomposites properties.

2.2 EPOXY-BASED NANOCOMPOSITES

One of the most used polymer matrices for carbon nanotubes based nanocomposites are the epoxy resin for their widely range of performance properties and the possibility of an easy process in lab scale. Notwithstanding the large amount of works dedicated to these CNTs nanocomposites, the results are still contradictory. Based on epoxy nanocomposites, a possibility is emerging to exploit an extensive rheological characterization to better understand the different morphology into which the carbon nanotubes structure themselves inside the polymer matrix, and how this nanostructured network influences not only the processing behavior, but also the enhancement of mechanical and electrical properties.

The aim of this work is to explore epoxy based nanocomposites containing different functionalized carbon nanotubes, to further comprehend the influence of the different functionalities on the dispersion processing and on curing processing. Moreover, rheological behavior is extensively investigated, to further comprehend how the different functionalities on the external wall could modify the microstructured network formed by carbon nanotubes, and how this interconnected network acts on mechanical properties enhancement. Induced electrical conductivity and electrical percolation concentration are also investigated to observe the modification from insulating to conductive behavior, induced by the carbon nanotubes presence, and how these are related on the CNTs' networked structure, that depends on the different functionalities on CNTs external wall.

An innovative and promising smart application of those nanocomposites, exploiting the conductivity induced by carbon nanotubes, is studied in this research. The effectiveness of applying epoxy based nanocomposites as sensors for following damage evolution is studied and related to the different microstructured morphology observed, to further clarifying the controversial found in literature and to move quickly to a near-terms application of this smarting behavior.

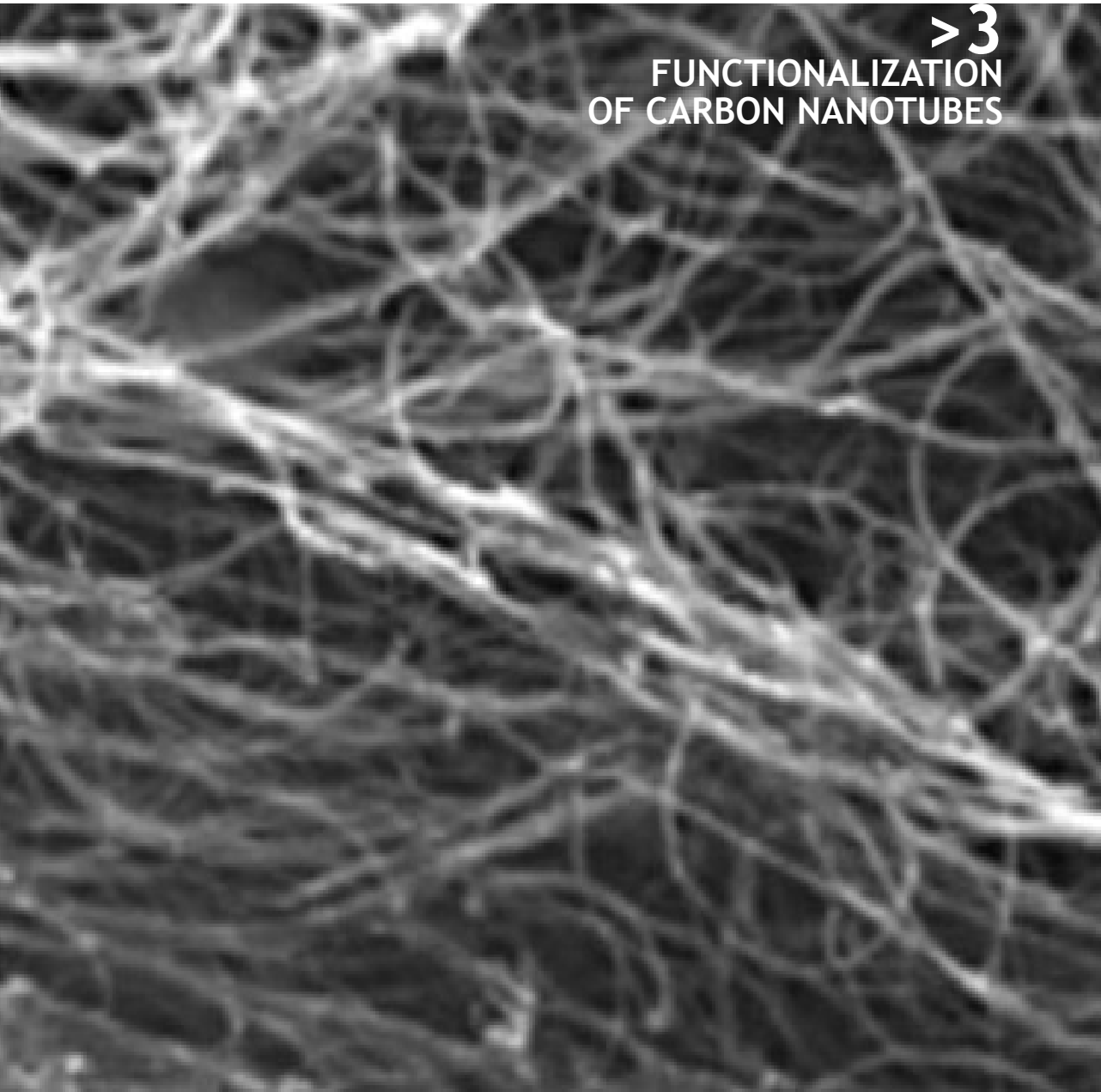
2.3 FLUORINATED POLYMERS-BASED NANOCOMPOSITES

Among the different polymer matrices studied in carbon nanotubes based nanocomposites, few attention were focused on fluorinated plastics. This lack of attention is mainly due to the particular applications in which these polymer matrix were used, such as superficial treatment to induce hydrophobic and oleophobic behavior for metal, leather and natural stone, and moreover as lubricant in critical condition. Notwithstanding the few amount of literature present, a very promising modification of present properties could be reached with the insertion of carbon nanotubes in those fluorinated polymer matrices.

This study is focused on two different perfluoropolyether based matrices, and on the dispersion of carbon nanotubes inside their structures. The aims is to achieve nanocomposites in which the dispersion of carbon nanotubes is more homogenous as possible, in order to enhance the peculiar mechanical and superficial properties of those matrices, that could permit a widening of the possible applications in which these nanocomposites could be exploited. Moreover this study tends to achieve a change in electrical conductivity, from an insulating to a conductive behavior, with the insertion of carbon nanotubes, in order to further extend the possible advanced applications of those nanocomposites.

The second part of this study is focused on a particular application for which perfluoropolyether based nanocomposites could be used, i.e. hydrophobic coating for gas diffusion layer in a PEM fuel cell system. Hydrophobic treatments on GDL are known to clear enhance the performances of the PEM fuel cell. Few attention on materials exploited for this particular treatment is present in literature, even if some good improvement are observed.

This research is focused on perfluoropolyether based nanocomposites containing carboxylic carbon nanotubes as coating treatment on carbon cloth. The aim is to optimize the nanocomposites formulation, at changing carbon nanotubes concentration, to obtain an effective hydrophobization treatment of carbon cloth that could give a less ohmic loss and better water management, to gain an higher performance in fuel cell system.



>3

FUNCTIONALIZATION
OF CARBON NANOTUBES

3.1 INTRODUCTION

Since their discovery carbon nanotubes have attracted considerable interest in potential application such as polymer composites ^[1-5]. To have an effective reinforcing effect, carbon nanotubes have to be well dispersed in polymer matrix with which CNTs has to be compatible ^[1,2-9]. Unfortunately, as it is well known, CNTs have a strong tendency to agglomerate within their self in the so called bundles, a rod like structure. Moreover, their sp^2 arrangement, their nanosize and their high surface energy, make them hardly compatible with polymer matrix ^[1,2,4,5].

Concerning the use of nanotubes in composite materials, the incorporation of chemical functionalized, mainly oxygen containing groups, is the crucial steps to facilitate the exfoliation of CNT bundles and to induce a uniform carbon nanotube distribution within the polymer matrix ^[9-14]. These functionalized groups could also act as stress transfer site, creating an inorganic/organic interface between CNT and polymer matrix ^[7,15].

Scientific literature shows different methods in order to induce a functionalization on CNTs' surface. The most common is obtained by chemical oxidation ^[9-11,13,14,16-18].

Oxidation acts on defects present on the carbon nanotubes surface, mainly at the tube ends and occasionally on the external sidewalls, and these defects are usually the prime sites for functionalization ^[1,2,13,14]. This oxidation creates nanotubes with carboxylic groups on the surface, that could be used for further functionalization ^[1,2]. The effect of the commonly used acid oxidations at elevated temperature on CNTs' surface morphology have been well documented in previous studies, and the functionalization of nanotubes is often discussed in articles reporting dispersion and interaction of carbon nanotubes with different materials ^[1,2,9-18]. Different acid mixtures are proposed in literature and a well established method suggests a combination of sulphuric and nitric acid (3:1 volume) ^[9-11,13,14,16-18]. Although this great effort to achieve dispersion improvement of CNTs in polymer matrices via functionalization and surface modifications, it is difficult to compare data between articles due to different procedure, adaptation and different starting CNTs' purity ^[13]. Moreover, these oxidation methods are seen to induce a sort of cut down of the peculiar aspect ratio value, showed by CNT, that could bring to an efficient incorporation in polymer matrices and to an ineffective modification of nanocomposite's properties ^[9,12-14].

Even if the oxidation methods are quite widely accepted, only few papers concentrate the interest in the study of functionalities concentration and the different effects induced in dispersion capability, due to some difficulties in the usual IR-based approaches and in time spending filtration and back titrations ^[9,13,14,17,18]. Another well established functionalization is the creation of amino groups on CNT surface ^[19-22]. The amino-functionalization method is more standardized and

proceeds usually via chemical manipulation of carboxylic acid residues present on the carbon nanotubes surface, with use of thionyl chloride solution. Even if some other methods are present that involve plasma treatments, the knowledge in this solvent free functionalization method is not fully completed and the method is not standardized yet, reducing the use of this CNTs modification ^[23]. Again only few interests are present in characterization of amino functionalities and how the concentration of these groups could change the effectiveness of dispersion in different media ^[19-22].

The main interest in this work is to try the most studied CNTs' oxidation methods presented in the literature, and to find out the more efficient ones, not only from a qualitative point of view, but also from a quantitative point of view, in order to insert the much more numbers of carboxylic functionalities. Moreover with same procedure, preserving as much as possible the ineluctable change in aspect ratio values.

3.2 EXPERIMENTAL SECTION

3.2.1 MWCNT and other materials

Multi walled carbon nanotubes were purchased from Nanocyl.

Nanocyl NC 3100 family are thin nanotubes with a great purity degree. They are synthesized via catalytic carbon vapor deposition and a following purification procedure. They show the following properties: average diameter of 9,5 nm, average length of 1,5 μm and carbon purity >95%.

Nanocyl NC 3101 (COOH-CNT commercial) are CNT of the same NC 3100 family with the presence of less than 4% of carboxylic group on the surface.

Nanocyl NC 3150 family are short thin CNTs and they are synthesized via catalytic carbon vapor deposition and a following purification procedure. They show the following properties: average Diameter of 9,5 nm, average length minor than 1 μm and carbon purity major than 95%.

Nanocyl NC 3152 (NH₂-CNT commercial) are CNTs from the same NC 3150 family with the presence of less than 0,5% of amino functionalities on the external surface.

All other chemicals are purchased by Sigma Aldrich.

3.2.2 Carboxylic functionalization.

As receive NC 3100 (further named CNT) were treated with a mixture of sulphuric acid, used at two different concentration (see Section 3.3.1), namely at 95% and at 69% obtained with deionized water dilution, and nitric acid (69%). Two quantities of CNT were used (0,1 g and 0,625 g) in order to study a briefly scale up of the functionalization method.

For every 0,1g of CNT used, 80 ml of the concentrated acid mixture H₂SO₄/H₂NO₃ (3:1 in volume) were added in a 100 ml round bottom flask and put under sonication (Sonic & Materials VCX130) for 30 minutes under 50% of instrumental amplitude. The flask was then equipped with a condenser and the dispersion was refluxed under magnetic stirring for different time, at two designed temperature (80°C and 60°C) (see Section 3.3.1). After these operations, the resulting dispersion was diluted in deionized water and collected on mixed cellulose ester filter with a pore size of 0,1 μm to reach a neutral pH. The resulting solid was then dried in vacuum at 60°C overnight.

The quantity of 0,625 g of CNT was dispersed in 500 ml of concentrate acid mixture H₂SO₄/H₂NO₃ (3:1 in volume) following the same sonicating and refluxing operations described above. The resulting dispersion was diluted in deionized water and filtered on mixed cellulose ester filter with a pore size of 0,22 μm . The same drying procedure already described was conducted in vacuum.

3.2.3 Amino functionalization

The carboxy-functionalized CNT (further named COOH-CNT) obtained via the oxidation procedures described above (100 mg), were inserted, after a complete dry out, in a three necked flask under inert environment in order to avoid the presence of water and other pollutants. 20 ml of thionyl chloride were added and the reaction was conducted at 75 °C for 24 h under magnetic stirring. After the acyl chlorination, the thionyl chloride was distilled. The compounds were then washed with 20 ml of THF, magnetically stirred for 20 min and then distilled. This washing operations were repeated three times in order to assure the removal of SOCl₂. The remaining solid (acyl-chlorinated functionalized CNT) was dried under vacuum. 75 g of acyl-chlorinated functionalized CNT were reacted with 50 ml of examethylenediamine solution under magnetic stirring at 100 °C for 48 h. After cooling to room temperature, the NH₂-CNTs were washed with ethanol for five times on PVDF filter (pore size 0,22 µm) to remove excess diamine. The amino-functionalized CNT (further named NH₂-CNT) was dried at room temperature overnight under vacuum.

3.2.4 Atomic force microscopy

Around 2,0 mg of CNTs were added in 4 ml of acetone and dispersed via sonication (Sonic & Materials VCX130) for 30 min under 50 % of instrumental amplitude. One to three microliters of the solutions were put onto cleaned purified silica wafer and spincoated (Laurell WS-400E-6NPP) at 2000 rpm for 20 seconds.

Atomic force microscopy was use for the qualitative evaluation of CNT length and aspect ratio before and after the oxidation procedure.

A NSCRIPTON™ DPNWriter™ (Nanoink, USA) in tapping mode was used. Commercial silicon cantilever/tips (SPM Probe ACT-10P) were used at their fundamental resonance frequencies of 320 kHz. The mean spring constant of these tips was 42 Nm⁻¹. A minimum of four scans was taken for each sample, at a resolution of 25 µm x 25 µm, from different area of the samples.

3.2.5 Electron microscopy

SEM samples were prepared in the same way of the AFM samples. One to three microliters of solution prepared with 2,0 mg of CNT in 4 ml of acetone, dispersed via sonication, were spincoated (2000 rpm for 20 s) on polished silica wafer. All specimens were sputtered with gold before imaging. Scanning electron microscope analyses were performed using a Cambridge Stereoscan 360 to evaluate the different morphology of samples.

1 mg of CNT was diluted in 1 ml of acetone and then sonicated in sonication bath for 45 min. One to three microliters of the dispersion was then diluted in 1

ml of acetone and sonicated in sonication bath for 15 minutes. One microliter was then cast onto TEM sample support mesh grid. Transmission electron microscope analyses were performed using a Zeiss EM 900 operating at 80 kV.

3.2.6 Fourier transfer infrared spectroscopy

Different sample of KBr with around 0,5 %wt of CNTs were prepared for FT-IR spectrometer. Carbon nanotubes and KBr were dry in vacuum overnight in order to reduce the presence of water. These compounds were then mechanical mixed and pressed into disc's shape. A FT-IR Perkin Elmer Auto Image System were used as spectrometer in the frequency range of 4000 to 400 cm^{-1} to analyze the chances in the surface chemical bonding.

3.2.7 Colloidal stability of the suspensions

Dispersion of CNT and COOH-CNT were prepared taking 0,2 g of CNTs and adding around 12 ml of different solvents: deionized water, ethanol, dimethylformamide, chloroform and chlorobenzene. The dispersions were sonicated 15 minutes in sonication bath and the samples were kept for 75 days.

3.2.8 Titration

The samples COOH-CNT were quantitatively analyzed by titration to determine the COOH concentration on the surface. In a typical experiment, a known amount of carboxylated nanotubes were added into a 35 ml of NaOH solution at 0,04 N and stirred for 48 h in order to allow the solid carbon nanotubes to equilibrate with the base solution and permit the reaction of the NaOH with all COOH functionalities present on the surface of the CNTs. Some hypothesis about the presence of COOH functionalities on the CNTs could be evaluated to estimate the maximum amount of nanotubes that could be analyzed by this experiment.

The first hypothesis that we took into account is that the NaOH solution is in large excess in the dispersion system, and precisely the $[\text{Na}^+]$ ions are double than the $[\text{COO}^-]$. This hypothesis will confirm that all the $[\text{COO}^-]$ ion present in the titration system will efficiently react with the NaOH solution. The second hypothesis is that we suppose that COOH-CNT could show 3 meq/g of carboxylic group per grams of carbon nanotubes, i.e. the best observed oxidation obtained in literature. Following these two hypothesis, with little algebra, we mark the maximum amount of COOH-CNT that could be dispersed in 35 ml of base solution as 0,222 g. In the typical experiment the amount of CNT is much lower than this guideline in order to obtain a better dispersion of the CNTs into the solution.

The mixture was then titrated with 0,04 N HCl solution to determine the excess

of NaOH present and so, the concentration of the carboxylic functionalities on COOH-CNT was calculated.

A similar procedure was followed in order to quantitative analyze the NH_2 functionalities present on the surface of NH_2 -CNT. The samples were added into a 35 ml of HCl solution at 0,04 N and stirred for 48 h at room temperature. The mixture was then titrated with 0,04 N NaOH solution to determine the excess of HCl present and so calculate the concentration of the amino functionalities on CNTs.

All the titration experiments were conducted at room temperature controlling the temperature with a water bath. For all titration characterization an Eutech Instruments PH 510 pHmeter was used.

3.3 RESULTS AND DISCUSSION

3.3.1 Functionalization

As already mentioned, acid oxidative treatments create carboxylic functionalities on CNTs external wall, acting on the defects present at surface [10,13,14,17,18]. The presence of COOH groups permits to better disperse carbon nanotubes in various media and permits a less presence of aggregation into bundle structure [1,2,5,13,14]. Beside these properties optimization that are usually achieved for incorporation of CNTs into polymer matrix, acidic oxidative treatments may also cause major alternation in nanotubes structure, and may lead to an appreciable etching of the carbon material even under moderate oxidation conditions [13,14,17,18]. The main challenge of this work is to find out a preparation of highly modified CNTs with no appreciable structural damage.

In order to find out the best practical procedure to obtain COOH-CNT with highly presence of carboxylic functionalities, we follow different procedure starting from the knowledge present in literature [13,14,17,18].

Table 1 tabulates different procedures of carboxylation with changes in acid concentration, time and temperature of refluxing and the average yield of the processes. Rule of thumb suggests that a moderate oxidation, that create a heavily functionalized CNTs, shows a low yield of processing [13,14].

Table 1 -Summary of carboxylic functionalization methods used.

| Method Name | Sample Mass (g) | Acid Concentration (H ₂ SO ₄ /HNO ₃) | Time and Temperature | Average Yield (%) |
|-------------|-----------------|--|----------------------|-------------------|
| a) | 0,1 | 95 / 69 | 6h 80° C | ≈ 0 |
| b) | 0,1 | 69 / 69 | 6h 80° C | 95,12 |
| c) | 0,1 | 95 / 69 | 2h 80° C | 0,47 |
| d) | 0,1 | 95 / 69 | 3h 60° C | 98,02 |
| e) | 0,625 | 95 / 69 | 3h 80° C | ≈ 0 |
| f) | 0,625 | 95 / 69 | 3h 60° C | 97,76 |

This behavior is explained by two different reasons [13,14]. First by heavy structural damages induced by oxidation, that create a carbon material with only partial CNTs structure, that could hardly remain in the filtration feed as precipitate. The second reason suggests that even if the tube structure is still present, nanotubes with many carboxylic functionalities show only few and small bundle structures. These structures decrease the efficiency of the filter that couldn't stop secluded carbon nanotubes, due to its pore size.

As observed the methods named a) and c), that are conducted with the 95%

concentration of H_2SO_4 at 80°C , show poor process yield, even if the time of the procedure is decreased from 6 to 2 hours. The same observation could be made for the method named e). Again, even in this scaled up configuration, the oxidation at 80°C is too heavy to obtain a reasonable yield. Method labeled b) shows a good process yield and (see Section 3.3.3 for titration results) a reasonable carboxylation. The methods labeled d) and f), that are conducted in the same way, with a difference only in the scale up configuration, were preferred to b) due to the easier and faster procedure obtained with similar results (see Section 3.3.3 for titration results). From those observations, the most efficient procedure of functionalization is a oxidation conducted in a mixture of $\text{H}_2\text{SO}_4/\text{H}_2\text{NO}_3$ (95%/69%) (3:1 in volume) for 3h at 60°C under magnetic stirring.

From the following sections, the carboxylic carbon nanotubes treated with the last mentioned oxidative methods, will be labeled COOH-CNT.

The amino-functionalization procedure instead (data not present in Table 1), was observed to show an average yield of around 60%.

3.3.2 Qualitative characterization of functionalization.

As it is well known and already discussed, CNTs have a strong tendency to agglomerate due to their nano size and their high surface energy [1-3,5]. However, when the surface is subjected to oxidation, chemical elements are adsorbed forming functional groups. In this case carboxylic acid groups. The presence of this functionalities on the surface of CNTs, enables them to repel from each other and, if dispersed in a solution, to keep the solution dispersed [13,14,17,18]. Evaluating the sedimentation it is possible to estimate the amount of functional groups adsorbed on the surface of CNTs.

Figure 1 shows the dispersion of COOH-CNT, in different solvent after 30 minutes of dispersion preparation.

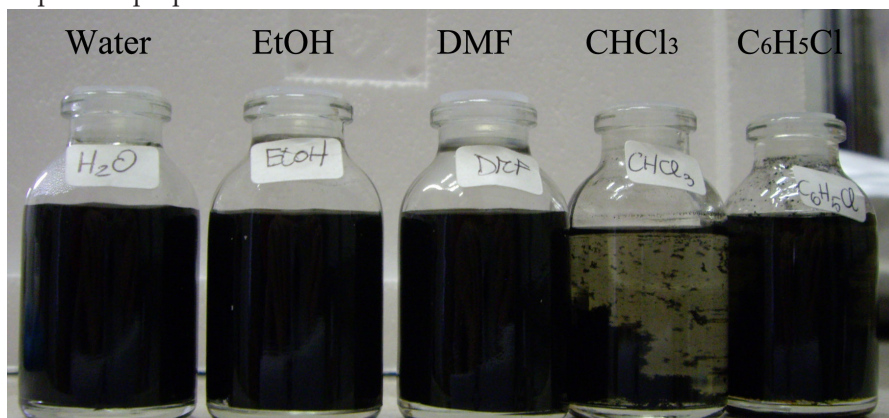


Figure 1 - Pictures of the dispersions of COOH-CNT in different solvents, taken after 30 minutes of dispersion preparation.

Good dispersion of COOH-CNT in solvent with different polarity are observed. Some clear precipitation can be seen in the dispersion with chloroform, and some difficult in colloidal stability could be suppose for the dispersion with chlorobenzene that show some swollen agglomeration. Same observations could be made for the same dispersion after 75 days as showed in Figure 2.

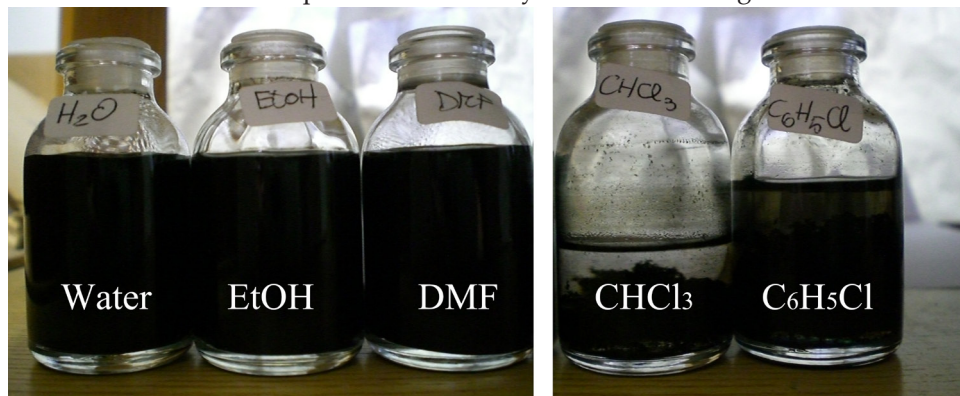


Figure 2 - Pictures of the dispersions of COOH-CNT in different solvents, taken after 75 days of dispersion preparation.

Figure 3 shows instead that the dispersions of untreated CNT in different solvent are quite unstable even at 30 minutes after the preparation. As observed in literature, nanotubes with COOH functionalities expel each other to loosen the bundle structure, and from this, they better interact with solvent creating a more stable dispersion.



Figure 3 - Picture of the dispersions of CNT in different solvents, taken after 30 minutes of dispersion preparation.

Another characterization exploited to qualitatively evaluate the presence of carboxylic groups was the fourier transfer infrared spectroscopy (FTIR).

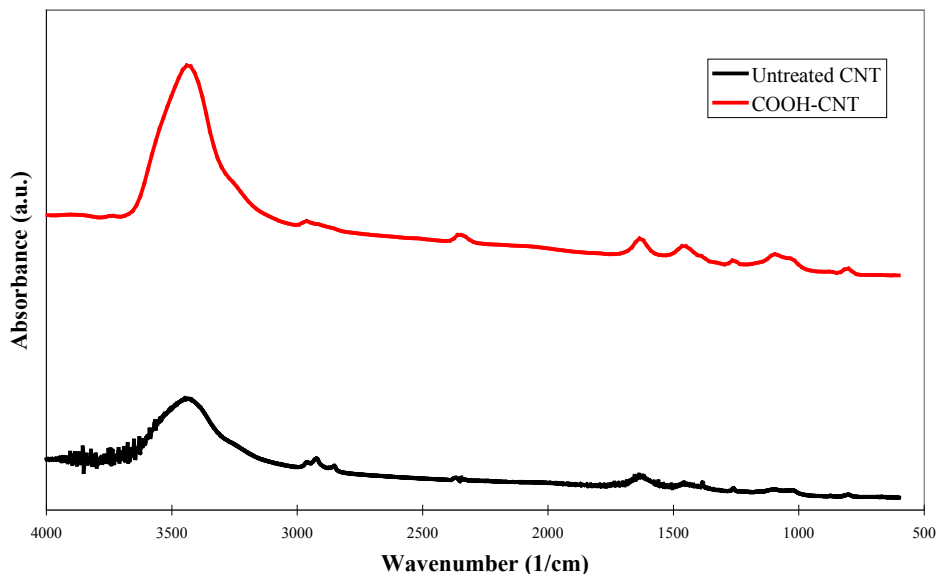


Figure 4 - IR spectra of untreated CNT and COOH-CNT sample.

Figure 4 shows the IR spectra of CNT and COOH-CNT samples. The band around 3500 cm^{-1} is attributed to the infrared absorption of the H-bonded hydroxyl group, and the band around 1640 cm^{-1} corresponds to the H-bonded carbonyl groups ($\text{C}=\text{O}$)^[17,18]. As observed, these IR bands, that suggest the presence of carboxylic functionalities on COOH-CNT surfaces, are still present in untreated CNT. At these values of absorptions the relative transmittances for untreated samples are lower than those observed for COOH-CNT samples, suggesting a low presence of carboxylic and hydroxylic functionalities on untreated CNT. The presence of these functionalities, even on untreated CNT, is explained by the oxidation that took place on nanotubes after exiting from the reactor, in order to obtain their highly purified carbon concentration. Same observations are confirmed with quantitative characterization obtained by titration. (see Section 3.3.3)

IR spectroscopy couldn't be used to mark out the difference obtained through functionalization, but could only suggest that some change in carboxylic functionalities took place during the oxidation process. For the same reason FTIR was not used to characterize the NH_2 -CNT functionalities.

3.3.3 Titration

A direct acid-base titration technique was performed to determine the concentration of groups on carbon nanotubes surface. Even if this characterization was time

spending and was difficult to carry out, requiring filtration and back titration, it was the only quantitative technique that could reveal important results on CNTs' functionalities [13,14,17].

In Table 1 the average mmol of acidic oxygen-containing surface groups per gram of CNT material, extracted by titration process, are given as a function of chemical treatment and the average yield of the process. In the same table are presented the data obtained with commercial untreated CNT and with commercial functionalized COOH-CNT.

Table 2 - Summary of carboxylic relative concentration after titration for different CNT samples.

| Method Name | Average Yield process | Average COOH groups (mmol/g) | Standad Deviation |
|---------------------|-----------------------|------------------------------|-------------------|
| CNT Untreated | Non-measurable | 0,70 | 0,14 |
| a | ≈ 0 % | Non-measurable | Non-measurable |
| b | > 90 % | 3,90 | 0,83 |
| c | ≈ 0,5 | 3,50 | 1,71 |
| d | > 90 % | 3,67 | 0,36 |
| e | ≈ 0 % | Non-measurable | Non-measurable |
| f | > 85 % | 3,94 | 0,48 |
| COOH-CNT commercial | Non-measurable | 2,53 | 0,09 |

First issues to point out is that the untreated CNTs show a small amount of COOH functionalities on external wall. This confirm the drafted data observed with FTIR (see Section 3.3.2), and prove what already suspected, that the process of purification on the nanotubes exiting the reactor creates a small amount of carboxylic functionalities on the external wall.

Titration results were also use to confirm the aim of this work that was looking for a good and easy functionalization method. Comparing the methods from a) to d), it is possible to confirm that the method named b) and d) create an efficient functionalization of CNTs' surface with similar results. Moreover these functionalization procedures were obtained with a reasonable yield. As already stated before in Section 3.3.1, the preference for the method named d) was induced by the easier preparation and less time consuming process. Same values of carboxylic functionalities are obtained with the scaling up oxidative method f).

A useful observation could be made for the average value obtained for commercial COOH-CNT samples. 2,53 mmol/g of CNT was observed for those commercial nanotubes, a lower values of carboxylic functionalities compared to 3,94 mmol/g

of COOH-CNT obtained from our best designed oxidation method.

Table 3 - Summary of carboxylic relative concentration after titration for different COOH-CNT's preparation methods.

| Method Name | Average Yield process | Average COOH groups (mmol/g) | Standad Deviation |
|-------------|-----------------------|------------------------------|-------------------|
| f | > 85 % | 3,94 | 0,48 |
| g | > 90% | 3,46 | 0,03 |
| h | > 90% | 2,46 | 0,48 |

Table 3 shows the contents of COOH groups of the acid-treated CNTs as a function of treatments conditions for the already described method f) and for two different methods g) and h). These two oxidation processes are conducted with the same configuration of method f) changing the time of the refluxing. For method g) the procedure was conducted for 2h at 60°C and for method h) for 1h at 60°C. These changes were studied in order to optimize the oxidation method and to reduce the time of the process, partially modifying the carboxylic functionalities on surface of CNTs. As Table 3 suggests, method h) creates a low number of carboxylic functionalization. Method g) instead, with a decreasing of just one hour of oxidative refluxing, shows a decrease in the presence of COOH groups on the external wall compared to the average value obtained with standard method f). The standard method f) was preferred for its reasonable average yield and for the efficiency in modification of CNTs' structures.

Table 4 shows the results for titration characterization on nanotubes with amino functionalities. Again the average results obtained with commercial NH₂-CNT samples could be used to evaluate the efficiency of the process of amino-functionalization described in Section 3.2.3. The amino values evaluated by titration, for our functionalization and for commercial amino modified CNTs are quite alike. This confirm the effectiveness of our amino-functionalization with a good process yield.

Table 4 - Summary of amino relative concentration after titration for different CNT samples.

| Name | Average Yield process | Average NH ₂ groups (mmol/g) | Standad Deviation |
|---------------------------------|-----------------------|---|-------------------|
| NH ₂ -CNT | ≈ 60% | 1,849 | 0,07 |
| NH ₂ -CNT commercial | Non-measurable | 1,96 | 0,39 |

3.3.4 Microscopy Characterization (TEM, SEM, AFM)

Oxidation as already stated, interacting with external wall of CNTs, inevitably change the morphology of the nanotubes ^[13,14,17,18]. A microscopy study is mandatory to characterize the modification of the aspect ratio values observed after oxidation.

3.3.4.1 Transmission Electron Microscopy

Transmission electron microscopy is often used to observe the length and diameter of carbon nanotubes ^[18]. Even if the rod like structure of CNTs couldn't make clearly possible to estimate the real value of the length and diameter, TEM could suggest changing in aspect ratio values. Figure 5 from a) to d) confirms that only a negligible change in aspect ratio occurs after oxidative process. These observations confirm the goodness of our carboxylic functionalization.

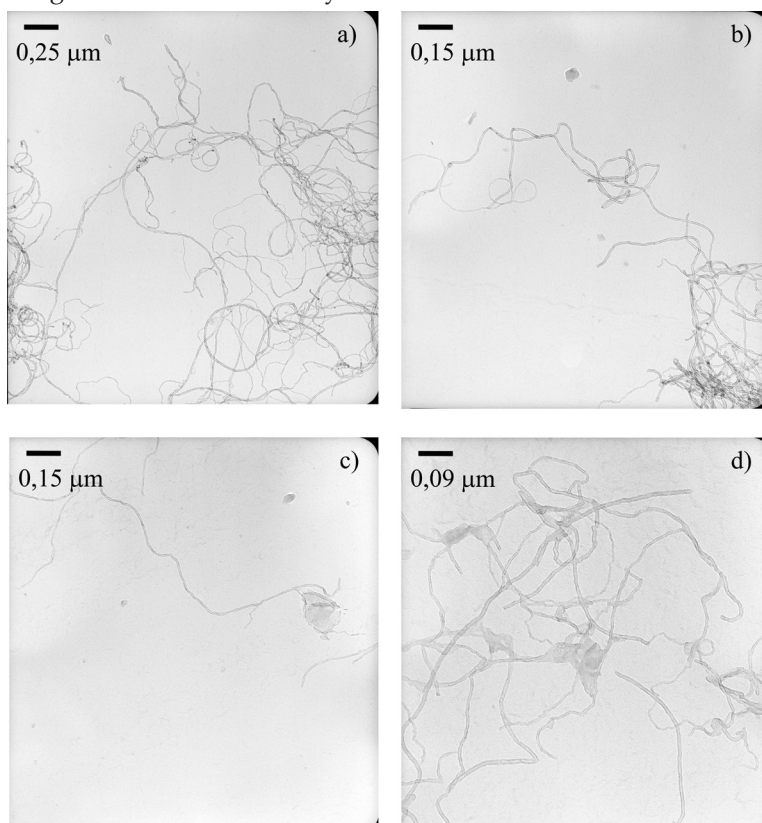


Figure 5 - TEM images of different CNTs: a), b) untreated CNT, c), d) COOH-CNT.

Figure 6 shows a TEM image of commercial COOH-CNT. Again the aspect ratio of these commercially used carboxylic nanotubes are comparable to the ones observed on our samples that have, as seen, a higher amount of functionalities

on their external wall (Figure 5 c,d). This again underline the efficiency of our oxidative process.

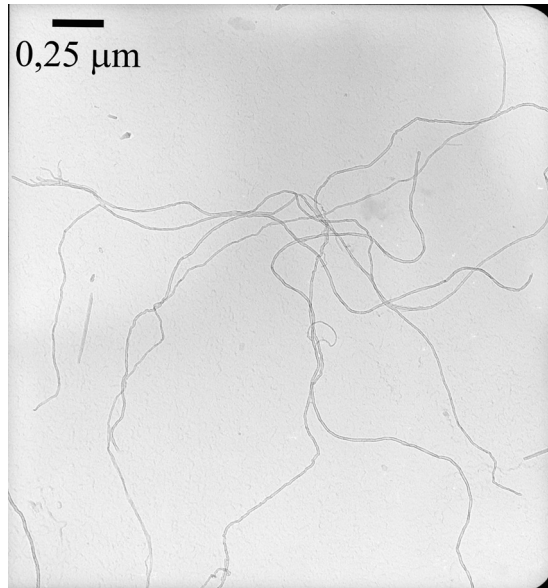


Figure 6 - TEM image of Commercial COOH-CNT.

Figure 7 instead shows the TEM image of NH_2 -CNT sample. As could be seen the amino functionalization that start from COOH-CNT do not induce any further change in aspect ratio, preserving a length and a diameter similar to untreated and commercial available CNT.

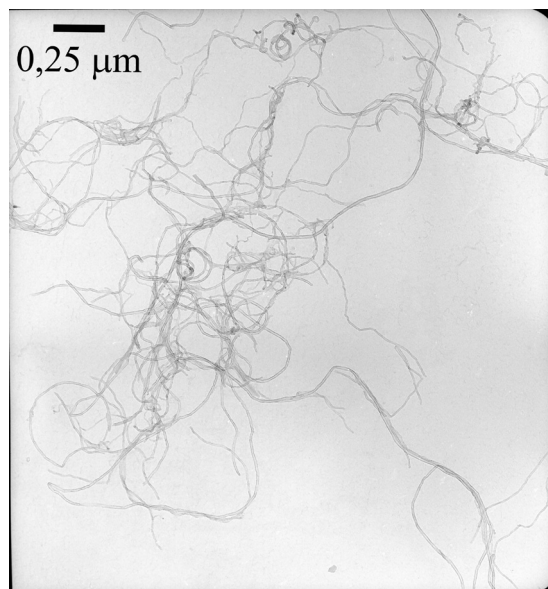


Figure 7 - TEM figure of NH_2 -CNT sample.

3.3.4.2 Scanning electron microscopy

Scanning electron microscopy was used also to confirm the possible morphological changes on functionalized CNTs.

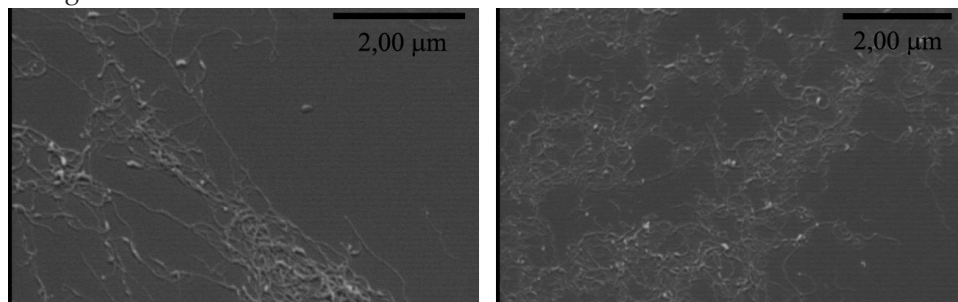


Figure 8 - SEM images of the untreated CNT a) and COOH-CNT samples b).

Concerning the oxidative treatment, no visible changes in the morphology of COOH-CNT are detected and the corresponding image Figure 8 b) seems to be similar with untreated CNT (Figure 8 a) used as starting sample. This is another indication that the oxydative treatment is not destructive for carbon nanotubes, while, at the same time, exceedingly functionalized materials are produced.

3.3.4.3 Atomic force microscopy

Atomic force microscopy was used to characterize the length of nanotubes or CNTs' bundles.

As already observed with other microscopy characterizations, no aspect ratio values change are observed with AFM for carboxylic functionalized samples as observed in Figure 9.

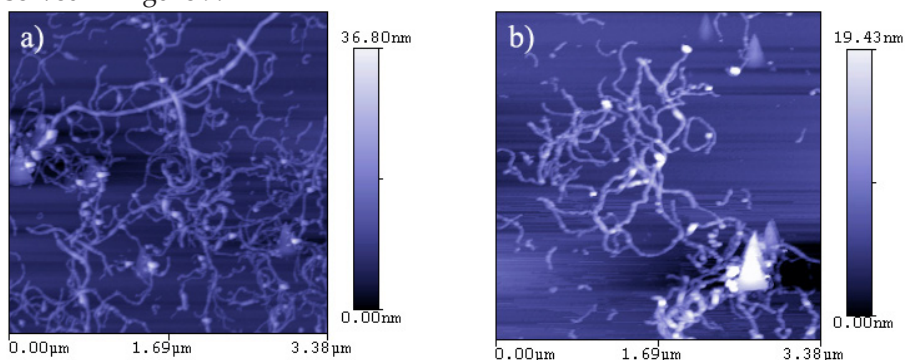


Figure 9 - AFM images of untreated CNT a) and carboxylic CNT b).

Height profiles showed that formation of bundles took place even after functionalization, as observed in Figure 9 b) that shows COOH-CNT samples.

3.4 CONCLUSIONS AND FUTURE CONSIDERATIONS

Strong acid treatments could create carboxylic functionalization on carbon nanotubes, but they damage the nanotubes structure. Functionalization is often required in order to better disperse CNT in various solvents and in polymer matrix.

Different chemical oxidation on nanotubes were conducted and the resulting material were characterized in different ways. A quantitative characterization of carboxylic concentration on the modified carbon nanotubes was approached in order to standardize an efficient functionalization method, with a resulting carboxylic concentration comparable with commercial COOH-CNT. This functionalization further shows a good process yield. Different characterizations (i.e. infrared spectroscopy and dispersion in different solvents) confirm the presence of carboxylic group on modified CNTs' external walls. Moreover COOH-CNT could create a more stable dispersion in a great variety of solvents. Additional microscopy characterization confirm the efficiency of oxidation that create carboxylic functionalities without a great change in peculiar aspect ratio values of those nanotubes.

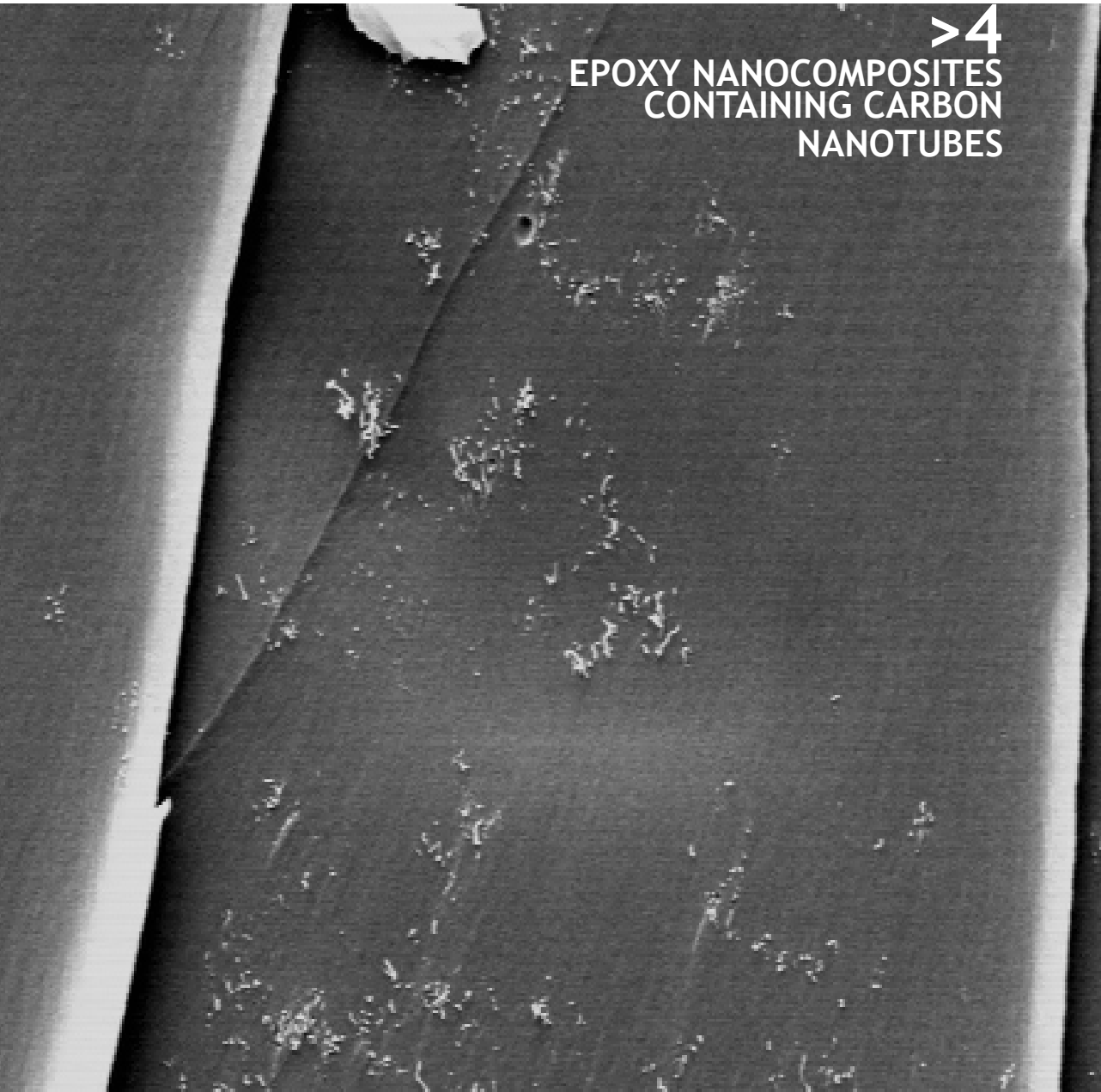
An efficient amino functionalization was also studied and the functionalities on external nanotubes' walls were estimate to be comparable with amino group values of commercial available NH_2 -CNT. As observed for COOH-CNT, this efficient functionalization was obtained without an observed change in nanotubes' aspect ratio values.

Future study will be directed to optimize the difference functionalization methods in terms of reducing the waste of time and chemical products used, and to develop a functionalization methodology that could be easily industrialized. Moreover, a relationship between the dispersion capability and the different concentration of the functionalities on the external wall must be investigated, in order to further optimize the better functionalized carbon nanotubes that could be easily dispersed in different polymer matrices.

3.5 REFERENCES

1. J. Coleman, U. Khan, W. Blau, Y. Gunko, Small but strong: A review of the mechanical properties of carbon nanotube-polymer composites, *Carbon*, 44, 1624-1652 (2006).
2. J. Coleman, U. Khan, Y. Gun'ko, Mechanical reinforcement of polymers using carbon nanotubes, *Advanced Material*, 18, 689-706 (2006).
3. J. Du, The present status and key problems of carbon nanotube based polymer composites. *Express polymer letters*, Vol 1 (5), 253-273 (2007).
4. H. Qian, E. Greenhalgh, M. Shaffer, A. Bismarck, Carbon nanotube-based hierarchical composites: a review, *Journal of Materials Chemistry*, 20, 4751-4762 (2010).
5. Z. Spitalsky, D. Tasis, K. Papagelis, C. Galiotis, Carbon nanotube-polymer composites: Chemistry, processing, mechanical and electrical properties, *Progress in Polymer Science*, 35, 357-401 (2010).
6. S.D. Bergin, Z. Sun, P. Streich, J. Hamilton, J. N. Coleman, New Solvents for nanotubes: approaching the dispersibility of surfactants, *The Journal of Physical Chemistry C*, 114, 231-237 (2010).
7. J. Bai, A. Allaoui, Effect of the length and the aggregate size of MWNTs on the improvement efficiency of the mechanical and electrical properties of nanocomposites-experimental investigation, *Composites Part A Applied Science and Manufacturing*, 34, 689-694 (2003).
8. K. Lau, M. Lu, H. Cheung, F. Sheng, H. Li, Thermal and mechanical properties of single-walled carbon nanotube bundle-reinforced epoxy nanocomposites: the role of solvent for nanotube dispersion, *Composites Science and Technology*, 65, 719-725 (2005).
9. J. Zhu, H. Peng, F. Rodriguez-Macias, J. L. Margrave, V. N. Khabashesku, A. M. Imam, K. Lozano, E. V. Barrera, Reinforcing Epoxy Polymer Composites through covalent integration of functionalized nanotubes, *Advanced Functional Materials*, 14 No.7, 643-648 (2004).
10. M. Abdalla, D. Dean, D. Adibempe, E. Nyairo, P. Robinson, G. Thompson, The effect of interfacial chemistry on molecular mobility and morphology of multiwalled carbon nanotubes epoxy nanocomposites, *Polymer*, 48, 5662-5670 (2007).
11. M. Abdalla, D. Dean, P. Robinson, E. Nyairo, Cure behavior of epoxy/MWCNT nanocomposites: The effect of nanotube surface modification, *Polymer*, 49, 3310-3317 (2008).

12. W. Zhang, R. C. Picu, N. Koratkar, The effect of carbon nanotube dimensions and dispersion of the fatigue behavior of epoxy nanocomposites, *Nanotechnology*, 19, 1-5 (2008).
13. M. Marshall, S. Popanita, J. Shapter, Measurement of functionalized carbon nanotube carboxylic acid groups using a simple chemical process, *Carbon*, 44, 1137-1141 (2006).
14. V. Datsyuk, M. Kalyva, K. Papagelis, J. Parthenios, D. Tasis, A. Siokou, I. Kallitsis, C. Galiotis, Chemical oxidation of multiwalled carbon nanotubes, *Carbon*, 46, 833-840 (2008).
15. L. S. Schadler, S. C. Giannaris, P. M. Ajayan, Load transfer in carbon nanotube epoxy nanocomposites, *Applied Physics Letters*, 73 (26), 3842-3844 (1998).
16. C. Jung, D. Kim, J. Choi, Surface modification of multi-walled carbon nanotubes by radiation-induced graft polymerization, *Current Applied Physics*, 9, S85-S87 (2009).
17. Y. Shieh, G. Liu, H. Wu, C. Lee, Effects of polarity and pH on the solubility of acid-treated carbon nanotubes in different media, *Carbon*, 45, 1880-1890 (2007).
18. A. Osorio, I. Silveira, V. Bueno, C. Bergmann, $H_2SO_4/HNO_3/HCl$ - Functionalization and its effect on dispersion of carbon nanotubes in aqueous media, *Applied Surface Science*, 255, 2458-2489 (2008).
19. J. Shen, W. Huang, L. Wu, Y. Hu, M. Ye, Study on amino-functionalized multiwalled carbon nanotubes, *Material Science and Engineering A*, 464, 151-156 (2007).
20. J. Wang, Z. Fang, A. Gu, L. Xu, F. Liu, Effect of amino-functionalization of multiwalled carbon nanotubes on the dispersion with epoxy resin matrix, *Journal of Applied Polymer Science*, Vol 100, 97-104 (2006).
21. J. Li, Z. Fang, L. Tong, A. Gu, F. Liu, Improving dispersion of multiwalled carbon nanotubes in polyamide 6 composites through amino-functionalization, *Journal of Applied Polymer Science*, Vol 106, 2898-2906 (2007).
22. J. Shen, W. Huang, L. Wu, Y. Hu, M. Ye, The reinforcement role of different amino-functionalized multiwalled carbon nanotubes in epoxy nanocomposites, *Composites science and technology*, 67, 3041-3050 (2007).
23. L. Valentini, D. Puglia, F. Carniato, E. Boccaleri, L. Marchese, J. M. Kenny, Use of plasma fluorinated single-walled carbon nanotubes for the preparation of nanocomposites with epoxy matrix, *Composites Science and Technology*, 68, 1008-1014 (2008).

A grayscale micrograph showing a dark, textured surface, likely a cross-section of an epoxy nanocomposite. The surface is covered with numerous small, bright, irregularly shaped particles and fibers, which are carbon nanotubes. A prominent diagonal crease or fold is visible on the left side of the image. The overall appearance is granular and fibrous.

>4
EPOXY NANOCOMPOSITES
CONTAINING CARBON
NANOTUBES

4.1 INTRODUCTION

Since the paper by Iijima, carbon nanotubes have been a focus of considerable research due to their mechanical and electrical performance^[1-4]. Their unique atomic structure, a very high aspect ratio, an extraordinary mechanical and electrical property make them the ideal reinforcing fillers^[1,2,4-6]. Much of earlier work focused their attention on the direct incorporation of nanotubes as reinforcement in different polymer matrices^[1-4]. However, the measured enhancements in properties due to the insertion of CNTs are significantly less than theoretically expected due to the difficulty of processing. The potential for mechanical and electrical properties enhancement is determined by both the degree of nanomaterial dispersion throughout the composite system and interfacial adhesion between the polymer matrix and dispersed phase^[1,2,7-12]. In order to overcome these difficulties, different functionalization of external wall of carbon nanotubes are studied and literature evidently highlight some better CNTs' properties exploitation using functionalized carbon nanotubes^[1-3,5,6,13].

Among different polymer matrices into which CNTs are used as fillers, epoxy resin is one of the most studied ones due to its importance as thermoset polymers^[1,2,7-10,13-15]. Epoxy resins are widely used for the manufacturing of advanced composites in application ranging from microelectronics to aerospace. Using CNTs as reinforcement in epoxy nanocomposites can widen their use in potential application such as coatings, adhesives, structural materials etc^[14,15]. Moreover epoxy matrix has shown extremely low percolation threshold when CNTs are added^[7-10,13-15]. This is an interesting issues in terms of industrial applications.

Furthermore one of the main reason for the wide number of literature studies on epoxy nanocomposites containing CNTs, is the easy availability and processability even in lab scale of this nanocomposites^[7-10,13-24].

Most of the epoxy composites' literature focused only on mechanical properties enhancement, observing the percolative threshold behavior, that could play a crucial role in the processing of these nanocomposites, even at very low loadings (commonly at 0,5 %wt for untreated CNTs)^[1,2,8-11,13-32]. However a few works concentrated their attention on the optimization of nanotubes dispersion in epoxy matrix, and on understanding how the different dispersions show different reinforcements^[13,18-23]. Accessibility of epoxy resin permits instead to increase knowledge on the ideal dispersion and on interfacial interactions of CNTs in polymer matrix, in order to reach the great expected theoretical properties of this promising nanocomposites. The realization of these ideal nanotube-reinforced epoxy can only be achieved by solving different problems. The most important is the poor dispersion of nanotubes in the epoxy matrix observed. With their fine size, with high surface energy and with intrinsic van der Waals forces, the untreated CNTs aggregate and entangle together spontaneously^[1,2,7-12]. This behavior could be restricted

with functionalization but couldn't be denied even for functionalized CNTs. In a CNTs/polymer composite, aggregation of CNTs may become a defect and cause the mechanical properties of the composite to deteriorate. Additional processing difficulties, come from the formation of high viscosity blends at low shear rates when the nanotubes are directly added [14-17].

In our study we focus our attention on CNTs dispersion in DGEBA matrix using untreated and different functionalized CNTs (carboxylic and amino functionalized). Rheological and microscopy characterizations were used in order to understand the different morphologies showed by epoxy nanocomposites with different functionalized CNTs, and how these differences modified the composites rheological behaviour.

Another important property showed by CNTs-epoxy nanocomposites is the electrical conductivity induced by the insertion of carbon nanotubes [6,12,19,30,31,33,34]. The enhancement of thermal and electrical characteristics of nanotube-epoxy nanocomposites, also observed with different polymer matrices, are attributed to the formation of a network of interconnected filler particles which can conduct heat and electrical current [6,11,12,19,30,31,33-43]. This event was found to be strongly related on nanotubes aspect ratio, on different functionalization of carbon nanotubes external wall, on dispersion of CNTs in polymer matrix, on dissimilar type of matrix polymer and on the processing of the nanocomposites [12,,19,,30,31,33,35-39]. Different literature works show an improvements in electrical conductivity with a percolation threshold below 1% of nanotubes weight fraction [19,30,33,35]. However these promising behavior, i.e. the connection between the degree of dispersion, the rheological performances and the electrical conductivity in nanotube-epoxy nanocomposites, has been practically ignored [19,35].

In our study on electrical characterization, our attention was focused on different electrical behavior showed by different nanocomposites containing functionalized CNTs. We also investigated specific features of electrical conductivity in comparison with results observed in rheology for our epoxy/CNT dispersions, in order to understand how different nanocomposites' morphologies are linked to the mechanical and electrical threshold.

In recent years, based on these promising results obtained in nanocomposites electrical conductivity, the conductive modification using small amounts of carbon nanotubes and subsequent damage monitoring through resistance measurements was introduced [44-48]. Usually the detection of damage in composites is conducted through invasive means. The electrical threshold due to CNTs electrically conductive network could be used to monitor damage initiation and possibly propagation in epoxy nanocomposites. Effectiveness and efficiency in damage sensing of using inducted electrical conductivity has been investigated.

4.2 EXPERIMENTAL SECTION

4.2.1 Carbon nanotubes, epoxy resin and other materials

Multi walled carbon nanotubes Nanocyl NC 3100 (labeled CNT), were purchased from Nanocyl. For further specific informations see Section 3.2.1.

For carboxylated nanotubes two different grades were used. The commercial available Nanocyl NC 3101 (labeled C COOH-CNT) purchased from Nanocyl, and the carboxylated nanotubes with the standard method described in Section 3.2.2 and studied in chapter 3 (labeled COOH-CNT).

For amino functionalized nanotubes again were used the commercial available Nanocyl NC 3152 (labeled C NH₂-CNT) purchased from Nanocyl, and the amino-CNT obtained from amino functionalization method described in Section 3.2.3 and studied in Chapter 3 (labeled NH₂-CNT).

For further details on commercial Nanocyl NC 3101 and Nanocyl NC 3152 please refer to Chapter 3.2.1.

In this study the labels COOH-CNT and NH₂-CNT are used without any distinction for commercial available carbon nanotubes and for functionalized CNTs with methods described in Section 3.2.2. This consideration is supported by preliminary study on all the different characterizations here further investigated, in which no dissimilar behavior is observed for our functionalized CNTs and nanocomposites in where are inserted, from the performance of commercial CNTs and in wherever nanocomposites are inserted. Epoxy resin used as polymer matrix is a commercial available transparent resin (Duroglass P5/1) purchased from Alcea Srl. The resin is a bicomponent epoxy resin. The first component (further labeled A) is a bisphenol A diglycidyl ether based liquid resin (DGEBA). The A component also contains a commercial aliphatic glycidyl ether (Epodil 748) as reactive thinner. The resin was Newtonian with a neat viscosity of around 2 Pa*s at 22 °C .

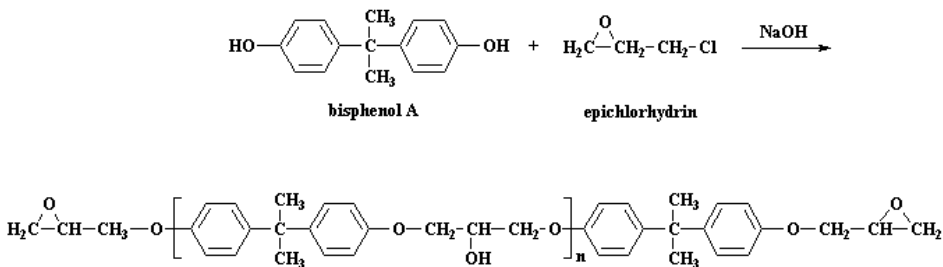


Figure 1 - Chemical reaction to products DGEBA.

An amino hardener (Versamine I74), 3-Aminomethyl-3,5,5-trimethylcyclohexylamine based, was used, with benzyl alcohol as plasticizer.

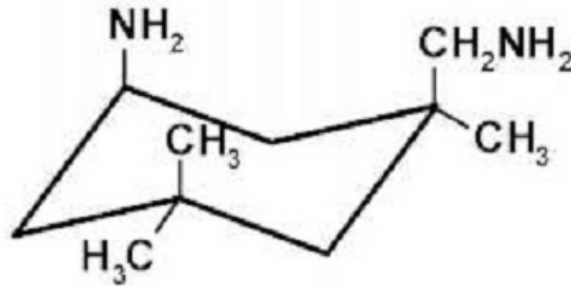


Figure 2 - 3-Aminomethyl-3,5,5-trimethylcyclohexylamine

Mixing procedure of part A and part B follow the indication of the manufacturer, that suggests, in order to balance the resin equivalences, to mix 100 parts of A component with 60 parts of hardener component. The crosslink procedure was conducted in the following way:

- room temperature for 24 hours,
- 2 hours at 80 °C
- 2 hours at 120 °C.

This long procedure, with time spending first step at room temperature, was chosen in order to let useful operative time for degasification. This will be more helpful when CNTs are added as described in Section 4.2.2. Differential scanning calorimetry analysis confirm the end of the crosslinking reaction with the above mentioned procedure. All other chemical, if not expressly mentioned, were provided by Sigma Aldrich.

4.2.2 Dispersion

Starting from knowledge underlined in few articles regarding CNTs dispersion at lab scale, acetone was chosen as solvent of the resin (it's a solvent of both resin's components) and as dispersing media into which CNT were dispersed ^[7-10,18-21].

CNT dispersions were formulated by mass fraction based on measured component weights. The mass fraction of carbon nanotubes in this study is always referred to the component A of the epoxy resin for easy labeling.

4.2.2.1 CNT/resin without curing agent dispersion

The liquid CNT/resin polymer mixture, with no curing agent present, were prepared in different steps. Around 50 grams of A component were prepared in a three necked round-bottom flask. First operation needs to disperse the CNT from their bundle agglomeration in acetone.

Appropriate amount of CNT, according to the final wished weight content, were added to a flat-bottom flask containing acetone (around 1,5 times of the resin weight). Carbon nanotubes are dispersed with three different operations. Firstly a mixing was conducted with magnetic stirring at 950 rpm for 30 minutes. The solution is then sonicated in a Starsonic 90 sonicator bath for 1 hour. The mixture was then sonicated with a Sonic & Materials VCX130 sonicator tip for 30 minutes at the 50% of the instrumental amplitude. Last step was conducted in ice bath in order to reduce the acetone evaporation. The acetone containing CNT was then added to the three necked flask that contains the A component. The dispersion of CNTs into A component of resin were conducted using a Heidolph RZR 2102. A Teflon stirring blade was used to mix the dispersion at 300 rpm for 3 hours. These operations created a good dispersion of CNTs into solvated resin.

The remaining acetone, used to disperse CNTs and to reduce the viscosity of the A/CNT blend, was then removed under vacuum with a mixing at 300 rpm for 1 hour at 60°C. The blend is then casted on Teflon plate and placed for the night in vacuum oven at 60 °C, in order to completely remove the acetone.

Rheological characterization was used in order to confirm the goodness of the above mentioned dispersion method. As the Figure 3 shows, three different samples with the same concentration of 0,5 %wt of CNT, rheologically behave in the same way.

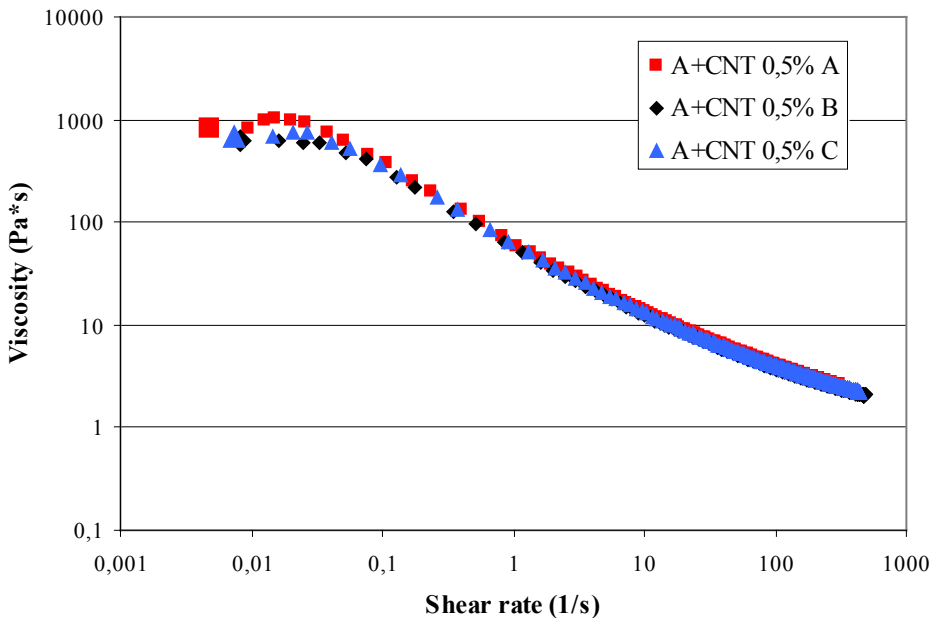


Figure 3 - Shear rate curves for different dispersion containing 0,5 % of CNT. A), B) curves are different curves on same dispersion, C) shear rate curve on different dispersion with the same composition of 0,5 %wt of CNT.

Same results were obtained for different functionalized CNTs (COOH-CNT, NH₂-CNT) confirming the goodness of the dispersion method. Those observations confirm that the dispersion procedure studied have a highly reproducibility. For instrumental condition in this rheological characterization see Section 4.2.5. For further rheological characterizations see the results in Section 4.3.2. The A+CNTs blend was then used for further rheological, calorimetric and microscopic characterizations. A+CNTs samples show high viscosity, even with the addition of small amount of carbon nanotubes. This viscosity growth couldn't permit a easy usage of the blend in the mix preparation with hardener. A solvent preparation was used also in this case when curing agent is needed.

4.2.2.2 CNT/resin with curing agent dispersion

The procedure to mix the CNT in A component and the following addition of the hardener component, was designed on the good dispersion method described above for the mixing of the CNTs into the DGEBA based components.

Around 50 grams of A component were prepared in a three necked round-bottom flask. The CNT dispersion in acetone were conducted with three different steps as already described above in Section 4.2.2.1. Appropriate amount of CNT were added to a flat-bottom flask containing acetone (around 1,5 times of the resin weight). The blend was mixed using a magnetic stirring at 950 rpm for 30 minutes, then sonicated using a Starsonic 90 sonicator bath for 1 hour. The mixture was then sonicated with a Sonic & Materials VCX130 sonicator tip for 30 minutes at the 80% of the instrumental amplitude. The acetone containing CNT blend was then added to the three necked flask that contains the A component.

The dispersion of CNTs into A component were conducted using a Heidolph RZR 2102 using a Teflon stirring blade at 300 rpm for 3 hours.

Part of the acetone, presents in the flask, is removed under vacuum with a mix at 300 rpm for 15 minutes at 60 °C. This operation is needed to reduce the amount of acetone in the final blend (after the adding of the hardener) in order to reduce the possible gas formation during solvent evaporation.

Hardener B was added in the right quantity (as already described 100 parts of A component is mixed with 60 parts of B component) . The system is then mixed using Heidolph RZR 2102 at 300 rpm for 30 minutes in a iced bath, in order to reduce the crosslinking reaction.

The composite is then cast on Teflon plate or in mold and put in vacuum overnight at room temperature in order to completely remove the solvent. The standard crosslinking procedure, already described in Section 4.2.1, was then continued reaching 24 hours at room temperature after the mixing. Then the crosslinking operation is continued with 2 hours at 80°C and 2 hours at 120 °C. Differential scanning calorimetry confirms the end of crosslinking reaction on all different composite samples.

4.2.3 Differential scanning calorimetry

Thermal characterization was used in order to comprehend the impact of carbon nanotubes insertion on the crosslinking reaction. Two different tests were performed in order to completely study the behavior of CNTs/resin nanocomposites during crosslinking. For all different characterizations a Mettler Toled DSC 823^e was used with a scanning temperature that starts from 25 °C to 250 °C. The speed of these scans was different for diverse tests.

The first test procedure was performed starting from A+CNTs samples obtained with dispersion method described in Section 4.2.2.1. An appropriate amount of component A containing untreated or functionalized CNTs was mixed using an extrusion process with the suitable amount of the curing agent. Using two syringes the resin A+CNTs and the curing agent were extruded into a mixing dispenser, purchased by Rs Components, that provide a 20 mixing elements in order to ensure a good dispersion. Several DSC aluminum pans were filled with the reaction mixture. The samples (around 10 mg) were then tested with a scanning temperature from 25 °C to 250 °C at 20 °C/min speed.

Every samples were tested pointing out the time passed after the mixing operation. The crosslinking residual enthalpy of every samples were calculated by a integral calculus of the exothermic peak observed from DSC scan for crosslinking reaction.

$$\Delta H = \int_{t_i}^{t_f} dH_p(t)$$

Equation 1 - Total enthalpy calculation

In Equation 1 T_i and T_f are the initial and end temperature at which the crosslinking reaction starts and ends (that means that the integral base line is tangent to the heat flux curve).

Another testing method was performed again starting from A+CNTs samples obtained with dispersion method seen in Section 4.2.2.1. An appropriate amount of component A containing untreated or functionalized CNTs was mixed using an extrusion process with the righteous amount of the curing agent. As already described two syringes containing the resin A+CNTs and the curing agent were exploited to efficiently extrude the samples and to ensure a good dispersion. Several DSC aluminum pans were filled with the reaction mixture. The samples (around 10 mg) were then tested with a scanning temperature from 25 °C to 250 °C at different scanning speed 5/10/20/30 °C/min. The scanning test was started exactly after 10 minutes of the mixing operation in order to study samples with the same crosslinking level. Crosslinking residual enthalpy of every samples were calculated by an integral calculus of the exothermic peak observed for crosslinking reaction.

4.2.4 Electron microscopy

4.2.4.1 Scanning electron microscope

Scanning electron microscope analyses were performed using a Cambridge Stereoscan 360 on different epoxy nanocomposite samples obtained with the dispersion method that produce the crosslinked nanocomposites (see Section 3.2.2.2). That characterization was used in order to determine the morphology and distribution of CNTs. For all the samples studied, fracture surfaces, created after a tensile test conducted until fracture elongation (data non presented in this work), was investigated with SEM characterization. All specimens were sputtered with gold before imaging.

4.2.4.2 Transmission electron microscope

Transmission electron microscope was used to support and to confirm the results, obtained with different characterizations (rheology, conductivity measurements ecc), regarding distribution of CNTs in nanocomposites and the morphology of the different samples. All crosslinked samples were microtomed in 50 nm slices at room temperature with Cryo-ultramicrotomy Leica EM FCS. The samples were then arranged on onto TEM sample support mesh grid. Transmission electron microscope analyses were performed using a Zeiss EM 900 operating at 80 kV.

4.2.5 Rheology characterization

Rheological characterizations were performed using a Rheometrics DSR 200 rheometer in 25 mm plate cone configuration at 40 °C. Steady shear and oscillating experiments were conducted to explore specific rheological behavior of CNT/epoxy suspension. All the samples investigated was prepared with dispersion method described in Section 4.2.2.1, that produce composites without curing agent. Steady shear test were performed for 5 minutes, starting from 0 to around 4500 Pa. The maximum value was chosen from sample to sample considering the viscosity showed by the sample itself.

Oscillating tests instead are conducted in two steps for every specimens. The first step was conducted at 1 Hz and with variable strain measurements in order to determine the linear viscoelastic regime. Within the linear viscoelastic region, the second steps provide a oscillatory measurement scanning the frequency between 10^{-2} and 10 rad/s.

4.2.6 Electrical Characterization

The electrical characterizations were conducted on samples that were prepared using the dispersion method described in Section 4.2.2.2. Following curing, the sample were cut in rectangular specimen of about 30 mm length, 25 mm width and 2 mm thickness, then they were grounded on all sides to obtain a flat and parallel surfaces. The samples were then annealed for 1 hour at 150 °C in order to achieve an almost defined morphology of the conductive network and to reduce the effect induced by residual superficial stress as a result of mechanical polishing. The cross-sectional areas were painted with conductive paint, electronically conductive paint - silver loaded 3g, provided by Rs Components, and then cured for 10 minutes at 150°C to enhance the conductance of the silver paint. 3g silver paint was used to provide a good contact with the two electrodes, that were pressed together on the sample, and to achieve an uniform electric field on the specimens.

All the test were performed with a Keithley 2612 multimeter at room temperature with needle point probe SPP4 S/F, purchased by Multi Contact, that provide a controlled tip's pressure on the specimen. The voltage between the two ends of the sample was varied from 0,1 V to 100 V dividing the scan in 50 steps. In every step the voltage was kept constant for 20 seconds. This long procedure was chosen to reduce the R-C circuit behavior observed in most of the samples, when a fast voltage change was induced. Conductivity of the nanocomposites were then calculated from resistance measurements using Ohm's law.

4.2.7 Electrical Characterization for damage sensing

Electrical characterization were also conducted on different sample in order to study the effectiveness of damage monitoring through resistance measurements.

All sample studied were prepared with dispersion method described in Section 4.2.2.2. After curing steps, all the samples were cut in small rectangular specimen of 20 mm length, 15 mm width and 2 mm tickness, and they were grounded on all sides to achieve a flat and parallel surfaces. Samples were then annealed as described above. The cross-sectional end areas were painted with conductive paint, electronically conductive paint - silver loaded 3g, provided by Rs Components, and then annealed for 10 minutes at 150°C to induce a better conductance of the silver paint. The paint was used to obtain the regular electric field required on the bulk of the specimens. All the test were performed with a Keithley 2612 multimeter at room temperature with needle point probe SPP4 S/F, purchased by Multi Contact, that provide a controlled tip's pressure on the specimens. The voltage was varied from 0,1 V to 100 V dividing the scan in 50 steps. Again every voltage step were kept constant for 20 seconds to reduce the R-C circuit behavior. Resistance was registered for every samples.

All the samples were then notched induced using a razor broching machine. The

machine is designed to notch the sample using a razor, sliding in a perpendicular direction to the one of the indentation, to easily remove the broched material. The razor have an edge curvature of $13\ \mu\text{m}$. This geometry was preferred for the reduced modification induced in the materials around the notch. Different cut depths were performed considering the different width of the sample studied, from $0,005\ a/W$ to $0,7\ a/W$, where a is the notch depth and W is the width of the sample. All the indentation depth are measured with optical microscopy after indentation. Notched samples are then electrically characterized at the same condition as before indentation, like described above. The difference in resistances from the pristine to the indented samples were pointed out.

4.3 RESULTS AND DISCUSSION

4.3.1 Calorimetry

The dispersion of carbon nanotubes into a crosslinking matrix, and in particular CNTs with functional groups on their external wall, could change the effectiveness and the behavior of crosslinking chemistry [18,25]. Moreover, in these thermoset nanocomposites' systems, the knowledge of modification that involve the processing is a focusing point. Differential scanning calorimetry is useful to analyze every change due the incorporation of different functionalized nanotubes into epoxy matrix. As described in Section 4.2.3 two different methodologies, with different objectives, were studied with calorimetric characterization.

The first procedure want to measure the total enthalpy of the crosslinking reaction and how the insertion of different functionalized carbon nanotubes could change this value. Pristine resin, as described in Section 4.2.1, starts to crosslink in the exact time in which the component A is mixed with the curing agent. This could make quite hard to measure the total enthalpy involved in the crosslinking reaction. In our study we took samples with different extent of reaction. Practically it involves, as seen in Section 4.2.3, to test samples at different time after the preparation of the specimen, i.e. the start of the crosslinking reaction, and to measure the residual crosslinking enthalpy, which results in the range of 305-312 J/g.

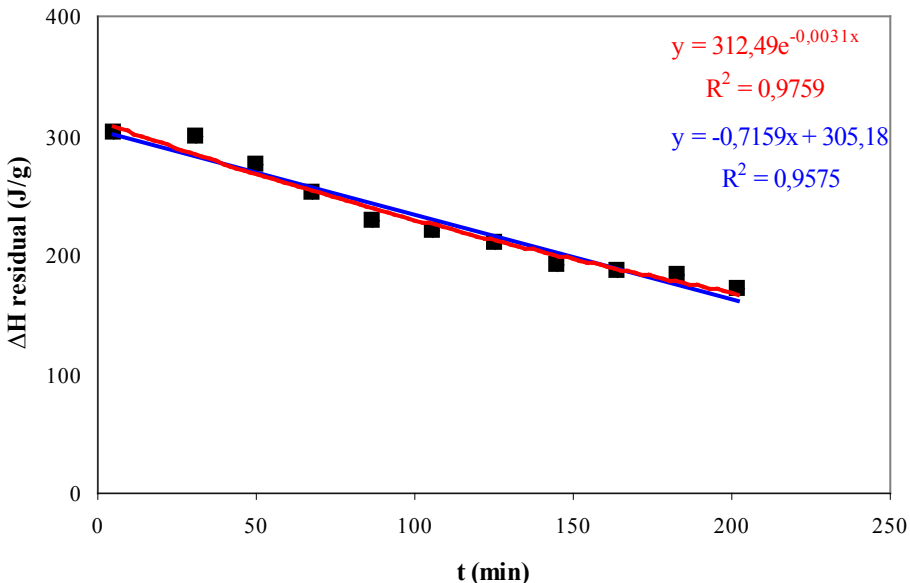


Figure 4 - Linear (blue line and blue coloured equation) and exponential (red line and red coloured equation) interpolation of residual ΔH of crosslinking reaction for composites with 0,1 %wt of CNT

The results for every sample are then plotted in graph, see an example in Figure 4. The linear and exponential regression of the residual enthalpy of the crosslinking reaction permit to extrapolate the enthalpy at time zero, i.e. the total crosslinking enthalpy.

Each sample tested shows the same behavior observed in Figure 4 for nanocomposites with 0,1 %wt of untreated CNT. The linear and exponential regression of the residual crosslinking enthalpy were always obtained with a R^2 values superior to 0,92 indicating the goodness in those interpolations.

Figure 5 shows the results of the extrapolation of total crosslinking enthalpy for all the samples. As could be seen the difference between the reaction enthalpy of the composites and the $\Delta H_{\text{crosslink}}(t=0)$ of the neat resin are quite similar for every composition and for every CNTs functionalization studied. The only significant change observed is with specimens with the 3 %wt presence of carbon nanotubes (untreated and carboxy-functionalized)

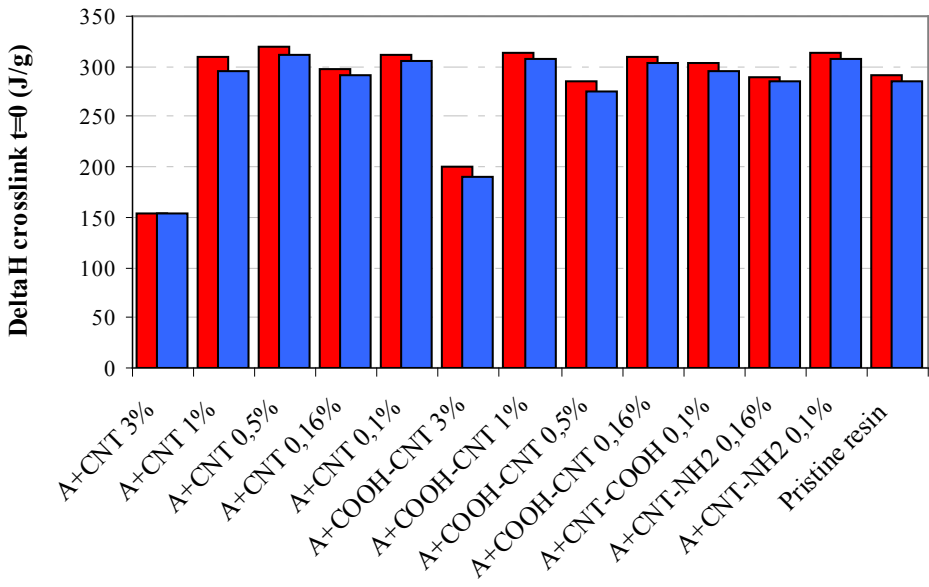


Figure 5 - $\Delta H_{\text{crosslink}}$ extrapolated at starting reaction time ($t=0$) from the $\Delta H_{\text{crosslink}}$ residual of samples containing different functionalized CNT. Red values are obtained with exponential interpolation, blue values are obtained with linear interpolation.

Any change in crosslinking enthalpy is intrinsically correlated with an alteration in chemical bonds that interact in the reaction. Therefore, the absence of modification in $\Delta H_{\text{crosslink}}(t=0)$ values, suggests that the concentration of the carbon nanotubes in the composites are too low to actively interact in the crosslink reaction. Moreover the carbon nanotubes functionalities, present on the external wall, introduced in the system, are definitely in lower number respect the amount of epoxy and curing

functionalities. This modest quantity indeed reduces the possible interaction with the crosslinking functional groups, and give a quite constant total enthalpy values.

The only change observed is with the highest concentration investigated (3 %wt with untreated and carboxylic-functionalized carbon nanotubes respect the A component). It could be hypothesized that with this relative high CNTs concentration, an effectively interaction among epoxy and carboxylic functionalities could be possible in the nanocomposite systems.

The second calorimetry procedure is focused on activation energy of the crosslinking reaction, and how the composition and the different chemical functionalities presented by CNTs could modify those values.

As described in Section 4.2.3, different specimens were prepared and tested from 25 °C to 250 °C at different scan speed (5, 10, 20, 30 °C/min). Moreover, samples were tested at the same time (10 minutes) after the start of the crosslinking reaction, i.e. the different specimens are at the same extent of reaction, in order to keep constant that variable. That procedure permits to analyze how the exothermal reaction is changed by different heating speed.

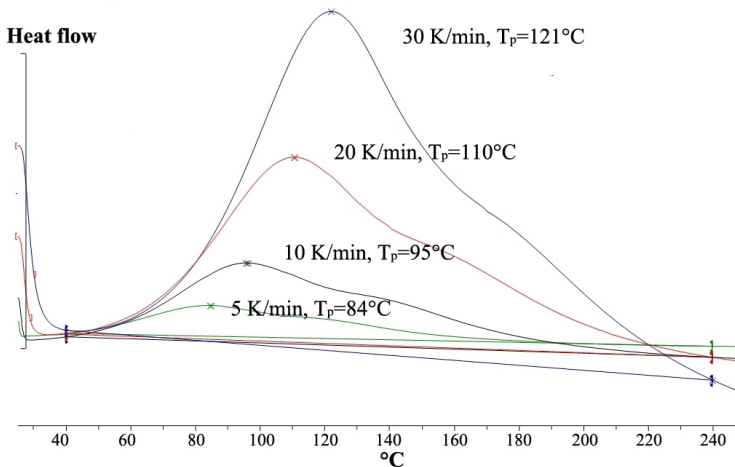


Figure 6 - Differences in crosslinking temperature peaks at different scanning speed observed for the sample containing 0,1 %wt of CNT.

As the Figure 6 shows, at different heating speeds, a different exothermal peak value is presented (T_p). With slow heating speed (5 °C/min) the crosslinking reaction is spread over great time, and this permit to the crosslinking chains to rearrange with theirselves. The maximum height of the exothermal peak show with this slow speed is at a lower values than that observed for fast heating rate (30 °C/min) in which the reaction is quickly conducted.

Values of exothermal peak are related with scanning speed (β) and activation energy E_a of the crosslinking reaction through two empirical equations named after their authors (Kissinger and Ozawa) ^[49], reported in Equation 2 and Equation

3.

$$\ln \frac{1}{\beta} = \frac{E_a}{R * T_p} + \text{constant}$$

Equation 2 - Ozawa equation

$$\ln \frac{T_p^2}{\beta} = \frac{E_a}{R * T_p} + \text{constant}$$

Equation 3 - Kissinger equation

With easy graphical calculations, the E_a values of different samples are obtained from the analyzing of DSC results. Figure 7 shows that no significance difference in activation energy is observed for every samples containing untreated, carboxylic and amino-functionalized carbon nanotubes. Moreover, no change in activation energy is observed for different CNTs concentrations.

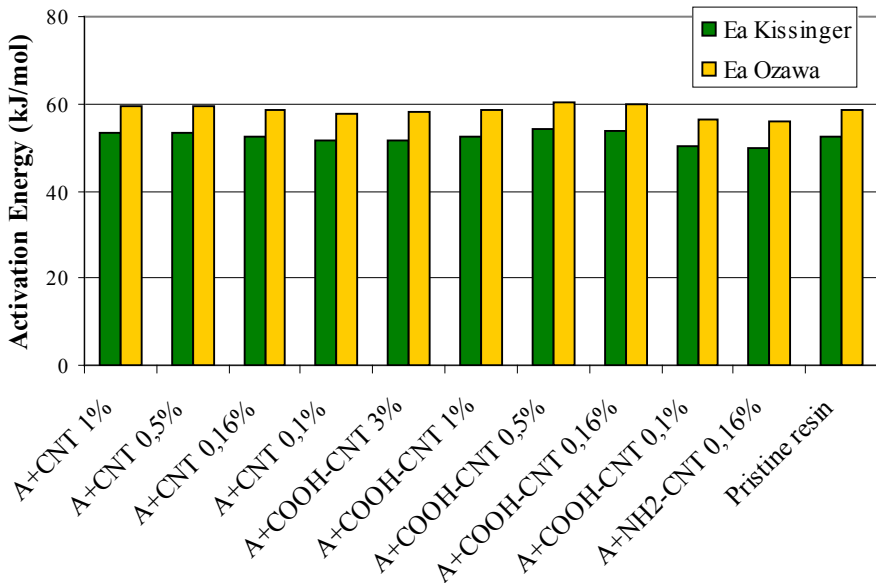


Figure 7 - Activation energy obtained from DSC data for different samples using Ozawa and Kissinger equations.

The analysis of data could be explained again by the low concentration of functionalized group inserted in the nanocomposite system, via the presence of carbon nanotubes. Those low number functionalities practically couldn't interact with the epoxy groups of the matrix.

As could be seen with differential scanning calorimetry, the insertion of different functionalized (untreated and modified) carbon nanotubes doesn't modify the crosslinking reaction from a thermodynamic and kinetic point of view. The presence of carbon nanotubes doesn't impact the processing of those composite and permit to go forward with the well known classical formulations of epoxy polymers.

4.3.2 Rheological Characterization

The rheological properties of polymer/CNT suspension play a crucial role in processing and manufacturing of such nanocomposites [13,18-28]. Moreover, this characterization is the main indicator of the quality of dispersions and how uniformly CNTs are distributed in the polymer matrix, and give crucial information on different morphologies of carbon nanotubes' network structures [13,18-25].

As described in Section 4.2.5 the samples studied are prepared with the dispersion of different functionalized carbon nanotubes (untreated, carboxylic and amino functionalized) in A component of the resin, and are characterized at 40°C.

4.3.2.1 Steady shear rheology

The A component of the resin shows a Newtonian behavior, and this is altered by the presence of carbon nanotubes.

As quickly described in Section 4.2.2.1, steady shear characterization is firstly studied to confirm the goodness of the dispersion method. As could be seen in Figure 3 for suspension with 0,5 %wt of untreated carbon nanotubes, and in Figure 8 for COOH-CNT at 0,1 %wt, the dispersion method shows a high repeatability between the same sample and in comparison with different samples with same CNTs concentration. Same results could be observed in composite containing NH₂-CNT.

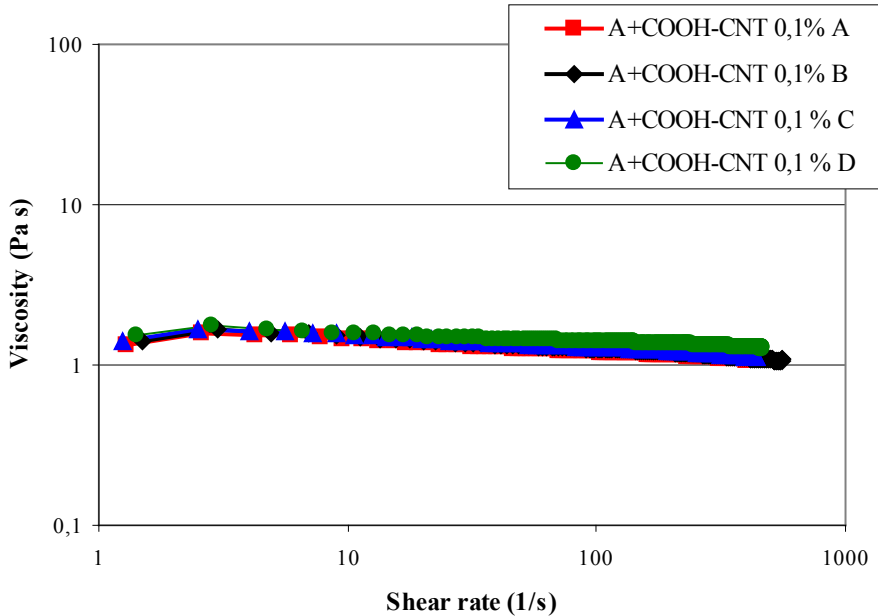


Figure 8 - Shear rate curves at 40°C for different dispersion containing 0,1 % of COOH-CNT. A), B) curves are different curves on same dispersion, C) shear rate curve on different dispersion with the same composition of 0,1%wt of COOH-CNT, D) shear rate curve of dispersion containing 0,1% of commercial carboxylated CNT.

Figure 9 shows the behavior of the dispersions of untreated CNT in epoxy polymer. As expected, and already seen in the dispersion preparation, the viscosity values increase with the raise of nanotubes concentration. This rise in viscosity is clearly seen especially for low shear rate values. The behavior change from a Newtonian fluid for the neat epoxy to a shear thinning one even at low CNT concentrations.

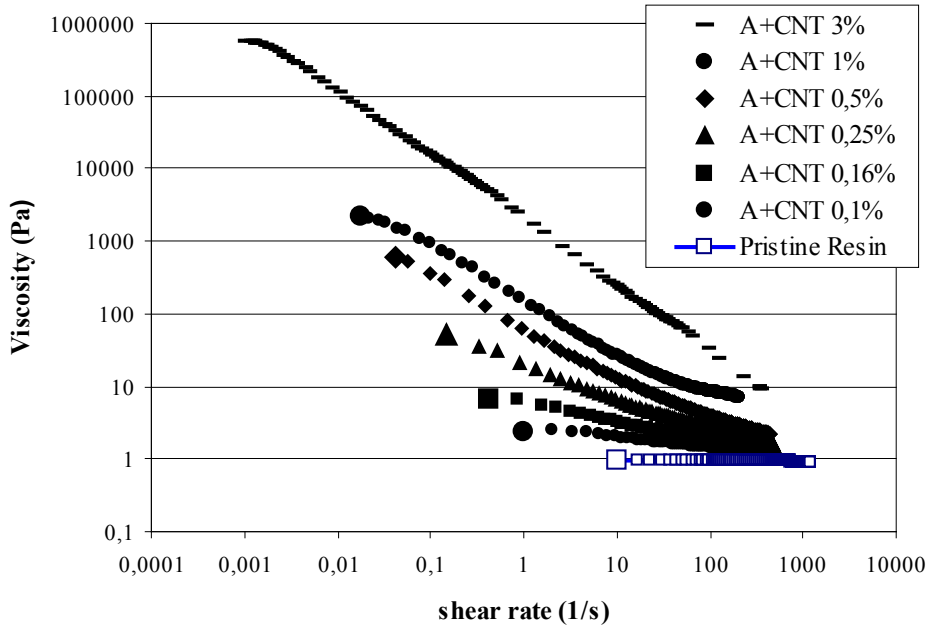


Figure 9 - Shear rate curves at 40°C for pristine resin and for nanocomposites with CNT at different concentrations.

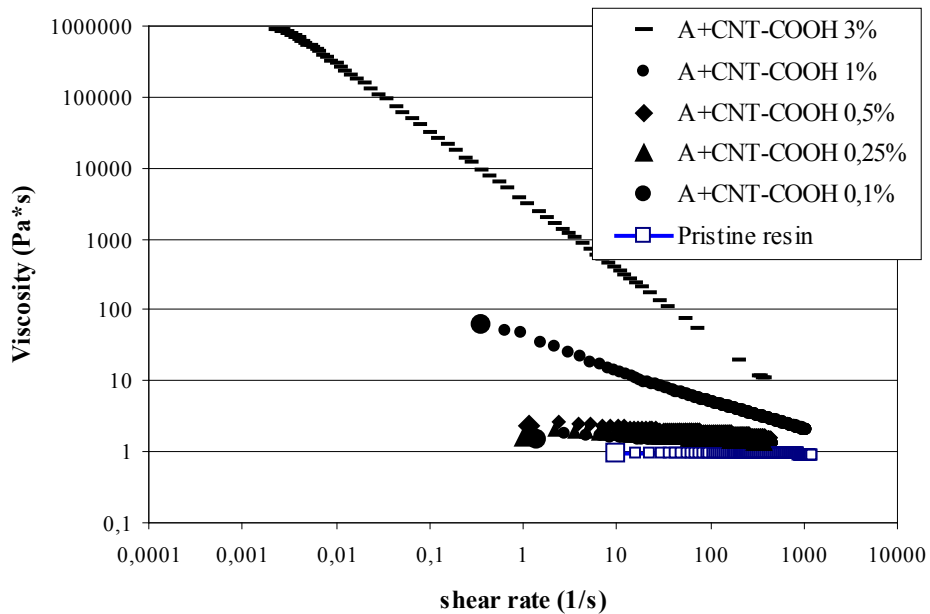


Figure 10 - Shear rate curves at 40°C for pristine resin and for nanocomposites with COOH-CNT at different concentrations.

The same behavior is observed in literature^[13,18-21]. The up to now main explanation for this pseudo-plastic behavior, observed in shear rate tests, implies the creation of interconnected CNTs network that partially stops the flowing of polymer matrix creating a gel-like behavior^[13,18-21].

Rheological characterizations on nanocomposites prepared with functionalized CNTs are even more interesting and a complex interpretation is required.

As Figure 10 shows, even for dispersion containing COOH-CNT, an increase in viscosity is observed with the rise of carbon nanotubes concentration. Notwithstanding this, a clear shear thinning behavior is observed only at the concentration higher than 1 %wt.

Same behavior is observed in some articles in literature, and a not completely supported theory is pointed out^[19,20]. In these articles the cause of this changing behavior between different nanocomposites was related to the low aspect ratio values of carboxylated CNT^[19,20]. Those functionalized CNTs, after oxidation, show a lower length than untreated nanotubes. This morphology change make more difficult the creation of the interconnected CNTs network that provide the shear thinning behavior. This theory is not supported by our TEM results as seen in Chapter 3 and here reported.

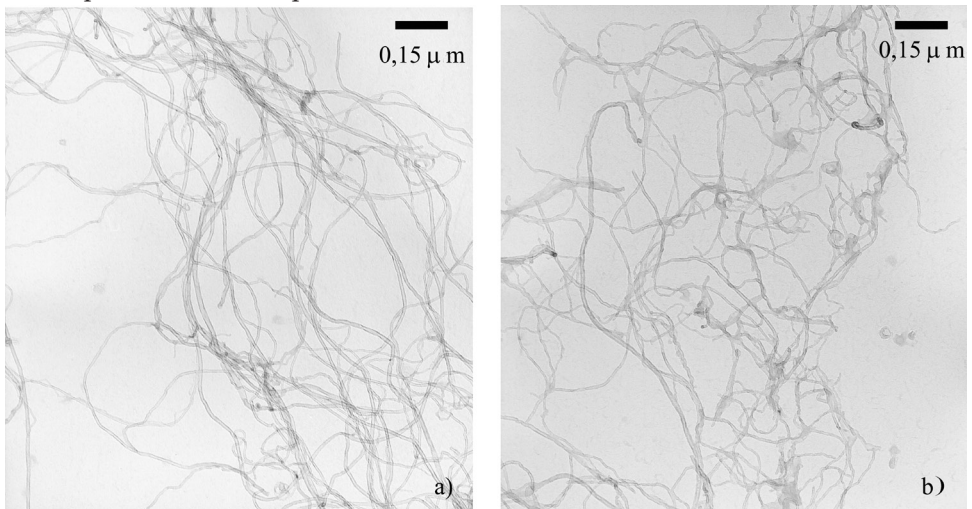


Figure 11 - TEM images of different functionalized CNTs: a) untreated CNT, b) COOH-CNT. The sample are dispersed in acetone and then casted on TEM grid.

No clear modification in aspect ratio could be observed for carboxy-functionalized carbon nanotubes, not supporting the explanation proposed in literature.

The cause of different behavior of functionalized CNTs, for the moment, remains under investigation. A more complex interpretation needs to be confirmed with oscillating rheological characterization described in Section 4.2.5.

Figure 12 compares the shear rate results for dispersions with untreated and

carboxylated nanotubes. As could be seen the viscosity values showed by dispersion with untreated CNT are far higher than the values of the dispersion with COOH-CNT at the same concentration.

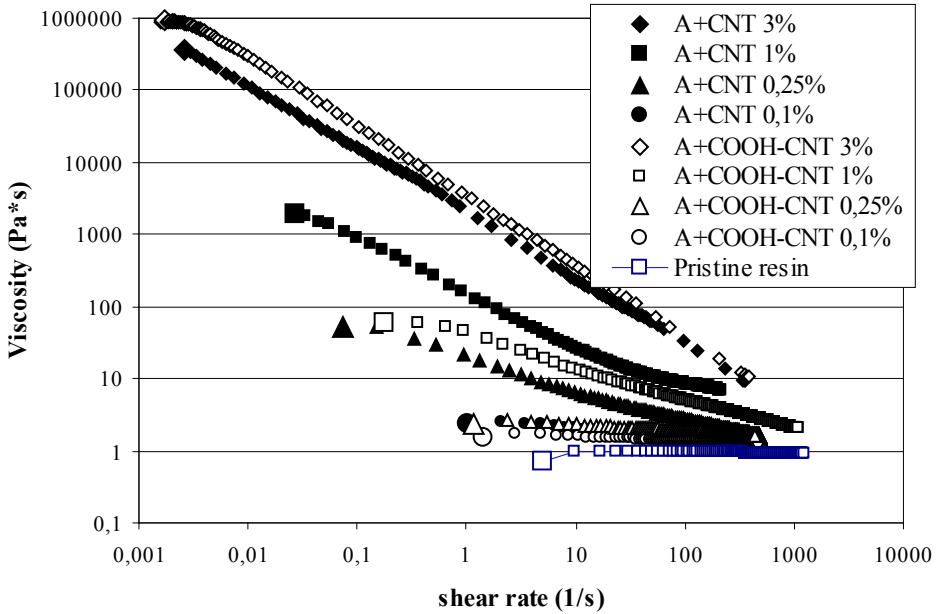


Figure 12 - Shear rate curves at 40°C of nanocomposites containing untreated CNT (black symbols) and COOH-CNT (white symbols).

Moreover, Figure 12 underlines the quickly increase of viscosity showed by composite with COOH-CNT at concentration above 1 %wt, that reach the shear thinning behavior of dispersions containing untreated CNT. Investigating the steady shear performances of the nanocomposites containing amino-functionalized CNT, a behavior similar with the one already seen for dispersion including COOH-CNT could be observed.

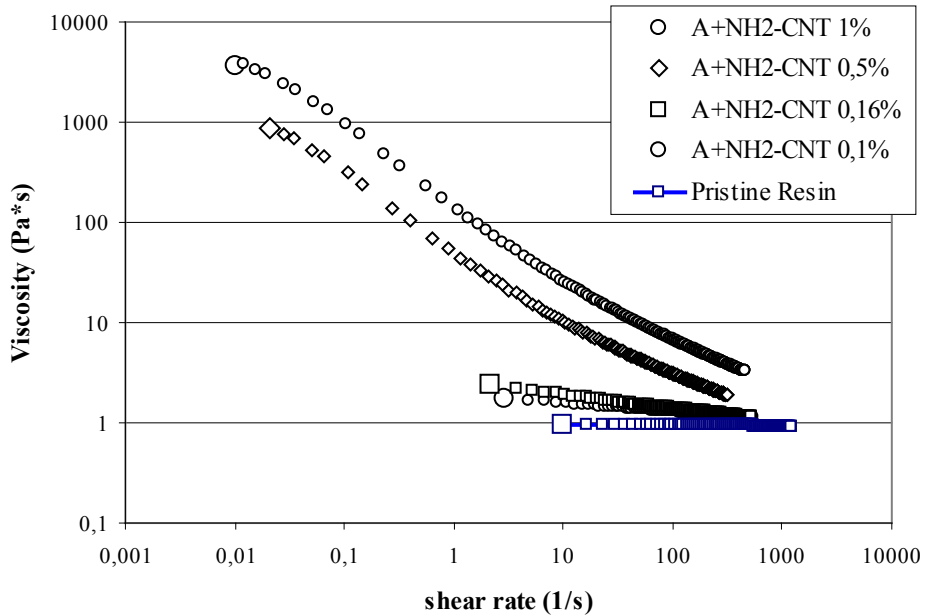


Figure 13 - Shear rate curves at 40°C of nanocomposites containing NH_2 -CNT.

Figure 13 points out that the change, from Newtonian to shear thinning behavior, happens only for high concentration of NH_2 -CNT, even if this alteration happens at lower concentration than that observed for COOH -CNT. For more detailed observations see Figure 14. The change in behavior for composites containing NH_2 -CNT happens around the concentration of 0,5 %wt, instead of the dispersions containing COOH -CNT in which this alterations is visible only at 1 %wt.

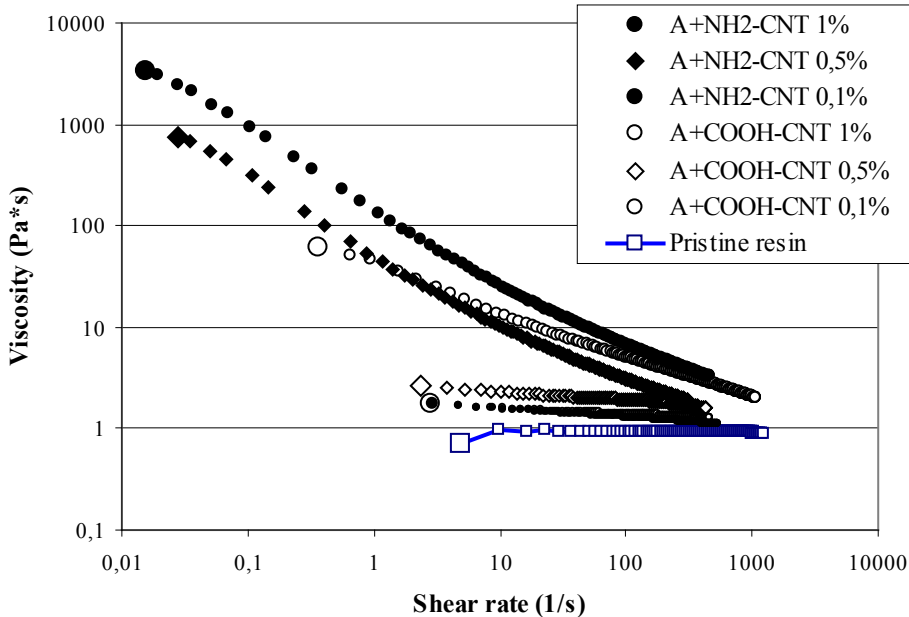


Figure 14 - Shear rate curves at 40°C of nanocomposites containing NH₂-NT (black symbols) and COOH-CNT (white symbols).

As already stated in Chapter 3, the amino-functionalization didn't evidently change the aspect ratio of the carbon nanotubes and so the observed performance is not related to a change in length of CNTs.

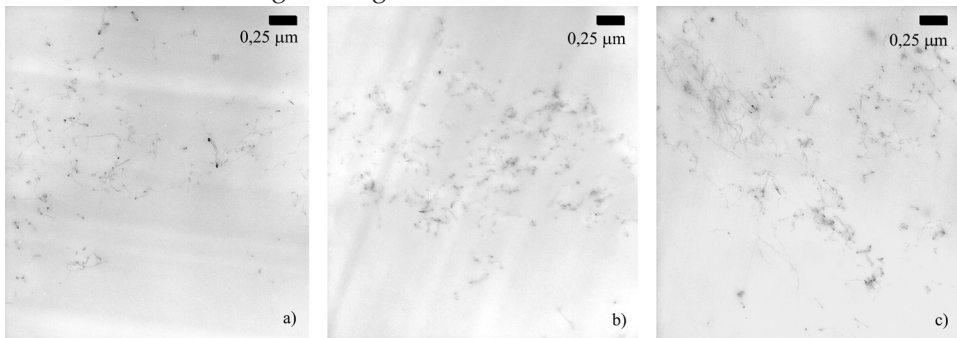


Figure 15 - TEM images of microtomed nanocomposites containing different CNTs: a) untreated CNT, b) COOH-CNT and c) NH₂-CNT.

Unfortunately Figure 15, as other TEM images, could only give a draft of the real dispersion of the different functionalized carbon nanotubes in epoxy matrix. The dispersed CNTs show a similarly good and homogenous dispersion in polymer matrix. Those different behaviors observed for nanocomposite containing dissimilar functionalized carbon nanotubes, could strongly depends only on the

diverse morphologies of the CNTs dispersion in polymer matrix. And as already stated in Chapter 1 the quality of dispersion depends directly to the differences in groups functionalities on the CNTs' external wall. A more detailed study will be made with oscillating rheological characterization.

Moreover, considering the processability of those nanocomposites, COOH-CNTs dispersed in polymer matrix show great benefits. These nanocomposites show a viscosity lower than the other carbon nanotubes filled polymer matrices at the same concentration (see Figure 16), permitting an easy flowing during processing, that is always advisable ^[20].

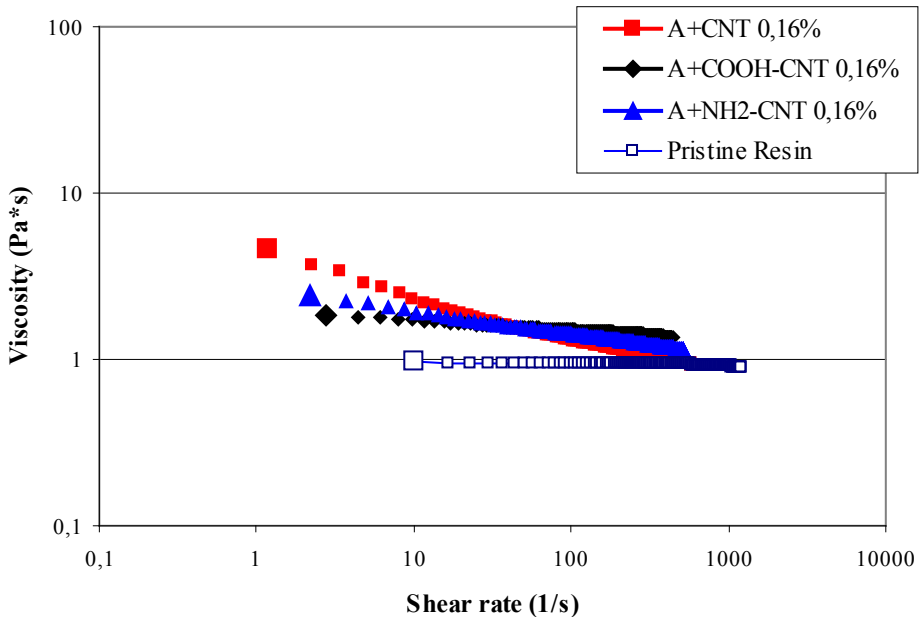


Figure 16 - Shear rate curves at 40°C of pristine resin and of dispersions containing: untreated CNT (Red symbols), COOH-CNT (black symbols) and NH₂-CNT (blue symbols) at concentration of 0,16 %wt.

4.3.2.2 Oscillating rheology

Oscillating rheological characterization and tracking the crossover value between moduli, is one of the best way to focusing on the evolution of a developing CNTs' network structure and CNTs' dispersion morphologies ^[13,18-23].

All the measurement, as already stated in Section 4.2.5, are conducted at 40°C. Analyzing the results, firstly we found that the dispersions containing untreated CNT show an increase in both storage modulus G' and the loss modulus G'' with the increasing concentration of CNTs. Figure 17 shows specifically the increase of G' with the raise of CNT in the dispersions. Moreover, storage modulus curves

show an independence from the frequency for the CNTs concentrations above 0,16 %wt. This plateau behavior of G' indicated the starting point of solid like performances of the nanocomposites. Literature, already discussed, describe this phenomena with the formation of entanglements or an interconnected network that rules the behavior of the nanocomposites [13,18-23].

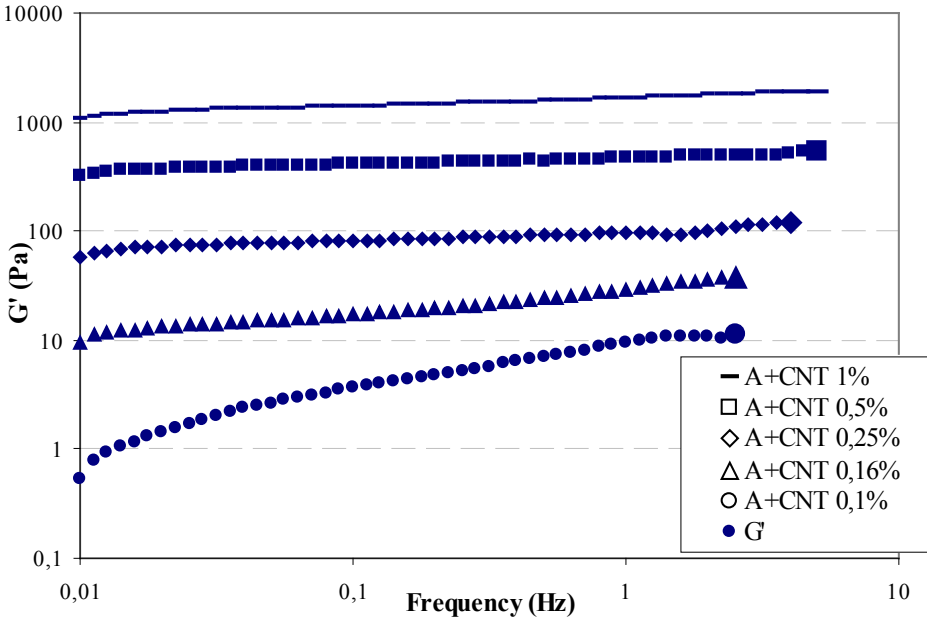


Figure 17 - Characterization of linear viscoelastic regime at 40 °C. Storage Modulus G' of dispersions containing untreated CNT at different concentrations.

In order to better investigate the developing of CNTs' network, is useful to analyze the presence of crossover between G' and the loss modulus G'' .

Figure 18 permits to observe the different behavior at increasing concentration of the composite with untreated CNTs.

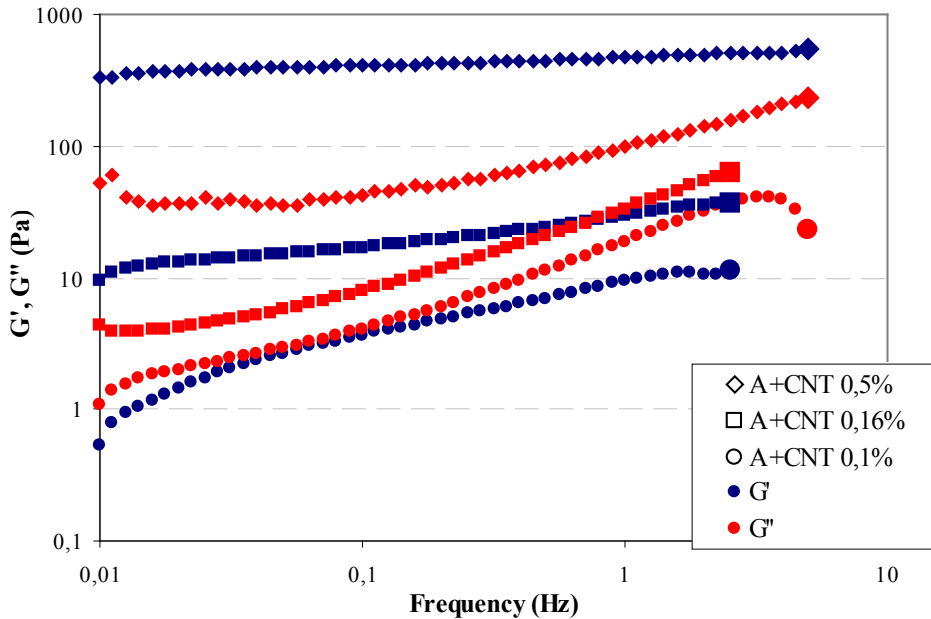


Figure 18 - Characterization of linear viscoelastic regime at 40°C. Storage Modulus G' (blue symbols) and Loss Modulus G'' (red symbols) of dispersion containing untreated CNT at different concentrations.

Dispersion with 0,1 %wt of CNT shows that the behavior is ruled by the loss modulus. At that low concentration, as observed in literature, the network is not so interconnected to let the nanocomposite behave like a solid. At 0,16 %wt of CNT a crossover point between the storage modulus and G'' is observed. The presence of this behavior points out a change in nanostructure, that leads from liquid-like to solid-like performances. For higher concentrations (above 0,16 %wt of CNT) G' have always a higher values than G'' (no more crossover point is observed), confirming the percolation threshold around 0,16 %wt and the change to a pseudo-plastic fluid behavior. This change is caused by the formation of a stronger interconnected network of CNTs that rule the rheological performances.

Determination of the percolation threshold based on the development of a shear thinning behavior could be better analyzed with Figure 19 a) as proposed recently in literature ^[21].

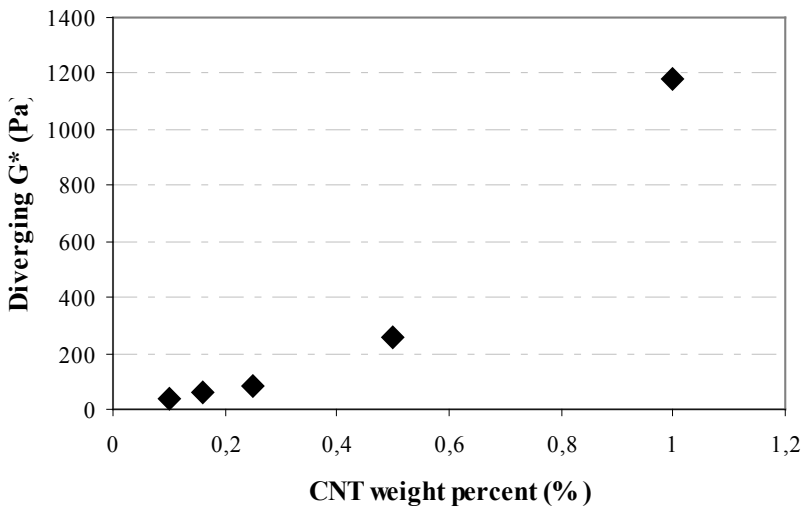
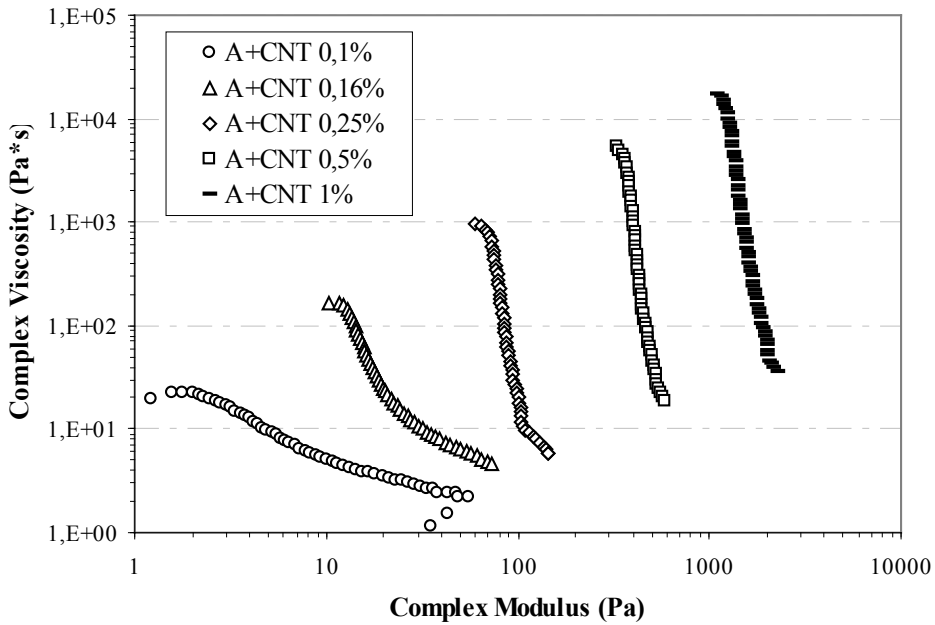


Figure 19 - Divergence plot of complex viscosity and complex modulus showing development of yield stress of dispersions containing untreated CNT at different concentration, at 40°C, above figure, Diverging Complex modulus, at 40°C, against weight loading for nanocomposites with CNT, below figure.

The plot of the overall flow resistance η^* against the overall deformation resistance G^* reveals divergent complex modulus behavior. Complex viscosity shows a decrease of an order of magnitude at constant value of G^* . That behavior is interpreted as pseudoplastic performance that appears for more than 0,16 %wt CNT content. With increasing concentration can be observed that this behavior becomes more prominent. The observed divergent complex modulus, i.e. the difference between the maximum and the minimum values of G^* , is plotted against CNT concentration in Figure 19 b). A rising in diverging modulus is more evident above concentration of 0,16 %wt.

Analyzing the nanocomposites containing COOH-CNT, a similar behavior is observed at different CNTs concentrations.

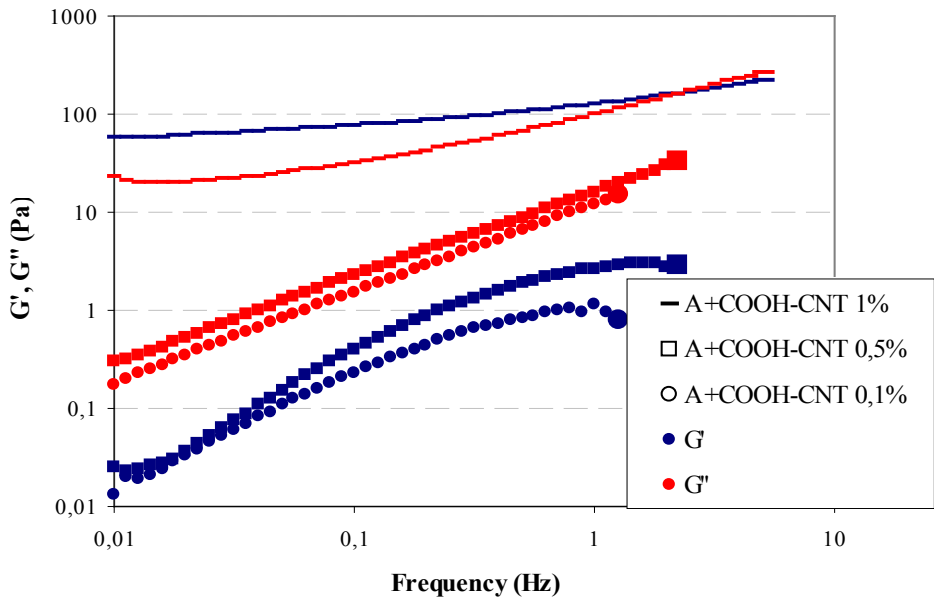


Figure 20 - Characterization of linear viscoelastic regime. Storage Modulus G' (blue symbols) and Loss Modulus G'' (red symbols) of dispersion containing COOH-CNT at different concentrations.

The solid like behavior for those dispersions is observed only at 1 %wt concentration as could be observed in Figure 20. At 1 %wt content of COOH-CNT, the storage modulus finally rule over G'' . Storage modulus shows a plateau behavior only at this high content of carbon nanotubes, even if a crossover point could be observed at higher frequencies. Hence a strong interconnected network is not formed, in dispersions containing COOH-CNT, until 1 %wt is reached.

Again it's useful to plot complex viscosity against complex modulus. Figure 21 a) confirms that only for concentration around 1 %wt the complex viscosity crumble down at constant G^* . Moreover the diverging modulus is observed only at this high concentration (Figure 21 b).

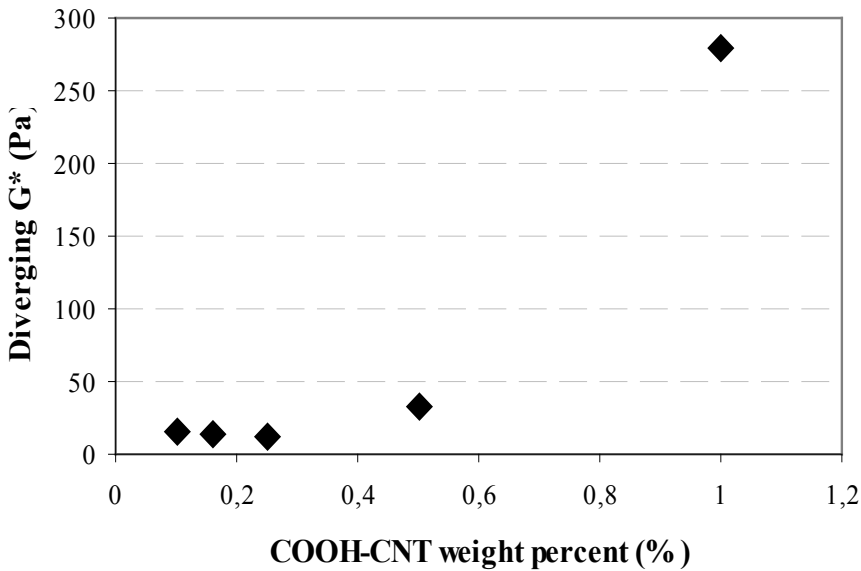
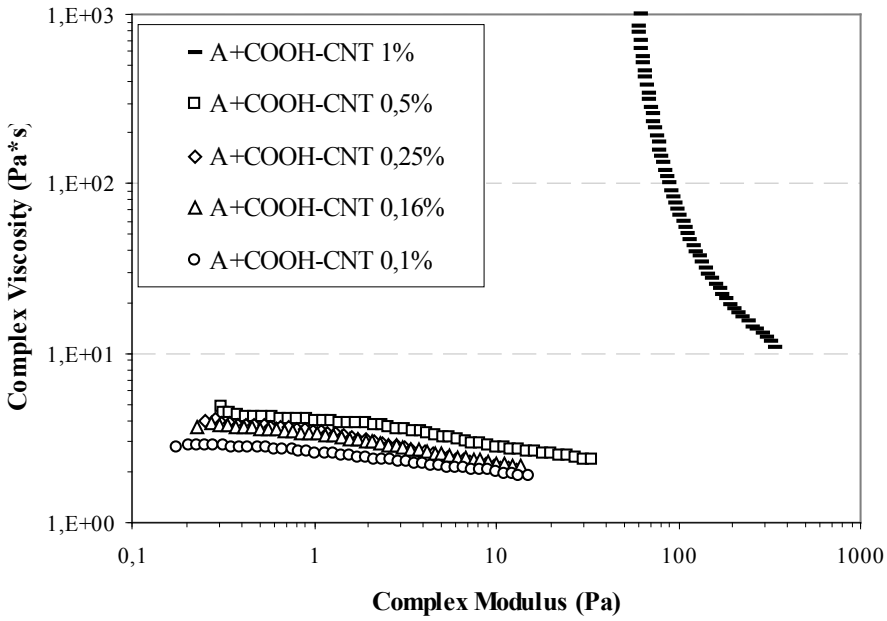


Figure 21 - Divergence plot of complex viscosity and complex modulus showing development of yield stress of dispersions containing COOH-CNT at different concentration at 40°C, above figure, Diverging Complex modulus, at 40°C, against weight loading for nanocomposites with COOH-CNT, below figure.

Summing up, nanocomposites with COOH-CNT create a strong interconnected network only at a higher concentration than untreated CNT. This difference is not due to different aspect ratio, as suggested in recent literature, as already stated in Section 4.3.2.1.

This phenomena is probably connected with the different functionalities present in the external wall and then with the difference ability of CNTs to disperse in polymer matrix.

COOH-CNTs, as seen in Section 3.3.2, show a better dispersion in different solvents. This behavior is confirmed also in polymer matrix (see Figure 15) with TEM characterization.

SEM characterization of fracture surface could show some better differences in morphology for the composites obtained with different functionalized CNTs.

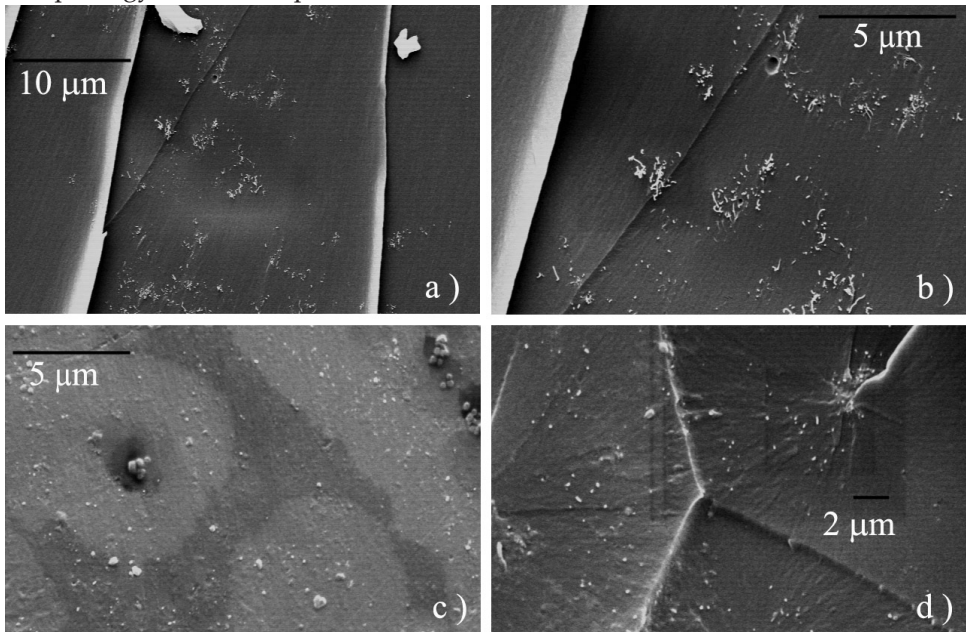


Figure 22 - Sem images of fracture surfaces obtained via tensile test for nanocomposites containing different CNTs: a), b) untreated CNT at 0,1 %wt, c), d) COOH-CNT at 0,1 %wt.

As could be observed in Figure 22 a), better dispersion and distribution of carboxylic carbon nanotubes is present also in the A component of resin. Figure 22 a) and Figure 22 b) clearly show a not dispersed agglomerate of untreated CNT in the nanocomposites. This confirms that the dissimilar behavior observed in oscillating rheology is due to the different functionalization that could rule the formation of different interconnected network.

COOH-CNT are broadly dispersed and this could cause a less interconnectivity of the network till a higher concentration of carbon nanotubes is reached. This lead us to hypothesize that the enhancement of pseudo-plastic behavior, i.e. a strong

interconnected network, is possible if some agglomeration, as the ones observed in dispersions with untreated CNT, is present.

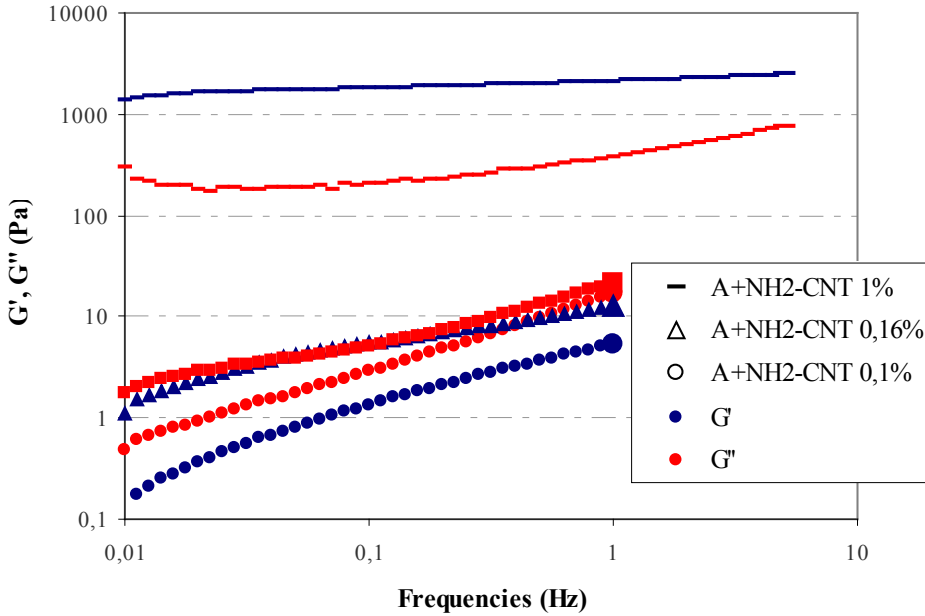


Figure 23 - Characterization of linear viscoelastic regime at 40°C. Storage Modulus G' (blue symbols) and Loss Modulus G'' (red symbols) of dispersion containing NH_2 -CNT at different concentrations.

The composites with NH_2 -CNT show a similar behavior. Figure 23 shows a crossover point for composite with 0,16 %wt of amino carbon nanotubes.

For dispersion with higher content than 0,16 %wt, the plateau of G' could be easily observed and storage modulus rules the pseudoplastic behavior. The percolation point could be pointed out around 0,16 %wt, even if a double crossover point is observed. This strange behavior, obtained for different specimens with the same 0,16 %wt concentration, is still under investigation.

Figure 24 shows the detailed analysis on percolation point. Again a decrease in complex viscosity, at a constant value of G^* , is observed starting from 0,16 %wt (see Figure 24 a). The rising of a diverging modulus could be ideally started exactly at 0,16 %wt (see Figure 24 b), at which the pseudoplastic behavior begins to rule the performances and a strong interconnected network is created. As could be seen the concentration of percolation are quite similar with the one observed for dispersion containing untreated CNT.

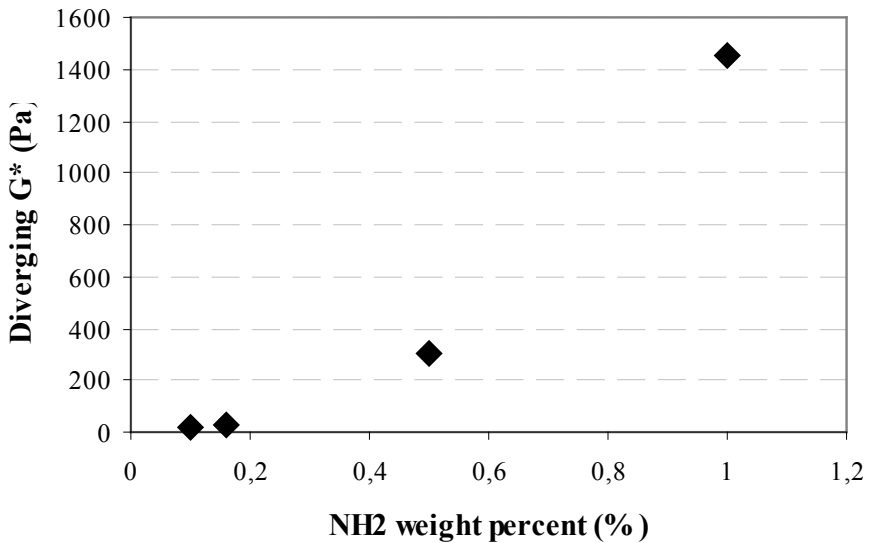
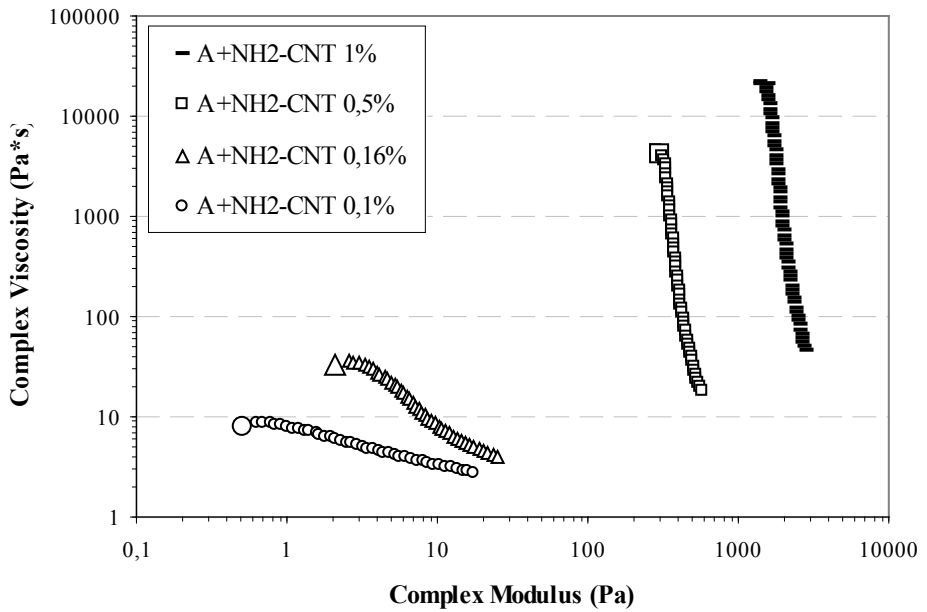


Figure 24 - Divergence plot of complex viscosity and complex modulus showing development of yield stress of dispersions containing NH₂-CNT at different concentration, at 40°C, above figure, Diverging Complex modulus, at 40°C, against weight loading for nanocomposites with NH₂-CNT, below figure.

Summing up, for concentration below the percolation threshold, the response observed in rheological characterization suggests a developing nanotubes network structure, that become interconnected as the concentration is raised. An interconnected structure is formed and a percolation behavior is observed. For higher concentration the structure is saturated in a tight network, and partial agglomeration could happens between the carbon nanotubes encouraging the pseudo-plastic behavior. Moreover this developing network is intrinsically structured by the dispersion capability of different functionalized carbon nanotubes as firstly stated in this study.

4.3.3 Electrical conductivity characterization

Induced electrical conductivity with the insertion of carbon nanotubes into insulating polymer matrix, is far beyond the most promising properties modification in CNTs nanocomposites [6,11,12,19,33]. Literature is increasingly working on inducing and controlling such property change. Moreover, electrical conductivity could be a good characterization used to understand the different morphologies of CNTs into the matrix, revealing the different network into which carbon nanotubes aggregate with their self [35,39].

Pristine epoxy resin, based on DGEBA, shows, from literature data, a conductivity of around 10^{-20} S/m, which is beyond the sensitivity of instrumentation available. Similar insulating behaviors, that it is outside the instrumentational limit, were observed also for some nanocomposites.

Figure 25 shows all the results obtained for different nanocomposites containing the three functionalized carbon nanotubes studied, i.e. untreated CNT, COOH-CNT and NH_2 -CNT.

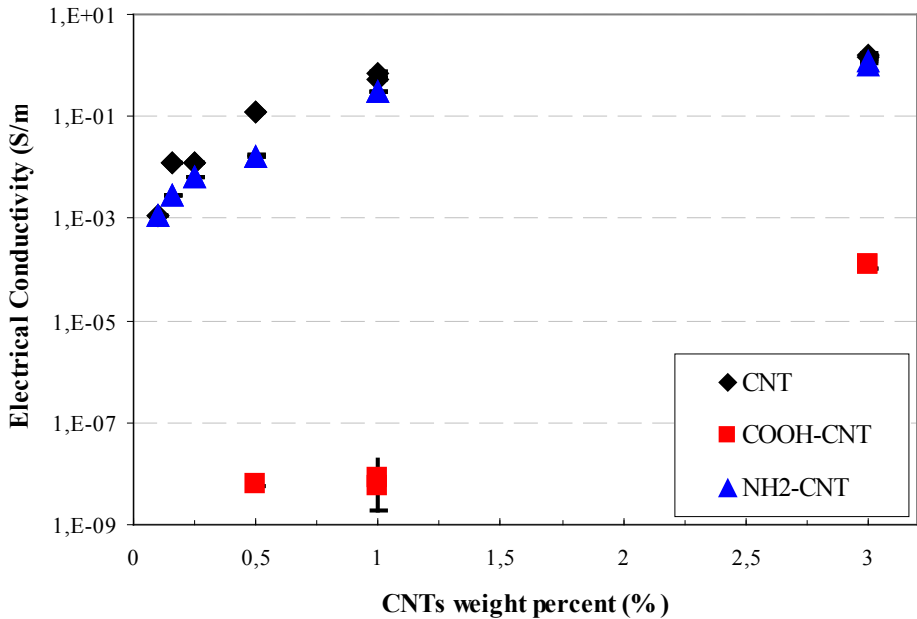


Figure 25 - DC conductivity of nanocomposites containing different CNTs: untreated CNT Black diamond symbols, COOH-CNT Red square symbols, NH₂-CNT Blue triangle, versus CNTs concentrations.

As could be seen for every samples studied, the error bar showing the oscillation of the measure, is quite small.

Concerning the nanocomposite containing untreated CNT (black diamond symbols), a good result is obtained even at the lowest CNT's concentration investigated. As Figure 25 shows, a measurable conductivity is observed with the insertion of 0,1 %wt of CNT in insulating epoxy matrix. A change from insulating to a conductive performance is gained by the insertion of carbon nanotubes.

The trend observed for nanocomposites with untreated CNT is similar to the trends analyzed in literature ^[6,11,12,19,30,33,35-39]. Moreover, the plot looks similar to those commonly presented for the electrical percolation transition in DC conductivity as a function of filler content ^[19,35-39]. A great increase from insulating behavior is caused by insertion of CNTs, then a plateau for conductivity is reached and no further increase in conductivity could be observed when more nanotubes are inserted. Performances at lower concentrations suggest that when small quantities of CNT (below 0,1 %wt) are added, a percolative tail behavior is displayed. Starting from those analysis an hypothetical percolation point, from insulating to pseudo-conductive behavior, could be pointed out below 0,1 %wt of CNT. This concentration of electrical percolation is below the one observed for rheological percolative behavior, that was around 0,16 %wt.

If we focus our attention to the electrical conductivity of the composite containing amino-functionalized CNT (blue triangle symbols), Figure 25 shows a similar performance to the one observed for dispersion with untreated CNT, and similar conclusions could be pointed out.

Again a plateau behavior for highest concentration and a percolation behavior could be observed. An hypothetical percolation changing point, from insulating to pseudo-conductive behavior, could be assumed at a concentration below 0,1 %wt.

Carboxylic functionalized carbon nanotubes inserted in polymer matrix, as observed with rheological behavior, show a similar behavior only at higher concentration.

Following the plot for nanocomposites containing COOH-CNT in Figure 25 (red squared symbols), it could be seen that at low CNTs' concentration (below 0,5 %wt) the conductivity is far too low to be measured by our instrumentation. At 0,5 %wt and at 1 %wt the conductivity plot shows a pseudo insulating behavior with a plateau. The conductivity start to increase only at higher COOH-CNT content, 3 %wt. For these nanocomposites couldn't be roughly hypothesized the percolation concentration above which the material change from insulating to pseudo-conductive. That value is above the investigated concentration's range of 3 %wt.

As could be seen in Figure 25 for every nanocomposite investigated, the insertion of carbon nanotubes changes the electrical behavior. The percolative change from insulating to pseudo-conductive is clearly explained, and here confirmed, with the formation of a network of carbon nanotubes, that could conduct the electrical charge inside the insulating polymer matrix. In literature works, the presence and the rules of this conductive network in the electrical percolative behavior, here observed, are analyzed ^[19,35-39].

As could be observed for nanocomposite containing untreated CNT and NH₂-CNT, the electrical percolation points are at lower concentration than the values observed for rheological characterization.

In literature, rheological percolation point is related, and here confirmed see Section 4.3.2, to the existence of a physical network constituted solely by carbon nanotubes interactions, an not by polymer chain/nanotubes interaction that permit the change in behavior ^[19,21,30]. So a physical contact between nanotubes is required for rheological percolation. No such contact is necessary for electrical percolation, because that is due by an hopping, tunneling process, mechanism. According to some detailed literature the electron hopping mechanism operate with tube-tube distances close to 5 nm ^[19]. This confirm that fewer nanotubes are required for electrical percolation threshold than for rheological percolation in which it is necessary a CTNs' touching interconnectivity.

Moreover, as the plateau behavior suggests, after a interconnected network is reached, the induced electrical conductivity couldn't increase further. Indeed the

carbon nanotubes are, in this structure, still touching each other and a maximum level of efficiency of charge transfer is reached.

As observed before in Section 4.3.2, nanocomposites with COOH-CNT behave in slightly different way. The higher electrical percolation value, here observed, in comparison with the values obtain for the composite with other functionalized carbon nanotubes, suggests that the minimum distance of 5 nm between close nanotubes is reached only at a concentration above the 1 %wt of COOH-CNT. In rheological way the nanocomposites with COOH-CNT show a higher percolation threshold above 1 %wt. This phenomena confirms the theory advanced in Section 4.3.2. Carboxylic-functionalized nanotubes, inserted in polymer matrix, create a more dispersed nanotubes structure that creates an efficient hopping network and a interconnected network only with high content of CNTs (above 1 %wt). Different functionalities, like carboxylic, that show a more easily dispersive carbon nanotubes in different media and higher functionalities concentration, see Table 2 of Chapter 3, create, when inserted in polymer matrix, a more enlarged and less interconnected network compared with nanotubes with other functionalities at same concentration.

Again, as observed when analyzing rheological behavior, it becomes more interesting a characterization that could observe the effective state of dispersion of carbon nanotubes at different concentration, especially at weight content that create the difference electrical and rheological percolation behaviors.

4.3.4 Damage sensing characterization

Starting from the seminal work by Thonstenson, from the insertion of small amount (< 1 %wt) of carbon nanotube and the induced conductive modification on the nanocomposite, a resistance measurements across samples is used for damage monitoring ^[44-48].

In our study a measurement of the possible usage of CNTs as crack sensor was investigated for nanocomposites containing, at low concentrations, different functionalized carbon nanotubes.

The procedure, described in Section 4.2.6, was conducted on nanocomposites with low amount of carbon nanotubes for the difficulties of obtaining a great number of specimens at high CNTs contents, due to the high viscosity showed by those samples.

Figure 26 shows clearly that for composites containing 0,16 %wt of untreated CNT the induced notches create a difference in resistance values before and after the defects creation ($\Delta R/R_0$ %), even for lower indentation length on specimens width parameters (a/W).

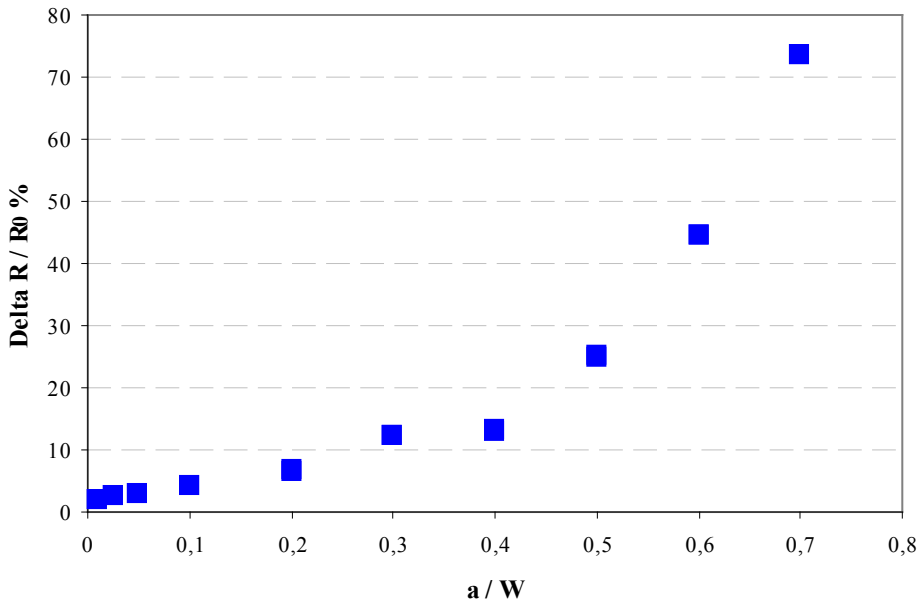


Figure 26 - Change in resistance against defects length parameter of nanocomposites containing untreated CNT at 0,16 %wt.

Before starting to fully investigate all our samples, we must take into account all the limitations, in this sensing characterization, that our instrumentation could give. In particular the sensitivity that our Multimeter has in terms of current measurement. Moreover a small theoretical analysis of the problems is required in order to face correctly the problematic issues of instrument sensibility.

Considering parallelepiped samples, see Figure 27, with length L , width W , thickness B and notches of length a is broached on only one side of the sample all over the sample's thickness B .

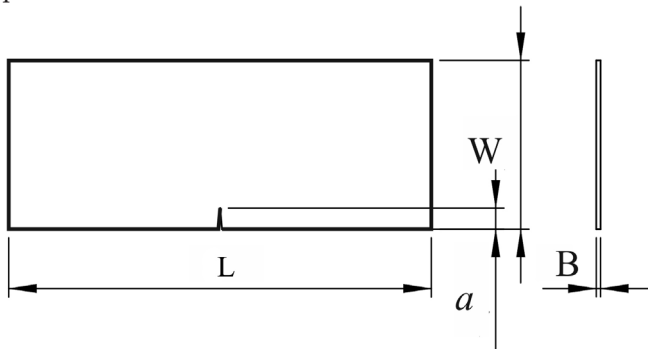


Figure 27 - Schematic draw of broached sample

Ohm law is the starting point for our consideration. $V = RI$ with $R = \frac{L}{\sigma WB}$

where σ is the conductivity of the samples. As described in Section 4.2.6 a scanning voltage were applied in our tests, and so our attention need to be focused on the difference of current that the sample could give before and after the notches creation.

For the pristine sample we consider $R_0 = \frac{L}{\sigma WB}$, instead for the broached sample

we could consider $R_1 = \frac{L}{\sigma W_1 B} = \frac{L}{\sigma(W - aW)B}$. We obviously consider the conductivity of the samples constant. This simplified theory consider the length of the notches, a , to be small enough to not influence on the deviation of the electric field lines and so, in an easy way, resistivity of the broached samples is considered like the resistivity of sample with reduced area, i.e. $(W_0 - aW_0)B$. The current

measured for the pristine sample when a voltage V is give is: $I_0 = \frac{V}{R_0} = \frac{V\sigma WB}{L}$

and the current measured for notched sample instead is

$I_1 = \frac{V}{R_1} = \frac{V\sigma W_1 B}{L} = \frac{V\sigma WB(1-a)}{L}$. On our samples we measured the difference

in current before and after the notches formation. So we measured $\Delta I = I_1 - I_0$.

With little algebra the result are presented in Equation 4.

$$\Delta I = -\frac{VBW}{L}\sigma a \text{ and } I_1 = I_0 - \frac{VBW}{L}\sigma a$$

Equation 4

As could be seen the difference in current is negatively influenced by the conductivity and the length of the notches. From this simplified theory, without taking account of the geometry factor that influence on the response, it comes that only a range of conductivity could make measurable value of the difference in current before and

after the notch. If the conductivity is high enough, the difference before and after the cut could become so little to not be efficiently measured. On the other side, if sample shows low conductivity, it can encounter to troublesome related to the accuracy of the instrumentation that maybe couldn't detect the current generated by the applied voltage in quasi-insulating materials. Even if this theory is simple and schematic, it could be taken into account when the response of broached samples are investigated.

For further usability also the relation with resistivity is calculated starting from the

same assumptions. $\Delta R = R_1 - R_0$ where R_0 is $\frac{L}{\sigma WB}$ and

$$R_1 = \frac{L}{\sigma W_1 B} = \frac{L}{\sigma(W - aW)B}.$$

With little algebra the difference in resistivity of the sample before and after the indentation is presented in Equation 5.

$$\Delta R = \frac{L}{WB} \left(\frac{La + L - 1}{1 - a} \right) \frac{1}{\sigma}$$

Equation 5

As could be seen the difference in resistivity is inversely proportional to the conductivity value of the sample, confirming that only a range of conductivity could give to detectable response.

With the above delineated draft theory, the promising crack sensing at low a/W leads us to investigate all the different nanocomposites created with untreated CNT, carboxylic and amino functionalized CNT.

Dispersion containing COOH-CNT couldn't be measured clearly at the low CNT concentration chosen. As stated in Section 4.3.3 a percolative network, that leads the electrical response from an insulating to a pseudo-conductive material, for the nanocomposite obtained with carboxylic-functionalized CNT, is not formed until a heavy content of carbon nanotubes is inserted. This difficulties in detecting the response of damage could be better comprehended with the theory here developed. The conductivity observed in samples containing COOH-CNT is small, and this lead the samples to response to the voltage applied with low current that, especially in indented samples, couldn't clearly be measured.

Promising results are instead observed for nanocomposites with NH_2 -CNT, and are showed in Figure 28.

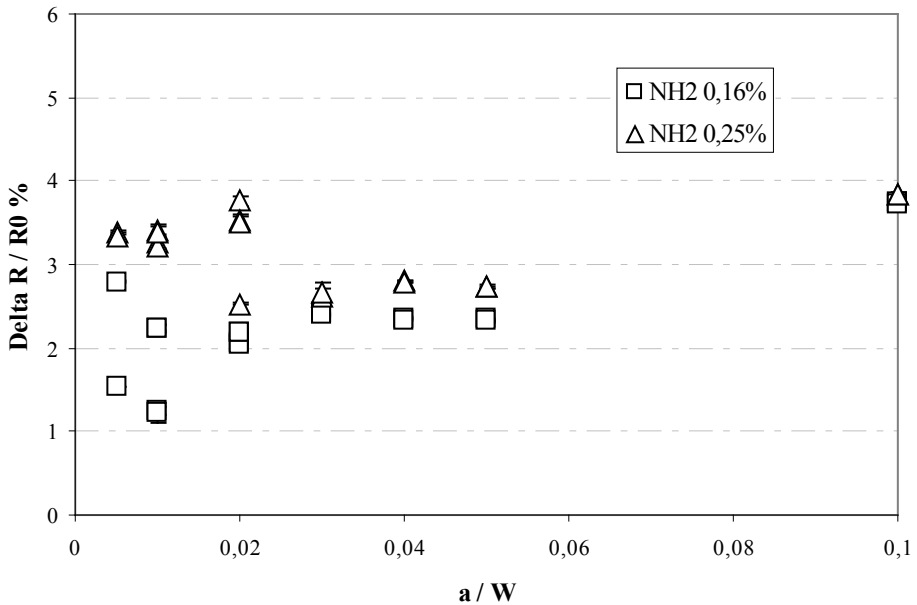


Figure 28 - Change in resistance against notches length parameter of nanocomposites containing NH_2 -CNT at 0,16 %wt and 0,25 %wt.

As could be observed a clear response of the crack presence is monitored. A change of 3 % on $\Delta R/R_0$ after defects creation is observed even for broaching machine limit, i.e. a/W around 0,005. Scattered results for different indentation length is observed till the value of a/W reach 0,1, confirming the potential of this damage sensing technique based on induced conductivity in nanocomposites with the insertion of carbon nanotubes.

Figure 29 shows the results obtained with nanocomposites containing untreated CNT. Again for the lowest concentration analyzed in this study, i.e. for 0,16 and 0,25 % wt of CNT, the damage sensing is efficient even for the smaller defects. The presence of broaching machine limit defect length (i.e. around 0,005 for a/W value) is monitored with a 2 % change in $\Delta R/R_0$ values. A lower efficiency is observed for the nanocomposites containing a higher concentration of untreated carbon nanotubes.

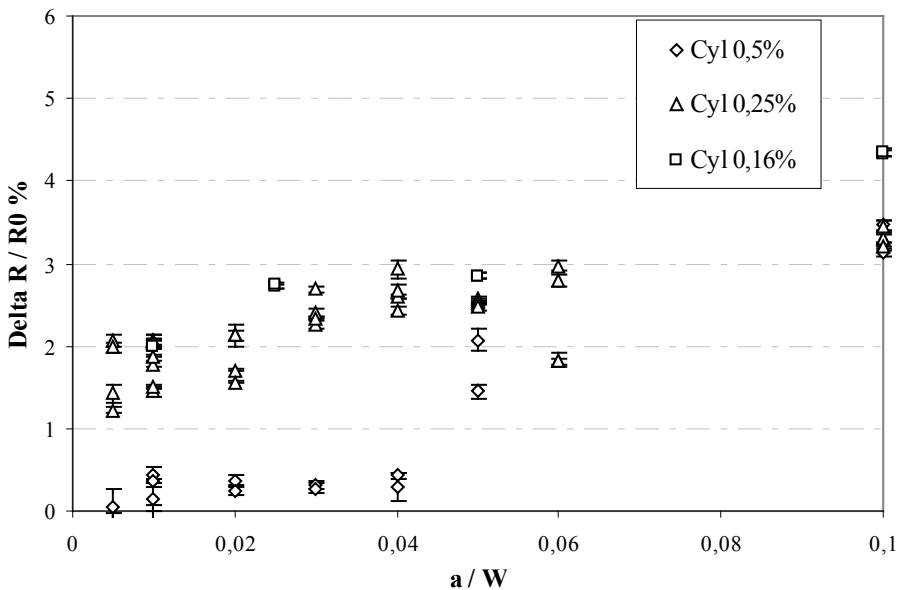


Figure 29 - Change in resistance against defects length parameter of nanocomposites containing NH_2 -CNT at 0,16 %wt, 0,25 %wt and 0,5 %wt.

Inserting 0,5 %wt in epoxy polymer the efficiency of this technique is quite neglected till a notch length with a a/W parameter of 0,05 is reached. This behavior could be explained with the drafted theory above delineated. The conductivity of samples containing pristine CNT at 0,5 %wt is high enough that the induced change before and after the notch creation is so small, and this led to a less response in damage sensing.

As noticed before, the drafted theory here developed didn't consider any change in electric field line direction when the notch is present, even if this change in direction obviously is expected. Moreover, this change in electric field line direction is more prominent when samples with high conductivity are investigated. The percolative network is, as well explained in Section 4.3.2, already created at 0,1 %wt. At 0,5 %wt also the rheological percolation value is reached and so an interconnected network between the carbon nanotubes is present. This network could permit to transfer the electron from the two sides of the specimen in the same way as the induced defect is not present. Only with high defects length the interconnected network is probably damaged and so a monitoring of the present of notches could be efficiently exploited.

These observations further confirm the remarks observed in rheological and electrical characterization on networking CNTs, that induce the changing behavior in the nanocomposites. Moreover, these suggest that the damage monitoring could

be efficiently exploited only in nanocomposites in which the CNTs are conformed in a developing interconnected network morphologies, and that this efficiency decrease when the CNTs' web become tight. That is, damage sensing could be easily exploited in nanocomposites containing CNTs only at a low concentration, above the percolation of electrical properties and below a contents of carbon nanotubes that provide a tight networking structure.

4.4 CONCLUSIONS AND FUTURE CONSIDERATIONS

A method, that could be conducted in lab scale without using machine providing high shear stress like an extruder, to disperse carbon nanotubes in a commercial epoxy resin was set up and studied. A good repeatability of the rheological and electrical behavior for the sample prepared with the dispersion process investigated is observed. Those characterizations are intrinsically related to the morphologies of the dispersion and so these observations confirm that the set up dispersion method produces nanocomposites with a good repeatability.

A calorimetry characterization on nanocomposites containing different functionalized carbon nanotubes was investigated. No change in enthalpy of crosslinking reaction from the value of pristine resin was found in the insertion of carbon nanotubes for the most used concentration (below 3 %wt). The concentration of functionalities, present of external wall of the CNTs, are too low in number to induce a change in the crosslinking reaction. Moreover the kinetic of the crosslinking reaction was not changed by the insertion of CNTs.

Rheological behavior of nanocomposite was studied extensively. A shear thinning behavior is observed when carbon nanotubes are inserted in the resin. This change in performance directly depend on functionalities present on external wall of the carbon nanotubes. A clear shear thinning behavior for nanocomposites containing COOH-CNT is observed only at a concentration above 1 %wt, a suitable performance for industrial processing of those composites. In dispersions with NH₂-CNT and untreated CNT, instead, the development of pseudo-plastic performances is observed starting at lower concentrations. Percolation between Newtonian fluid to pseudo-plastic was investigates with oscillating rheology characterization. The presence of crossover points between the storage modulus and the loss modulus was found to depend on the different kind of carbon nanotubes inserted.

The rheological behavior are directly connected with the developing nanotube microstructure. The interconnected network that provide the crossover to a pseudo-plastic behavior was correlated with the variation in dispersion capability of the different carbon nanotubes, due to the functionalities present on their external walls.

Electrical behavior of nanocomposites show an induced conductivity that depend on the morphologies in which the inserted carbon nanotubes structured their self, and so on the different functionalities of inserted CNTs. The percolative behavior from insulating to pseudo-conductive, for nanocomposites containing COOH-CNT was observed only at concentration above 1%. For nanocomposites containing untreated CNT and amino-functionalized CNT, a conductivity is experimented starting from 0,1 %wt.

The induced conductivity was further investigated for a promising use of this peculiar properties as a novel damage detection in nanocomposites. A promising

feasibility for this non invasive method of detection was observed. The efficiency is related with the induced conductivity and the morphologies in which the carbon nanotubes is structured inside the nanocomposites. A high content of carbon nanotubes provide a tight network that could easily bypass the notch without changing the performances.

The future step will be directed in better comprehend the dispersion morphology of the carbon nanotubes in polymer matrix and how the difference in functionalization could modify this morphology. Rheology and electrical behavior are the best way to indirectly investigate the interconnected morphology of the dispersed CNTs, and so those technique will be further exploited. A more exhaustive investigation on the influence of the notch on the electric properties needs to be developed, and in the same time a methodology to study the damage sensing response in line with the propagation of the crack must be examined.

4.5 REFERENCE

1. J. Coleman, U. Khan, W. Blau, Y. Gunko, Small but strong: A review of the mechanical properties of carbon nanotube-polymer composites, *Carbon*, 44, 1624-1652 (2006).
2. J. Coleman, U. Khan, Y Gunko, Mechanical reinforcement of polymers using carbon nanotubes, *Advanced Materials*, 18, 689-706 (2006).
3. H. Qian, E. S. Greenhalgh, M. S. P. Shaffer, A. Bismarck, Carbon nanotube-based hierarchical composites: a review, *Journal of Materials Chemistry*, 20, 4751-4762 (2010).
4. F Galindo-Rosales, P. Moldenaers, J. Vermant, Assessment of the Dispersion Quality in Polymer Nanocomposites by Rheological Methods, *Macromoleculars Materials and Engineering*, 296, 331-340 (2011).
5. M. Cadek, J. Coleman, K. P. Ryan, V. Nicolosi, G. Bister, A. Fonseca, J. B. Nagy, K. Szostak, F. Béguin, W. J. Blau, Reinforcement of polymers with carbon nanotubes: The role of nanotube surface area, *Nanoletters*, 4(2), 353-356 (2004).
6. F. Du, R. C. Scogna, W. Zhou, S. Brand, J. E. Fischer, K. I. Winey, Nanotube networks in polymer nanocomposites: Rheology and electrical conductivity, *Macromolecules*, 37, 9048-9055 (2005).
7. J. Wang, Z. Fang, A. Gu, L. Xu, F. Liu, Effect of amino-functionalization of multiwalled carbon nanotubes on the dispersion with epoxy resin matrix, *Journal of Applied Polymer Science*, Vol 100 (1), 97-104 (2006).
8. J. Shen, W. Huang, L. Wu, Y. Hu, M. Ye, The reinforcement role of different amino-functionalized multiwalled carbon nanotubes in epoxy nanocomposites, *Composites science and technology*, 67, 3041-3050 (2007).
9. J. Zhu, H. Peng, F. Rodriguez-Macias, J. L. Margrave, V. Khabashesku, A. M. Imam, K. Lozano, E. V. Barrera, Reinforcing Epoxy Polymer Composites through covalent integration of functionalized nanotubes, *Advanced Functional Materials*, 14 No. 7, 643-648 (2004).
10. K. Lau, M. Lu, H. Cheung, F. Sheng, H. Li, Thermal and mechanical properties of single-walled carbon nanotube bundle-reinforced epoxy nanocomposites: the role of solvent for nanotube dispersion, *Composites Science and Technology*, 65, 719-725 (2005).
11. D. S. Bangarusam, H. Ruckdäschel, V. Altstädt, J. K. W. Sandler, D. Garray, M. S. P. Shaffer, Rheology and properties of melt-processed poly(ether ether ketone)/multi-wall carbon nanotube composites, *Polymer*, Vol. 50 (24), 5803-

- 5811 (2009).
12. L. Chang, K. Friedrich, L. Ye, P. Toro, Evaluation and visualization of the percolating networks in multi-wall carbon nanotube/epoxy composites, *Journal of Materials Science*, Vol 44 (15), 4003-4012 (2009).
 13. M. Abdalla, D. Dean, D. Adibempe, E. Nyairo, P. Robinson, G. Thompson, The effect of interfacial chemistry on molecular mobility and morphology of multiwalled carbon nanotubes epoxy nanocomposites, *Polymer*, 48, 5662-5670 (2007).
 14. F.H. Gojny, M.H. Wichmann, B. Fiedler, K. Schulte, Influence of different carbon nanotubes on the mechanical properties of epoxy matrix composites – A comparative study, *Composites science and Technology*, 65, 2300-2313 (2005).
 15. L. S. Schadler, S. C. Giannaris, P. M. Ajayan, Load transfer in carbon nanotube epoxy nanocomposites. *Applied Physics Letters*, 73 (26), 3842-3844 (1998).
 16. W. Zhang, R. C. Picu, N. Koratkar, The effect of carbon nanotube dimensions and dispersion on the fatigue behavior of epoxy nanocomposites, *Nanotechnology*, 19, 1-5 (2008).
 17. Y. S. Song, Rheological characterization of carbon nanotubes/poly (ethylene oxide) composites, *Rheologica Acta*, 46, 231-238 (2006).
 18. M. Abdalla, D. Dean, P. Robinson, E. Nyairo, Cure behavior of epoxy/MWCNT nanocomposites: The effect of nanotube surface modification, *Polymer*, 49, 3310-3317 (2008).
 19. M. Chapartegui, N. Markaide, S. Florez, C. Elizetxea, M. Fernandez, A. Santamaría, Specific rheological and electrical features of carbon nanotube dispersion in an epoxy resin, *Composites science and technology*, 70, 879-884 (2010).
 20. Z. Fan, S. G. Advani, Rheology of multiwall carbon nanotube suspensions, *Journal of Rheology*, 51 (4), 585-604 (2007).
 21. M. J. Kayatin, V. A. Davis, Viscoelasticity and Shear Stability of Single-Walled Carbon Nanotube/Unsaturated Polyester Resin Dispersions, *Macromolecules*, Vol 42 (17), 6624-6632 (2009).
 22. Y. Y. Huang, S. V. Ahir, E. M. Terentjev, Rheology of concentrated carbon nanotube suspensions, *The Journal of chemical physics*, Vol 126 (12), 124907 (2006).
 23. E. Hobbie, Shear rheology of carbon nanotube suspensions, *Rheologica Acta*, 49 (4), 323-334 (2010).

24. D. T. N. Chen, K. Chen, L. A. Hough, M. F. Islam, A. G. Yodh, Rheology of Carbon Nanotube Networks During Gelation, *Macromolecules*, Vol 43 (4), 2048-2053 (2010).
25. J. Shen, W. Huang, L. Wu, Y. Hu, M. Ye, Study on amino-functionalized multiwalled carbon nanotubes, *Materials Science and Engineering: A*, 464, 151-156 (2007).
26. J. Xu, S. Chatterjee, K. W. Koelling, Y. Wang, S. E. Bechtel, Shear and extensional rheology of carbon nanofiber suspensions, *Rheologica Acta*, 44, 537-562 (2005).
27. A. W. K. Ma, F. Chinesta, M. R. Mackley, The rheology and modeling of chemically treated carbon nanotubes suspensions, *Journal of Rheology*, 53 (3), 547-573 (2009).
28. I. A. Kinloch, A rheological study of concentrated aqueous nanotube dispersions, *Polymer*, 43, 7483-7491 (2002).
29. P. Hubert, B. Ashrafi, K. Adhikari, J. Meredith, S. Vengallatore, J. Guan, B. Simard, Synthesis and characterization of carbon nanotube-reinforced epoxy: Correlation between viscosity and elastic modulus, *Composites Science and Technology*, Vol 69 (14), 2274-2280 (2009).
30. Z. Spitalsky, D. Tasis, K. Papagelis, C. Galiotis, Carbon nanotube-polymer composites: Chemistry, processing, mechanical and electrical properties, *Progress in Polymer Science*, 35, 357-401 (2010).
31. J. Bai, A. Allaoui, Effect of the length and the aggregate size of MWNTs on the improvement efficiency of the mechanical and electrical properties of nanocomposites-experimental investigation, *Composites Part A Applied Science and Manufacturing*, Vol 34 (8), 689-694 (2003).
32. P. Guo, H. Song, X. Chen, Interfacial properties and microstructure of multiwalled carbon nanotubes/epoxy composites, *Materials Science and Engineering A*, Vol 517 (1-2), 17-23 (2009).
33. W. Bauhofer, J. Z. Kovacs, A review and analysis of electrical percolation in carbon nanotube polymer composites, *Composites Science and Technology*, Vol 69 (10), 1486-1498 (2009).
34. S. Yuen, C. M. Ma, H. Wu, H. Kuan, W. Chen, S. Liao, C. Hsu, H. Wu, Preparation and thermal, electrical, and morphological properties of multiwalled carbon nanotube and epoxy composites, *Journal of applied polymer science*, 103, 1272-1278 (2007).
35. I. Alig, T. Skipa, D. Lellinger, P. Pötschke, Destruction and formation of a

- carbon nanotube network in polymer melts: Rheology and conductivity spectroscopy, *Polymer*, 49, 3524-2532 (2009).
36. A. Battisti, A. A. Skordos, I. K. Partridge, Percolation threshold of carbon nanotubes filled unsaturated polyesters, *Composites Science and Technology*, Vol 70 (4), 633-637 (2010).
 37. A. Battisti, A. A. Skordos, I. K. Partridge, Monitoring dispersion of carbon nanotubes in a thermosetting polyester resin, *Composites Science and Technology*, Vol 69 (9), 1183-1189 (2009).
 38. I. D. Rosca, S. V. Hoa, Highly conductive multiwall carbon nanotube and epoxy composites produced by three-roll milling, *Carbon*, Vol 47 (8), 1958-1968 (2009).
 39. Q. Wang, J. Dai, W. Li, Z. Wei, J. Jiang, The effects of CNT alignment on electrical conductivity and mechanical properties of SWNT/epoxy nanocomposites, *Composites Science and Technology*, Vol 68 (7-8), 1644-1648 (2008).
 40. C. H. Lau, R. Cervini, S. R. Clarke, M. Ginic Markovic, J. G. Matisons, S. C. Hawkins, C. P. Huynh, G. P. Simon, The effect of functionalization on structure and electrical conductivity of multi-walled carbon nanotubes, *Journal of Nanoparticle Research*, Vol 10 (S1), 77-88 (2008).
 41. S. Yuen, C. M. Ma, H. Wu, H. Kuan, W. Chen, S. Liao, C. Hsu, H. Wu, Preparation and Thermal, Electrical, and Morphological Properties of Multiwalled Carbon Nanotube and Epoxy Composites, *Journal of Applied Polymer Science*, Vol 103 (2), 1272-1278 (2007).
 42. Y. Song, J. Youn, Influence of dispersion states of carbon nanotubes on physical properties of epoxy nanocomposites, *Carbon*, Vol 43 (7), 1378-1385 (2005).
 43. J. Sandler, M. S. P. Shaffer, T. Prasse, W. Bauhofer, K. Schulte, A. H. Windle, Development of a dispersion process for carbon nanotubes in an epoxy matrix and the resulting electrical properties, *Polymer*, Vol 40 (21), 5967-5971 (1999).
 44. A. S. Lim, Q. An, T. Chou, E. T. Thostenson, Mechanical and electrical response of carbon nanotube-based fabric composites to Hopkinson bar loading, *Composites Science and Technology*, Vol 71 (5), 616-621 (2011).
 45. L. Gao, T. Chou, E. T. Thostenson, Z. Zhang, A comparative study of damage sensing in fiber composites using uniformly and non-uniformly dispersed carbon nanotubes, *Carbon*, Vol 48 (13), 3788-3794 (2010).
 46. E. T. Thostenson, T. W. Chou, Carbon Nanotube Networks: Sensing of

Distributed Strain and Damage for Life Prediction and Self Healing, *Advanced Materials*, Vol 18 (21), 2837-2841 (2006).

47. M. D. Rein, O. Breuer, H. D. Wagner, Sensors and sensitivity: Carbon nanotube buckypaper films as strain sensing devices, *Composites Science and Technology*, Vol 71 (3), 373-381 (2011).
48. M. A. Bily, Y. W. Kwon, R.D. Pollak, Study of Composite Interface Fracture and Crack Growth Monitoring Using Carbon Nanotubes, *Applied Composite Materials*, Vol 17 (4), 347-362 (2009).
49. J. P. Elder, The general applicability of the Kissinger equation in thermal analysis, *Journal of thermal analysis*, Vol. 30, 657-669 (1985).

>5
FLUORINATED
NANOCOMPOSITES
CONTAINING CARBON
NANOTUBES



5.1 INTRODUCTION

The scientific and industrial interest in fluorinated polymers has grown considerably in the last 15 years for the possible wide use of their peculiar properties, like their unmatched thermal stability and chemical resistance^[1-4]. Family of fluoroelastomers represent one of the most promising class of fluorinated polymers for their high performances in a variety of sectors, notwithstanding their high cost, for example in sealing and applications in which water-oil repellence is required^[1-4]. Classical fluoroelastomers are based on statistical copolymers of well known fluorinated monomers like perfluorovinylethers, hexafluoropropene and the commonly famous tetrafluoroethylene^[1,2]. As a rule of thumbs, the unrivaled thermal and chemical resistance increases with the fluorine content, at the same time cost and polymer's glass transition increase^[1-4]. When a good sealing properties at low temperature is wanted, it can be very difficult to achieve materials with this increasing fluorine content approach^[1,5].

A potentially interesting alternatives are the perfluoropolyethers (PFPE) based elastomers that show a low glass transition, in the range of -50 to -100 °C, depending on their highly flexible chain composition^[1,3,5].

Moreover, another heavily exploited field in scientific literature and in industrial applications are the polyurethane thermoplastic elastomers that gave enthusiastic results for their excellent mechanical properties (abrasion resistance, toughness and tensile strength) in low temperature applications^[3-10].

Combining these two polymer families the class of linear segmentated polyurethane perfluoropolyethers gives commercial success for their unique balance of properties, such as high solvent and chemical resistance, low surface energy and low glass transition^[3,5-9, 11-13].

These perfluoropolyether derivatives show, as expected, besides an unique mechanical performances, a very good insulating behavior and could be an ideal candidate for the incorporation of carbon nanotubes in order to enhance their electrical properties for particular applications^[1,7,11-14].

To best of the author's knowledge only few works focus their attention in nanocomposites containing carbon nanotubes based on perfluoropolyethers^[1,14]. This lack of interest in this promising field, in contrast with the huge amount of articles present in literature on nanocomposites containing CNTs with different polymer matrices, is mainly due to the very specific field of application of this advanced nanocomposites, like highly specialized electronic industry, or hydrophobization coating for gas diffusion layer for PEM fuel cells^[1,7,13,14].

In our study we focused our attentions on two different perfluoropolyethers derivatives in aqueous dispersions. Those PFPE chains were made water-reducible through functionalization with ionic side or end group. The insertion of carboxylated carbon nanotubes to create advanced nanocomposites was

investigated with rheological, mechanical, thermal and superficial characterizations. These characterizations were chosen to observe the modification of CNTs in the most industrially exploited perfluoropolyethers properties, such as coatings with water-oil repellence, low temperature processing, high temperature stability and chemical resistance, and most important to analyze the change in mechanical properties due to the change of glass transition temperature. Electrical properties was also studied on perfluoropolyethers nanocomposites to confirm, also in this polymer family, the expected percolative behavior induced by the presence of carbon nanotubes in the matrices. It will be a very promising opportunity of inducing a conductivity change in fluorinated polymers, traditionally exploited as insulator, permitting a widening of possible innovative applications for those nanocomposites.

5.2 EXPERIMENTAL SECTION

5.2.1 Perfluoropolyethers, carbon nanotubes and other materials

Two different perfluoropolyether (PFPE, fluorine content close to 67% w/w) polymers were used in this study.

Fluorolink® P56 (P56), developed and purchased by Solvay Solexis, is a aqueous dispersions of anionic segmented polyurethane containing perfluoropolyether (PFPE) blocks and carboxylate side groups (see structure in Figure 1, tetralkylammonium counterions have been omitted) . The solid content of the water dispersion is of around 26% w/w. The P56 shows a M_w of around 20000 g/mol.

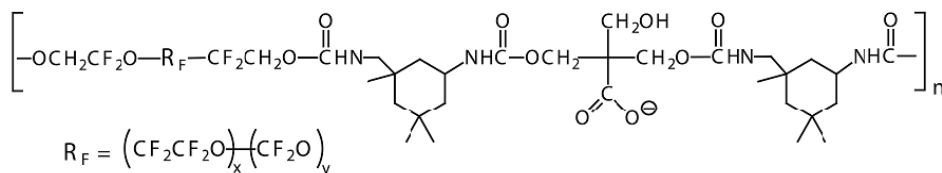


Figure 1 – Molecular structure of fluorinated polyurethane Fluorolink® P56.

Fluorolink® TLS 5007 (TLS), developed and purchased by Solvay Solexis, is a aqueous microdispersion of perfluoropolyether phosphate ammonium salt. The dispersion shows a solid content of around 29% w/w and the molecular weight of TLS is around 2000 g/mol (see Figure 2).

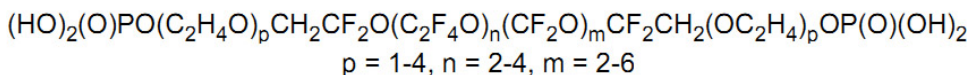


Figure 2 – Molecular structure of perfluoropolyether phosphate Fluorolink® TLS 5007

P56 and TLS are made water reducible by their functionalized chain with ionic side. Those PFPE polymers show low molecular values in comparison with the standard molecular weight of polytetrafluoroethylene and are commonly used as lubricant in critical conditions or as coating agent on natural stone and metal to induce water and oil repellence.

Carboxylated nanotubes were used for their better compatibilization with aqueous media in which the perfluoropolyethers are microdispersed ^[15-17]. The commercial available Nanocyl NC 3101, based on Nanocyl NC 3100 (for further informations see Section 3.2.1) were purchased by Nanocyl and the carboxylated nanotubes, functionalized with the standard method described in Section 3.2.2 and studied in Chapter 3, were used. Commercial COOH-CNT and owner carboxylated nanotubes are used without any distinction and simply labeled COOH-CNT.

This decision, as already observed in Section 4.2.1 for epoxy nanocomposites, is supported by preliminary study with no dissimilar behavior observed on all the different characterizations here further investigated.

All other chemicals, if not expressly mentioned, were provided by Sigma Aldrich.

5.2.2 Nanocomposites dispersion preparation

For easy preparation, the two perfluoropolyether microdispersions were diluted at a solid content of 10 % w/w with deionized water, and mixed with magnetic stirring at 600 rpm for 30 minutes in order to create a homogeneous and stable (more than 1 year) dispersions.

Starting from the knowledge acquired for epoxy nanocomposites' systems, see Chapter 4, the dispersion of COOH-CNT into aqueous microdispersion of perfluoropolyethers' polymer matrices were conducted in different steps.

In the first step a wished amount of carboxylated nanotubes was added in a flat-bottom flask containing around 100 ml of the 10 %wt aqueous dispersion of PFPE matrices. A mechanical mix was conducted with magnetic stirring at 950 rpm for 30 minutes. The dispersion was then sonicated in a Starsonic 90 sonicator bath for 1 hour. The mixture was finally sonicated with a Sonic & Materials VCX130 sonicator tip for 30 minutes at the 80% of the instrumental amplitude. Last step was conducted in ice bath in order to reduce the water evaporation to maintain the designed solid concentration.

All dispersions were formulated by mass fraction based on measured component weights. The mass fraction of carbon nanotubes in these study is always referred to the perfluoropolyether polymer matrix content for easy labeling.

All the dispersion containing COOH-CNT show a stable dispersion for more than 1 year after the first preparation.

5.2.3 Rheology characterization.

Rheological characterizations were performed using a Rheometrics DSR 200 rheometer in 25 mm plate cone configuration at 25 °C. Steady shear test were performed for 3 minutes, starting from 0 to around 120 Pa for nanocomposites containing P56 and to around 12 Pa for the samples containing phosphate matrix TLS. The maximum value was chosen from specimen to specimen considering the viscosity showed by the sample itself. The purpose of this characterization was to evaluate the repeatability of the dispersion method and to suggest the structure that the carbon nanotubes will form inside the perfluoropolyether nanocomposites.

5.2.4 Differential scanning calorimetry

Thermal characterization was used in order to comprehend the impact of carbon

nanotubes insertion. The aqueous dispersion of the two perfluoropolyether based matrices (P56 and TLS), containing different concentrations of COOH-CNT, were cast on PTFE plate and dried for 48 hours at 40°C. The cast samples were then heated in air-forced oven at 100°C for 24 hours till a weight leakage is excluded. A film with a thickness of around 0,1 mm were formed. Several DSC aluminum pans were filled with film slices. The samples (around 10 mg) were then tested using a Mettler Toledo DSC 823^e instrumentation, with a scanning method that provide three steps at a scanning speed of 20 °C/min. Firstly a scan from 0 °C to 200 °C were realized in order to completely melt the nanocomposites at the bottom of the aluminum pan, to analyze the other two scanning steps with better precision. The second step starts from 200 °C and go to -140 °C. Finally the ascent step starts from -140 °C to 200 °C. Same scanning steps were analyzed, for specific specimen, with two different scanning speeds of 10 °C/min and 30 °C/min.

From differential scanning calorimetry, glass transition temperatures, T_g , were evaluated from the second and third scan as the temperature at the inflection point of heat capacity change.

5.2.5 Dynamic mechanical analysis

Mechanical analysis were performed in order to analyze the reinforcement induced by the insertion of COOH-CNT into perfluoropolyether polymers, and the change in performance in particular at high temperature.

An around 0,1 mm films of P56 nanocomposite, containing different concentrations of COOH-CNT, were obtained by casting the aqueous dispersions on PTFE plate. The drying procedure provides a 48 hours at 40 °C followed by 24 hours in an air-forced oven at 100 °C, till a no change in weight is observed. Circular specimens with a diameter of 0,5 cm were obtained and tested in shear-sandwich mode with a Mettler DMA/SDTA861^e dynamic-mechanical analyzer. The dynamic scans were conducted from -30 °C to 180 °C at successive frequencies of 0,5, 1, 5 and 10 Hz, with a specimen deformation less than 0,5%. Samples were re-clamped at -30 °C to counteract the thermal shrinkage.

The measurement were not performed on TLS nanocomposites due to their pseudo-liquid behavior, that not permit a creation of solid film that could be cut in a self sustained circular specimen. This difference is due by the low molecular weight of the TLS polymer (M_w of 2000 vs 20000 g/mol for P56 PFPE)

5.2.6 Contact angle measurements

One of the most exploited properties of fluoroelastomers is their water-oil repellence [3,4,7,9,10,13]. Contact angle measurements were performed in order to analyze the change induced by CNTs presence on these peculiar characteristics of perfluoropolyether matrices.

Static contact angles against bidistilled water and highest purity grade of diiodomethane were measured at 25 °C with a DataPhysics OCA 20, equipped with a 500 µl Hamilton syringe to dispense liquid droplets. Measurements were made by means of the sessile drop technique. Results were expressed as the average of at least 30 independent measurements. The delivered volume was of 7 µl and the measurements were carried out after 1 s after drop deposition. Surface energy and its dispersive and polar components were calculated applying the Wu harmonic mean approximation that could better calculate the surface energy of polymer film. Wu harmonic mean is defined by the Equation 1, in which which γ_{LV} is the interfacial tension for a liquid vapour system, γ_{SV} is the interfacial tension for a solid vapour system, and the angle θ is referred to the contact angle. The apex d and p are referred to the dispersive and polar components of the surface tension.

$$\gamma_{LV}(1 + \cos \theta) = \frac{4\gamma_{SV}^d \gamma_{LV}^d}{\gamma_{SV}^d + \gamma_{LV}^d} + \frac{4\gamma_{SV}^p \gamma_{LV}^p}{\gamma_{SV}^p + \gamma_{LV}^p}$$

Equation 1.

From Advancing and receding contact angles against water were also measured with sessile drop method. Any measurements were composed by three advancing-receding cycle with a delivered volume of 1 µl, a steady time for measurement of 3 seconds and a delay time between measurements of 2 seconds. All the results were expressed as the average of at least 15 independent measurements.

5.2.7 Roughness characterization

In order to further comprehend the behavior observed in contact angle measurement, is necessary to perform a roughness characterization.

All the measurement were performed with UBM Microfocus profilometer. Results were expressed as the average of at least 5 independent measurements. The length investigated was of 1,25 mm with 1400 points/mm. The parameters considered were firstly the arithmetic average of the absolute values of all points of the profile.

$R_a = \sum_{i=1}^N \frac{|y_i|}{N}$ where N is the number of points in the analyzed area. The other parameter considered is the root means square of the values of all points of the

profile: $R_q = \sqrt{\frac{1}{N} \sum_{i=1}^N y_i^2}$.

5.2.8 Scanning electron microscopy

Scanning electron microscopy analyses were performed using a Cambridge Stereoscan 360 on different film obtained from the dispersion with heating procedure described in Section 5.2.4 That characterization was used only to monitor the morphological characteristic of the fluorinated film and the difference induced by the COOH-CNT presence. Moreover, to further observe the morphology and distribution of CNTs in the matrix. All specimens were sputtered with gold before imaging.

5.2.9 Electrical characterization

Carbon nanotubes as fillers were found to impart electrical properties on insulating polymer matrices ^[1,14,18,19]. Starting from dispersion containing nanocomposites with P56 polymer matrix, an around 0,1 mm thickness film was obtained from a cast on PTFE plate. The drying procedure was conducted for 48 hours at 40 °C, followed by 24 hours in an air-forced oven at 100 °C till a constant weight is reached.

Samples were cut in rectangular specimen of about 25 mm length, 10 mm width. The cross-sectional areas were painted with conductive paint, electronically conductive paint - silver loaded 3g, provided by Rs Components, and then cured for 10 minutes at 120°C to enhance the conductance of the silver paint. 3g silver paint was used to provide a good contact with the two electrodes, that were pressed together on the sample, and to achieve an uniform electric field on the specimens. All the test were performed with a Keithley 2612 multimeter at room temperature with needle point probe SPP4 S/F, purchased by Multi Contact, that provide a controlled tip's pressure on the specimen. The voltage between the two ends of the sample was varied from 0,1 V to 200 V dividing the scan in 50 steps. In every step the voltage was kept constant for 20 seconds. This long procedure was chosen to reduce the R-C circuit behavior observed in most of the samples when a fast voltage change was induced. Conductivity of the nanocomposites were then calculated from resistance measurements.

5.3 RESULTS AND DISCUSSION

5.3.1 Rheological characterization of dispersions

As observed in literature and as outlined in Chapter 4, rheological characterization is a powerful technique that could efficiently describe the effectiveness of dispersion and distribution of carbon nanotubes in polymer matrices [18-22]. Moreover, the insertion of carboxylic carbon nanotubes could strongly modify the performances of PFPE nanocomposites, and therefore a rheological characterization is necessary [1,3,7,8,18,21,22]. All rheological characterizations were conducted at 25°C, as stated in Section 5.2.3.

Firstly steady shear characterization was used in order to confirm the goodness and repeatability of perfluoropolyether dispersions containing CNTs, dispersed as described in Section 5.2.2. As could be seen in Figure 3 dispersions with the 10% wt of polyurethane perfluoropolyether on water, with the insertion of COOH-CNT at the concentration of 5 %wt on P56 weight, show a very good repeatability.

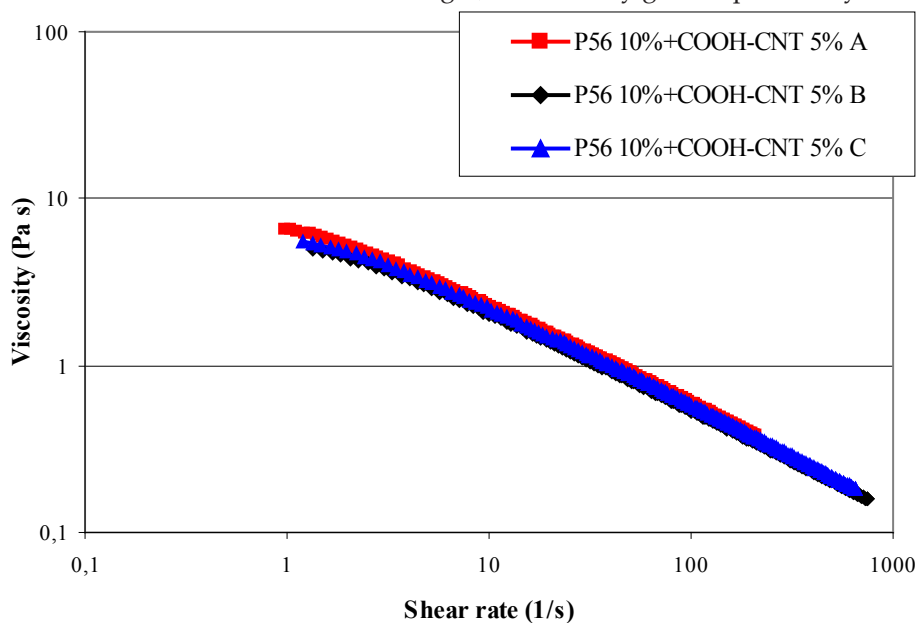


Figure 3 - Shear rate curves, at 25°C, for different dispersions containing 10 % wt of P56 polymer and 5 %wt (on polymer) COOH-CNT. A), B) curves of different dispersions with same composition of 5 %wt of COOH-CNT, C) shear rate curve of dispersion with the same composition of 5 %wt with carboxylic carbon nanotubes functionalized with method described in Chapter 3.

The behavior of different dispersions, labeled A and B in Figure 3, containing the same concentration (5 %wt) of commercial available carboxylated CNTs, and the

dispersion labeled C, obtained adding COOH-CNT functionalized with the method described in Chapter 3, is very similar. The same repeatability is observed for every dispersion of P56 in water, containing a concentration of COOH-CNT, from 1 %wt to 5 %wt, suggesting, as observed in Chapter 4 for rheology characterization with epoxy nanocomposites, that the distribution of carbon nanotubes could be very good repeated with the above mentioned dispersion method.

A complete rheological study of all the different dispersions of P56 nanocomposites containing COOH-CNT at concentrations from 1 %wt to 5 %wt are presented in Figure 4.

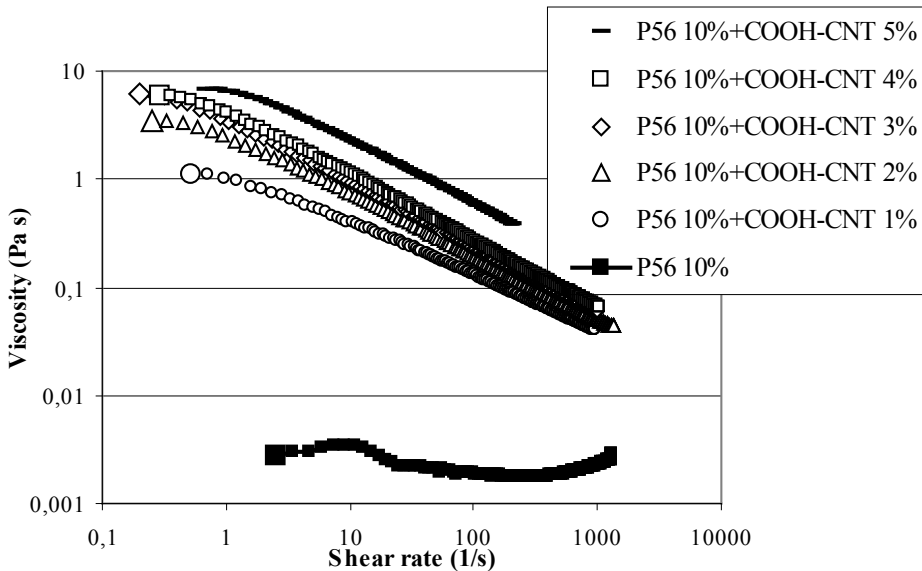


Figure 4 - Shear rate curve, at 25 °C, of dispersion of P56 nanocomposites containing COOH-CNT at different concentrations.

Before discussing the results, it is necessary to point out further that the dispersions studied in this study are mainly composed by water solution (around 90 % wt of the total dispersion). This will lead the rheological behavior of the nanocomposite dispersions to act merely like a liquid. Any change observed, induced by insertion of carbon nanotubes, will lead to a small change in viscosity values due to these low concentrations of our investigated systems. Notwithstanding this, a draft of bigger change induced by carbon nanotubes insertion on nanocomposites (i.e. P56+COOH-CNT) could even be pointed out with this dilute systems. As expected the viscosity of the dispersion is increased by the presence of carbon nanotube. The neat perfluoropolyether dispersion shows a Newtonian behavior, as expected due to the mass presence of water. Instead, the dispersions containing COOH-CNT, show a shear thinning behavior, more visible at low shear rate values, even if the concentration of carbon nanotubes on the overall dispersion is

low (ranging from 0,1 to 0,5 % wt on the whole dispersions) as stated before. The changing behavior observed by the carboxylic functionalized carbon nanotubes insertion, even in this diluted case, is similar to the one observed in Chapter 4, and well known in literature for nanocomposite with different polymer matrices^[18,21,22]. Same observations, outlined in Section 4.3.2.1 for shear rate tests on epoxy nanocomposites, could be made for these systems, and so a creation of interconnected network between the carbon nanotubes inserted in the nanocomposites could be certainly hypothesized. The creation of this network partially stops the flowing of polymer matrix, leading to a gel-like behaviors.

A clear increase in viscosity values is observed, starting from the concentration of 1 %wt to the higher concentrations of carbon nanotubes. This observation suggests that a great change in CNTs network structure, from a lightly connected to a clear interconnected network, could be hypothesized (due to the dilute dispersion) below the 1 %wt of COOH-CNT.

Moreover, as stated for epoxy nanocomposites in Chapter 4, a very good dispersion of carbon nanotubes in the nanocomposites, could be hypothesized due to well known tendencies of carboxylic carbon nanotubes to uniformly disperse and interact with different polymer matrices and water.

For dispersions containing phosphate perfluoropolyether derivatives (TLS), similar characterizations were analyzed.

Steady shear tests were firstly used to confirm the goodness and repeatability of the dispersion method described in Section 5.2.2 . As could be seen in Figure 5 the rheological behavior of two diverse dispersions (sample A and sample B), containing the same concentration of TLS (10 %wt on total dispersion) and COOH-CNT (5 %wt on perfluoropolyether content), shows a similar performance. The same behavior is observed when carboxylic nanotubes, obtained with "hand-made" oxidation method described in Chapter 3, are inserted in the same concentration (sample labeled C). Again, as observed for nanocomposites with P56 matrix, the dispersion method described in Section 5.2.2, permits to disperse carboxylic carbon nanotubes in perfluoropolymer matrices with a good repeatability.

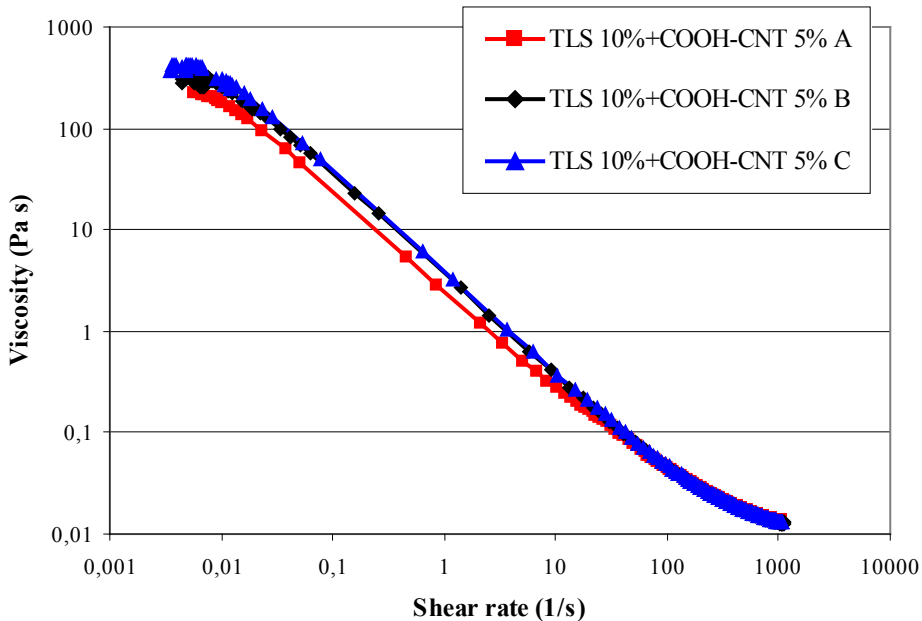


Figure 5 - Shear rate curves, at 25°C, for different dispersions containing 10 % wt of TLS polymer and 5 %wt (on polymer) COOH-CNT. A), B) curves of different dispersions with same composition of 5 %wt of COOH-CNT, C) shear rate curve of dispersion with the same composition of 5 %wt with carboxylic carbon nanotubes functionalized with method described in Chapter 3.

Analyzing the rheological behavior of the overall dispersions taken into account in this study (i.e. TLS dispersions with COOH-CNT from 1 to 5 %wt on perfluoropolyether content), a great similarity could be made with the observation underlined for nanocomposites containing P56 perfluoropolyether.

As could be observed in Figure 6, the dispersion containing only the PFPE polymer at 10 %wt shows a Newtonian behavior during the steady stress test. The viscosity showed by this dispersion is in good agreement with the values observed for the dispersion containing pristine P56, suggesting that the different polymer structure, in particularly the different molecular weight of the perfluoropolyether polymer chain, couldn't strongly modify the behavior of this diluted solutions.

As the carboxylic modified carbon nanotubes are inserted, a clear shear thinning behavior is observed above the 2 %wt COOH-CNT concentrations. As stated for P56 nanocomposites, the shear thinning behavior observed could be caused by the creation of a interconnected network between the carbon nanotubes present, that slows the rheological flow, especially at low shear rate, of these dilute dispersions. A jump, from a quasi liquid behavior to a clear shear thinning performances, is observed clearly above the concentration of 1% wt that could be hypothesized as the limit to percolation.

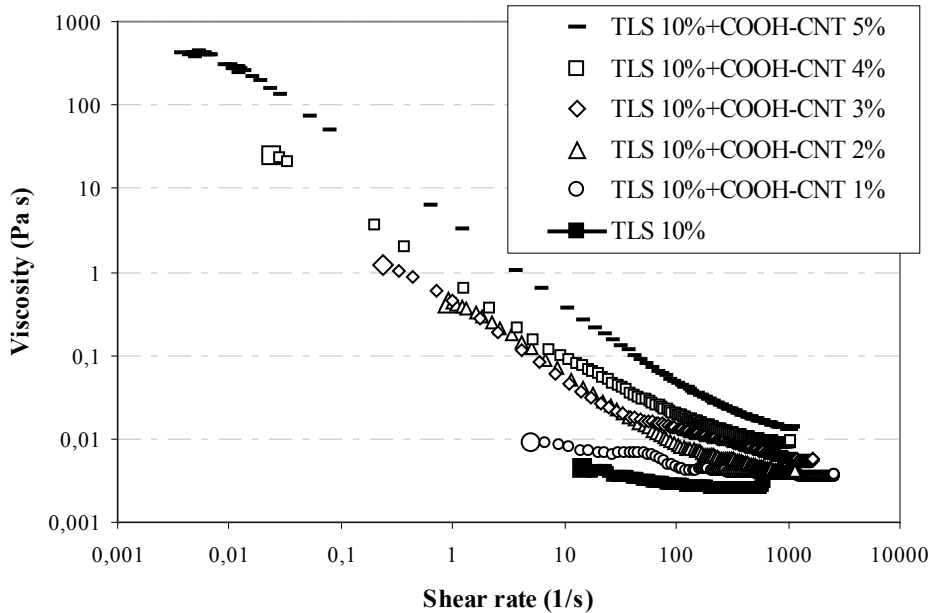


Figure 6 - Shear rate curve, at 25 °C, of dispersion of TLS nanocomposites containing COOH-CNT at different concentrations.

Moreover, if a comparison is made between the viscosity values obtained in steady stress tests for the two perfluoropolyether based nanocomposites, a clear difference could be observed, reported in Figure 7 for selected nanotubes concentrations. Nanocomposites with P56 show a higher viscosity values than the TLS nanocomposites at measured shear rate. This difference is less pronounced when a high concentration of COOH-CNT are present (3 and 5 %wt). At those concentrations, for TLS nanocomposites, a noticeable shear thinning behavior is observed. Moreover, the viscosity at higher shear rate is dominated at all concentrations by the P56 composites. The highlighted difference in the viscosity values for perfluoropolyether nanocomposites with same COOH-CNT concentrations could be explained by the different molecular weight of the two PFPE polymer matrices. As pointed out in Section 5.2.1, P56 shows a M_w of around 20000 g/mol against the one order of magnitude lower value of M_w for TLS.

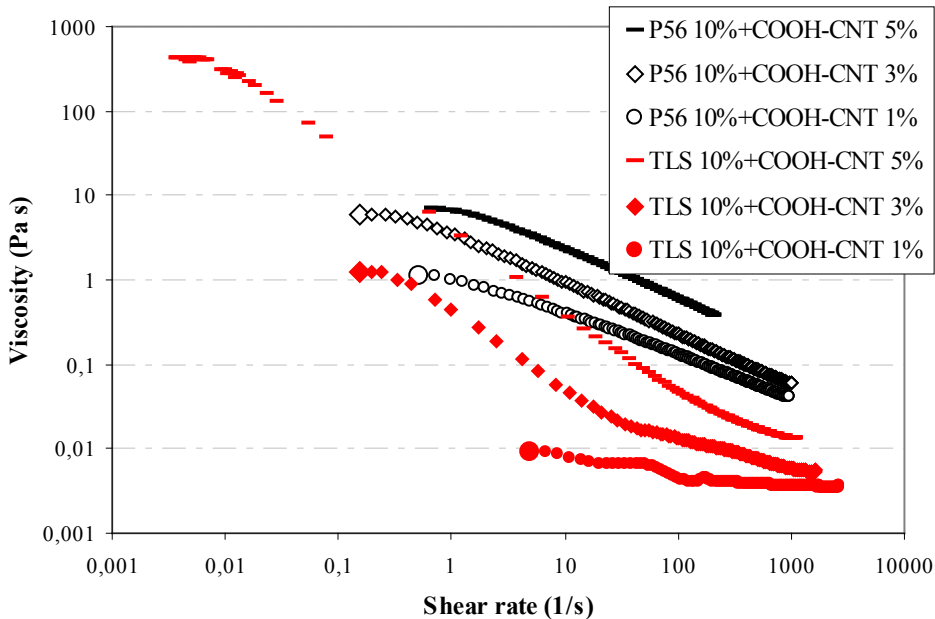


Figure 7 - Confrontation between shear rate curve, at 25 °C, of dispersion of P56 and of TLS nanocomposites containing 1, 3, 5 %wt of COOH-CNT.

Nanocomposites' dispersions based on TLS fluorinated matrix, with the observed low molecular weight, express an higher number of polymer chain at the same weight concentration. The presence of more chains leads to a higher concentration of ionomeric functionalities inside the dispersion than the ones observed in P56 based dispersions. Those ionomeric functionalities could better interact, with carboxylic groups present on the external wall of the inserted carbon nanotubes. Carbon nanotubes interaction permits to reduce the mobility of the TLS polymer chain in a higher way than the effect present in P56 based dispersions. The phenomena observed here, in Figure 7, is hypothetically related in the different ionomeric concentration of the different fluorinated polymer matrix considered. This will lead the focus on controlling the ionomeric functionalities of perfluoropolyether polymers, and the molecular weight of those fluorinated matrices, in order to better control the processing of those dispersion when carbon nanotubes are inserted, and to efficiently manage the nanofiller dispersion inside those matrices and hence the induced properties of those novel nanocomposites.

Unfortunately no dynamic characterization was made due to the low value of viscosity observed, and this will limit the confirmation of the hypothesis claimed with shear rate tests. A wide and intense rheological characterization, testing perfluoropolyether nanocomposites, not only in water dispersions but also after drying the water solutions, will be required to further confirm the observation

here stated and to better highlight the interconnected carbon nanotubes network structure here only hypothesized.

5.3.2 Thermal characterization

Differential scanning calorimetry is widely used in literature in order to analyze the improvement in the thermal properties of fluorinated polymers [1,3,5-10,13]. As stated in Section 5.1, perfluoropolyether polymers are selected for their stability at high temperature and for their peculiar low T_g , in the range of -50 to -100 °C depending on chain composition, that significantly differs them from other fluorolefin copolymers [1-3,5,7-9].

As well known and expected, the insertion of carbon nanotubes in polymer matrices modify the glass transition temperature [18-22]. In particular an increase of T_g as the COOH-CNT concentrations rising will be explained by the hardness of CNTs, that induce a more stiffness to the polymer chain.

Notwithstanding the observation stated in different articles in literature, in which differential scanning calorimetry scarcely detects perfluoropolyether thermal behavior, a thermal characterization on nanocomposites with selected COOH-CNT was done [6-9].

As well known in literature, most of perfluoropolyethers containing polyurethane groups, like P56, show a clear biphasicity with two separated glass transition temperature, that could be related to two segregated different phases [3,6-9]. This phase segregation is often present on a submicron or nanoscale, and it is explained by the different solubility parameter of the perfluoropolyether and urethane chain. The T_g observed at lower temperature, between -100 and -50 °C, is related to the soft fluorine chain phase, instead the glass transition that is observed at higher temperature, from 60 to 150 °C, is related to hydrogenated stiff chain [3,5-9,13].

As could be observed in Figure 8, the insertion of carbon nanotubes induces only a small change in T_g of the fluorinated phase, even for the nanocomposites containing 10 %wt of COOH-CNT.

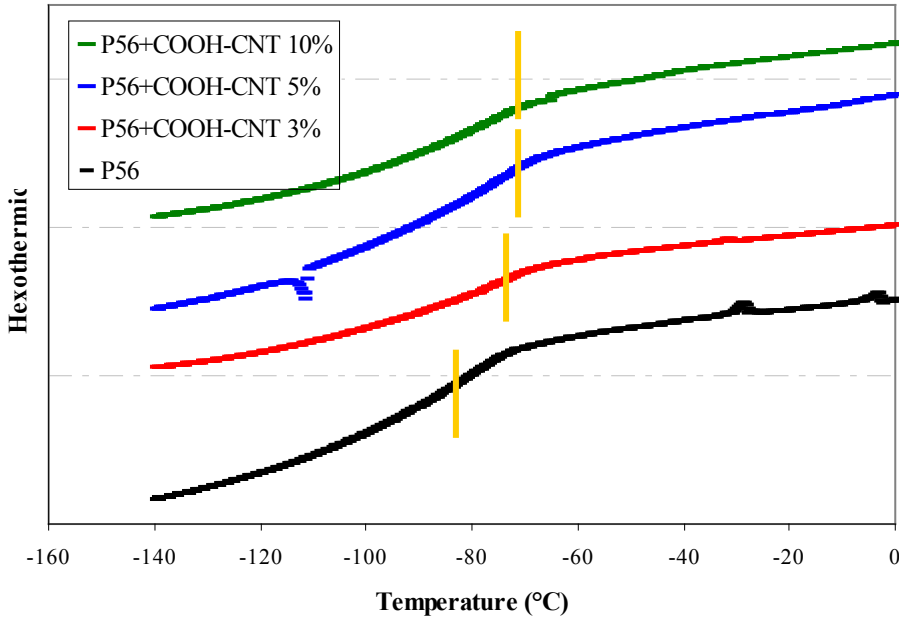


Figure 8 - Differential scanning calorimetry trace for P56 nanocomposites at different concentrations versus temperature showing glass transition related to fluorinated chain. Gold lines represent the calculated glass transition temperature reported in Table 1.

All the measured glass transition temperature were calculated during the second scanning curve, i.e. the cooling scan, and are reported in Table 1 that shows also the thermal behavior of pristine P56 and nanocomposite with 10 %wt of COOH-CNT at different scanning speeds (10 and 30 °C/min).

Table 1- Glass transition values of fluorinated chain for P56 nanocomposites.

| Name | COOH-CNT concentration (%wt) | Scanning Speed (°C/min) | Fluorinated glass transition (°C) |
|------------------|------------------------------|-------------------------|-----------------------------------|
| P56 | - | 20 | -81 |
| P56+COOH-CNT 3% | 3 | 20 | -74 |
| P56+COOH-CNT 5% | 5 | 20 | -77 |
| P56+COOH-CNT 10% | 10 | 20 | -77 |
| P56 | - | 10 | -120 |
| P56+COOH-CNT 10% | 10 | 10 | -110 |
| P56 | - | 30 | -33 |
| P56+COOH-CNT 10% | 10 | 30 | -35 |

As roughly observed in Figure 8, the insertion of carbon nanotubes, even at high concentration, induces only a small increase, almost neglected, in the observed glass transition temperature.

The hydrogenated glass transition temperature of perfluoropolyether-polyurethane matrices, are usually observed at a temperature above the ambient [3,5-9,13]. This peculiar property of fluoropolyurethane markedly affects the mechanical behavior at room temperature, since the polymer behaves like toughened plastics, with rubbery and glassy domains that are simultaneously presents, and could impart hardness and deformability [3,7].

Figure 9 and Table 2 show the modification induced by the carbon nanotubes insertion. The measured glass temperatures were calculated during the third scan, i.e. heating scan, that show a better sensitivity in detecting the glass transition temperature when carbon nanotubes are inserted.

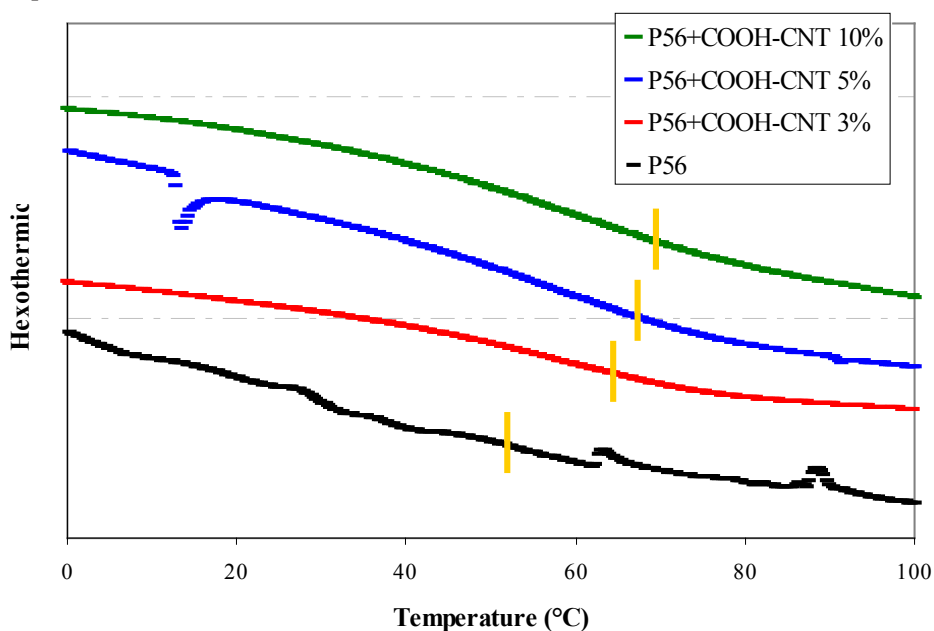


Figure 9 - Differential scanning calorimetry trace for P56 nanocomposites at different concentration versus temperature showing glass transition related to hydrogenated chain. Gold lines represent the calculated glass transition temperature reported in Table 2.

Table 2 - Glass transition values of hydrogenate chain for P56 nanocomposites at different concentrations.

| Name | COOH-CNT concentration (%wt) | Scanning Speed (°C/min) | Hydrogenated glass transition (°C) |
|------------------|------------------------------|-------------------------|------------------------------------|
| P56 | - | 20 | 51 |
| P56+COOH-CNT 3% | 3 | 20 | 63 |
| P56+COOH-CNT 5% | 5 | 20 | 66 |
| P56+COOH-CNT 10% | 10 | 20 | 70 |

A broad glass transition is observed for every samples, making hard to clearly detect the exact values of the glass transition. Notwithstanding this difficulty in detecting the glass transition at these temperatures, well known in literature as stated before, a clear increase of T_g values, related to this hydrogenate chain, hard phase, is observed with the insertion of carbon nanotubes. Pointing out the attention on these two glass transitions, the rise of T_g related to the hard phase is higher than the small increase observed in the fluorine chain glass transition values, for nanocomposites with same COOH-CNT insertion. This will led us to hypothesize a better affinity of carbon nanotubes with the hydrogenated chain instead of the fluorinated chain, probably due to the presence of carboxylic group on the CNTs external wall. Moreover, COOH-CNT could partially be specifically segregated around hard phase, i.e. around domains with hydrogenated chain, and here interact better with the polymer chain and rule the increase of glass transition. The same phenomena is only partially observed on fluorinated domain, hypothetically due to a lower affinity of this polymer area with the COOH-CNT structure.

As could be analyzed the insertion of carbon nanotubes into fluoro-polyurethane matrix couldn't extremely modify the particular thermal behavior of those polymer. Moreover, COOH-CNT presence amplifies the range of temperature into which the nanocomposites could behave like a toughened plastic, widening this peculiar characteristic, exploited in very different industrial applications.

Differential scanning calorimetry were analyzed also on nanocomposite with phosphate perfluoropolyether (TLS). The structure of this matrix, e.g. M_w of 2000 g/mol and no polyurethane structure, permit to observe only a glass transition at low temperature, related, as observed for P56 nanocomposites, to the fluorinated chain.

Figure 10 and Table 3 show the modification induced by the insertion of carbon nanotubes in these perfluoropolyether based nanocomposites. Same observation already stated for nanocomposites containing fluoro-polyurethane could be easily made. The insertion of carbon nanotubes slightly changes the fluorinated chain

behavior, maintaining the peculiar glass transition temperature at low values, as required in many industrial application for those perfluoropolyether polymers.

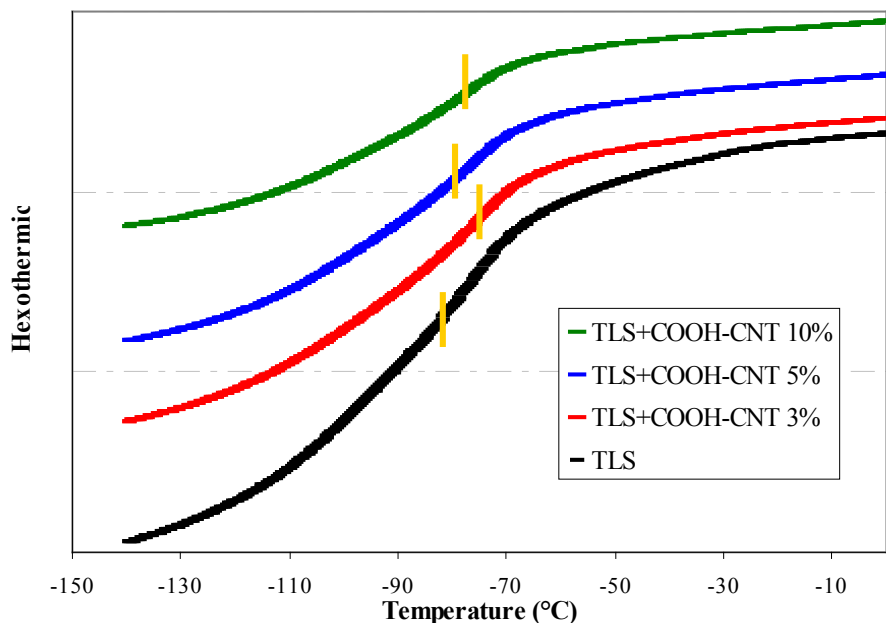


Figure 10 - Differential scanning calorimetry trace for TLS nanocomposites at difference COOH-CNT concentrations versus temperature showing glass transition related to fluorinated chain. Gold lines represent the calculated glass transition temperature reported in Table 3.

Table 3 - Glass transition values of fluorinated chain for TLS nanocomposites at difference COOH-CNT concentrations.

| Name | COOH-CNT concentration (%wt) | Scanning Speed (°C/min) | Fluorinated glass transition (°C) |
|-----------------|------------------------------|-------------------------|-----------------------------------|
| TLS | 0 | 20 | -83 |
| TLS 10% CNT 3% | 3 | 20 | -71 |
| TLS 10% CNT 5% | 5 | 20 | -79 |
| TLS 10% CNT 10% | 10 | 20 | -74 |

5.3.3 Dynamic mechanical analysis

Dynamic mechanical analysis were conducted only on fluorinated polyurethane nanocomposites (P56). TLS nanocomposites, due to the low molecular weight of

the phosphate perfluoropolyether matrix (M_w around 2000 g/mol), couldn't create a self sustained film and couldn't be analyzed with our selected instrumentation and procedure described in Section 4.2.5.

DMA is well exploited in literature on perfluoropolyether matrices in order to comprehend the peculiar mechanical properties of those polymers [1,3,5-9]. On fluorinated polyurethane matrix, DMA spectra, in dynamic scans, allowed the determination of T_g and other relaxation phenomena with a more accuracy than DSC analysis [3,6,7]. Moreover DMA could better analyze the peculiar mechanical behavior, as toughened plastic, observed for these fluoropolyurethane family between the two glass transition temperatures of the two immiscible phases [3,5-9].

The insertion of carbon nanotubes could strongly change the mechanical behavior of P56 nanocomposites, and in particular a change at high temperature is expected.

Figure 11 shows the temperature dependence of storage shear modulus (G') at 0,5 Hz for the P56 nanocomposites with increasing COOH-CNT composition.

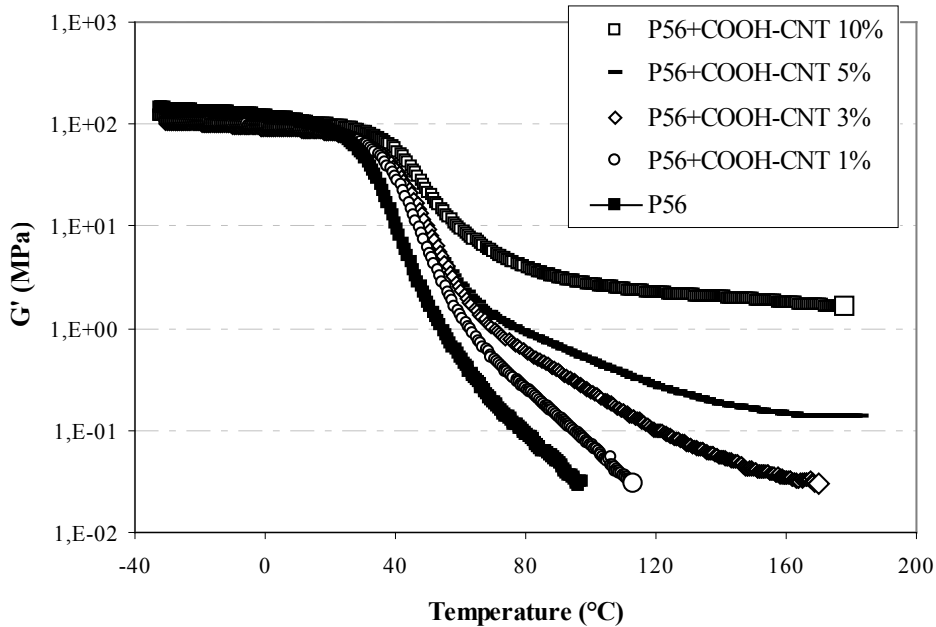


Figure 11 - Dynamic mechanical spectra of storage modulus against temperature for P56 nanocomposites at different COOH-CNT concentrations measured at 0,5 Hz.

The dynamical scans analyzed are better described in Section 5.2.5. Unfortunately, due to problems in clamping at low temperature, scans start only above -40 °C, and so DMA couldn't detect the change induced by CNTs, in mechanical behavior, around and below the glass transition temperature related to the fluorinated chain.

A first observation could be made on the plateau modulus observed around

the ambient temperature. These values, in the order of 100 MPa, is not effected by the insertion of carbon nanotubes. As already observed during calorimetric characterizations, this plateau, that is noticed at temperature above the ambient, is a peculiar property of fluorinated polyurethane, that make them behave like a toughened polymer for the presence of both rubbery and glassy domains at the same time, imparting hardness and high deformability ^[3,7]. Same behavior are observed at different scanning frequency studied, as could be seen for example at 10 Hz in Figure 12.

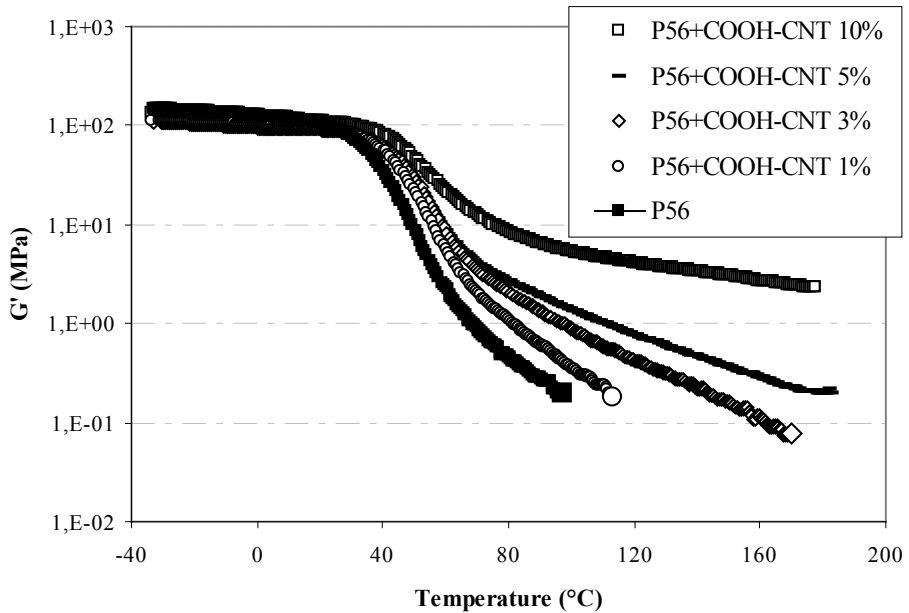


Figure 12 - Dynamic mechanical spectra of storage modulus against temperature for P56 nanocomposites at difference COOH-CNT at different concentrations measured at 10 Hz.

As the COOH-CNT concentration rise, the observed transition at temperatures above 40 °C starts to wide over two decade of temperature, not permitting a complete analysis of the modification induced by the carbon nanotubes presence on the transition value. In order to better comprehend this relaxation is useful to observe the loss tangent dependence on temperature for the investigated nanocomposites. As could be seen in Figure 13 at 0,5 Hz, a clear peak in $\tan \delta$ could be observed only in pristine P56 sample. As the carbon nanotubes are inserted, a more undefined peak with a broaden right wing is examined.

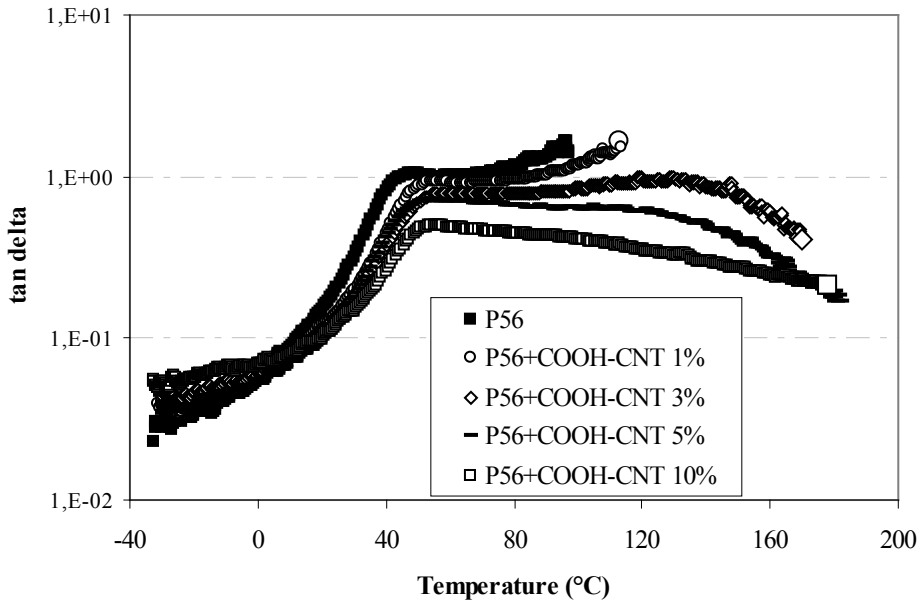


Figure 13 - Dynamic mechanical spectra of tangent δ against temperature for P56 nanocomposites at different COOH-CNT concentrations measured at 0,5 Hz.

Same loss tangent behavior is obviously observed at different scanning frequencies investigated.

Moreover, it is interesting to examine the observed $\tan \delta$ values during this relaxation, reported in Table 4. Insertion of carbon nanotubes decreases the loss tangent values, i.e. as roughly observed before, the relaxation transition is spread in a wide temperature range, and so the behavior is showed in a less sigmoid way.

Table 4 – Dynamical mechanical values of tangent δ (G''/G') for P56 nanocomposites at difference COOH-CNT concentration versus different frequencies investigated.

| Name | % CNT | Tan δ value at 0,5 Hz | Tan δ value at 1 Hz | Tan δ value at 5 Hz | Tan δ value at 10 Hz |
|------------------|-------|------------------------------|----------------------------|----------------------------|-----------------------------|
| P56 | - | 1,04 | 1,02 | 0,96 | 0,95 |
| P56+COOH-CNT 1% | 1 | 0,94 | 0,93 | 0,88 | 0,86 |
| P56+COOH-CNT 3% | 3 | 0,79 | 0,79 | 0,75 | 0,75 |
| P56+COOH-CNT 5% | 5 | 0,72 | 0,71 | 0,68 | 0,66 |
| P56+COOH-CNT 10% | 10 | 0,50 | 0,50 | 0,47 | 0,46 |

When the temperature is higher than 100 °C, a clear different behavior is observed in P56 nanocomposites as the COOH-CNT concentration is risen. Pristine anionic segmented polyurethane containing perfluoropolyether couldn't be studied with DMA's shear sandwich method at a temperature higher than 100 °C. This is caused by the low storage modulus values of this pristine PFPE, that make the sample to slip on instrument grips, and scattered values are provided by DMA instrument (data not shown). As the concentration of carbon nanotubes is increased, a plateau behavior above the relaxation temperature is observed in Figure 11 and in Figure 12. G' values on this "rubbery" plateau are increased as the COOH-CNT concentration is risen, and the extension of the plateau reach the maximum temperature studied in our experimentation (i.e. 180 °C). As could be observed, the insertion of carbon nanotubes could create a broad "rubberlike" plateau that extends to an higher temperature than the ones observed for pristine perfluoropolyether, providing a very promising spreading of the peculiar PFPE mechanical properties at high temperature, that could be industrially exploited.

5.3.4 Contact angle measurements

Contact angle measurements between liquids and polymer solids are often used for the evaluation of the surface energy and wettability characteristics of materials [3,7,9-13]. Surface properties modification is one of the most exploited characteristic of perfluoropolyether polymers in industrial applications, due to their specific performances like water and oil repellence [3,7,9-13]. The possibility of a change in surface properties, induced by carbon nanotubes insertion, needs to be studied due to the great importance of such properties for any PFPE nanocomposites applications.

5.3.4.1 Static contact angle measurements

The first characterization were made using static contact angle with two different investigating liquids, water and diiodomethane. P56 based nanocomposites show a clear hydrophobic oleophobic behavior as could be observed in Figure 14, and show a good filming capability with sticking behavior. It could be pointed out that an above 100 ° surface contact angle, versus water, values are present for all nanocomposites containing carbon nanotubes.

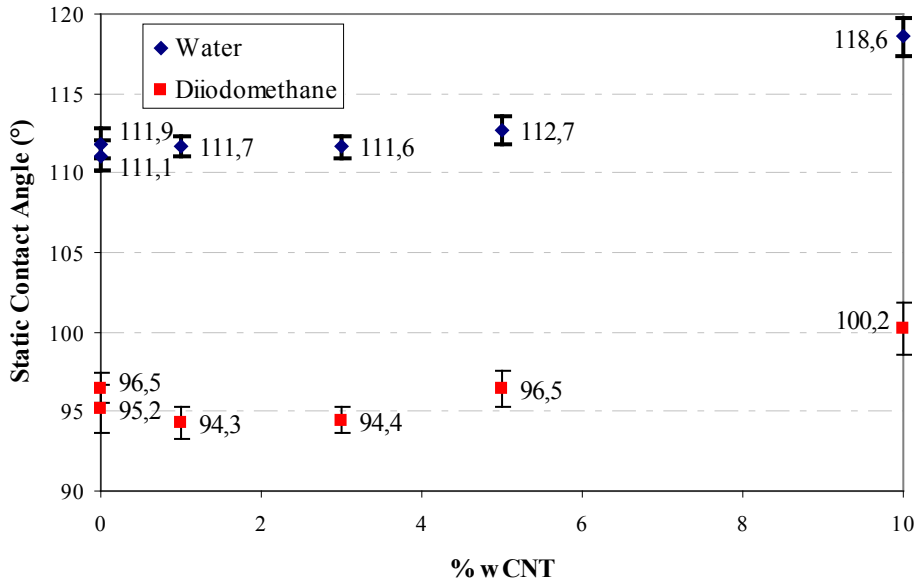


Figure 14 - Static contact angle against water (blue symbols) and against diiodomethane (red symbols) for P56 nanocomposites at difference COOH-CNT concentrations.

An increasing contact angle value against water and diiodomethane could be observed as the concentration of COOH-CNT is augmented, confirming a slightly increased hydrophobic/oleophobic behavior for nanocomposites with CNTs.

For nanocomposites with TLS polymer matrix, a similar behavior is observed in Figure 15. Unfortunately, due to the low molecular weight of phosphate based PFPE, a metastable contact angle against water and against diiodomethane is observed, invalidating the measurements for pristine polymer specimen and for nanocomposites containing small concentrations of COOH-CNT. Films formed by pristine TLS and by nanocomposites with small concentrations of carboxylic carbon nanotubes, look not completely regularly formed. This behavior is once again explained by the low molecular weight of TLS. Liquid drop induces a rearranging of polymeric chains that was eased by the low value of M_w of those nanocomposites.

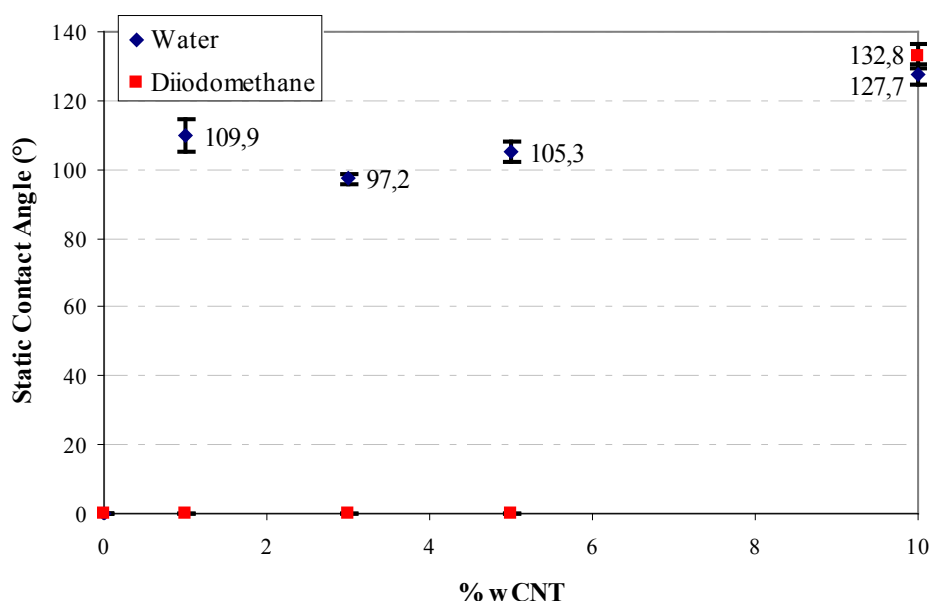


Figure 15 - Static contact angle against water (blue symbols) and against diiodomethane (red symbols) for TLS nanocomposites at difference COOH-CNT concentrations.

When carbon nanotubes are inserted at high concentrations, a stable measurements against water could be observed for TLS nanocomposites containing COOH-CNT. With diiodomethane investigation liquid, only at a CNT's concentration of 10 %wt a stable measurement could be observed. This changing behavior, from a metastable to a stable contact angles, as the CNTs are inserted, could be explained by the hardening effect of carbon nanotubes introduction, that permits the creation of a more rigid film of these TLS nanocomposites, that reduces the rearrangements of polymeric chains, and so permits a more stable contact angle measurement. Moreover, only for this sample with 10 %wt of COOH-CNT, the morphology of the film looks more uniform.

A clear characterization of surface behavior could be analyzed with the calculation of surface tension and its components, disperse and polar, using the results obtained with the different investigated liquids. As could be seen in Figure 16, the total surface energy is slightly reduced, for P56 based nanocomposites, only when the concentration of carbon nanotubes is above the 3 %wt. A small decrease of both dispersive (Van der Walls) component and polar component (caused by the presence of polar group on the film surface) is observed when the composition of COOH-CNT reaches the highest level investigated.

From these analysis, it could be stated that carbon nanotubes insertion didn't quantitative modify the peculiar surface energy of PFPE matrices and the hydrophobic/oleophobic behavior for those nanocomposites is maintained.

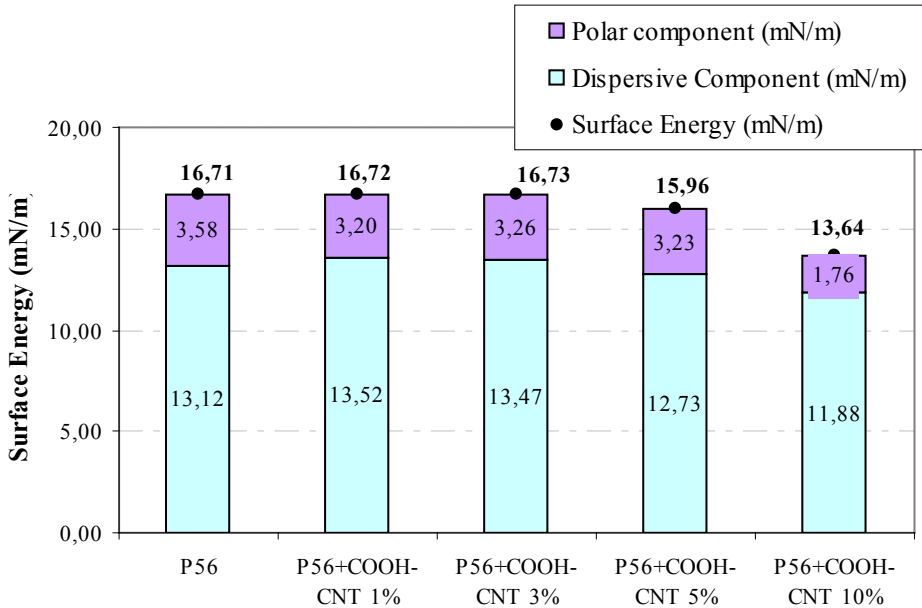


Figure 16 - Surface energy, polar component and dispersive component for P56 nanocomposites at difference COOH-CNT concentrations.

No such analysis could be made for TLS nanocomposites, due to the above mentioned difficulties in measuring stable contact angle with the investigated liquids.

5.3.4.2 Dynamic contact angle measurements, morphology and roughness characterization

Perfluoropolyether polymers are also intensively studied using dynamic contact angle measurements for their peculiar behavior, in this characterization, due to their particular biphasic molecular structure. It is well know that the polyphasic structure of PFPE polymers will induce a strong thermodynamic hysteresis [3,7,9-13]. The introduction of carbon nanotubes could change the polyphasicity, and so one of the peculiar behavior of those nanocomposites.

In Figure 17 the average of advancing and receding contact angle against water and the difference between these two values, for nanocomposites with P56 matrix, are showed. As could be observed, large hysteresis are present, confirming the presence of a strongly polyphasic fluorinated surface with domains of higher energy hydrogenated moieties. This behavior is not modified by the presence of carbon nanotubes. Only a small trend could be identified for nanoosites with high COOH-CNT concentrations, for which a little increase of the difference between the advancing and receding contact value is observed.

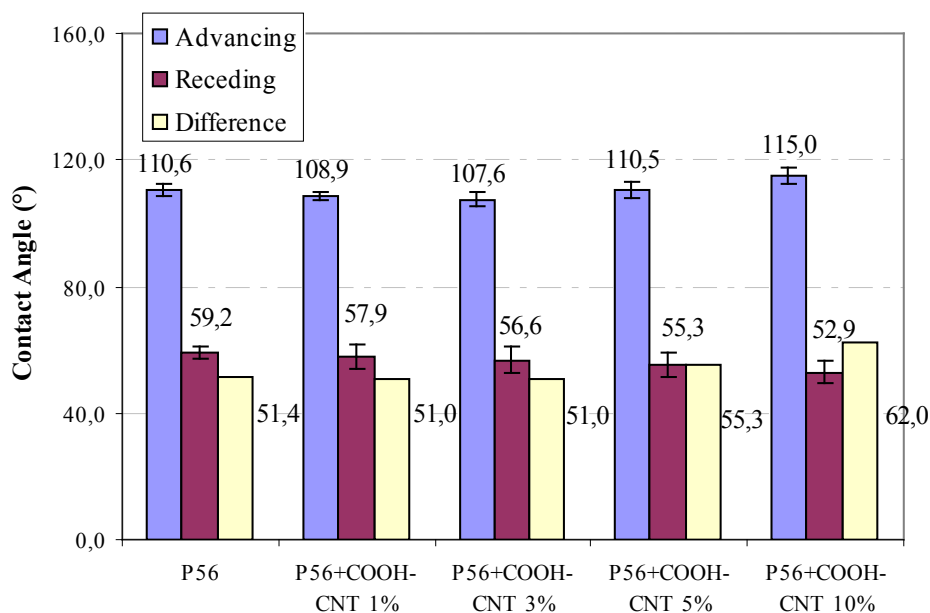


Figure 17 - Dynamic contact angle against water average values: advancing, receding and difference between these two values for P56 nanocomposites at difference COOH-CNT concentrations.

The small increase in the difference between advancing and receding contact angles, at increasing carbon nanotubes concentrations, could be better understood with morphological analysis of the samples.

Scanning electron microscopy images clearly state that some change in roughness is present with the insertion of the carbon nanotubes.

Figure 18 shows the surface of P56 pristine film and the nanocomposites with COOH-CNT at 5 %wt, and a clear increase in roughness is observed for latter sample.

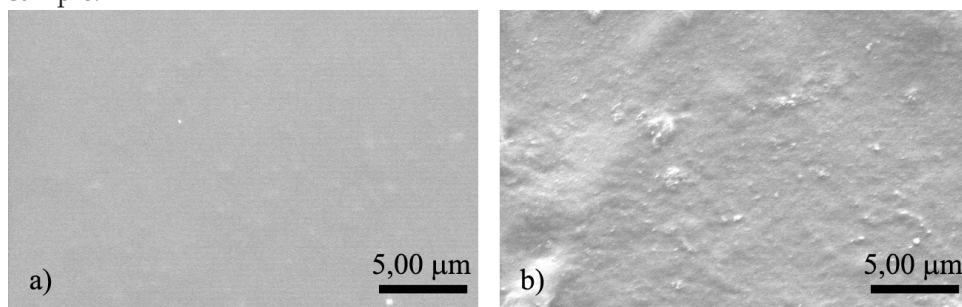


Figure 18 - SEM images of fluorinated film: a) P56 pristine, b) P56 nanocomposites containing 5 %wt of COOH-CNT.

Profilometer further confirms this observation. Figure 19 shows the average roughness values for selected samples based on P56. As observed, an increased roughness of the film is induced by the presence of the nanoparticles, even if those increase is not so consistent.

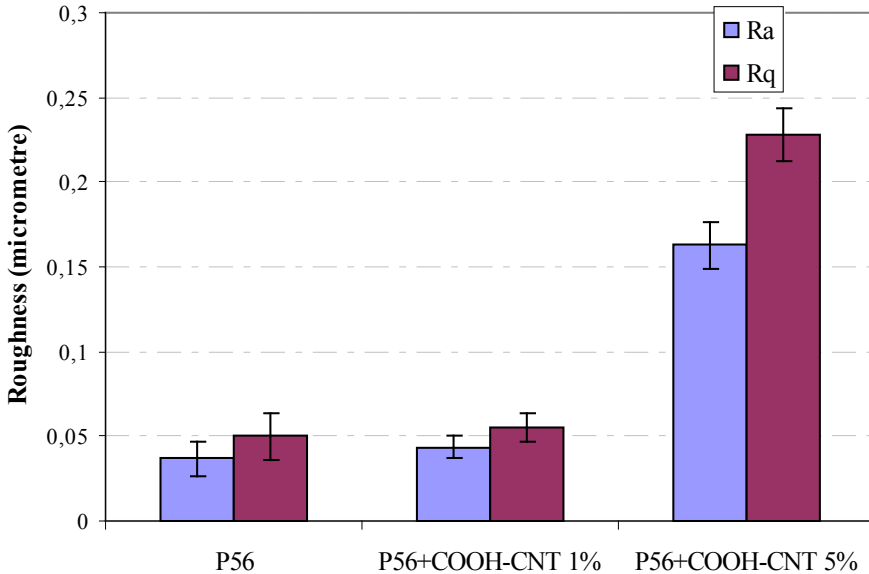


Figure 19 - Roughness, R_a arithmetic average, R_q root mean squared average, for pristine P56 and nanocomposites at increasing COOH-CNT concentrations.

This tendency of increased roughness, with increased COOH-CNT concentration, will explain easily the small raise of the difference between advancing and receding contact angle, with a creation of Cassie Baxter effects [23]. As well known, when dealing with a heterogeneous surface, the contact angle measurement has to be taken into account also the air that is trapped inside the roughness, underneath the liquid drop, that tends to slightly increase, as suggested by the Cassie Baxter model, the contact angle itself [23].

A different behavior is observed for the nanocomposites containing TLS phosphate matrix. As already observed in Section 5.3.4.1 with static measurements, a measure of contact angle versus water was not possible with pristine TLS polymer, due to the physic adsorption of the dropped liquid. For these nanocomposites, as could be seen in Figure 20, only samples containing COOH-CNT could be analyzed. The insertion of carbon nanotubes largely decreases the difference between advancing and receding contact angle versus water.

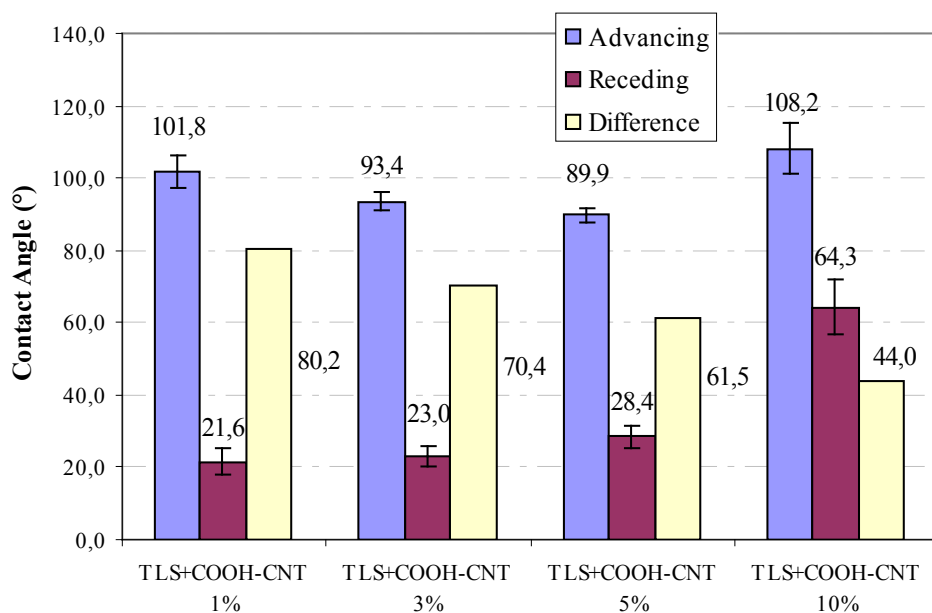


Figure 20 - Dynamic contact angle against water average values: advancing, receding and difference between these two values for TLS nanocomposites at difference COOH-CNT concentrations.

This modification, that seems in contrast with the results obtained with P56 nanocomposites, could be understood taking into account the differences between the two perfluoropolyether matrices here studied. TLS-PFPE matrix, with its low molecular weight, no urethane moieties and phosphate groups in polymer chain, could be easily modified by the presence of CNTs and their carbon structure, reducing the polyphasicity present on the surface. Moreover, an analyzing of the scanning electron microscopy images could outline the difference in morphologies induced by the presence of the carboxylic functionalized carbon nanotubes.

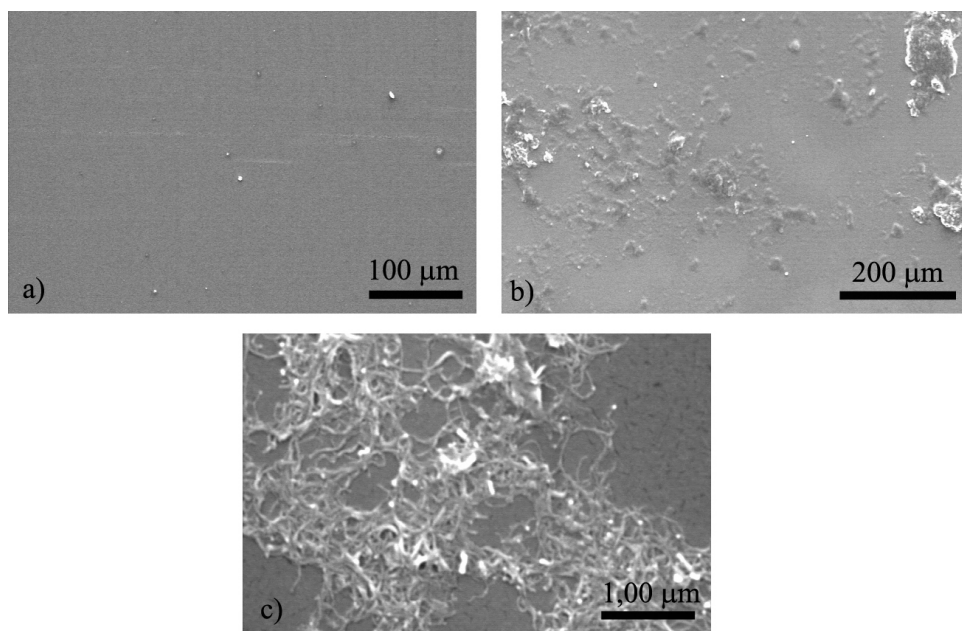


Figure 21 - SEM images of fluorinated film: a) TLS pristine, b) and c) TLS nanocomposites containing 5 %wt of COOH-CNT at different magnification. c) image show the morphology appearance of COOH-CNT in bulky agglomeration.

As Figure 21 delineates, the TLS pristine oligomer, even in its difficulty in film formation, due to the low molecular weight and high surface tension, shows a very plain morphology. When COOH-CNT are inserted, a roughness surface is formed, with some agglomerations of carbon nanotubes surrounded by fluorinated polymer. Inside those agglomeration, it's possible to clearly distinguish the carbon nanotubes presence. This behavior is rather different from the one observed for P56 nanocomposites, in which the surface is modified by the insertion of carbon nanotubes as well, but with less roughness induced and no CNT aggregation visible. Therefore the roughness analysis on TLS nanocomposites' film gives some more details on morphology.

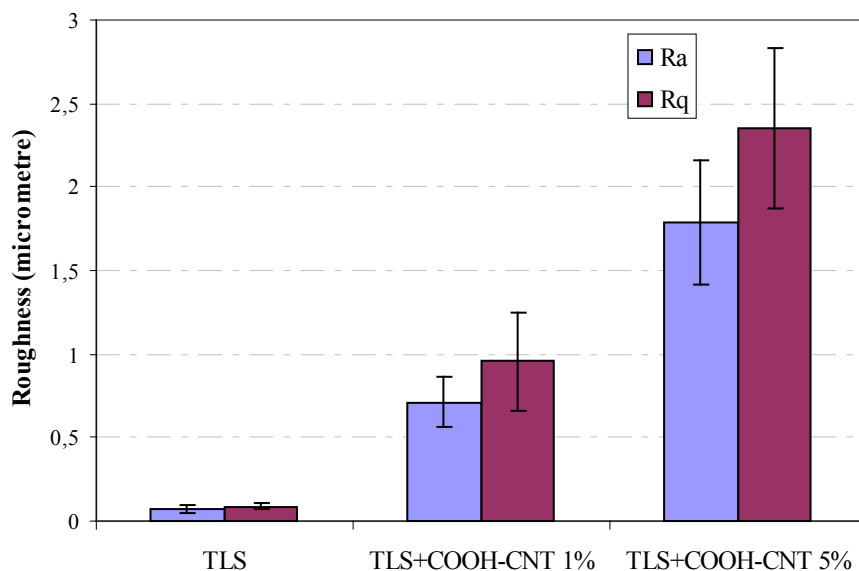


Figure 22 - Roughness, R_a arithmetic average, R_q root mean squared average, for pristine TLS and nanocomposites at increasing COOH-CNT concentrations.

Figure 22 shows that, as the concentration of carbon nanotubes are increased, the film passes from smooth surface of the pristine TLS to a strong roughness of nanocomposites with 5 %wt of COOH-CNT. This further confirms the observation made on SEM images.

With those observations, a better analysis of the dynamic contact angles measurements could be made. An increased roughness on surface, here clearly noticed when COOH-CNT are inserted, gives an higher hysteresis between advancing and receding contact angles as well explained by the Cassie Baxter equation^[23]. So, the decrease of that difference value, here observed in Figure 20, as COOH-CNT concentration is increased, couldn't be explained by the difference in roughness values analyzed.

As noticed, an advancing contact angle of around 108° is observed for the film formed by the TLS nanocomposite with lowest concentration of COOH-CNT, i.e. 1 %wt. This value is lower than expected for an highly hydrophobic perfluoropolyether based nanocomposites. As the concentration of COOH-CNT is increased, higher advancing values is noticed when the concentration reach the 5 %wt. So, we hypothesized that the behavior observed by TLS nanocomposite is caused by the low molecular weight of the oligomer matrix. As low concentration of COOH-CNT is inserted, the nanocomposites behaves in similar way like the pristine polymer. As the water is dropped, the low molecular weight of the matrix

permit an arrangement of the chain domains. This movements is only partially stopped by the presence of carbon nanotubes, that contribute to induce a more rigid structure. As the concentration of COOH-CNT is risen, this stiffening of the chain is more present and contribute to completely stop the fluorinate chain and so, let the film to behave as expected by a film of polyphasic polymer. This stiffening induced behavior clearly explains the difference observed in Figure 20 and could be confirmed by observing that film formation is easier when nanocomposites containing high concentration of COOH-CNT are laid.

Kinetic hysteresis are generally caused by surface swelling or reorganization of polyphasic hydrophilic-hydrophobic structure. For all nanocomposites analyzed, based on both P56 and TLS, in this dynamic contact angle characterization, kinetic hysteresis is weak. Advancing contact angles decrease less than 2° after 3 cycles for all the samples.

5.3.5 Electrical properties

Perfluoropolyethers' molecular structure makes them a prototype of a successful polymer insulator ^[1,3,5,13,14]. The insertion of carbon nanotubes in polymer matrices is widely know to enhance the electrical conductivity of the nanocomposites, as describe in Chapter 4 for epoxy nanocomposites ^[18,19]. Inducement of electrical conductivity in perfluoropolyether based blend, with the incorporation of carbon nanotubes, could create a very promising nanocomposites with high thermo-chemical stability, and good conductivity properties for high performance applications. The modification of electrical conductivity on this classes of nanocomposites are barely investigated in literature, and the application of the growing knowledge of carbon nanotubes conductivity inducement could open to further interesting properties in innovative technological fields ^[1,13,14].

Figure 23 shows the electrical conductivity of P56 nanocomposites. As could be observed, with our instrumentation, a measurable conductivity could be detected only for nanocomposites containing COOH-CNT above 3 %wt. Starting from the calculation analyzed in Section 4.3.4, an hypothesized conductivity value for nanocomposites containing 1 %wt of COOH-CNT stands below $1 \cdot 10^{-11}$ S/m. Pristine P56, even with its ionized side chain, couldn't be measured by our instrumentation, and to best of our knowledge, the conductivity values of this matrix is not presents in literature. Starting from confrontation with other insulating fluorine polymer matrices, we could hypothesized that the conductivity values of pristine P56 polymer stand well below the value of 10^{-15} S/m.

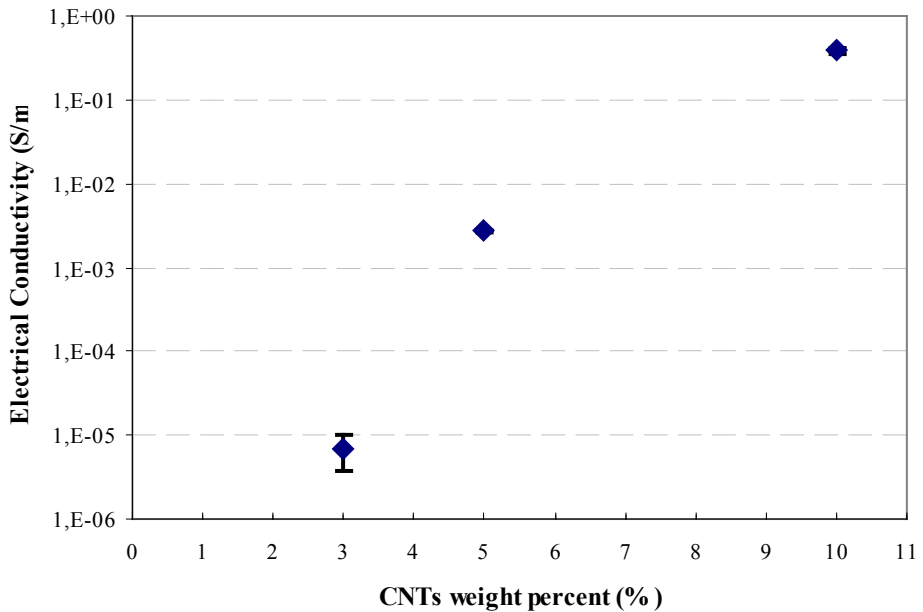


Figure 23 - DC conductivity of P56 nanocomposites versus COOH-CNT concentrations.

Based on these observations, the insertion of carbon nanotubes will provide a semi-conductive behavior for PFPE nanocomposites at concentration above 3 %wt. Only a drafted conductivity plateau could be hypothesized for concentrations of COOH-CNT above 10 %wt. No guess for percolation carbon nanotubes concentration could be made from these few analyzed samples.

Notwithstanding these few results, a very promising properties modification could be realized with the incorporation of CNTs, that could permit to add, for those nanocomposites, to well known performances, like high thermal stability and hydrophobicity, a pseudo-conductive behavior that could be exploited in different applications, for example in exploit them as hydrophobization coating of gas diffusion layer for PEM fuel cells ^[1,13,14].

5.4 CONCLUSIONS AND FUTURE CONSIDERATIONS

Two perfluoropolyether based nanocomposites containing COOH-CNT were analyzed. A method for dispersing carboxylic carbon nanotubes in perfluoropolyether based matrices were set up. A clear repeatability of the rheological behavior, for the diluted dispersions containing different concentrations of CNTs, confirmed the goodness of the dispersion method provided. A shear thinning behavior was observed for every diluted dispersions containing carbon nanotubes, with some differences caused by the differences polymer matrix and their different molecular weight. Rheological characterization, that are strongly connected with the nanotubes nanostructures, suggests that the creation of well dispersed carbon nanotubes structure, with an interconnected network, is present in all our nanocomposites.

Thermal characterization of perfluoropolyether based nanocomposites showed that non extensive modification on glass transition temperatures were made with the insertion of carbon nanotubes, permitting to maintain the peculiar thermal properties showed by pristine PFPE.

Dynamical mechanical characterizations were conducted on fluorinated polyurethane nanocomposite. The insertion of carbon nanotubes enlarges to higher temperature the relaxation transition registered above room temperature. Moreover, a plateau behavior at high temperature, above the relaxation temperature, with storage modulus value higher than 1 MPa, is observed to get higher as the carbon nanotubes concentration is increased. This will lead to wide the possible mechanical applications of those nanocomposites to higher temperatures than the ones usually exploited.

A no modification of superficial properties were observed in contact angle measurements with the insertion of carbon nanotubes, confirming the peculiar oleophobic/hydrophobic behavior for those nanocomposites. For polyurethane based nanocomposites, the insertion of carbon nanotubes didn't modify greatly the morphologies of those film. Instead, for phosphate based nanocomposites, as the concentration of carbon nanotubes are risen, a more easily film formation is observed with a high roughness values. COOH-CNT permit to increase the stiffness of the polymer chain.

A clear conductivity is induced with COOH-CNT insertion on perfluoropolyether composites. This exceptional property modification could wide the possible applications of perfluoropolyether based nanocomposites. The most promising application will be further described in Chapter 6, and is concerned on the usage of PFPE-COOH-CNT nanocomposites for the hydrophobization of the carbon cloth used as gas diffusion layer for a PEM fuel cell systems.

Starting from all those observations a promising step is to create nanocomposites with the insertion of NH_2 functionalized carbon nanotubes. Those nanoparticles

could react easily with the functionalized side chain of fluoropolymers, and so they could better create an homogenous nanocomposites. In addition, more studies will be directed in order to modify the functionalization of perfluopolyether matrices, in order to tune up further the exploitation of those polymers with the insertion of carbon nanotubes.

5.5 REFERENCE

1. T. Pham, V. Sridhar, J. Kim, Fluoroelastomer-MWNT nanocomposites – 1: Dispersion, morphology, physico-mechanical, and thermal properties, *Polymer Composites*, Volume 30 (2), 121–130 (2009).
2. R. Valsecchi, L. Torlaj, S. Turri, C. Tonelli, M. Levi, Barrier properties in hydrogenated acrylonitrile butadiene rubber compounds containing organoclays and perfluoropolyether additives, *Journal of Applied Polymer Science*, Vol 119, 3476-3482 (2011).
3. S. Turri, M. Scicchitano, R. Marchetti, A. Sanguineti, in: *Fluoropolymers 2: Properties*, G. Hougham, P.E. Cassidy, K. Johns, T. Davidson, Kluwer Academic, 145 (1999).
4. T. Trombetta, European Patent, EP 1 559 733 B1 (2005).
5. C. Tonelli, T. Trombetta, M. Scicchitano, G. Simeone, G. Airoidi, New fluorinated thermoplastic elastomers, *Journal of Applied Polymer Science*, Vol. 59, 311-327 (1996).
6. S. Turri, R. Valsecchi, M. Levi, M. Cristini, A. Sanguineti, Microstructure to property relations in a family of millable polyurethane fluoroelastomers, *European Polymer Journal*, 44, 2951-2961 (2008).
7. S. Turri, M. Levi, T. Trombetta, Waterborne anionomeric polyurethane-ureas from functionalized fluoropolyethers, *Journal of Applied polymer science*, Vol. 93, 136-144 (2004).
8. S. Turri, M. Levi, M. Cristini, A. Sanguineti, Rheological properties and thermal transitions in millable polyurethane fluoroelastomers, *Polymer International*, 54, 698-704 (2005).
9. T. Trombetta, P. Iengo, S. Turri, Fluorinated segmented polyurethane anionomers for water-oil repellent surface treatments of cellulosic substrates, *Journal of Applied Polymer Science*, Vol. 98, 1364-1372 (2005).
10. S. Turri, A. Sanguineti, S. Novelli, R. Lecchi, Preparation and properties of poly(urethane-urea) crosslinked coatings from perfluorocopolyethers and polyfunctional isocyanurates, *Macromolecular Materials and Engineering*, 287, 319-329 (2002).
11. M. Licchelli, S. J. Marzolla, A. Poggi, C. Zanchi, Crosslinked fluorinated polyurethanes for the protection of stone surfaces from graffiti, *Journal of Cultural Heritage*, 12, 34-43 (2010).
12. S. J. Marzolla, Modified fluorinated polymers for the protection of stone surface from mural writings, *Scientifica Acta*, 2 (2), 12-16 (2008).

13. P. Gallo Stampino, D. Molina, L. Omati, S. Turri, M. Levi, C. Cristiani, G. Dotelli, Surface treatments with perfluoropolyether derivatives for the hydrophobization of gas diffusion layers for PEM fuel cells, *Journal of Power Sources*, 196, 7645-7648 (2011).
14. X. Zhao, A. Koos, B. Chu, C. Johnston, N. Grobert, P. Grant, Spray deposited fluoropolymer/multi-walled carbon nanotube composite films with high dielectric permittivity at low percolation threshold, *Volume 47 (3)*, 561-569 (2009).
15. V. Datsyuk, M. Kalyva, K. Papagelis, J. Parthenios, D. Tasis, A. Siokou, I. Kallitsis, C. Galiotis, Chemical oxidation of multiwalled carbon nanotubes, *Carbon*, 46, 833-840 (2008).
16. M. Bystrzejewski, A. Huczko, H. Lange, T. Gemming, B. Buchner, M. Rummeli, *Journal of Colloid and Interface Science*, 345, 138-142 (2010).
17. Y. Shieh, H. Wu, Y. Twu, Y. Chung, *Colloid and Polymer Science*, 288 (4), 377-385 (2010).
18. M. Chapartegui, N. Markaide, S. Florez, C. Elizetxea, M. Fernandez, A. Santamaría, Specific rheological and electrical features of carbon nanotube dispersion in an epoxy resin, *Composites science and technology*, 70, 879-884 (2010).
19. I. Alig, T. Skipa, D. Lellinger, P. Pötschke, Destruction and formation of a carbon nanotube network in polymer melts: Rheology and conductivity spectroscopy, *Polymer*, 49, 3524-2532 (2009).
20. M. J. Kayatin, V. A. Davis, Viscoelasticity and Shear Stability of Single-Walled Carbon Nanotube/Unsaturated Polyester Resin Dispersions, *Macromolecules*, Vol 42 (17), 6624-6632 (2009).
21. Z. Fan, S. G. Advani, Rheology of multiwall carbon nanotube suspensions, *Journal of Rheology*, 51 (4), 585-604 (2007).
22. M. Abdalla, D. Dean, P. Robinson, E. Nyairo, Cure behavior of epoxy/MWCNT nanocomposites: The effect of nanotube surface modification, *Polymer*, 49, 3310-3317 (2008).
23. S. Wu, *Polymer Interface and Adhesion*, Dekker, 1982.

>6
FLUORINATED
NANOCOMPOSITES
COATINGS ON GAS
DIFFUSION LAYER



6.1 INTRODUCTION

Fuel Cells (FC) are electrochemical devices which convert chemical energy into electrical energy, without pollutant emission^[1-4]. Among the different type of FCs, depending on the different electrolytes used, the so-called polymer electrolyte membrane or proton exchange membrane (PEM) fuel cells are the best choice for automotive applications, for small-scale power generation and also for portable devices^[1,4-7]. However all these favorable points, PEMFCs must overcome certain engineering and economic obstacle to become commercially and popularly viable^[5-7]. As described in Chapter 1, the heart of PEM fuel cell is the membrane electrode assembly (MEA), which consist of a proton exchange membrane and two catalyst layers, anode and cathode, onto which the reaction is performed. Many interests were devoted on developing high performance MEA, in order to compete with the conventional energy conversion technologies^[1,4-7]. Membrane electrode assemblies are usually sandwiched by two electrode plate, containing channels for gases (fuel) insertion and water (emission) disposal. Electrodes are frequently mirrored, when cell are stacked together in series, to obtain greater voltages, and are called, for their configuration, bipolar plates (BP).

As observed in literature and widely explained in Chapter 1, the reactants, gases, and the product, water vapor or liquid water, enter and exit through the diffusion path in the electrode^[1,4-7]. In general an hydrophobic gas diffusion layer (GDL) and an additional microporous layer (MPL) are placed between the catalyst layer and the flow channel plate^[1,5-17]. Although the GDL and MPL have no electrochemical reaction sites, they are widely known to play an important role in the overall PEMFCs efficiency^[6-19]. They indeed provide a very efficient access of reactants to the catalytic sites, and they effectively remove the produced water from the electrode.

Most of the past researches in literature are focused on how to optimize the MPL morphologically, compositionally and dimensionally, for better water management and higher catalyst utilization^[7,16,18,19]. GDL properties optimization are nowadays one of the challenging topics to properly allow the fuel cells to operate at their optimal performances and to prolong their life span^[7-19]. This attention on gas diffusion layer is due by the fact that GDL plays a critical role in water and gases management, and is a critical electrical link between the electrochemical reaction site and the system engineering needed to construct a fuel cell^[7-19].

Gas diffusion layer are usually made of either a nonwoven carbon paper or a woven carbon cloth, in any case modified with different hydrophobic agents^[7-10,14]. This particular structure is needed for the different and often conflicting properties required in this particular layer as described in Chapter 1. GDL must be electrical conductive, highly hydrophobic, permeable to gas. It must have an optimized pore size distribution, a high corrosion stability and it must possess a

good mechanical stiffness [7-10].

Water management is critical in obtaining a stable cell performance. Usually both anode and cathode GDLs are coated with a fluoropolymer such as polytetrafluoroethylene (PTFE) or fluorinated ethylene propylene (FEP), in order to obtain the wished hydrophobic properties [7,9-14,16-18,20]. Several articles concerning PTFE and FEP coating outline that the optimal amount of hydrophobic agent is around 10-15%wt, in order to optimize the removal of product water, without interrupting the flux of the reactant and in the same time permitting a correct hydration of MEA [7,9-14,16-18,20].

In our study we introduce the perfluoropolyether (PFPE) polymers, described in Chapter 4, as alternatives to standard fluoropolymer for the modification of carbon cloths that will be used in PEM fuel cell. As described, PFPE are available in form of aqueous dispersion and could be processed without the needing of high temperature thermal sintering treatment, typical of PTFE [7,9-14,16-18,20,21]. This novel fluoropolymers are not yet used in fuel cell systems, instead they show great effectiveness in imparting water repellence and soil release to very different substrates [22-24]. Their efficiency in water-repellence will be widely studied and exploited in hydrophobization of gas diffusion layer and in modification of all conflicting properties required for this particular components in order to achieve a challenging FC performances.

Moreover in Chapter 5, we have efficiently introduced multi walled carbon nanotubes (CNT) into perfluoropolyether polymer matrices, to enhance mechanical properties and to induce a conductivity in the resulting nanocomposites. As previously noticed, a gas diffusion layer must efficiency transfer electrons to the electrochemical sites and usually this properties is reduced by the insertion of hydrophobic additives. The induced conductivity in perfluoropolyether is a very promising property, when these novel nanocomposites are used in fuel cell system, that could match one of the conflicting requirements of GDL. Furthermore, as observed in Chapter 5, PFPE nanocomposites show an higher G' values than the pristine perfluoropolyether at temperature higher than room temperature. This increased mechanical properties are one of the necessary properties required by the ideal gas diffusion layer in PEMFC system, and further create good expectation on those PFPE nanocomposites used as coating agent. Carbon nanotubes are usually exploited in microporous layer, for their high conductivity and microporous morphology, to replace or assist carbon black in minimizing the electric contact resistance with the adjacent catalyst layer and to enhance water management efficiency [25-29]. Starting from their conductivity, their microporous morphology and their high mechanical performances, other exploitations of CNTs are studied as novel free standing gas diffusion layer and as component in membrane [25-28]. Insertion of carbon nanotubes in the nanocomposites used for hydrophobization of gas diffusion layer is expected to modify the complex

water management of this unit, in order to improve the fuel cell efficiency. The modification of properties of coated carbon cloth, that will be used as gas diffusion layer, with pristine perfluoropolyether and PFPE nanocomposites containing carbon nanotubes were investigated with contact angle measurement in order to follow their hydrophobic behavior. Permeability and microscopic characterizations were examined to evaluate their change in film formation on carbon cloth fibers, and so their capability in gas diffusion when operating in fuel cell system. Conductivity of those hydrophobized carbon cloths were measured to observe the modification when carbon nanotubes are inserted in the system. Electrochemical performances of treated carbon cloths, used as gas diffusion layer, without the presence of any microporous layer, were investigated to evaluate the water management capability of those coated GDLs with these different perfluoropolymers and fluorinated nanocomposites.

6.2 EXPERIMENTAL SECTION

6.2.1 Gas diffusion layer, perfluoropolyethers derivatives, carbon nanotubes and other materials

A commercial carbon cloth (SCCG 5N), purchased by SAATI, is used in this study as gas diffusion layer (GDL). The perfluoropolyethers (PFPEs) used are fully described in Chapter 4, and here reported. Fluorolink® P56 (P56) purchased by Solvay Solexis, is a aqueous dispersion of anionic segmented polyurethane, containing perfluoropolyether blocks and carboxylated side group. Figure 1 reports the P56 structure (tetraalkylammonium counterions have been omitted).

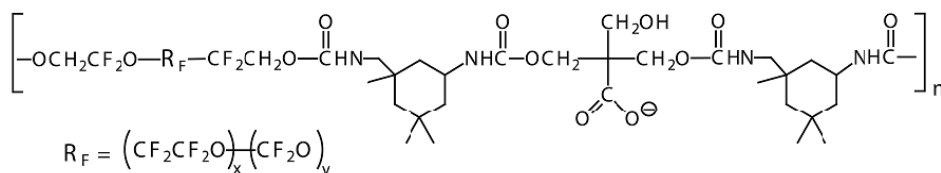


Figure 1 - Molecular structure of fluorinated polyurethane Fluorolink® P56.

Fluorolink® TLS 5007 (TLS) purchased by Solvay Solexis, is a aqueous microdispersion of perfluoropolyethers phosphate ammonium salt.

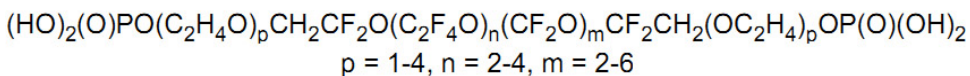


Figure 2 - Molecular structure of perfluoropolyether phosphate Fluorolink® TLS 5007.

For benchmarking purpose an aqueous polytetrafluoroethylene (PTFE) dispersion, Allogflon® D 1214X purchased by Solvay Solexis is used.

As already explained in Chapter 5, carboxylated nanotubes were inserted in perfluoropolyether to create nanocomposites that show the modified properties described in that chapter. Commercial available Nanocyl NC 3101, based on Nanocyl NC 3100 (for further informations see Section 3.2.1), were purchased by Nanocyl (COOH-CNT).

All other chemicals, if not expressly mentioned, were provided by Sigma Aldrich.

6.2.2 Dispersion and preparation of gas diffusion layers

For easy preparation, the two perfluoropolyether microdispersions and the PTFE dispersion were diluted at a solid content of 10 % w/w with deionized water, and mixed with magnetic stirring at 600 rpm for 30 minutes, in order to create homogenous and stable (more than 1 year) dispersions.

All dispersions were formulated by mass fraction based on measured component

weights. The concentration of the dispersions are always referred to the mass fraction of fluorinated dispersion in water. Instead for dispersions containing carbon nanotubes the mass fraction of carbon nanotubes is always referred to the fluorinated content for easy labeling.

6.2.2.1 Perfluoropolyether coated GDLs

PFPE dispersions were diluted with deionized water up to a concentrations ranging from 1 to 10 %w, depending on the samples. Carbon cloth, cut in wished dimensions, was then dipped in fluorinated dispersion for 10 min. The dipping procedure were conducted in a appropriate glassware that permit the complete covering of carbon cloths with the fluorinated dispersion. The ratio of fluorinated dispersion with carbon cloth area was keep constant at 56 mm²/ml. The treated samples were then roll squeezed and dried in oven at a temperature of 150 °C to completely dry off the water. Dry pick up values were calculated from sample's weight percentage difference before dipping and after heating procedures.

6.2.2.2 Polytetrafluoroethylene coated GDLs

The same operations described above for PFPE coating of carbon cloth were performed for PTFE dispersion. The only difference were in drying operations. For this PTFE coated carbon cloths, the sample were put in oven and ramp heated from ambient temperature to 90 °C for 50 minutes, following heated at 120 °C for 40 minutes, then at 280 °C for 40 minutes and finally at 350 °C for 50 minutes. This complex heating procedure was optimized in precedent work, in order to completely drying all components present in PTFE dispersion and efficiently sintering the perfluoropolyether on carbon cloth structure.

6.2.2.3 Perfluoropolyether nanocomposite coated GDLs

Starting from the knowledge acquired in Chapter 5 on dispersing COOH-CNT into PFPE dispersion, the same dispersion procedure was performed in preparing the nanocomposite dispersions for the hydrophobization of carbon cloth.

The dispersion of carbon nanotubes was conducted in different steps. A wished amount of carboxylated nanotubes was added in a flat-bottom flask containing desired amount of the aqueous dispersion of PFPE polymers. A mechanical mix was then conducted with magnetic stirring at 950 rpm for 30 minutes. The dispersion were then sonicated in a Starsonic 90 sonicator bath for 1 hour. The mixture was finally sonicated with a Sonic & Materials VCX130 sonicator tip for 30 minutes at the 80% of the instrumental amplitude. Last step was conducted in ice bath in order to reduce the water evaporation to maintain the designed solid concentration. At this point the homogeneous and stable dispersion was used for

the hydrophobization of carbon cloths. As described in Section 6.2.2.1 the GDLs were cut and dipped in fluorinated dispersion for 10 min. The same ratio between fluorinated dispersion and carbon cloth area was kept constant at 56 mm²/ml, in order to ensure the complete covering of the carbon cloth. The samples are then dried out from water in oven at 150 °C.

6.2.2.4 Polytetrafluoroethylene nanocomposite coated GDLs

The same dispersion procedure of carbon nanotubes described above, Section 6.2.2.3, was used with PTFE dispersions. The same dipping operations described were conducted. The drying process was then carried out with the heating cycle described in Section 6.2.2.2.

6.2.3 Water transmission rate

Carbon cloths for this characterization were cut in dimensions of 80 x 75 mm. An ad hoc test tube provided with gasket flange, see Figure 3, were used.



Figure 3 - Ad hoc test tube used for permeability characterizations.

The test tube, with 41 mm diameter, were filled with 50 g of deionized water and the hydrophobized carbon cloths were inserted between the gasket. The flange were closed in order to avoid the water leaking. The tube were then turned upside down to let the water place upon the treated carbon cloth, inside the test tube. The test were conducted in thermostatic room at 23 °C and keeping constant the relative humidity of 42 %. The complete apparatus, containing the treated carbon cloth, was weighted before and during the test to monitor the water transmission rate through the hydrophobized sample.

6.2.4 Scanning electron microscopy

Scanning electron microscopy analyses were performed using a Cambridge Stereoscan 360 on different carbon cloths, treated with different fluorinated dispersions and fluorinated nanocomposite dispersions. This characterization was used to monitor the morphological characteristics and the distribution of the different fluorinated polymers. For the samples treated with nanocomposites containing COOH-CNT, SEM images were exploited to determine the change in morphology induced by insertion of the nanoparticles. All specimens were sputtered with gold before imaging.

6.2.5 Contact angle measurements

Contact angle measurements were performed in order to analyze the hydrophobic behavior induced on carbon cloths by treatments with fluorinated dispersions.

Static contact angles against bidistilled water were measured at 25 °C with a DataPhysics OCA 20 equipped with a 500 µl Hamilton syringe to dispense liquid droplets. Measurements were made by means of the sessile drop technique. Results were expressed as the average of at least 30 independent measurements. The delivered volume was of 7 µl, dispensed with a 1,5 µl/s speed. The measurements were carried out after 1 s after drop deposition.

6.2.6 Electrical characterization

In-plane electrical characterization of carbon cloths was performed on hydrophobized samples with a 20 x 80 mm dimensions. All the tests were performed with a Keithley 2612 multimeter at room temperature using the 4-terminal technique. This technique was chosen for the very low impedance observed for these materials. An ad hoc cell was adopted, see Figure 4, that permit a measurement on these specific samples. The cell has the contacts' dimension with a width of 20 mm and a length of 30 mm. The current was varied from 0,1 A to 1 A dividing the scan in 50 steps. In every step the current was kept constant for 2 seconds. Conductivity of the treated carbon cloth was then calculated from resistance measurements.

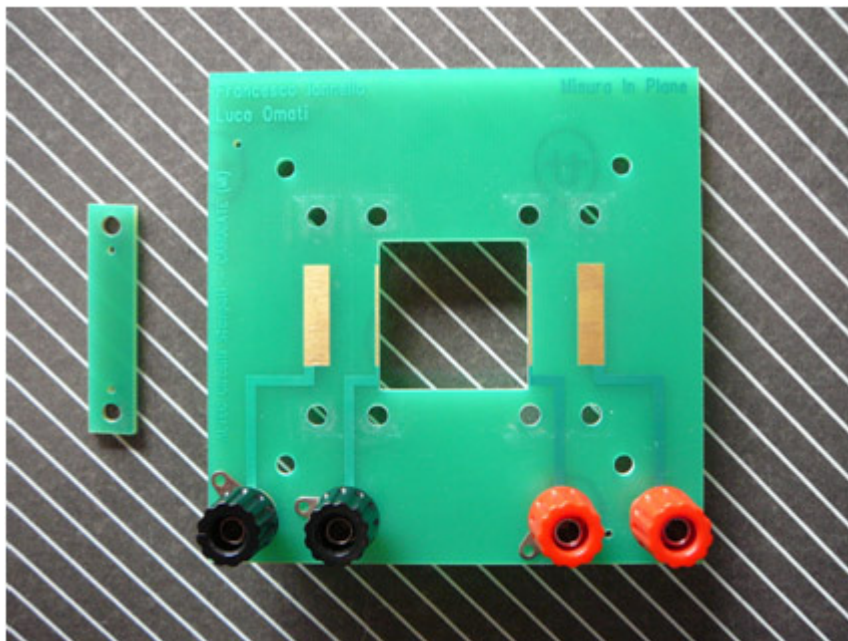


Figure 4 - Ad hoc cell used for electrical characterization with in-plane configuration, developed for carbon cloth.

6.2.7 Single cell polarization measurement

Electrochemical performances of the treated GDLs were tested in two different test station.

The first test station is a commercial single cell provided by Fuel Cell Technologies, with an active area of 25 cm² area. Treated carbon cloths were then cut in two different square of 5 x 5 cm. The bipolar plates (no stack configuration is designed, the serpentine are present only in one side of the plate) have a single serpentine at the anode and a triple parallel serpentine at the cathode. MEA were assembled using a Nafion® 212 membrane with a thickness of 50 μm and an active area of 25 cm². Catalyst Coated Membrane (CCM), provided by Baltic Fuel Cell, was coated directly onto membrane with a loading of platinum of 0,3 mg/cm² at the anode, and of 0,6 mg/cm² at the cathode. CCM was supplied with Mylar gasket, thickness 25 μm, around the active area to reduce gas leakages.

The treated carbon cloths were placed at the anode and cathode side, assembling together the MEA inside the cell. A torque on cell screw of 10 Nm were provided in order to obtain a fixed compression of GDLs at 70 % of the original thickness (about 380 μm). This compressed thickness was kept constant with an uncompressible glass fiber gasket, inserted around the active area, that further prevent gas leakages. Pure hydrogen and air were fed at the anode and cathode respectively.

The flow rate, controlled with mass flow controllers provided by Brooks, were 0,2 NI/min of hydrogen at the anode and 1 NI/min of air at the cathode. Reactant gases were humidified with bubbling procedure in humidification systems, provided by Fuel Cell Technologies, that provide a 80 % of relative humidity at anode side and a variable relative humidity for air at the cathode side (100 or 60 % HR). Cell temperature was controlled by a controller provided by Alcon and set in variable values (60 and 80 °C). Thermocouple to control cell temperature were placed as close as possible to the graphite plate. All systems operate at room temperature and in ambient pressure.

An electronic load, RBL 488-50-150-800 provided by TDI Power, to control voltage, current and generated electric power, was connected to the cell. Polarization curves were recorded under galvanostatic conditions, measuring the current density in the range from Open Circuit Voltage potential (OCV) to 0,87 A/cm². A step of 0,085 A/cm² were recorded for 420 seconds. A single measured point was traced every second. Potential values were averaged from the last 300 recorded points of every steady state, to minimize experimental artifacts due to transient phenomena.

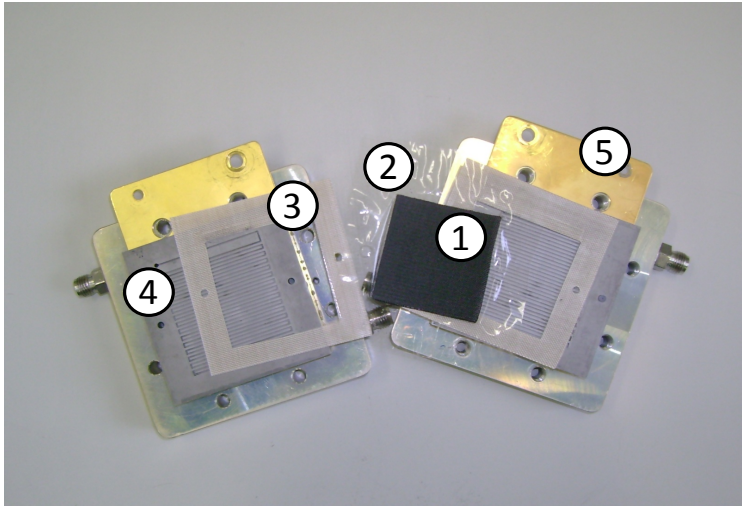


Figure 5 - Fuel Cell equipment. 1: GDL sample, 2: Catalyst Coated Membrane CCM, 3: Glass fiber Gasket, 4: Graphite plate, 5: Current collector.

The second test station have the same technical characteristic of the first test station already described, with some differences here reported. A different batch of CCM, provided from Baltic Fuel Cell, were used. The nominal catalyst layer values of platinum loadings were again 0,3 mg/cm² at the anode and of 0,6 mg/cm² at the cathode. Some differences in membrane's ion transport capability is not clearly observed, even if an evident difference in fuel cell performance is experimented. The BP have a difference configuration for the external feeding. Another technical differences is about the electronic load. An Agilent N3300A electronic load

were connected to the cell. This load permit only a potentiostatic measurement. Polarization curves were indeed recorded under potentiostatic condition in the potential range from OCV to 0,3 V with a 0,05 V step. Each step was maintained for 400 seconds and a point is recorded every second. Potential values were averaged over all 400 points. All other technical details of second test station are kept alike to the first test station.

6.3 RESULTS AND DISCUSSION

6.3.1 Preparation of Gas Diffusion Layers

As widely studied in literature, proper gas diffusion layer design is essential to allow the fuel cell operating at their optimal performance [7,9,10,11,14]. GDL should be a porous material and good electric conductor. Additionally, to prevent liquid water molecules from filling the pores of the GDL, impeding the delivery of the reaction gas, gas diffusion layer must undergo hydrophobic treatment in advance. Moreover on the anode side the membrane tends to dry out. As well known, an appropriate water management, in which as seen conflicting requirements are needed, is critical to ensure the strong performances of a PEMFC [7,9,10,15,19]. Usually carbon cloths are typically treated by partially coating them with polytetrafluoroethylene (PTFE) [7-12,14,16-18]. As a rule of thumb literature suggests that a 10 %wt loading of PTFE is sufficient to create a hydrophobic surface, to facilitate liquid water removal without a reduce in gases transportation, but only few articles concentrate their attention on material designing the hydrophobic polymer [14,20,21]. Starting from this kind of traditional GDL's hydrophobization approach, new fluorinated polymers were studied to enhance the PEMFC performances.

6.3.1.1 GDL preparation using perfluoropolyether and PTFE

In order to limit the possible variable in GDL hydrophobization, and to reduce the step of processing, looking for a future industrial preparation, a simple methodology for coating carbon cloths is studied and presented in Section 6.2.2. The first variable that needs to be considered, is the concentration of the aqueous dispersions of different fluorinated polymers. The variation of weight pick up of carbon cloth, after the hydrophobization treatments, could give an efficient indication of the effectiveness of this procedure and could be optimized in order to reduce material and time consumption.

In Section 6.2.2 the process of hydrophobization with dipping technique is fully described. Different concentration of PFPE and PTFE aqueous dispersions were used and the percentage weight dry pick up values of carbon cloth are reported in Figure 6.

As could be easily seen, the standard hydrophobization method used in literature, i.e. with a solution of 10 %wt of PTFE give a pick up values with elevated dispersion. This great deviation from the average values could easily lead to difference in hydrophobized GDLs, and so to different PEMFC performances. With a aqueous dispersion of 1 %wt of PTFE instead, a narrow dispersion of the pick up values is observed. Unfortunately this last hydrophobization method was not efficient (contact angle measurements show low values), confirming the observations

presented in literature in which at least a content of 5 %wt of PTFE is necessary for a good hydrophobization of GDL [7,10,11,14,17,20].

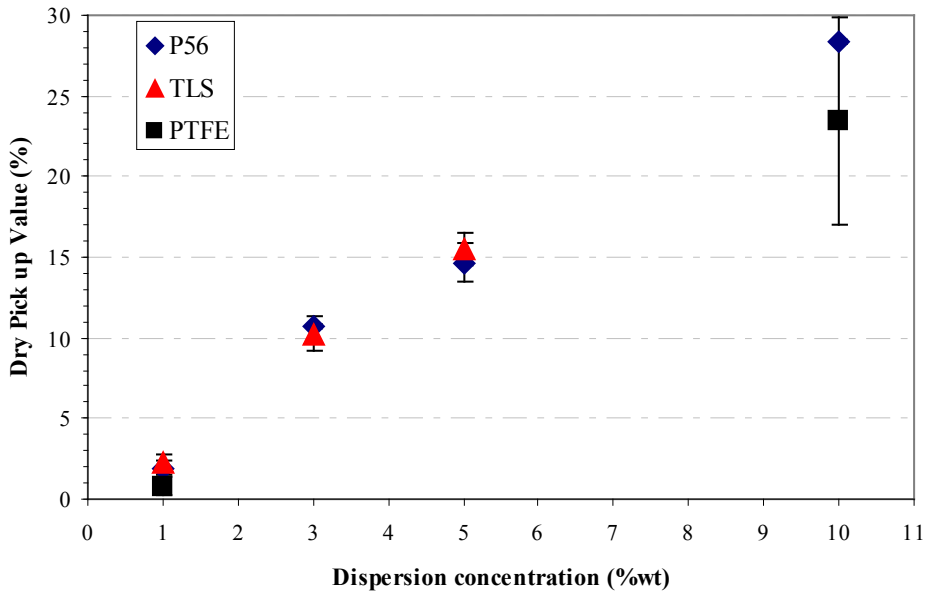


Figure 6 - Dry pick up values of carbon cloth coated with different fluorinated polymers at increasing dispersion concentration.

When the treatments were applied with the pristine perfluoropolyether polymers, different and promising results were observed. As could be seen in Figure 6, when the hydrophobization of carbon cloth is processed with PFPE dispersions, P56 and TLS, the pick up values show a low deviation from average value, and a good reproducibility with linear correlation between the dispersion compositions were observed. As could be seen in the following characterizations, carbon cloths treated with the two perfluoropolyether dispersion described, show very good performances even when the hydrophobization is processed with just 1 %wt, confirming the effectiveness of these fluorinated materials in gas diffusion layer treatments. The hydrophobization procedure with PFPE dispersions shows indeed a high reproducibility, a lower material consumption than the standard PTFE processing, obtained with similar results and, a lower temperature of processing than the sintering temperature required in PTFE treatments. These observations clearly underline the promising interest in using PFPE polymers in common carbon cloth hydrophobization treatments, in particular when a industrialization of the process will be developed

From the observation outlined above, the insertion of carboxylic carbon nanotubes were processed in 1 %wt fluorinated dispersions, permitting to focus the attention

only on the dispersion with lower perfluoropolyether amounts, that show good performances. For benchmarking purpose, COOH-CNT were also dispersed in aqueous dispersion with a 10 %wt content of polytetrafluoroethylene that represent the standard hydrophobization mixture used in literature. Carbon nanotubes, with their excellent conductivity properties, good chemical stability and large surface area, are expected to enhance the performances of the treated carbon cloths when inserted in PEMFC systems.

The percentage dry pick up values of treated carbon cloths, with different perfluoropolyether and PTFE dispersions, containing different concentrations of COOH-CNT, are present in Figure 7. As could be easily seen, the hydrophobization with polytetrafluoroethylene dispersions at 10 %wt shows a great dispersion for every content of carbon nanotubes, confirming the low reproducibility of those “standard” process. When COOH-CNT are inserted in the two perfluoropolyether polymer dispersions, the dry pick up values of the carbon cloths show quite constant values, confirming the reproducibility of those fluorinated system in hydrophobization procedure.

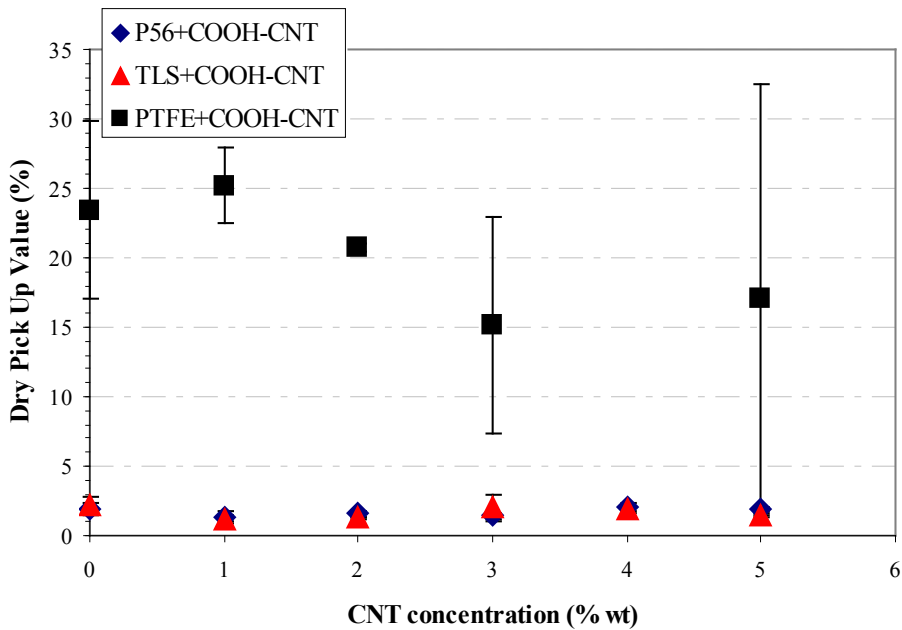


Figure 7 - Dry pick up values of carbon cloth coated with different fluorinated polymers at increasing COOH-CNT concentrations.

6.3.2 Water transmission rate and electron microscopy

Water permeability is a useful characterization, that could easily suggest the behavior of treated carbon cloths in water management. When this characterization

is proceeded with untreated carbon cloths, i.e. no hydrophobization were carried out, water leaks in short time. Instead with fluorinated polymer coating present on carbon cloth structure, as the permeability test is started, no leakage is observed, and only a decrease of weight is registered that is caused by the water evaporation. This evaporation inevitably occurs through the free pore of the hydrophobized carbon cloths, suggesting that this procedure could efficiently acquire information on the water management induced by hydrophobization.

Figure 8 shows the water transmission rate through carbon cloth treated with the two PFPE polymers and PTFE. The weight loss is normalized onto the area of permeation and the thickness of the membrane, in order to measure the transmission rate. The carbon cloths treated with a PTFE dispersion at 1 %wt of fluorine polymer couldn't be measured due to its leaking behavior. This further confirm that the effectiveness of hydrophobization with PTFE dispersions is showed only with high pick up values. P56 and TLS dispersions instead show a reproducibility of hydrophobization even if the treatment of carbon cloths were made with dispersion of 1 %wt. As stated before this reproducibility, obtained with lower polymer coating, is one of the promising characteristics of those fluorinated polymers.

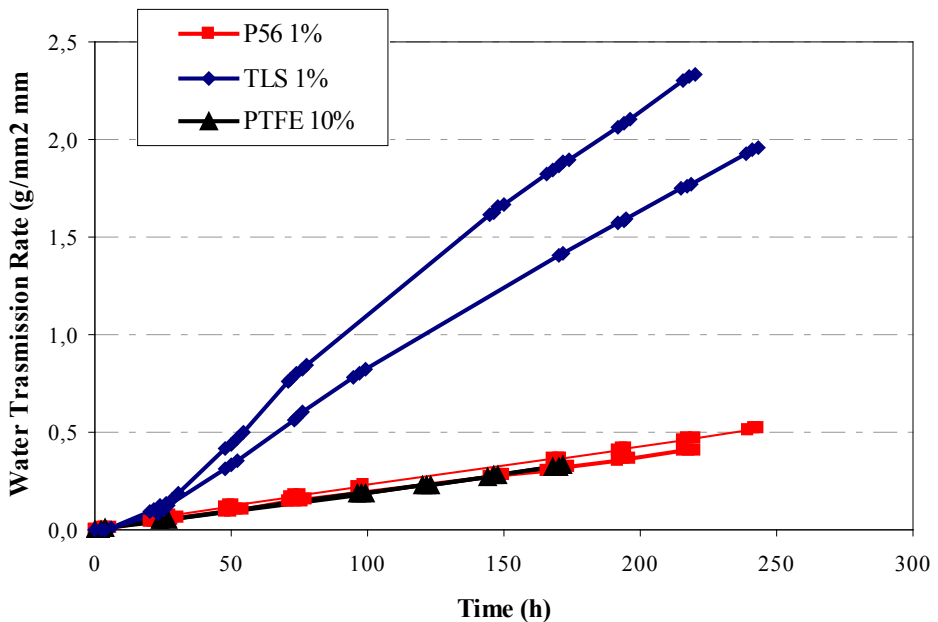


Figure 8 - Water transmission rate of carbon cloth treated with different fluorinated polymers.

The behavior of the carbon cloths treated with P56 dispersion at 1 %wt shows a very similar behavior with the carbon cloths coated with standard PTFE dispersion

at 10 %wt. The carbon cloths coated with TLS at 1 %wt instead, show a higher water transmission rate. These behavior could be further analyzed observing SEM images on those samples.

Figure 9 shows, at low magnification, the morphology of carbon cloths treated with different fluorinated polymers. It could be possible to observe the texture of the carbon cloth that induce the peculiar porosity. Fluorinated coating is dispersed all over the carbon surface with similar macroscopic morphology. As expected, an extensive film, that could fill all the pores denying the gas transportation, is not formed. Only small agglomeration of fluorinated polymers is observed.

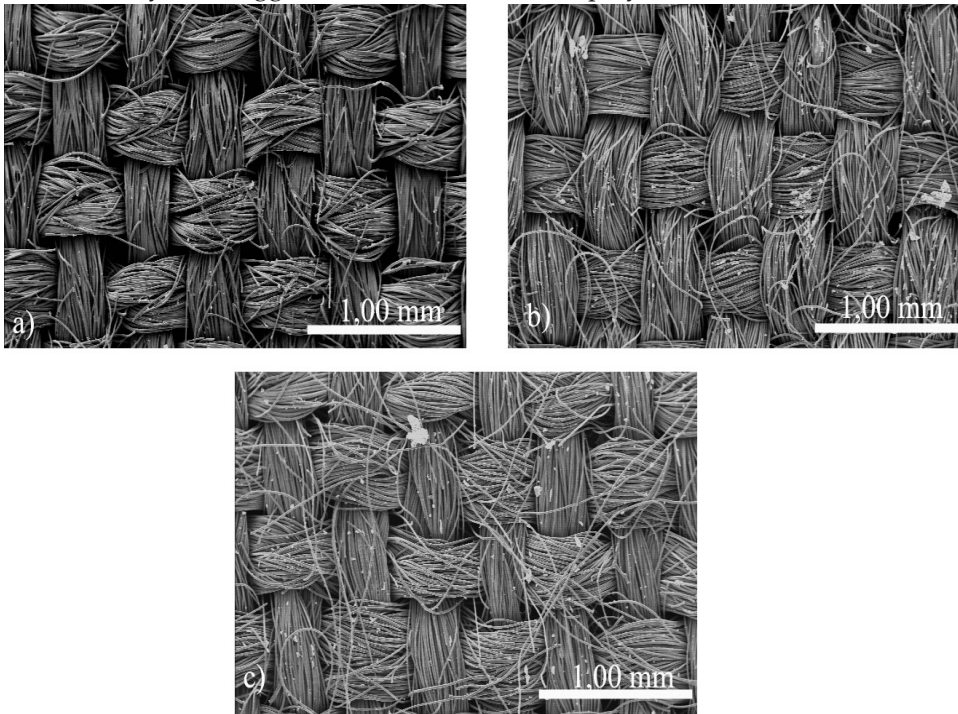


Figure 9 - SEM figure of the carbon cloth treated with different fluorinated polymers: a) PTFE dispersion at 10 %wt, b) P56 dispersion at 1 %wt, c) TLS dispersion at 1 %wt.

At higher magnification, Figure 10, SEM images show that a microscopic film is present on all fibers, and this morphology permits the hydrophobic behavior required. A difference in filming morphology could be observed. A more granular film between the fiber is present with carbon cloths treated with PTFE dispersion, while a more plain intra fiber film is observed when P56 is used as coating. This observation could be further confirmed by the observed film sticking ability of pristine P56 observed and described in Chapter 5 (see Figure 18 a). At those magnification some agglomerations that partially close the space between the fiber, is observed in similar way for those fluorinated polymers. These observations suggest that even if there is some differences in filming morphologies, the similar

intra fibers agglomeration, is expressed with similar water transmission behavior as observed in Figure 8 for coatings obtained with PTFE and P56 polymers.

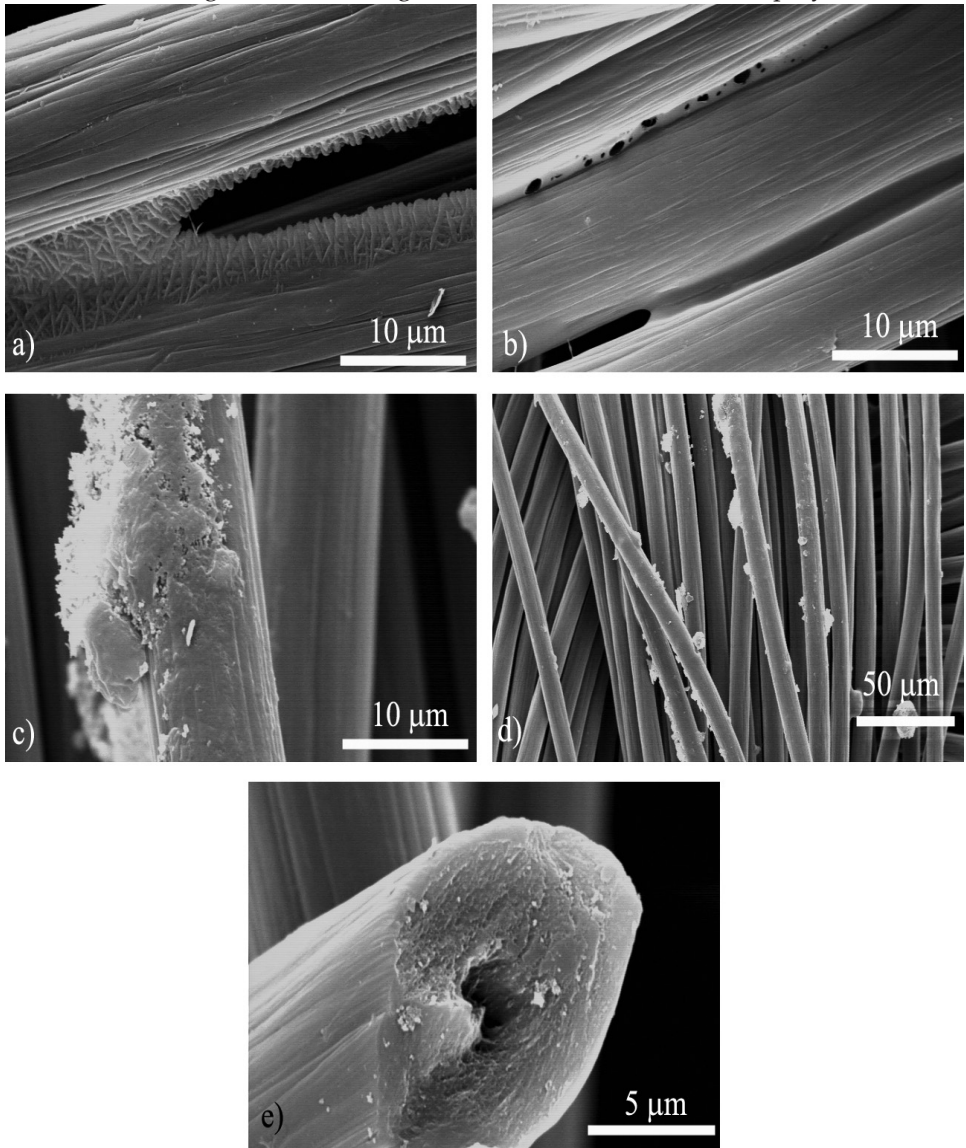


Figure 10 - SEM images of carbon cloth treated with different fluorinated polymers. A) PTFE dispersion at 10 %wt, b) P56 dispersion at 1 %wt, c) and d) TLS dispersion at 1%wt at difference magnifications. e) section of filament of carbon cloth treated with TLS dispersion at 1 %wt.

TLS coating instead show some differences. As could be seen in Figure 10 the film formation is rather granular, but the agglomeration didn't extend on close fiber. Again this behavior on carbon cloth fibers is peculiar of the TLS fluorinated polymer. In Chapter 5, Figure 21 a), a clear film formation difficulty is observed

for TLS samples, confirming this tendency even on the roughness of carbon cloth texture. This suggests that lower amount of fiber are connected with TLS fluorinated coating, proving the higher water transmission rate behavior observed in Figure 8 for those samples.

SEM images confirm once more that PFPE polymers could effectively coat the carbon cloth with lower amount of material involved, lower processing temperature and higher reproducibility of the coating process.

Starting from observation with pristine fluorinated coating, the effect of carbon nanotubes was investigated on dispersion containing 1 %wt of PFPE and on standard 10 %wt aqueous dispersion of PTFE, to observe the difference induced by the functionalized CNTs.

As could be analyzed in Figure 11 the addition of carbon nanotubes didn't evidently affect the water transmission rate when PTFE and P56 nanocomposites were used as coating agent of carbon cloth. Even at high CNT concentration, 5 %wt on fluorinated polymers, the transmission rate values show similar results with pristine coated carbon cloths presented in Figure 8. When TLS nanocomposites at low carbon nanotubes concentrations were used as hydrophobization agent, the transmission rate values didn't change from the observed behavior with pristine TLS coating. A clear difference of these transmission rate values, from pristine, is observed only when 5 %wt of COOH-CNT is inserted. A drop of permeated water is clearly measured. This decrease in water transmission rate values could be explained hypothesizing that more pores are macroscopically closed when TLS nanocomposite, with 5 %wt of COOH-CNT, is used as coating. As seen, the drop of permeated water values make the TLS nanocomposites, with 5 %wt of COOH-CNT, to act like the P56 and PTFE nanocomposites.

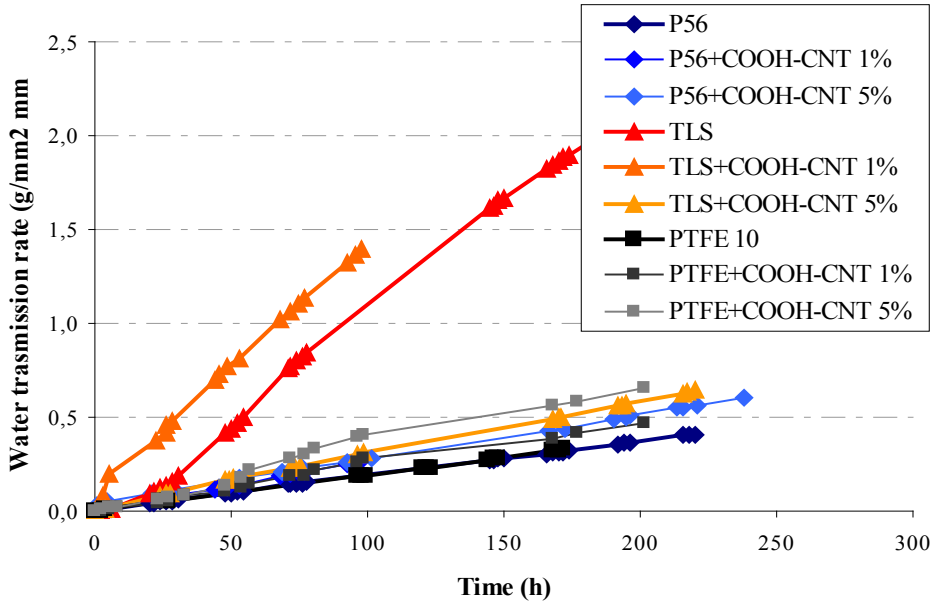


Figure 11 - Permeated water normalized on carbon cloth of GDL with different fluorinated polymers and with different fluorinated nanocomposites at increasing COOH-CNT concentrations.

SEM images, at low magnifications, of carbon cloths treated with fluorinated nanocomposites containing COOH-CNT didn't clearly reveal a morphology change induced by carbon nanotubes presence. As could be seen in Figure 12, showing samples coated with P56 and TLS nanocomposites with COOH-CNT at 5 %wt, film formations are similar to samples treated with pristine fluorinated polymer, and so similar observations could be repeated. This could be explained by the low concentration of CNTs that didn't induce any visible morphological change in the coating at those magnifications, i.e. no change in microscopical morphology of the coating.

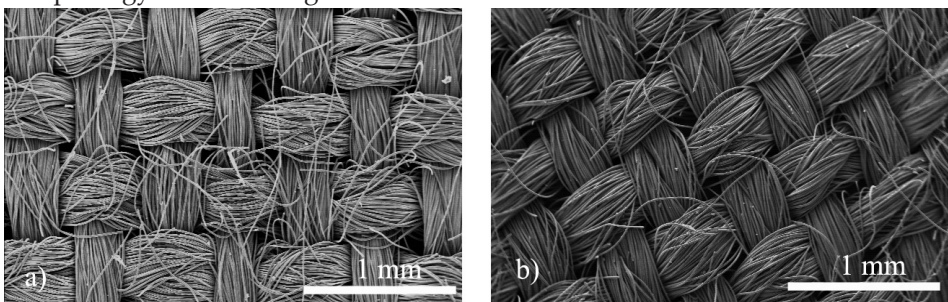


Figure 12 - SEM images of carbon cloth treated with perfluoropolyether nanocomposites. a) P56 dispersion containing 5 %wt of COOH-CNT, b) TLS dispersion containing 5 %wt of COOH-CNT.

Some difference instead could be observed at increasing magnification presented in Figure 13. The intra fiber aggregation, that in coating with pristine P56 are showed with plain film morphology, are replaced with a granular appearance when 5 %wt of COOH-CNT are present in the coating. This increased roughness were observed also for P56 nanocomposites film described in Chapter 5, see Figure 18 b), and induced by the presence of carbon nanotubes. Similar with the observations of Chapter 5, no great change in film capability is observed due to carbon nanotubes, and this behavior, applied on carbon cloth weave, didn't induce any change in film morphology between the fibers. This further proves the little change in water transmission rate observed for those samples. A bigger difference could be observed in samples coated with TLS nanocomposites in which some agglomeration between fiber is finally observed.

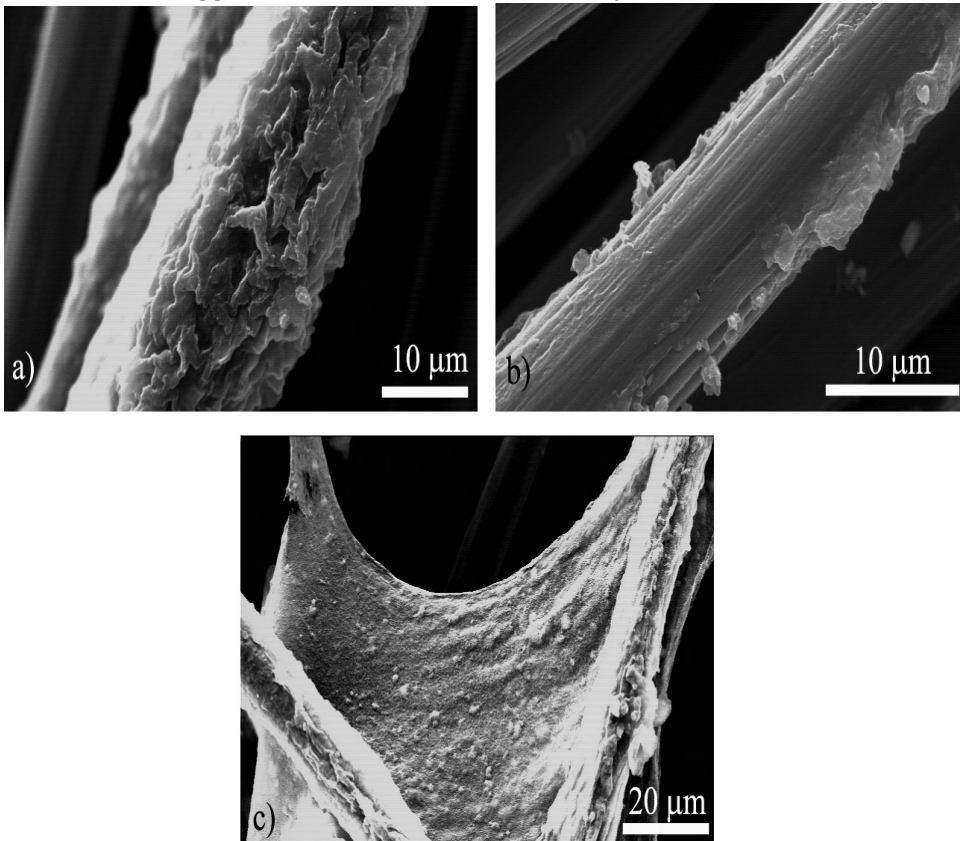


Figure 13 - SEM images of carbon cloth treated with perfluoropolyether nanocomposites. a) P56 dispersion containing 5 %wt of COOH-CNT, b) and c) TLS dispersion containing 5 %wt of COOH-CNT.

It could be possible to observe some CNTs agglomeration in Figure 13 c). These bulks of nanocomposite film between fiber are not present when pristine TLS were used, suggesting that this morphology change could be caused by the CNT

presence. This bulk formation clearly close partially the peculiar pores of carbon cloth, and so could be seen as the source of the drop in water transmission rate values for samples coated with TLS containing 5 %wt of COOH-CNT. Same observation of different film capability induced by the insertion of COOH-CNT and the presence of agglomeration were observed for TLS nanocomposites' film in Chapter 5, see Figure 21 b) and c), and here further proved to be characteristic of those nanocomposites.

This capability of carbon nanotubes to partially change the morphology of the coating and so the permeability of the carbon cloth, needs to be more cleared and studied in order to further tune different perfluoropolyethers and different functionalities of those perfluoropolyether matrices, to exploit this morphology change in enhancement of PEMFC performances.

6.3.3 Contact angle measurements

Static contact angle measurements are the easiest way to confirm the effectiveness of the hydrophobization treatment on carbon cloth. This characterization is widely used as preliminary assessment before the insertion of the cloth in the PEMFC systems [7,10,17,18,21].

As widely known, the pristine carbon cloth didn't show any measurable contact angle against water. The dropped water fall down into the porous weave of carbon cloth [10,17,18,21]. When carbon cloth is treated with hydrophobic polymer instead, the behavior change completely, and a contact angle against water is observed with values above 120 ° [7,10,17].

Figure 14 shows the contact angle measurements of treated carbon cloths with different fluorinated dispersions. The graph is plotted against the weight gain observed after hydrophobization treatments, in order to better observe the differences induced by the fluorinated polymers.

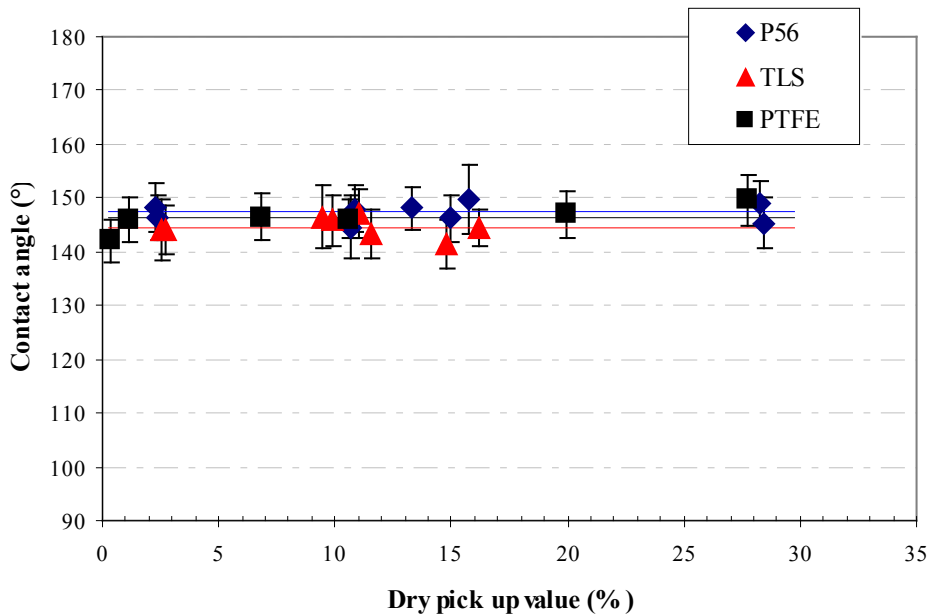


Figure 14 - Contact angle measurement of carbon cloth treated with different fluorinated polymers.

As could be easily seen, the contact angles are constant for every samples, at values around 144-147, with small dispersion of the data. This observation confirms the effectiveness of the hydrophobization treatments of carbon cloth with perfluoropolyether polymers, even at low dispersion concentrations, i.e. 1 %wt of fluorinated polymer, without any observable change in surface behavior from the properties induced by the standard dipping process that exploit dispersion with 10 %wt of PTFE.

Moreover, the elevated contact angle values here observed are caused also by the different roughness of the carbon cloth surface. In fact, the pristine PFPE materials show contact angle measurements, see Section 5.3.4, against water of around 112 °. The higher values here observed are mainly caused by the great roughness of the surface here studied, i.e. the roughness of weaved cloth, that creates when investigated with water drop, a well known Cassie-Baxter effects ^[30].

As the carbon nanotubes are inserted, some changes are expected in surface behavior due to their peculiar high surface area. Figure 15 shows the contact angle measurements of carbon cloths treated with the two perfluoropolyether polymers dispersion at 1 %wt and, for benchmarking purpose, the carbon cloth processed with PTFE dispersion at 10 %wt, with increasing concentration of carbon nanotubes. As could be analyzed, the insertion of carbon nanotubes seems to increase only slightly the contact angles observed in carbon cloth treated with

pristine fluorinated polymer. This increased could be explained with an increased Cassie-Baxter surface morphology, induced by the presence of carbon nanotubes. Furthermore, carboxylated carbon nanotubes, has seen in Section 6.3.2, change the film formation of perfluoropolyether polymers and their insertion creates a surface with more microscopically roughness, that is confirmed here by the increased contact angle values.

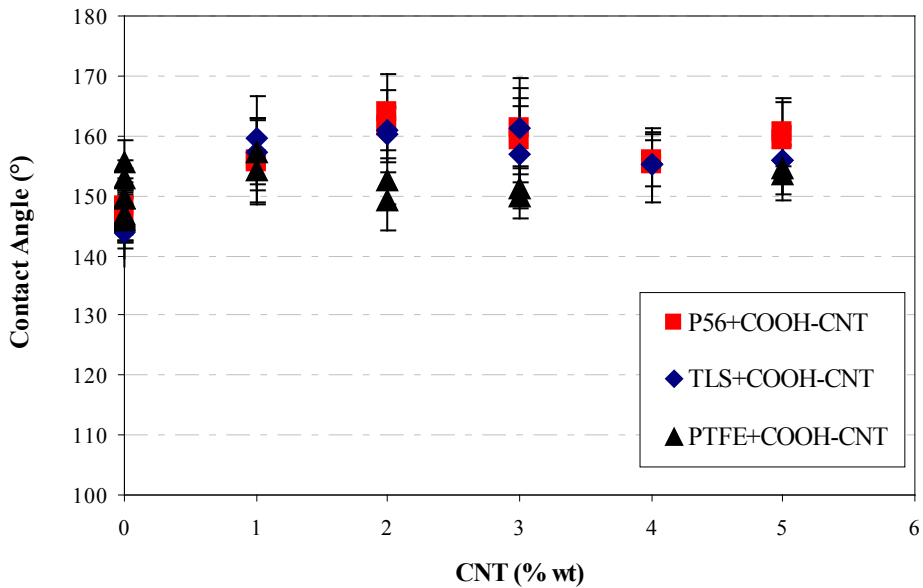


Figure 15 - Contact angle measurement of carbon cloth treated with different fluorinate nanocomposites containing different concentration of COOH-CNT.

All these observations suggest that the carbon cloths, treated with nanocomposites containing COOH-CNT, could efficiently be used as gas diffusion layer in PEMFC systems. The same good water management observed for GDLs treated with pristine PFPE and PTFE will hypothetically be present even with the presence of carbon nanotubes inside the hydrophobization coating.

6.3.4 Electrical characterization

Before the measurement of the performance of the treated carbon cloths in FC systems, electrical characterizations, with in-plane configuration, were used to further observe the modification induced by perfluoropolyether and nanocomposites, containing carbon nanotubes, used as carbon cloth's coating. Figure 16 shows the in-plane conductivity of carbon cloths treated with different fluorinated polymers against the weight gain of hydrophobic process. As could be seen the hydrophobization procedure, described in Section 6.2.2, that produces an

effective hydrophobic behavior on carbon cloths, as seen in Section 6.3.2, doesn't considerably change the overall conductivity of carbon cloths, confirming the goodness of this dipping process. All the membranes treated with fluorinated polymer show similar conductivity, at the same order of magnitude as pristine carbon cloth. Even if the measurements show a narrow dispersion of samples' data, the pristine carbon cloth shows some deviation, probably due to some weave differences that induce a change in conductivity values.

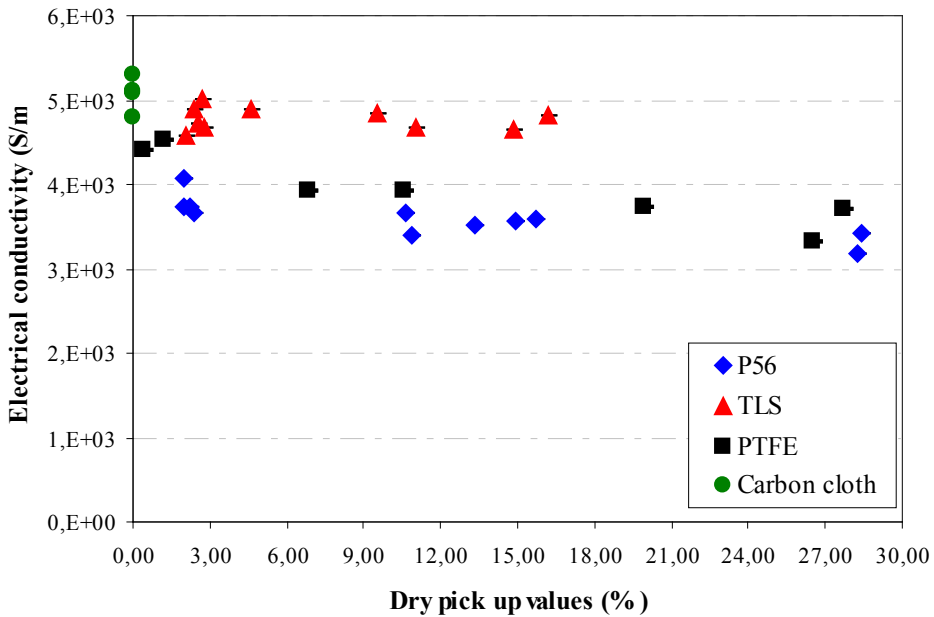


Figure 16 - Electrical conductivity of pristine carbon cloth and carbon cloth treated with different fluorinate polymers.

Considering only in plane conductivity, a slightly better treatment could be indicated in TLS perfluoropolyether. For the carbon cloths treated with this PFPE polymer, the conductivity is slightly decreased from pristine carbon cloth's values by the presence of the hydrophobic and insulating coating.

The insertion of conductive carbon nanotubes could change the electrical conductivity of those coated samples. As could be observed in Figure 17 only a small increase from the values of carbon cloths coated with pristine polymers is observed when the hydrophobic coating of carbon cloth is obtained with nanocomposites containing high carbon nanotubes concentration, i.e. 5 %wt. Again, the best coating, with lower decrease from the conductivity values of pristine carbon cloth, is the TLS nanocomposites. These observations suggest that the insertion of carbon nanotubes in the coating nanocomposites, didn't effectively increase the in-plane conductivity of gas diffusion layer, but their behavior is more

prominent in the sum up of all the other different requirements necessary by GDLs in PEMFC systems.

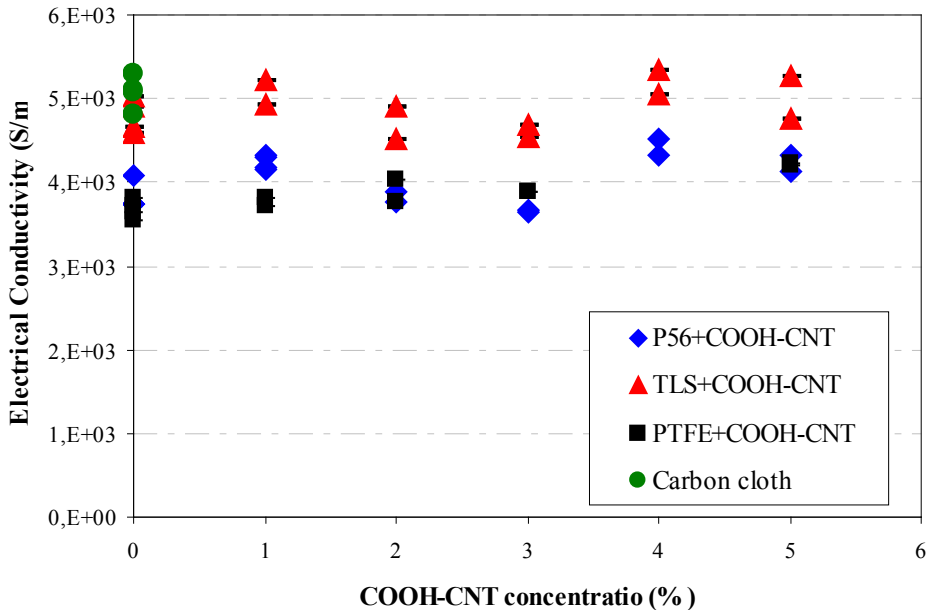


Figure 17 - Electrical conductivity of pristine carbon cloth and carbon cloth treated with different fluorinate nanocomposites at different COOH-CNT concentrations.

6.3.5 Single cell polarization measurement

All the observation analyzed with the above mentioned characterizations, lead us to effectively use the treated carbon cloths in a PEM fuel cell system as gas diffusion layers. This characterization is the main focus of the fluorinated materials used as hydrophobization agent, and their further modification with carbon nanotubes. As stated in Section 6.1 and in Chapter 1, PEMFC system is rather complex, and a small change in one parameter leads to a modification of other factors that could give some unexpected modification of fuel cell performances ^[1,7,10,14]. In order to test mainly the hydrophobic effect obtained with perfluoropolyether polymers and PFPE based nanocomposites, the samples were characterized with test stations described in Section 6.2.6 without a microporous layer coating. This strongly reduce the amount of different variables that could change the fuel cell performances, reducing the observation on different materials used in the modification of the GDLs.

In order to asses mainly the effectiveness of the GDLs' hydrophobic treatments with PFPE, the single cell polarization measurements were conducted only at high values of relative humidity of gases, i.e. RH 80% for idrogen at the anode, and

RH 100% for air at the cathode side. These conditions of relative humidity permit to assure a condition in which the membrane could be considered efficiently humidified.

Figure 18 shows the polarization curves and the power density curves at 60°C of the single cell, assembled mounting GDLs treated with two perfluoropolyether polymers dispersions at 1 %wt and, for benchmarking purpose, a GDL treated with PTFE dispersion at 10 %wt. Cell technical details are fully described in Section 6.2.6.

It is worth noting that the addition of PFPE polymers as GDL coating, even in as small amount as 1 %wt, positively influences the cell performances at all current density in comparison with the results of the PTFE, that is the standard in PEM fuel cell experiments.

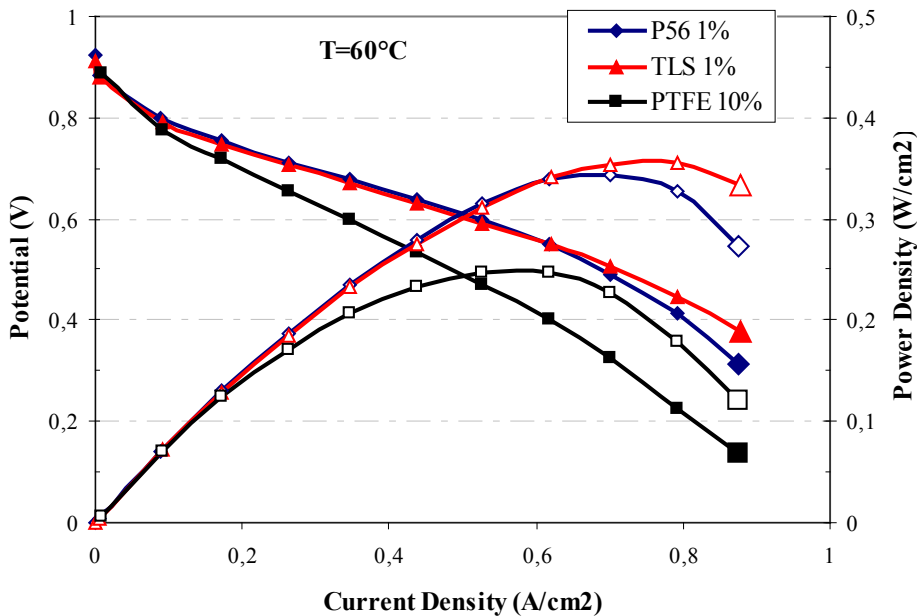


Figure 18 -Polarization (filled symbols) and power density (hallow symbols) curves at 60°C and RH 80/100 air/H₂ of single cell assemblies mounting three GDLs treated with different fluorinated dispersions.

The assembly, with the GDLs treated with PFPEs, shows polarization curves with lower ohmic losses than the one observed when PTFE is inserted. This phenomena could be explained by the lower amount of insulating fluorinated material inserted in GDL when PFPE were used as coating. Moreover, this less ohmic losses, for treatments with perfluoropolyether polymers, couldn't be clearly observed in the conductivity measurement conducted with in-plane configuration, described in Section 6.2.5 and in particular in Figure 16, in which no such differences between carbon cloths treated with P56 perfluoropolyether and PTFE were observed. This

suggests that the a difference in conductivity of treated GDLs, could be understood better only in through-plane configuration.

PFPE treated GDLs measurably improves the cell performance more evidently in the high current density region, where the cell is more stressed and the amount of water generated by cathodic reaction is maximum. This could us assert that the PFPE coatings permit a better water management during cell operations, preventing both the drying of the membrane and the flooding of GDLs at the cathodic side. This better water management observed, from the hydration of membrane point of view, could be also the reason for the reduction of ohmic losses for those samples. This improvement couldn't be clearly understood with the water transmission rate values analyzed in Section 6.3.2 in which the observed values for carbon cloths with P56 and PTFE show similar values. TLS coating instead, as observed in Figure 8, shows an higher permeability to water than the other fluorinated polymers, and this behaviour could explain the performance at high current density observed for this sample. For GDL treated with TLS dispersion, a slightly less concentration/diffusive losses is noticed, and could be hypothesized to be caused by the high permeability observed.

In terms of power density, GDLs treated with PFPEs are superior with the benchmark of PTFE treated carbon cloth. The peak value is about 0,34 and 0,35 W cm^{-2} for P56 and TLS treated GDLs respectively, while, when PTFE is used, the power density reach only 0,25 W cm^{-2} .

When the temperature is raised to 80 °C, the effect of perfluoropolyethers is more controversial. Figure 19 shows the polarization curves and power density curves for the three samples at 80 °C. As could be observed, the difference in the part of the curves due to the ohmic losses shows a less enhancement when PFPE coating is used. As expected, the rise in temperature decrease the ohmic losses and so the different performances for these samples is less evident. Notwithstanding this, a similar behaviour with the one observed at 60 °C is observed for the improved performances when PFPE treatments are inserted.

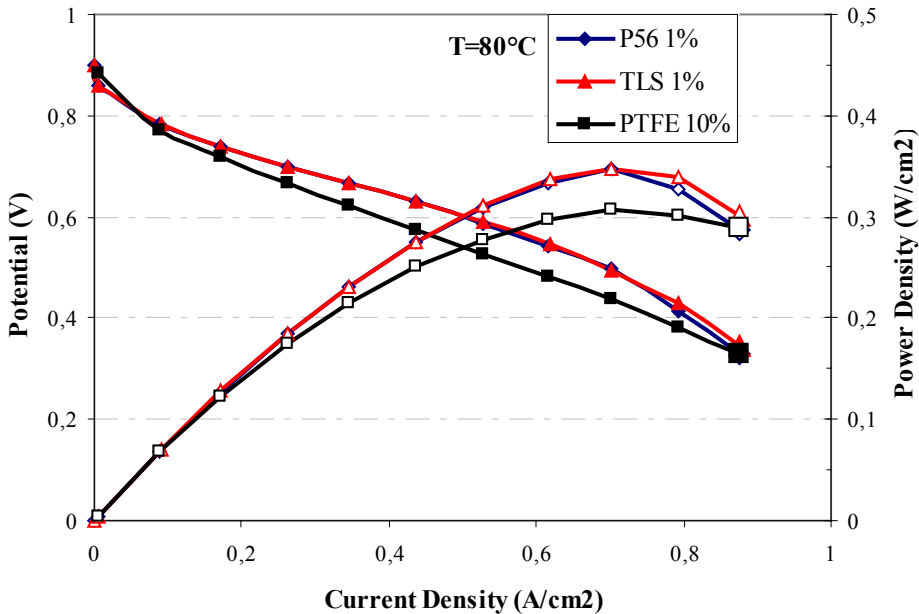


Figure 19 - Polarization (filled symbols) and power density (hallow symbols) curves at 80°C and RH 80/100 air/H₂ of single cell assemblies mounting three GDLs treated with different fluorinated dispersions.

As the temperature is raised, it could be seen that in high current density region, i.e. when cell is more stressed by the generated water, the GDLs with PFPEs show curves with diffusive losses similar to the one observed when PTFE is used as coating. So the highly efficient water management observed for PFPEs is reduced at higher temperature, suggesting that the best operating temperature for those perfluoropolyethers is reached at 60 °C.

Again, the power density of GDLs treated with PFPEs are superior than the performances observed with PTFE. The peak value is about 0,34 W cm⁻² for both the P56 and TLS treated carbon cloths, while a value of 0,30 W cm⁻² is observed when PTFE is used as coating.

As observed with the other preliminary characterizations described above, the insertion of carbon nanotubes in fluorinated polymer partially modify the behaviour of carbon cloths treated with those nanocomposites.

The samples of GDLs coated with PFPE nanocomposites and other GDLs coated with pristine perfluoropolyether, for benchmark purpose, were characterized in the second fuel cell test station assembly described in Section 6.2.6. The main difference of those configuration, that give also problematical issues, is the change in the Catalyst Coated Membrane batch purchased by Baltic Fuel Cell. Unfortunately, even if the nominal platinum loading is the same as the CCM used

in first test station, a great difficulty in obtaining reproducible results for same GDL-PFPE samples were observed. No confrontation between data obtained with first test station and the second test station were possible, even over same treated GDL samples.

Figure 20 shows the polarization curves and power density curves for GDLs treated with P56 pristine and P56 nanocomposites at 1 and 5 %wt of COOH-CNT content, at 60 °C.

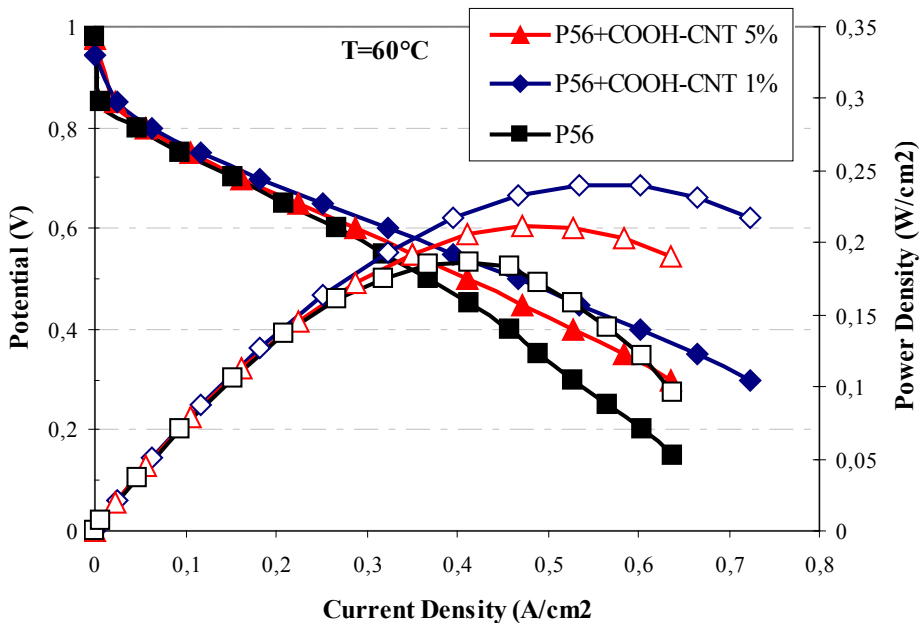


Figure 20 - Polarization (filled symbols) and power density (hallow symbols) curves at 60 °C and RH 80/100 air/H₂ of single cell assemblies mounting GDLs treated with P56 pristine polymer and P56 nanocomposites at different COOH-CNT concentrations.

As could be easily seen, the ohmic losses for all the samples are so important that no sign of diffusion losses is observed. These losses are present in all samples studied with the above mentioned batch of CCM, and this common behaviour could be hypothesized to be due exclusively by the catalyst coated membrane's lower performances. A reduce in those ohmic losses is observed for samples with GDLs treated with perfluoropolyether nanocomposites. Carbon nanotubes insertion could indeed partially increase the conductivity of the gas diffusion layer in PEM fuel cell system.

Carbon cloths, treated with the nanocomposites, didn't show any difference in all the preliminary characterizations analyzed during the work. No clear explanation of the small difference observed for the two GDLs coated with nanocomposites here studied could be presented. The low performances attributed to CCM, and its variability behaviour, rules

over all the small possible differences induced by the variation of concentration of carbon nanotubes present in the nanocomposite used as GDL coating. No diffusive losses could be observed and so no further analysis of the change in morphology, observed as the COOH-CNT concentration is risen, could be made in term of the induced change in performances of the fuel cell.

Same difficulties in interpretation could be stated when the curves of polarization and power density are presented at 80 °C for the GDLs treated with P56 nanocomposites, as seen in Figure 21.

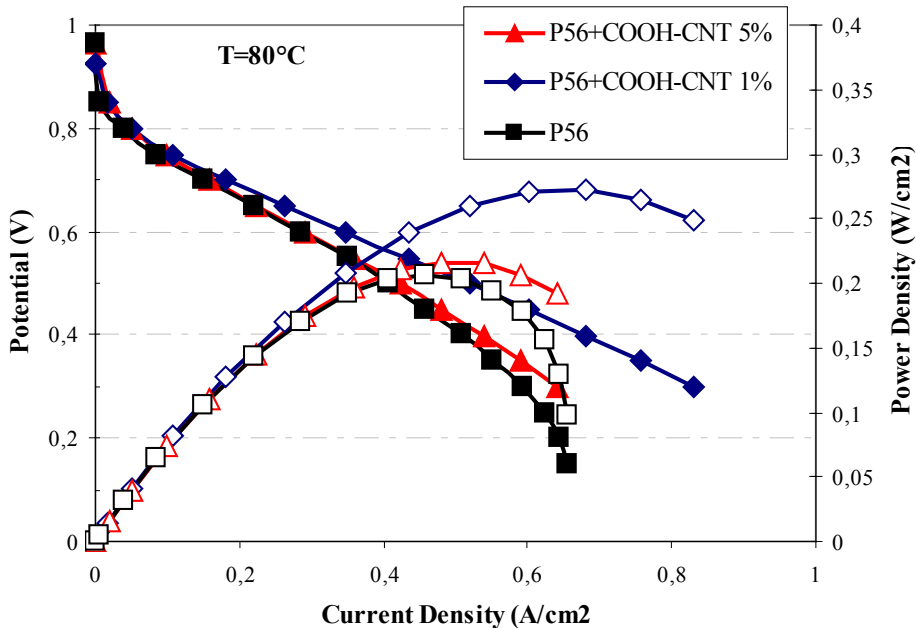


Figure 21 - Polarization (filled symbols) and power density (hallow symbols) curves at 80 °C and RH 80/100 air/H₂ of single cell assemblies mounting GDLs treated with P56 nanocomposites at different COOH-CNT concentrations.

Again, as observed at 60 °C, the ohmic losses, due to the inefficient CCM, rules over all other losses, and cover up the differences induced by the increased COOH-CNT concentrations. Again the performances of the GDLs treated with perfluoropolyether nanocomposites are higher than those observed with pristine perfluoropolyether. A decrease in ohmic losses observed when nanocomposites are present could be explained by the higher conductivity induced by the COOH-CNT content. A small diffusive behaviour could be observed at high current density region, i.e. when cell is more stressed and water generated at the cathode is maximum. This behaviour is observed for GDL treated with pristine polymer, already analyzed in Figure 19 with a CCM layer that permit more detailed observation of those losses, and only for nanocomposites containing 5 %wt of carbon nanotubes. As observed in Figure 13, this high carbon nanotubes concentration creates a slightly difference

in coating morphology, that could be recalled as the cause of a different water management observed in the diffusion loss for this sample.

As stated before, CCM troublesome couldn't resolve the observed power density peak for those nanocomposite coated GDLs, even if the general performances of the fuel cell are higher than the one observed with pristine P56 perfluoropolyether.

Even with difficulty of using such CCM, samples of GDLs coated with TLS oligomer and TLS nanocomposites containing 1 and 5 %wt of COOH-CNT were studied, and the polarization and power density curves at 60 °C for those samples were presented in Figure 22.

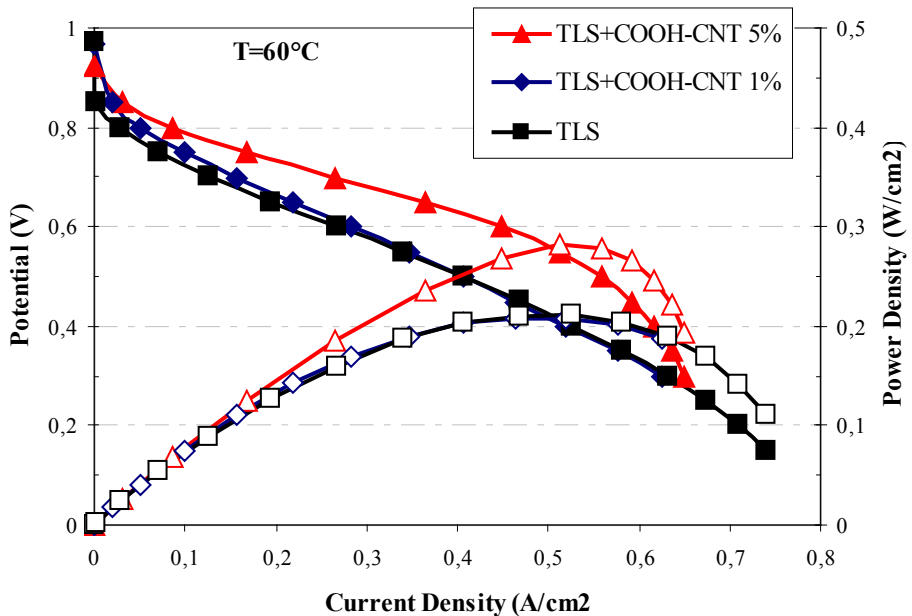


Figure 22 - Polarization (filled symbols) and power density (hallow symbols) curves at 60 °C and RH 80/100 air/H₂ of single cell assemblies mounting GDLs treated with TLS pristine polymer and TLS nanocomposites at different COOH-CNT concentrations.

Again, CCM induced ohmic losses partially cover all the other variables and make difficult an extensive analysis of PEM different performances at increasing CNTs. An higher polarization curve than other samples is observed when GDLs were treated with TLS at 5 %wt of COOH-CNT. This behaviour suggests that a less ohmic losses are present when a nanocomposites coating with high CNTs concentration is used. Considering the conductivity, with in-plane configuration a similar behaviour of TLS+COOH-CNT 5 % is observed in comparison with the nanocomposites with just 1 %wt of CNTs and pristine TLS. Therefore, this slightly higher conductivity induced by CNTs insertion are confirmed in PEM performances.

Moreover a clear bend of polarization curve at high current density region is observed only for nanocomposites with 5 %wt. This bend is due to the diffusion

losses. This particular behaviour, observed when high content of COOH-CNT (5 %wt) are inserted could be confirmed with the preliminary permeability characterization reported in Section 6.3.2, in which for this sample a significant drop in water transmission rate value is calculated, and a different coating morphology between the coating with pristine TLS perfluoropolyether is observed. This morphology, as analyzed in Section 6.3.2, induces a film formation that partially reduce pores and this is confirmed with the reduced performances at high current density.

Pristine TLS perfluoropolyether at those cell condition showed a very efficient water management, see Figure 18, that could partially be observed here in this test station, due to the importance of the ohmic losses induced by CCM batch. Same good water management behaviour is observed also when the GDL treatment is hydrophobized with TLS nanocomposites with 1 %wt of COOH-CNT. This similarity between pristine TLS and TLS nanocomposites with 1%wt coated GDL further confirms the previous results observed in terms of permeability, see Figure 11. The presence of the carbon nanotubes induce an higher conductivity of the hydrophobized GDL, but at the same time induce a film morphology that partially decrease the permeability, and so reduce the water management behaviour in PEMFC systems.

At 80 °C the behaviours, reported in Figure 23, of polarization and power density curves with GDLs treated with TLS nanocomposites containing 1 and 5 %wt are very comparable with results already discussed, and same observation stated for lower temperature, 60 °C, could be confirmed.

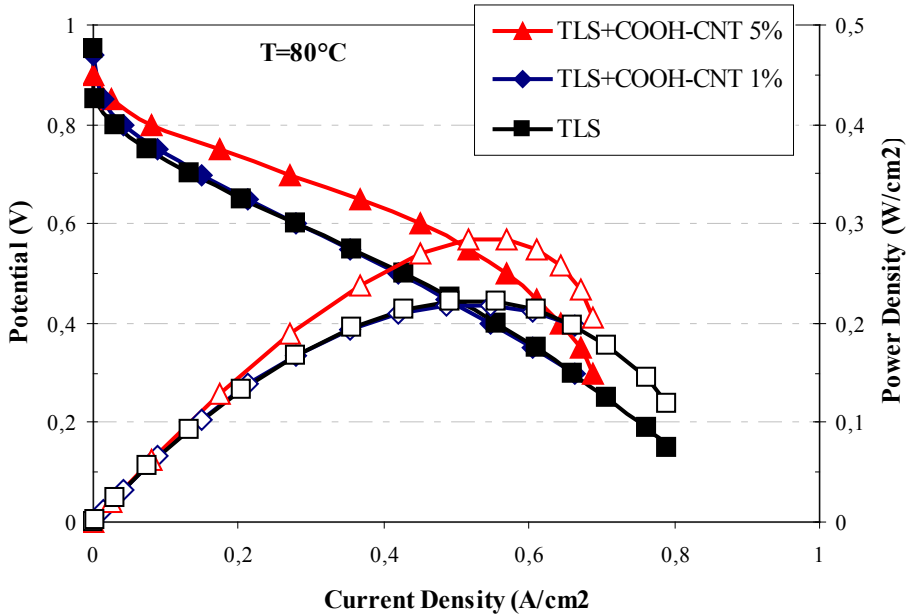


Figure 23 - Polarization (filled symbols) and power density (hallow symbols) curves at 80°C and RH 80/100 air/H₂ of single cell assemblies mounting GDLs treated with TLS nanocomposites at different COOH-CNT concentrations.

A similar behaviour between GDLs treated with pristine TLS and GDLs treated with nanocomposites, containing low COOH-CNT amount (1 %wt), is observed. The ohmic losses observed in samples containing 5 %wt of carbon nanotubes are lower than the other samples, confirming that an increase in conductivity is induced with the rise of the COOH-CNT concentration. At the same time, the diffusion losses are more preeminent for those nanocomposites with high nanotubes inserted. This behaviour is induced by the COOH-CNT presence, and the different morphology and permeability that are created by their insertion. In any case the performances observed in fuel cell system, when the TLS nanocomposites containing COOH-CNT are used as hydrophobization treatment of GDLs, are far higher than the already high-performances observed with samples treated with pristine TLS.

6.4 CONCLUSIONS AND FUTURE CONSIDERATIONS

An efficient use of two perfluoropolyether polymers as hydrophobic surface treatments for carbon cloths, exploited as Gas Diffusion Layer in Polymer Electrolyte Membrane Fuel Cell, is presented. Moreover, the insertion of carboxylic carbon nanotubes into fluoropolymer were investigated, and their influence on carbon cloths modification were underlined. The application procedure of PFPEs on carbon cloths were effective and efficient. Coating with Perfluoropolyether polymers shows a very good dry pick up, even at low dispersion concentration, with a simpler procedure without the needing of the high sintering cycling temperature required in the well used hydrophobization methodology that exploit PTFE dispersions at 10%wt. The insertion of carbon nanotubes in the PFPE matrices didn't influence the effectiveness of the coating procedure. PFPEs polymers and their nanocomposites with COOH-CNT, used as hydrophobic agents, will fairly reduce the problematical issues in industrialization of the carbon cloths coating procedure.

The coated carbon cloths' performances were investigated with preliminary characterizations to better understood the behaviour of those hydrophobic treatments before the insertion in PEM fuel cell system.

Morphology and water transmission rate of PFPE treated carbon cloths show that the effectiveness of those coating procedures permit an efficient hydrophobization without the formation of extended film, and so without occluding the peculiar pores of the carbon cloth, required in gas transportation. The insertion of carbon nanotubes in fluorinated polymers changes slightly the morphology of the coating, and partially reduces the high water rate transmission values observed in pristine PFPEs. In any case the behaviour is similar to the one observed with PTFE coating that represent the benchmark in this study.

Effectiveness of the hydrophobic treatments was specifically confirmed with the high contact angle values for the two PFPEs even at low dispersion concentration. The insertion of carbon nanotubes didn't change this high hydrophobic behaviour required in GDL structure. Electrical conductivity of the carbon cloth were slightly reduced by the coating procedure with PFPEs, with similar performances observed with PTFE. A little higher conductivity were observed when the carbon nanotubes were inserted the in coating.

A good performances in electrochemical performances of Fuel Cell were observed with the use of PFPE polymers as coating agent with dispersion containing just 1%wt of perfluoropolyether. The treated GDLs clearly show a better water management during cell operation, especially at 60°C, at which the best performances for PFPE materials are observed. An improvement over the standard hydrophobization method, that exploit a PTFE dispersion with higher (10%wt) concentration, is clearly analyzed. All those observations permit to assure the

goodness of the two perfluoropolyether dispersions here studied as alternatives to standard polytetrafluoroethylene in hydrophobization of the gas diffusion layer in PEM fuel cells systems.

Insertion of carbon nanotubes increase the performances of pristine PFPEs in electrochemical response of th Fuel Cell. A lower ohmic loss is observed as the concentration of COOH-CNT are increased. Unfortunately all the behaviour couldn't clearly be understood due to some problematic issues related to Catalyst Coated Membrane properties. Moreover, the different morphologies induced by the carbon nanotubes presence modify the behaviour at high current density.

More work is however needed to further improve the performances. An extensive electrochemical impedance spectroscopy is needed to understand clearly the specificity of the improvement here observed. Moreover, an optimization of the composition and the functionalization of the perfluoropolyether polymers and a modification of the properties of the PFPE nanocomposites (i.e. carbon nanotubes functionalization and concentration) is required to enhance the peculiar properties needed by gas diffusion layer in PEM Fuel Cell systems. As the electrochemical characterization has underlined, a further improvement in PEMFC performances needs to be reached with the modification of the functionalities of the perfluoropolyethers and the induced modification of insertion of carbon nanotubes. This tune up is needed in order to enhance the mechanical, thermal and superficial properties of those materials at the common temperatures used in fuel cell system. Moreover, an enhancement of the conductivity is required. A specific control on the morphology change, induced by COOH-CNT, needs to be controlled with different carbon nanotubes functionalization and different pristine perfluoropolyethers. All those material related modifications must be confirmed in the coating capability of the carbon cloth, and at the end, in the performances of the Polymer Electrolyte Membrane Fuel Cells.

6.5 REFERENCES

1. F. Barbir, *PEM Fuel Cells, Theory and Practice*, Elsevier, 2005.
2. C. S. Spiegel, *Designing & Building Fuel Cells*, Mc Graw-Hill Editore, 2007.
3. J. Larminie, A. Dicks, *Fuel Cell Systems – Explained*, Wiley John & Sons, Second Edition, 2003.
4. L. Carrette, K. Friedrich, U. Stimming, Fuel Cells – Fundamentals and Applications, Fuel Cells, Volume 1 (1) 5-39 (2001).
5. S. Litster, G. McLean, PEM fuel cell electrodes, Journal of Power Sources, 130, 61-76 (2004).
6. H. Li, Y. Tang, Z. Wang, Z. Shi, S. Wu, D. Song, J. Zhang, K. Fatih, J. Zhang, H. Wang, Z. Liu, R. Abouatallah, A. Mazza, A review of water flooding issues in the proton exchange membrane fuel cell, Journal of Power Sources, 178, 103-117 (2008).
7. L. Cindrella, A. Kannan, J. Lin, K. Saminathan, Y. Ho, C. Lin, J. Wertz, Gas Diffusion layer for proton exchange membrane fuel cells – A review, Journal of Power Sources, 194, 146-160 (2009).
8. Y. Pai, J. Ke, H. Huang, C. Lee, J. Zen, F. Shieu, CF_4 plasma treatment for preparing gas diffusion layers in membrane electrode assemblies, Journal of Power Sources, 161, 275-281 (2006).
9. C. Tseng, S. Lo, Effects of microstructure characteristics of gas diffusion layer and microporous layer on the performance of PEMFC, Energy Conversion and Management, 51, 677-684 (2010).
10. C. Lim, C. Wang, Effects of hydrophobic polymer content in GDL on power performance of a PEM fuel cell, Electrochimica Acta, 49, 4149-4156 (2004).
11. M. Prasanna, H. Ha, E. Cho, S. Hong, I. Oh, Influence of cathode gas diffusion media on the performance of the PEMFCs, Journal of Power Sources, 131, 147-154 (2004).
12. P. Wilde, M. Mändle, M. Murata, N. Berg, Structural and Physical Properties of GDL and GDL/BPP Combinations and their Influence on PEMFC Performance, Fuel Cells, 4 (3), 180-184 (2004).
13. H. Lee, J. Park, D. Kim, T. Lee, A study on the characteristics of the diffusion layer thickness and porosity of the PEMFC, Journal of Power Sources, 131, 200-206 (2004).
14. A. Li, M. Han, S. Chan, N. Nguyen, Effects of hydrophobicity of the cathode catalyst layer on the performance of a PEM fuel cell, Electrochimica Acta, 55,

- 2706-2711 (2010).
15. E. Kimball, J. Benziger, Y. Kevrekidis, Effects of GDL Structure with an Efficient Approach to the Management of Liquid water in PEM Fuel Cells, *Fuel Cells*, 10 (4) 530-544 (2010).
 16. M. Ismail, T. Damjanovic, D. Ingham, M. Pourkashanian, A. Westwood, Effect of polytetrafluoroethylene-treatment and microporous layer-coating on the electrical conductivity of gas diffusion layers used in proton exchange membrane fuel cells, *Journal of Power Sources*, 195, 6619-6628 (2010).
 17. J. Lin, T. Ko, W. Kuo, Y. Lin, C. Huang, W. Chen, Effect of Various Hydrophobic Concentrations and Base Weights of Gas Diffusion Layer for Proton Exchange Membrane Fuel Cells, *Fuel Cells*, 10, 118-123 (2010).
 18. P. Gallo Stampino, C. Cristiani, G. Dotelli, L. Omati, L. Zampori, R. Pelosato, M. Guilizzoni, Effect of different substrates, inks composition and rheology on coating deposition of microporous layer (MPL) for PEM-FCs, *Catalysis Today*, 147, S30-S35 (2009).
 19. G. Park, Y. Sohn, T. Yang, Y. Yoon, W. Lee, C. Kim, Effect of PTFE contents in the gas diffusion media on the performance of PEMFC, *Journal of Power Sources*, 131, 182-187 (2004).
 20. C. Lee, Y. Pai, Y. Zen, F. Shieu, Characterization of Teflon-like carbon cloth prepared by plasma surface modification for use as gas diffusion backing in membrane electrode assembly, *Materials Chemistry and Physics*, 114, 151-155 (2009).
 21. P. Gallo Stampino, D. Molina, L. Omati, S. Turri, M. Levi, C. Cristiani, G. Dotelli, Surface treatments with perfluoropolyether derivatives for the hydrophobization of gas diffusion layers for PEM fuel cells, *Journal of Power Sources*, 196, 7645-7648 (2011).
 22. T. Trombetta, P. Iengo, S. Turri, Fluorinated segmented polyurethane anionomers for water-oil repellent surface treatments of cellulosic substrates, *Journal of Applied Polymer Science*, Vol. 98, 1364-1372 (2005).
 23. M. Licchelli, S. J. Marzolla, A. Poggi, C. Zanchi, Crosslinked fluorinated polyurethanes for the protection of stone surfaces from graffiti, *Journal of Cultural Heritage*, 12, 34-43 (2010).
 24. S. Turri, R. Valsecchi, M. Levi, M. Cristini, A. Sanguineti, Microstructure to property relations in a family of millable polyurethane fluoroelastomers, *European Polymer Journal*, 44, 2951-2961 (2008).
 25. V. Ijeri, L. Cappelletto, S. Bianco, S. Tortello, P. Spinelli, E. Tresso, Nafion and

- carbon nanotube nanocomposites for mixed proton and electron conduction, *Journal of Membrane Science*, 363, 265-270 (2010).
26. J.M. Tang, M. Itkis, C. Wang, X. Wang, Y. Yan, R. Haddon, Carbon nanotube free-standing membrane as gas diffusion layer in hydrogen fuel cells, *Micro and Nano Letters*, Volume 1 (1), 62–65 (2006).
 27. H. Gharibi, M. Javaheri, R. Mirzaie, The synergy between multi-wall carbon nanotubes and Vulcan XC72R in microporous layers, *International Journal of Hydrogen Energy*, 35, 9241-9251 (2010).
 28. P. Gallo Stampino, L. Omati, C. Cristiani, G. Dotelli, Characterisation of Nanocarbon-based Gas Diffusion Media By Electrochemical Impedance Spectroscopy, *Fuel Cells*, 10 (2), 270-277 (2010).
 29. Y. Gao, G.Q. Sun, S.L. Wang, S. Zhu, Carbon nanotubes based gas diffusion layers in direct methanol fuel cells, *Energy*, 35, 1455-1459 (2010).
 30. S. Wu, *Polymer Interface and Adhesion*, Dekker, 1982.



>7

CONCLUSIONS

The research work in the present thesis has been directed in three different issues, to further clarify the effect of inserting different functionalized carbon nanotubes in various polymer matrices, to obtain a dispersed CNTs microstructure, enhanced properties of nanocomposites and possible widen applications of those materials.

7.1 FUNCTIONALIZATION OF MULTIWALLED CARBON NANOTUBES

Efficient functionalization methods were optimized, to prepare CNTs with carboxylic and amine functionalities, and were carried out with a high yield (more than 80%). A quantitative characterization of the concentration of functionalities on the external wall were efficiently used, in order to determine a selected functionalization process that permits to obtain functionalized carbon nanotubes with a resulting functionalities concentration comparable with commercial available carbon nanotubes. Microscopic characterizations were performed on functionalized carbon nanotubes and no significant change of aspect ratio were observed, confirming the efficiency of the functionalization methods here optimized to reduce the morphology change of carbon nanotubes.

7.2 EPOXY-BASED NANOCOMPOSITES

Epoxy based nanocomposites were intensively investigated, to better comprehend the influence of the interconnected morphology created by carbon nanotubes insertion on the different properties of the nanocomposites. A dispersion method of carbon nanotubes, based on solvent mixing procedure, in a DGEBA based resin was efficiently developed. A great stability of the resulting dispersions was observed. Moreover, rheological characterizations of dispersions confirm the good repeatability of the dispersion process of pristine, carboxylic and amino functionalized carbon nanotubes. The insertion of carbon nanotubes didn't show a modification of the crosslinking reaction due to low concentration of functionalities present in the systems. Rheology characterizations were extensively investigated. A change from Newtonian fluid to shear thinning behavior were observed for all the dispersions studied. The CNTs concentrations at which this change occurs were found to be dependent on the different functionalities present on the external wall. Oscillating rheological characterization further clarify the dependences on the different functionalization of carbon nanotubes in modifying the percolation concentration from a Newtonian to pseudo-plastic behavior. Observed rheological behaviors are directly connected with the developing nanotubes nanostructure and they correlated the different dispersion capability of the functionalized carbon nanotubes with the interconnected CNTs network itself. Moreover, rheological characterizations were confirmed to be efficiently investigated as a sensitive tool to assess the quality of carbon nanotubes dispersion. Electrical conductivity were efficiently induced with the presence of carbon nanotubes inside the polymer matrix, and the different percolation concentrations observed, were found to be related to the diverse morphologies in which the different functionalized carbon nanotubes structured themselves. Electrical conductivity induced by the presence of carbon nanotubes were further investigate to use the nanocomposites material as non invasive detector of presence of damage. A promising feasibility of exploiting nanocomposites as crack sensor is confirmed. The sensibility of the damage presence were found to be dependent on the morphologies in which the carbon nanotubes are structured inside the nanocomposites.

7.3 FLUORINATED POLYMERS NANOCOMPOSITES

Two different perfluoropolyether based nanocomposites were investigated to observe the modification induced by carbon nanotubes on the peculiar properties of those polymers. An efficient dispersion method was developed, permitting a stable dispersion of carboxylic carbon nanotubes. Rheological behaviors were investigated, confirming the repeatability of the dispersion methodology provided on those nanocomposites. Rheology characterizations were further studied to related the interconnected structure, that well dispersed carbon nanotubes create inside the polymer matrices, and the change from Newtonian behavior of the polymer dispersion to shear thinning behavior as the carbon nanotubes are inserted. Carbon nanotubes insertion was observed to slightly change the peculiar glass transition temperatures of the two perfluoropolyether polymers. Dynamical mechanical characterizations, performed on fluorinated polyurethane nanocomposites, show, as the concentration of carbon nanotubes inserted is increased, the creation of a rubber like plateau at high temperature, with storage modulus value higher than 1 MPa. This modification permits a widening at higher temperature of the possible mechanical applications of those nanocomposites. Carbon nanotubes didn't modify the peculiar hydrophobic/oleophobic behavior showed by perfluoropolyether matrices and instead a slightly change in film capability is observed, especially for the low molecular weight fluorinated polymer considered. A clear conductivity were observed as the concentration of carbon nanotubes is increased, permitting to promising broaden the applications of those nanocomposites.

Perfluoropolyether nanocomposites were investigated as advanced hydrophobic surface treatments of gas diffusion layer in PEM fuel cell systems. The application procedure developed was effective and efficient, with good dry pick up values even at low dispersion concentrations, and the treatment could be conducted at lower temperature than the standard hydrophobization method with PTFE. The use of pristine PFPE and PFPE nanocomposites could fairly reduce the problematical issues of industrialization of the carbon cloth coating procedure. Morphology of the coating and the water rate transmission values confirm the effectiveness of the coating with those nanocomposites in a efficient water managing inside the cell. The slightly change of film morphology, when carbon nanotubes are inserted, already observed when investigating nanocomposites' film, could open to a possible tune up of PFPEs' and CNTs' functionalities for improving the water management of treated gas diffusion layer. The hydrophobization effectiveness of PFPE nanocomposites were confirmed with contact angle characterizations, and a slight increase of conductivity were observed at increasing carbon nanotubes concentration. Electrochemical characterizations of treated GDLs in fuel cell clearly demonstrate an increased performances, compared with standard PTFE coating, when PFPE and PFPE nanocomposites were used, confirming those materials as best substitutes for the hydrophobization treatment of gas diffusion layer.



**APPENDIX 1
GLOSSARY**

| | |
|----------------------|--|
| AFM | Atomic Force Microscopy |
| β | Scanning speed of Differential Scanning Calorimetry |
| CCM | Catalyst Coated Membrane |
| CL | Catalyst Layer |
| CNT | Carbon nanotube (untreated) |
| COOH-CNT | Carboxylic functionalized carbon nanotube |
| CVD | Chemical Vapour Deposition |
| DGEBA | Diglycidyl ether of bisphenol-A |
| DMF | Dimethylformamide |
| DSC | Differential Scanning Calorimetry |
| E_a | Activation energy |
| EtOH | Ethanol |
| FC | Fuel Cell |
| FT-IR | Fourier Transform Infrared Spectroscopy |
| GDL | Gas Diffusion Layer |
| HR | Relative Humidity |
| MEA | Membrane Electrolyte Assembly |
| MPL | Microporous Layer |
| MWCNT | Multiwalled carbon nanotube |
| NH ₂ -CNT | Amino functionalized carbon nanotubes |
| OCV | Open Circuit Voltage |
| P56 | Anionic segmented polyurethane containing perfluoropolyether blocks |
| PEM | Polymer Electrolyte Membrane |
| PFPE | Perfluoropolyether |
| PTFE | Polytetrafluoroethylene |
| R-C | Resistor-capacitor circuit |
| SEM | Scanning Electron Microscopy |
| SWCNT | Singlewalled Carbon nanotube |
| TEM | Transmission Electron Microscopy |
| T_g | Glass transition temperature |
| TLS | Perfluoropolyether phosphate ammonium salt |
| T_p | Exothermal peak temperature |



APPENDIX 2
LIST OF PUBLICATIONS

- Publications on international journals with referees
 1. P. Gallo Stampino, S. Latorrata, **D. Molina**, S. Turri, M. Levi, G. Dotelli, "Investigation of hydrophobic treatments with Perfluoropolyether Derivatives of Gas Diffusion Layers by Electrochemical Impedance Spectroscopy in PEM-FC", *Solid State Ionics*, submitted.
 2. P. Gallo Stampino, **D. Molina**, L. Omati, S. Turri, M. Levi, C. Cristiani, G. Dotelli, "Surface treatments with perfluoropolyether derivatives for the hydrophobization of gas diffusion layers for PEM fuel cells", *Journal of Power Sources*, 2011, 196, 7645-7648.
- Proceedings of national congresses
 3. **D. Molina**, G. Clerici, M. Levi, S. Turri, "Reologia di compositi epossidici contenenti nanotubi di carbonio multiparete", *Atti del XI Convegno Nazionale di Reologia*, Trieste, 23-26 Maggio 2010 pag 281-286.
 4. **D. Molina**, L. Sacchetti, M. Levi, M. Rink, F. Briatico, S. Turri, "Funzionalizzazione di nanotubi di carbonio e il loro ruolo nel comportamento reologico e meccanico di nanocompositi a matrice epossidica, *Atti del 10° Convegno Nazionale AIMAT*, Capo Vaticano (VV), 5-8 Settembre 2010 pag 425-428.

The following article was published in international journal:



Contents lists available at ScienceDirect

Journal of Power Sources

journal homepage: www.elsevier.com/locate/jpowersour

Short communication

Surface treatments with perfluoropolyether derivatives for the hydrophobization of gas diffusion layers for PEM fuel cells

P. Gallo Stampino*, D. Molina, L. Omati, S. Turri, M. Levi, C. Cristiani, G. Dotelli

Politecnico di Milano, Dipartimento di Chimica, Materiali e Ingegneria Chimica "Giulio Natta", P.zza Leonardo da Vinci 32, 20133, Milano, Italy

ARTICLE INFO

Article history:

Received 12 January 2011

Received in revised form 27 March 2011

Accepted 19 April 2011

Available online 23 April 2011

Keywords:

Perfluoropolyether

GDL

PEM fuel cells

Hydrophobicity

Water management

ABSTRACT

In the present work, preliminary results of different hydrophobic surface treatments for gas diffusion layer (GDL) for PEM fuel cells are presented. This hydrophobic coating consists of new perfluoropolyether (PFPE) derivatives, in comparison to standard polytetrafluoroethylene (PTFE) dispersions. Experimental conditions for an efficient coating of fluoropolymers onto carbon clothes were explored by wet chemical methods. The GDLs obtained were tested in a single fuel cell at the lab scale. The cell testing was run at two temperatures (60 °C and 80 °C) with a relative humidity (RH) of the feeding gases of 80/100%, hydrogen/air respectively. The new PFPE coatings measurably improve the cell performances, and this effect is more evident at 60 °C with respect to 80 °C.

© 2011 Elsevier B.V. All rights reserved.

1. Introduction

Fuel cells (FC) are electrochemical devices, which produce electricity through clean chemical reactions without the emissions common to combustion processes; the benefits of FC include highest energy efficiency (50–60%) in the conversion of fuel (typically H₂ and air) to energy and environmentally friendly emissions (water) [1].

At present, the so-called polymer electrolyte membrane or proton exchange membrane (PEM) fuel cells are the best choice for automotive applications [2], for small-scale distributed power generation and also for portable applications [1].

The heart of the PEM fuel cell is the membrane electrode assembly (MEA), which consists of a proton exchange membrane and two catalyst layers (i.e. anode and cathode). MEA is typically sandwiched by two flow field plates that are often mirrored to make a bipolar plate (BP), when cells are stacked in series for greater voltages. Usually, a gas diffusion layer (GDL) is inserted between the BP and the MEA [3,4].

The GDL is a key component because it plays a critical role in the water and reagent gases management of the fuel cell [5]. It must control the homogeneous transportation of reactant gases from the flow field to the catalyst layer (so it has to be porous) [6], it must easily transport electrons from the bipolar plate to the catalyst (electrically conductive) [7,8], conduct heat from the catalyst to

the cooling channels in the bipolar plate (thermally conductive) [9] and it must manage the removal of reaction products (liquid and gas) from the catalyst (hydrophobic) [5,6,10].

Most of these requirements are met by carbon fiber-based materials, i.e. carbon clothes and carbon papers, due to their high porosity and electric conductivity. Moreover, GDLs must be made hydrophobic in order to avoid flooding in their porous microstructure. Usually, both anode and cathode GDLs are coated with an hydrophobic agent, typically a fluoropolymer such as polytetrafluoroethylene (PTFE) [11,12] or fluorinated ethylene propylene (FEP) [13] dispersions. These conventional treatments usually involve dipping or spraying technique followed by a heat treatment at around 350 °C [14]. Several articles in the literature concern the use of PTFE and FEP coatings, and it was found that the optimal amount is around 10–15 wt% [5,13,14].

Moreover, some works reports on the hydrophobic properties of GDLs hydrophobized by plasma treatment with fluoruous gases [15]. The hydrophobic properties are largely improved but obviously this is a more expensive method than standard wet chemical processes like dip coating [15].

The aim of the present work was to investigate the behaviour of perfluoropolyether (PFPE) derivatives as alternatives to standard fluoropolymer. Several grades of PFPE are available in form of aqueous dispersions, and allow for an easy processing without the need of using high temperature thermal sintering treatment typical of PTFE. To the best of the author's knowledge PFPEs derivatives have not been used for application on GDL, but they are commonly exploited to impart water repellence and soil release to different substrates like paper, textiles, and stones [16–18]. Particularly, in

* Corresponding author. Tel.: +390 223 993 234; fax: +390 270 638 173.
E-mail address: paola.gallo@polimi.it (P.G. Stampino).

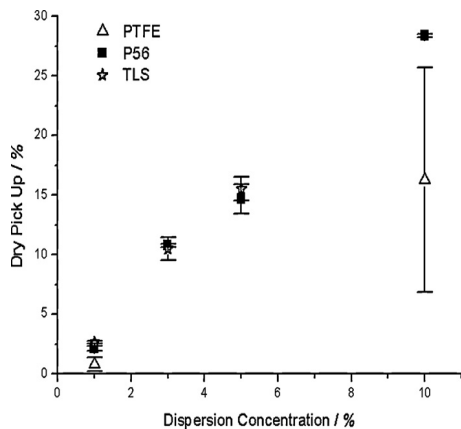


Fig. 1. Dry pick up of GDL coated with different fluorinated derivatives at increasing dispersion concentrations.

the present work, only the hydrophobic effect onto the substrates was investigated, the three samples tested are not coated with the microporous layer, as the key point of the present paper is to evaluate only the hydrophobicity of the carbon clothes coated with different fluoropolymers.

2. Experimental

2.1. Preparation of gas diffusion layers

The gas diffusion layer (GDL) used in this study is a commercial carbon cloth (SCCG 5N purchased by SAATI S.P.A., Italy) [19]. The perfluoropolyether derivatives used are commercially available products (Fluorolink® P56 and Fluorolink® TLS 5007, from Solvay Solexis s.p.a., Italy). The former perfluoropolyether (P56) is an anionic, segmented polyurethane with high molecular weight, while the latter (TLS) is a phosphate ammonium salt with lower molecular weight. It was also used an aqueous polytetrafluoroethylene (PTFE) dispersion (Algoflon® D 1214X, Solvay Solexis s.p.a., Italy) for benchmarking purposes.

PFPE dispersions were diluted with distilled water up to concentrations ranging from 1 to 10 wt%. The GDL was then dipped in the fluorinated dispersions for 10 min. The treated samples were

roll squeezed, then put in oven at a temperature of 150 °C for the GDLs treated with perfluoropolyethers, in order to obtain the complete dry off the water, and at a temperature of 350 °C for the one treated with PTFE.

The dry pick up values were calculated from the sample's weight percentage difference before dipping and after heating procedures.

2.2. Contact angle measurements

Static contact angles with bi-distilled water were measured according to the sessile drop technique with a OCA 20 Dataphysics instruments. Values were averaged from at least 20 measurements for each sample.

2.3. Morphological analysis

Microscope analyses were performed using a scanning electron microscope (SEM) Cambridge Stereoscan 360 to evaluate the different morphology of samples.

2.4. Single cell polarization measurement

Electrochemical performances of the GDLs were tested in a single cell (Fuel Cell Technologies). The BPs have a single serpentine at the anode and a triple parallel serpentine at the cathode side. The GDLs were placed at the anode and cathode side clamping the screw of the cell at a torque of about 10 Nm. The compression of GDLs was fixed at 70% of the original thickness (about 380 μm) and kept constant with an uncompressible glass fiber gasket. The MEA was assembled using a Nafion®212 membrane with a thickness of 50 μm and an active area of 25 cm²; the catalyst layer was coated directly onto the membrane with a platinum loading of 0.3 mg cm⁻² at the anode (A) and of 0.6 mg cm⁻² at the cathode (C). Pure hydrogen and air were fed at the anode and cathode, respectively. The flow rates were 0.2 Nl min⁻¹ of hydrogen and 1.0 Nl min⁻¹ of air, corresponding to a stoichiometric ratio $\lambda = 1.2$ –2.0 A/C @ 1 A cm⁻², and were controlled and detected by a calibrated flow meter.

In the present experimental work the *I*-*V* curves were made at constant flow rate both for H₂ and air, and the cell was operated at ambient pressure. The degree of humidity and the gas temperature were controlled by saturators and temperature controllers: the temperature of the cell was kept at 60 °C and 80 °C, the relative humidity of reactants was kept constant both for anode and cathode. In particular, at the anode it was set at 80%RH, while at the cathode at 100%RH. An electronic load (RBL488-50-150-800) was connected to the cell, which measures and controls the voltage,

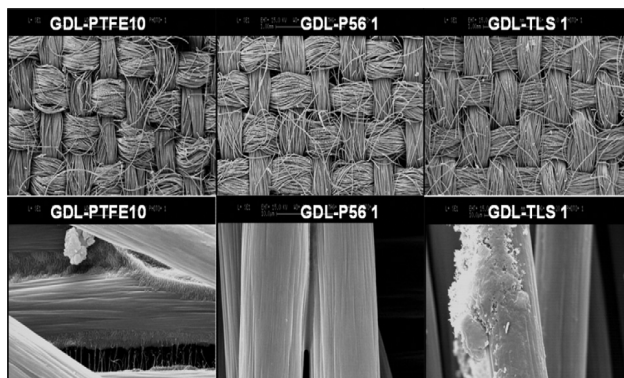


Fig. 2. Microscopical analysis of the three samples analyzed: GDL-PTFE 10, GDL-P56 1 and GDL-TLS 1.

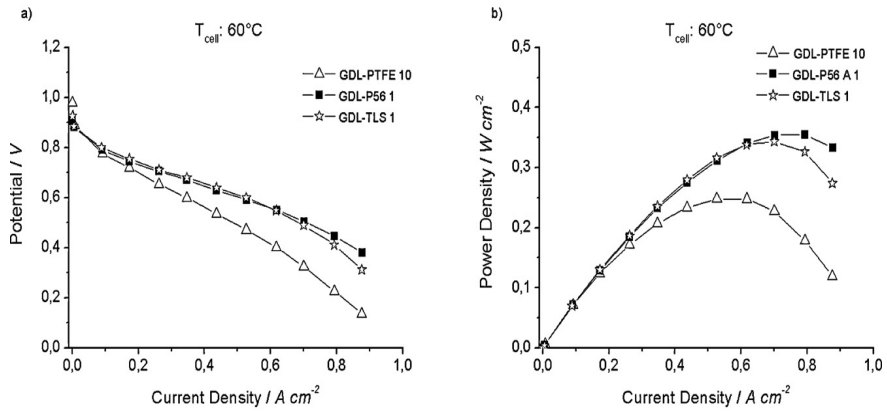


Fig. 3. Polarization (a) and power density (b) curves of single cell assemblies mounting three different GDLs (GDL-P56 1, GDL-TLS 1 and GDL-PTFE 10) at 60 °C and RH 80/100 air/H₂.

the current and the generated electric power. Polarization curves were recorded under galvanostatic conditions in the current density range from OCV to 0.87 A cm⁻², with steps of 0.085 A cm⁻², and at each step the resulting potential was recorded (galvanostatic mode, 420 s per step, 1 pt per s recorded). Potential values plotted in the steady-state polarization curves result from the averaging of the last 300 pts recorded at each step in order to minimize experimental artefacts due to transient phenomena.

3. Results and discussions

The two perfluoropolyether derivatives were described in details in the literature [16,17]. The hydrophobic PFPE chains were made water-reducible through functionalization with ionic side or end groups. In spite of this, it has been shown that the PFPE derivatives have good film forming properties and effectively make hydrophobic the treated surfaces, which become predominantly fluorinated [18]. The GDL samples coated with PFPE dispersions show (Fig. 1) a high dry pick up value and an overall good reproducibility of the application. A linear correlation between the fluorinated dispersion concentration and dry pick-up after coat-

Table 1

Contact angle measurements of GDL coated with different fluorinated derivatives.

| Sample name | Contact angle (°) | St. deviation |
|-------------|-------------------|---------------|
| GDL-PTFE 10 | 147.3 | 4.31 |
| GDL-P56 1 | 147.3 | 4.37 |
| GDL-TLS 1 | 144.0 | 5.16 |

ing can be observed. On the other hand the carbon cloth samples treated with PTFE show a lower pick-up and lower reproducibility.

Three different samples were selected for contact angle measurement and for the fuel cell testing: a GDL coated with an aqueous dispersion of PFPE polyurethane (P56) at 1 wt% (*GDL-P56 1*) and a GDL coated with an aqueous dispersion of phosphate (TLS) at 1 wt% (*GDL-TLS 1*); for sake of comparison, as reported by literature [5], a GDL coated with an aqueous dispersions of polytetrafluoroethylene 10 wt% (*GDL-PTFE 10*) was included in the experiments.

As-received GDL shows an immeasurably low contact angle value due to its porous microstructure. Some contact angle measurements for selected coated samples are presented in Table 1. As observed the application of PFPE dispersions at 1 wt% makes the

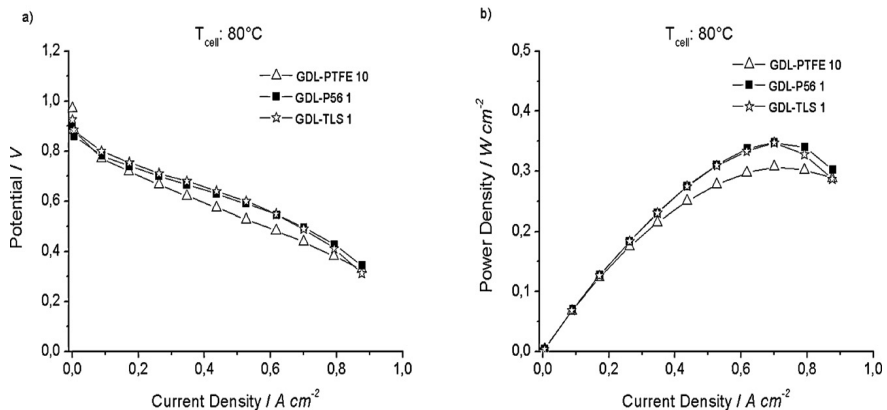


Fig. 4. Polarization (a) and power density (b) curves of single cell assemblies mounting three different GDLs (GDL-P56 1, GDL-TLS 1 and GDL-PTFE 10) at 80 °C and RH 80/100 air/H₂.

GDL surface very hydrophobic, in quite the same way of PTFE coated samples.

The three GDLs were observed with the electronic microscope in order to identify the presence of the polymeric agglomerates among the carbon fibres. In Fig. 2 are shown the carbon fibres of GDL treated with different polymer. It is possible to observe the presence of polymer onto the carbon fibres in the samples considered. Some polymer agglomerates were found in GDL-PTFE 10 and GDL-TLS 1 while GDL-P56 1 seems to present a more uniform distribution.

In order to assess the effectiveness of the GDLs hydrophobic treatments only high values of relative humidity of gases (i.e. RH80–100% H₂–Air) were adopted in the present work. Moreover, these conditions should assure that the membrane be fully humidified. Analyzing the experimental results, it is worth noting that the addition of different PFPE polymers, even in as small amounts as 1 wt%, positively influences the cell performances at all current density values, as reported in Figs. 3 and 4.

Particularly, when operating at 60 °C, the assembly with the PFPE treated GDL measurably improves the cell performances; this effect is even more evident in the high current density region, where the cell is more stressed and the amount of water generated by the cathodic reaction is maximum. In terms of power density GDL-P56 1 and GDL-TLS 1 are superior to GDL-PTFE 10; the peak value is about 0.35 and 0.34 W cm⁻² for GDL-P56 1 and GDL-TLS 1, respectively, while GDL-PTFE 10 gets only 0.25 W cm⁻².

At 80 °C the effect of perfluoropolyethers is more controversial. Also at this working temperature the PFPE based system performs better than PTFE, but the enhancement is less evident. Again, the power density of GDL-P56 1 and GDL-TLS 1 are superior to GDL-PTFE 10; at 80 °C the peak value is about 0.34 W cm⁻² both for GDL-P56 and GDL-TLS, while for GDL-PTFE 10 the value is 0.30 W cm⁻².

The slope of the polarization curve in the quasi-linear central region is known to be strictly correlated to the FC ohmic resistance, which is mainly due to membrane resistance, bulk resistance of GDLs and contact resistances between different elements of the assembly.

At 60 °C the polarization curve of the cell assembled with GDL-PTFE 10 shows a lower slope than the two PFPE's slopes, that is indicative of an higher overall cell resistance mounting PTFE treated GDLs. This effect is mitigated at 80 °C, where all the polarization curves have quite the same slope.

We can assume that at 60 °C the PFPE probably shows a better water management during the cell operation preventing both the drying of the membrane and the flooding of the GDL at the cathodic side.

4. Conclusive remarks

In this work some preliminary data about the use of perfluoropolyether derivatives as hydrophobic surface treatments for GDL were presented. It was interesting to observe that the application of a small amount of PFPE (1 wt% of PFPE to coat GDLs, with respect to the 10 wt% of PTFE) allowed for a clear improvement in electrochemical performances. Moreover, the application procedure of PFPEs seems quite simple and user-friendly, showing a very good dry pick-up even at low dispersion concentration, and being quite effective even without the high temperature sintering cycle typically needed for PTFE coatings. More work is however needed to further improve the performances and optimize the composition (i.e. average molecular weight and functionalities) of the perfluoropolyether derivatives.

Acknowledgments

The Authors thank Fondazione Cariplo for financial support (Project 2008-2372: "Advanced Materials for Gas Diffusion Electrodes (GDE) in Polymer Electrolytes Membranes Fuel Cells (PEMFCs); superhydrophobic textiles and nanocarbon based inks").

References

- [1] L. Carrette, K.A. Friedrich, U. Stimming, *Fuel Cells* 1 (2001) 5.
- [2] G. Frenette, D. Forthoffer, *Int. J. Hydrogen Energy* 34 (2009) 3578.
- [3] F. Barbir, *PEM Fuel Cells: Theory and Practice*, Elsevier Academic Press, Oxford, 2005.
- [4] S. Lister, G. McLean, *J. Power Sources* 139 (2004) 61.
- [5] L. Cindrella, A.M. Kannan, J.F. Saminatha, Y. Ho, C.W. Lin, J. Wertz, *J. Power Sources* 194 (2009) 146.
- [6] E.E. Kimball, J.B. Benzinger, Y.G. Kevrekidis, *Fuel Cells* 4 (2010) 530.
- [7] P.M. Wilde, M. Mandle, M. Murata, N. Berg, *Fuel Cells* 4 (2004) 180.
- [8] T. Zhou, H. Liu, *J. Power Sources* 161 (2006) 444.
- [9] I. Nitta, O. Himanen, M. Mikkola, *Fuel Cells* 8 (2008) 11.
- [10] P.G. Stampino, G. Dotelli, L. Omati, P. Fracas, D. Brivio, P. Grassini, *Smart Textiles* 60 (2009) 128.
- [11] M.S. Ismail, T. Damjanovic, D.C. Ingham, L. Ma, M. Pourkashanian, *J. Power Sources* 195 (2010) 6619.
- [12] J.-H. Lin, T.-H. Ko, W.-S. Kuo, Y.-H. Lin, C.-C. Huang, W.-C. Cheng, *Fuel Cells* 10 (2010) 118.
- [13] C. Lim, C.Y. Wang, *Electrochim. Acta* 49 (2004) 4149.
- [14] V.A. Paganin, E.A. Ticianelli, E.R. Gonzalez, *J. Appl. Electrochem.* 26 (1996) 297.
- [15] C.-M. Lee, Y.-H. Pai, J.-M. Zen, F.-S. Shieu, *Mater. Chem. Phys.* 114 (2009) 151.
- [16] T. Trombetta, P. Iengo, S. Turri, *J. Appl. Polym. Sci. Part A: Chem.* 98 (2005) 1364.
- [17] A. Russo, C. Tonelli, E. Barchiesi, *J. Polym. Sci. Part A: Chem.* 43 (2005) 4790.
- [18] R. Canteri, G. Speranza, M. Anderle, S. Turri, S. Radice, *Surf. Interface Anal.* 35 (2003) 318.
- [19] P. Fracas, P. Grassini, G. Dotelli, P. Gallo Stampino, D. Brivio, *ECS Trans.* 12 (2007) 51.

ACKNOWLEDGEMENTS >>

It is rather difficult to properly thank everyone that help me in this three year work. I switch to their mother language to thank them all. Ringrazio i professori Stefano e Marinella, senza il loro gruppo di ricerca, questa difficile ed entusiasmante esperienza non ci sarebbe mai stata. Ringrazio i miei compagni e colleghi di laboratorio, con cui ho condiviso ogni singola scoperta, ogni singola fatica giornaliera, ma sempre con il sorriso sulle labbra. Un grazie a Gianmarco, il compagno ideale di dottorato, tra i suoi consigli scientifici, le ricerche nella colonna infame e il costante supporto/apporto morale. Giuseppe, che mi ha insegnato molto di più di quanto mai credevo possibile, umanamente e culturalmente, anche se il suo regime alimentare lo rende di difficile approccio. Frapic, per la grande simpatia, le grasse risate e la forza bruta necessaria in un laboratorio chimico. Raffaella, per la sua saggezza e capacità di ascoltare e attentamente consigliare, in bocca al lupo per tutto. Un grazie particolare va a Gigliola, la cui presenza costante rimane il pilastro fondamentale di tutto questo lavoro di ricerca, e il cui aiuto in ogni momento ha reso tutto pieno di gioia. Un grazie agli altri colleghi, Francesca Torino per cui sono un vero nerd, Francesca Frosty e Massimo per aver allietato le veloci pause nutrimento, tra il mio "non ho tempo", con mille aneddoti divertenti, Stefano per le sue mille domande, Carmela per i consigli su come condurre l'OCA, Barbara e Serena a cui faccio i più grandi incoraggiamenti per rendere il laboratorio più funzionale e d'eccellenza. Grazie ai tesisti con cui ho condiviso parte del mio percorso: Claudio, Alessandro e soprattutto Giacomo e le sue scorpacciate di pizza kebab con monster annessa, senza il vostro apporto non sarei mai giunto qui. Un grazias a Luciana, con cui ho condiviso la frustrazione della ricerca, ma anche la sua immensa gioia. Il prof. Briatico e la professoressa Rink, vi ringrazio per i vostri consigli e il supporto professionale. Un grazie al prof. Dotelli e alla prof. ssa Cristiani, a Paola, Luca e Saverio, che mi hanno fatto apprezzare la ricerca sotto differenti punti di vista rispetto a quelli a cui ero abituato. Un enorme ringraziamento va a Filomena e gli altri del dipartimento, che lo fanno andare avanti ogni giorno veramente tra mille difficoltà. Un grazie va poi a Francesco Caimmi, con cui per molto tempo ho condiviso le mattine, i pensieri apocalittici, la filosofia della scienza e la gayna musicale, permettendo a tutte le giornate di partire di slancio. Ringrazio poi i miei più vicini amici, per avermi dato forza nei momenti di difficoltà. 26per1 tutta, ma soprattutto l'idea di fondo. Frani che con poche parole capisce. Carolina che invece mi regala sempre un sorriso. Simone che è diventato sempre più una sicurezza da "piano quinquennale". Ringrazio i miei genitori e la mia famiglia, per avermi veramente permesso di arrivare fino a qui. Senza il vostro sostegno non sarebbe stato possibile. Spero di ricambiare presto. Grazie Mamma mi manchi tantissimo. Grazie Papà per essere così forte. Grazie Matteo e Marinella per sostenermi anche nella difficoltà. Per ultimo ringrazio Alice, che sposerò presto. Con la tua presenza riesco veramente ad essere meglio di quanto mai avrei voluto essere. Ti amo infinitamente ogni giorno di più.